



PhD-FSTC-2016-17  
The Faculty of Sciences, Technology and Communication

## DISSERTATION

Defense held on 18/05/2016 in Belvaux

to obtain the degree of

DOCTEUR DE L'UNIVERSITÉ DU LUXEMBOURG

EN BIOLOGIE

by

**Nadia BATTELLO**

Born on 25 December 1983 in Luxembourg (Luxembourg)

# THE IMPLICATION OF ONCOSTATIN-M IN HIF-1-MEDIATED METABOLIC REPROGRAMMING IN HEPATOCELLULAR CARCINOMA CELLS AND IMMORTALIZED HEPATOCYTES

## Dissertation defense committee

Dr. Karsten Hiller, Dissertation supervisor  
*Associate Professor, University of Luxembourg, Luxembourg*

Dr. Thomas Sauter, Chairman  
*Professor, University of Luxembourg, Luxembourg*

Dr. Laurent Vallar, Vice-chairman  
*Luxembourg Institute of Health, Luxembourg*

Dr. Sarah-Maria Fendt  
*Associate Professor, KU Leuven, Belgium*

Dr. Daniel Tennant  
*Associate Professor, University of Birmingham, United Kingdom*

UNIVERSITY OF LUXEMBOURG

**The implication of Oncostatin-M in  
HIF-1-mediated metabolic reprogramming  
in hepatocellular carcinoma cells and  
immortalized hepatocytes**

by

Nadia Battello

A thesis submitted in partial fulfillment for the  
degree of Doctor of Biology

in the

FACULTY OF SCIENCE, TECHNOLOGY AND COMMUNICATION  
LUXEMBOURG CENTRE FOR SYSTEMS BIOMEDICINE

July 2016

# Declaration of Authorship

I hereby confirm that the PhD thesis entitled "The implication of Oncostatin-M in HIF-1-mediated metabolic reprogramming in hepatocellular carcinoma cells and immortalized hepatocytes" has been written independently and without any other source than cited.

Luxembourg,

---

Name and Signature:

---

# *Acknowledgements*

This thesis is the result of two and a half years of research and would not have been possible without the support of my supervisor, my colleagues and my family. I would like to take the opportunity to thank everybody who has help me during this time.

First, I wish to express my gratitude to my supervisor, Karsten Hiller, for accepting me as his PhD student and always being faithful that I can manage my PhD in less time than usual. This work would not have been possible without his expertise, his support and his indestructible optimism.

I would like to thank my thesis committee members, Thomas Sauter and Laurent Vallar for their guidance and encouragement throughout my PhD and for critically revising my work. Furthermore I would like to thank my defence committee members, Sarah-Maria Fendt and Dan Tennant, for their interest in my work and for joining my committee.

I would like to thank our collaborators on this project, Iris Behrmann, Claude Haan and Andreas Zimmer.

I would like to thank Rob Moritz and his whole team, especially Ulli Kusebauch, for giving me the opportunity to stay at ISB for a couple of months.

A special thanks goes to the fantastic metabolomics group. I would like to thank Andre for his invaluable support throughout this project, for his patience with me, for introducing me to *LATEX* and *Inkscape* and for revising this thesis. I am grateful to Xiangyi for her terrific technical support and most importantly, for always making me laugh. I would like to thank Sylvie for providing me with her "*bible*" that truly contains the best written protocols and for revising my thesis so carefully. I would like to thank Jenny for her technical assistance, her help throughout this whole project and for her precious advice on the materials and method section of this work. I would like to thank Daniel and JP for helping me whenever I had a problem in *R* (and this was often the case). I would like to thank Sean for debugging my *LATEX* scripts, for his advice while writing this thesis and for making me aware how well potato chips go with lunch. I would like to thank Christian, for his wonderful help and support on the GC-MS instruments. I wish to thank Elodie, who made miracles happen with my proteomics data. I want to thank "Lieschen" for never saying no to a beer in the evening and to Yannick for always providing us with a fresh supply of beer.

I want to thank my wonderful husband Mario and my son Milo for their endless love and encouragement.

I wish to thank my parents, who always love and support me.

*“Voici mon secret. Il est très simple: on ne voit bien qu’avec le cœur. L’essentiel est invisible pour les yeux.”*

Le Petit Prince

## Abstract

The majority of hepatocellular carcinomas (HCCs) develop in a setting of chronic inflammation, which is accompanied by the persistent activation of macrophages and long-lasting infiltration of lymphocytes into the liver. Inflammatory microenvironments comprise a battery of cytokines and growth factors that stimulate liver regeneration but also favour malignant transformation and support neoplastic growth. One important group of inflammatory mediators present within this inflammatory microenvironment are IL-6-type cytokines which induce a growth-promoting transcriptional program by activating signal transducer and activator of transcription 3 (STAT3). While the expression of STAT3 target genes supports cellular survival and stimulates proliferation, STAT3 activation might also play an important role in the regulation of cellular metabolism. STAT3 induces the expression of the metabolic key regulator hypoxia-inducible factor-1 $\alpha$  (HIF-1 $\alpha$ ) which orchestrates the regulation of hundreds of target genes, many of which play key roles in the adaptation of cellular metabolism to low oxygen tension. Both, aberrant STAT3 signalling and HIF-1 $\alpha$  expression are associated with cancer development and progression. While aberrant STAT3 expression drives cellular proliferation, the particular impact of STAT3-mediated HIF-1 $\alpha$  induction on cellular metabolism under normoxic conditions remained to be elucidated. Thus we aimed to determine whether IL-6 type cytokines induce changes within central carbon metabolism that would support the metabolic requirements of carcinogenesis.

In this work, we used the IL-6-type cytokine Oncostatin M (OSM) to induce HIF-1 $\alpha$  expression under normoxic conditions in HCC cell lines and in immortalized hepatocytes. We performed stable-isotope assisted metabolomics to decipher whether OSM-induced HIF-1 $\alpha$  results in a hypoxia-like metabolic phenotype and thus has the ability to promote neoplastic growth.

We found that short-term OSM treatments induced metabolic reprogramming in immortalized hepatocytes while the metabolism of HCC cell lines remained unaffected. OSM-mediated changes within central carbon metabolism were characterized by a reduced pyruvate dehydrogenase complex activity, thus a diminished entry of glucose-derived carbon into the TCA cycle and an increased reductive glutamine metabolism. We provided evidence that OSM-mediated metabolic changes in immortalized hepatocytes were HIF-1 $\alpha$ -dependent and that the HIF-1 $\alpha$  target gene pyruvate dehydrogenase kinase 1 plays an essential role. Although OSM-induced HIF-1 $\alpha$  protein levels under normoxia were comparable to those observed under hypoxia, OSM-mediated metabolic reprogramming was less pronounced.

While cellular metabolism of HCC cell lines was unaffected by short-term OSM treatments, we showed that chronic OSM exposure leads to drastic metabolic changes in the HCC cell line JHH-4. Chronic OSM treatment in JHH-4 cells did not induce HIF-1 $\alpha$ , suggesting that the metabolic effects are HIF-1 $\alpha$  independent. Chronic OSM stimulation did not effect PDC activity while reductive glutamine metabolism to generate lipogenic citrate was induced,

pointing towards OSM-induced changes in fatty acid metabolism.

Our results reveal that inflammatory conditions, which frequently coincide with HCC development and progression, might assist carcinogenesis by regulating growth promoting changes in cellular metabolism.

# Contents

|   |            |
|---|------------|
| <b>Declaration of Authorship</b>  | <b>i</b>   |
| <b>Acknowledgements</b>   | <b>ii</b>  |
| <b>Abstract</b>   | <b>iv</b>  |
| <b>List of Figures</b>  | <b>ix</b>  |
| <b>List of Tables</b>   | <b>xi</b>  |
| <b>Abbreviations</b>  | <b>xii</b> |
| <br>  |            |
| <b>1 Introduction</b>   | <b>1</b>   |
| 1.1 Inflammation promotes hepatocellular carcinoma development . . . . .  | 1          |
| 1.2 The implication of STAT3 in cancer development . . . . .  | 2          |
| 1.3 STAT3 activation by IL-6-type cytokines . . . . .   | 2          |
| 1.3.1 The IL-6-type cytokine Oncostatin M . . . . .   | 4          |
| 1.4 The implication of STAT3 in HCC . . . . .   | 5          |
| 1.5 The metabolic effects of STAT3 . . . . .  | 6          |
| 1.6 Hypoxia-inducible factor 1- $\alpha$ . . . . .  | 6          |
| 1.6.1 Oxygen-dependent HIF-1 $\alpha$ induction . . . . .   | 8          |
| 1.6.2 Oxygen-independent HIF-1 $\alpha$ induction . . . . .   | 10         |
| 1.6.2.1 Interactions between STAT3 and HIF-1 $\alpha$ . . . . .   | 10         |
| 1.6.3 The transcriptional and metabolic consequences of HIF-1 $\alpha$ stabilization<br>under hypoxia . . . . . | 11         |
| 1.7 The metabolism of proliferating cells . . . . .   | 15         |
| 1.8 The Warburg effect . . . . .  | 15         |
| 1.9 Metabolomics . . . . .  | 20         |
| 1.9.1 Metabolomics workflow . . . . .   | 20         |
| 1.9.2 Mass isotopomer distribution . . . . .  | 21         |
| 1.9.3 Metabolic flux analysis . . . . .   | 22         |
| 1.10 Aims and scope of the thesis . . . . .   | 25         |
| <br>  |            |
| <b>2 Material and Methods</b>   | <b>27</b>  |
| 2.1 Cell culture and reagents . . . . .   | 27         |



---

|          |   |           |
|----------|---|-----------|
| 2.2      | Stable isotope labelling experiments . . . . .  | 28        |
| 2.3      | siRNA-mediated silencing of PDK1 and HIF-1 $\alpha$ . . . . .   | 28        |
| 2.3.1    | OSM stimulation . . . . .   | 29        |
| 2.3.2    | Short-term OSM stimulation . . . . .  | 29        |
| 2.3.3    | Long-term OSM stimulation . . . . .   | 30        |
| 2.4      | Extraction of intracellular metabolites . . . . .   | 30        |
| 2.5      | Medium preparation for GC-MS analysis . . . . .   | 31        |
| 2.6      | Cell counting . . . . .   | 32        |
| 2.7      | GC-MS analysis . . . . .  | 32        |
| 2.8      | GC-MS data analysis . . . . .   | 33        |
| 2.8.1    | Mass isotopomer distribution analysis . . . . .   | 33        |
| 2.8.2    | Relative quantification of metabolites . . . . .  | 33        |
| 2.9      | Reverse transcription and quantitative PCR procedure . . . . .  | 34        |
| 2.10     | Western blots . . . . .   | 34        |
| 2.11     | Statistical analysis . . . . .  | 36        |
| <b>3</b> | <b>Results</b>  | <b>37</b> |
| 3.1      | Effects of hypoxia on cellular metabolism of HCC cells and immortalized hep-<br>atocytes . . . . .                              | 38        |
| 3.1.1    | Hypoxia reduces glucose-derived carbon entry into the TCA cycle . . . . .   | 38        |
| 3.1.2    | Metabolic consequences of hypoxia on glucose and glutamine metabolism . . . . .   | 40        |
| 3.2      | OSM-mediated metabolic effects in HCC cell lines and immortalized hepatocytes . . . . .   | 44        |
| 3.2.1    | Effects of OSM on glucose- and glutamine-derived carbon contribution<br>to central carbon metabolism . . . . .                  | 44        |
| 3.2.2    | Effects of OSM on glucose and glutamine metabolism . . . . .  | 45        |
| 3.2.3    | OSM-mediated HIF-1 $\alpha$ upregulation in hepatoma and hepatic cells . . . . .  | 46        |
| 3.2.4    | OSM does not induce metabolic changes in HepG2-C3A and SK-Hep1<br>HCC cells despite HIF-1 $\alpha$ induction . . . . .          | 49        |
| 3.2.5    | OSM-mediated metabolic effects in PH5CH8 cells are concentration<br>dependent . . . . .   | 50        |
| 3.2.6    | OSM-mediated metabolic effects in PH5CH8 cells are HIF-1 $\alpha$ dependent . . . . .   | 51        |
| 3.2.7    | OSM-induced metabolic effects are partially dependent on PDK1 . . . . .   | 53        |
| 3.2.8    | Oncostatin-M induces a hypoxia-like metabolic phenotype in other PH5CH<br>clones . . . . .                                      | 56        |
| 3.2.9    | Long-term OSM treatment effects cellular metabolism in hepatocellular<br>carcinoma cells and immortalized hepatocytes . . . . . | 58        |
| 3.3      | Results summary . . . . .   | 60        |
| <b>4</b> | <b>Discussion and Perspectives</b>  | <b>61</b> |
| 4.1      | Discussion . . . . .  | 61        |
| 4.1.1    | The metabolic phenotype of HCC cell lines and immortalized hepatocytes . . . . .  | 62        |
| 4.1.2    | Hypoxia inhibits glucose-derived carbon entry into the TCA cycle and<br>induces reductive glutamine metabolism . . . . .        | 64        |
| 4.1.3    | OSM does not induce a hypoxia-like metabolic phenotype in HCC cell<br>lines . . . . .   | 64        |
| 4.1.4    | OSM induces hypoxia-like metabolic changes in immortalized hepatocytes . . . . .  | 67        |
| 4.1.5    | OSM-induced metabolic reprogramming in immortalized hepatocytes<br>is HIF-1 $\alpha$ -dependent . . . . .                       | 69        |

---

|          |   |            |
|----------|---|------------|
| 4.1.6    | OSM-induced metabolic reprogramming in immortalized hepatocytes is partially dependent on PDK1 . . . . .              | 69         |
| 4.1.7    | Long-term OSM treatment results in HIF-1 $\alpha$ -independent metabolic changes in the HCC cell line JHH-4 . . . . . | 70         |
| 4.1.8    | Conclusions . . . . .   | 72         |
| 4.2      | Perspectives . . . . .  | 73         |
| <br>     |   |            |
| <b>A</b> | <b>Supplemental figures</b>   | <b>76</b>  |
| <b>B</b> | <b>Supplemental Material and Methods</b>  | <b>84</b>  |
| <b>C</b> | <b>Publications</b>   | <b>86</b>  |
| <br>     |   |            |
|          | <b>Bibliography</b>   | <b>142</b> |

# List of Figures

|      |  |    |
|------|--|----|
| 1.1  | The JAK/STAT3 signalling cascade . . . . .   | 3  |
| 1.2  | HIF-1 target genes . . . . .   | 7  |
| 1.3  | Mechanisms of HIF-1 $\alpha$ stabilization . . . . .   | 9  |
| 1.4  | The effects of HIF-1 $\alpha$ on glycolysis . . . . .  | 12 |
| 1.5  | The effects of HIF-1 $\alpha$ on the TCA cycle . . . . .   | 14 |
| 1.6  | Glucose metabolism in resting and proliferating cells . . . . .  | 16 |
| 1.7  | Glutamine metabolism in proliferating cells . . . . .  | 18 |
| 1.8  | Mass isotopomer distribution . . . . .   | 23 |
| 1.9  | Mass isotopomer distributions from uniformly labelled glucose . . . . .  | 24 |
| 1.10 | Mass isotopomer distributions from uniformly labelled glutamine . . . . .  | 25 |
| 2.1  | Experimental scheme of the long-term OSM stimulation . . . . .   | 31 |
| 3.1  | Hypoxia-mediated changes in glucose- and glutamine-derived carbon contributions . . . . .                                      | 40 |
| 3.2  | Hypoxia-mediated changes in glucose and glutamine metabolism in hepatoma cells and immortalized hepatocytes . . . . .          | 43 |
| 3.3  | OSM-mediated changes in carbon contributions in hepatoma cells and immortalized hepatocytes . . . . .                          | 45 |
| 3.4  | OSM-mediated changes in glucose and glutamine metabolism in hepatoma cells and immortalized hepatocytes . . . . .              | 47 |
| 3.5  | The effect of OSM on HIF-1 $\alpha$ expression in PH5CH8 immortalized hepatocytes and HepG2 and JHH-4 hepatoma cells . . . . . | 48 |
| 3.6  | OSM-mediated metabolic effects in Sk-Hep1 and HepG2-C3A hepatocellular carcinoma cells . . . . .                               | 50 |
| 3.7  | OSM-mediated metabolic changes in PH5CH8 are concentration-dependent . . . . .   | 51 |
| 3.8  | The metabolic effects of HIF-1 $\alpha$ silencing on the OSM-induced hypoxia-like metabolic phenotype in PH5CH8 . . . . .      | 52 |
| 3.9  | The metabolic effects of PDK1 silencing on the OSM-induced hypoxia-like metabolic phenotype in PH5CH8 . . . . .                | 54 |
| 3.10 | The metabolic effects of PDK1 silencing intracellular metabolite levels . . . . .  | 55 |
| 3.11 | The metabolic effects of PDK1 silencing on the OSM-induced hypoxia-like metabolic phenotype in PH5CH1 and PH5CH7 . . . . .     | 57 |
| 3.12 | Long-term OSM stimulation in PH5CH8 and JHH-4 cells . . . . .  | 59 |
| 4.1  | Model of OSM-mediated HIF-1 $\alpha$ upregulation and effects on metabolism . . . . .  | 71 |
| A.1  | Glucose uptake and lactate secretion rates in PH5CH8 . . . . .   | 77 |
| A.2  | PDK1 expression and PDC phosphorylation in HepG2 and JHH-4 . . . . .   | 78 |

---

|     |   |    |
|-----|---|----|
| A.3 | PDK1 expression and PDC phosphorylation in PH5CH8 cells . . . . .                         | 79 |
| A.4 | Metabolic effects of OSM in combination with hypoxia in HepG2, JHH-4 and PH5CH8 . . . . . | 80 |
| A.5 | The metabolic effects of PDK1 silencing in HCC cell lines . . . . .                       | 81 |
| A.6 | Response of PH5CH1 and PH5CH7 non-neoplastic hepatocytes to OSM . . .                     | 82 |
| A.7 | Response of PH5CH1 and PH5CH7 non-neoplastic hepatocytes to OSM . . .                     | 83 |

# List of Tables

|     |   |    |
|-----|---|----|
| 2.1 | Overview on HCC cell lines and immortalized hepatocytes. . . . .          | 28 |
| 2.2 | siRNA sequences . . . . .   | 29 |
| 2.3 | Cell seeding densities for stable isotope labelling experiments . . . . . | 30 |
| 2.4 | GC-MS analysis: Details on the SIM method . . . . .                       | 33 |
| 2.5 | Primer sequences . . . . .  | 34 |
| 2.6 | Antibody dilutions and suppliers . . . . .                                | 36 |
| B.1 | Metabolite Detector Settings . . . . .                                    | 84 |
| B.2 | MID Wizard settings . . . . .   | 85 |

# Abbreviations

|                                 |                                       |
|---------------------------------|---------------------------------------|
| <b>ATP</b>                      | adenosine 5'-triphosphate             |
| <b>ACL</b>                      | ATP citrate lyase                     |
| <b>ACN</b>                      | Acetonitrile                          |
| <b>ACSL</b>                     | Acyl-CoA synthetase long-chain family |
| <b><math>\alpha</math>-KGDH</b> | $\alpha$ -Ketoglutarate dehydrogenase |
| <b>ATP</b>                      | Adenosine triphosphate                |
| <b>ChIP</b>                     | Chromatin immunoprecipitation         |
| <b>CLCF-1</b>                   | Cardiotrophin-like cytokine           |
| <b>CNPF</b>                     | Ciliary neurotrophic factor           |
| <b>CS</b>                       | Citrate synthase                      |
| <b>CT-1</b>                     | Cardiotrophin 1                       |
| <b>COX</b>                      | Cytochrome c oxidase                  |
| <b>DEN</b>                      | Diethylnitrosamine                    |
| <b>DMEM</b>                     | Dulbecco's modified eagle medium      |
| <b>DPBS</b>                     | Dulbecco's phosphate-buffered saline  |
| <b>EGF</b>                      | Epidermal growth factor               |
| <b>EPO</b>                      | Erythropoietin                        |
| <b>ERK</b>                      | Extracellular signal-regulated kinase |
| <b>FAD<sup>+</sup></b>          | Oxidized flavin adenine dinucleotide  |
| <b>FADH<sub>2</sub></b>         | Reduced flavin adenine dinucleotide   |
| <b>FAS</b>                      | Fatty acid synthase                   |
| <b>FBS</b>                      | Fetal bovine serum                    |
| <b>FGF</b>                      | Fibroblast growth factor              |
| <b>FH</b>                       | Fumarate hydratase                    |
| <b>FIH</b>                      | Factor inhibiting HIF                 |

---

|                        |  |
|------------------------|--|
| <b>G6PC</b>            | Glucose-6-phosphatase catalytic-subunit                |
| <b>GC</b>              | Gas chromatography                                     |
| <b>GLUT</b>            | Glucose transporter                                    |
| <b>gp130</b>           | Glycoprotein 130                                       |
| <b>HCC</b>             | Hepatocellular carcinoma                               |
| <b>HGF</b>             | Hepatocyte growth factor                               |
| <b>HIF</b>             | Hypoxia-inducible factor                               |
| <b>HK</b>              | Hexokinase   |
| <b>IDH</b>             | Isocitrate dehydrogenase                               |
| <b>IL-11</b>           | Interleukin-11   |
| <b>IL-11R</b>          | Interleukin-11 receptor                                |
| <b>IL-6</b>            | Interleukin-6  |
| <b>JAK</b>             | Janus kinase   |
| <b>JNK</b>             | Jun amino-terminal kinase                              |
| <b>LDH</b>             | Lactate dehydrogenase                                  |
| <b>LDLR</b>            | Low density lipoprotein receptor                       |
| <b>LIF</b>             | Leukaemia inhibitory factor                            |
| <b>LIFR</b>            | Leukaemia inhibitory factor receptor                   |
| <b>MAPK</b>            | Mitogen-activated protein kinase                       |
| <b>MEF</b>             | Mouse embryonic fibroblasts                            |
| <b>MDH</b>             | Malate dehydrogenase                                   |
| <b>ME</b>              | Malic enzyme   |
| <b>MID</b>             | Mass isotopomer distribution                           |
| <b>MS</b>              | Mass spectrometry                                      |
| <b>mTOR</b>            | Mechanistic target of rapamycin                        |
| <b>NAD<sup>+</sup></b> | Oxidized nicotinamide adenine dinucleotide             |
| <b>NADH</b>            | Reduced nicotinamide adenine dinucleotide              |
| <b>NOS</b>             | Nitrogen oxide species                                 |
| <b>OSM</b>             | Oncostatin M   |
| <b>PC</b>              | Pyruvate carboxylase                                   |
| <b>PDC</b>             | Pyruvate dehydrogenase complex                         |
| <b>PDP2</b>            | Pyruvate dehydrogenase phosphatase catalytic subunit 2 |
| <b>PEPCK</b>           | Phosphoenolpyruvate carboxykinase                      |

---

|                                |  |
|--------------------------------|--|
| <b>PFK</b>                     | Phosphofructokinase                              |
| <b>PHD</b>                     | Prolyl hydroxylase dioxygenase                   |
| <b>PI3K</b>                    | Phosphatidylinositide 3-kinase                   |
| <b>PIAS</b>                    | Protein inhibitor of activated STAT              |
| <b>PK</b>                      | Pyruvate kinase                                  |
| <b>PKB</b>                     | Protein kinase B                                 |
| <b>PKM2</b>                    | Pyruvate kinase muscle isozyme 2                 |
| <b>PTP</b>                     | Protein tyrosine phosphatase                     |
| <b>RCC</b>                     | Renal clear cell carcinoma                       |
| <b>ROS</b>                     | Reactive oxygen species                          |
| <b>SDH</b>                     | Succinate dehydrogenase                          |
| <b>siRNA</b>                   | Small interfering RNA                            |
| <b>SOCS</b>                    | Suppressor of cytokine signalling                |
| <b>STAT</b>                    | Signal transducer and activator of transcription |
| <b>TCA</b>                     | Tricarboxylic acid                               |
| <b>TNF-<math>\alpha</math></b> | Tumor necrosis factor $\alpha$                   |
| <b>VEGF</b>                    | Vascular endothelial growth factor               |
| <b>VHL</b>                     | Von Hippel-Lindau                                |



*Dedicated to Milo*

# Chapter 1

## Introduction

### 1.1 Inflammation promotes hepatocellular carcinoma development

Chronic inflammation precedes 70% to 90% of all hepatocellular carcinomas (HCCs), which indicates that inflammatory conditions promote malignant growth [El-Serag and Rudolph, 2007]. Chronic hepatitis B and C virus infections, amongst other causes, induce liver cirrhosis which is accompanied by a continuous activation of liver resident macrophages, the Kupffer cells, and long-lasting infiltration of lymphocytes [El-Serag and Rudolph, 2007, Fausto, 1999]. This condition stimulates hepatocyte regeneration while driving hepatocarcinogenesis and is accompanied by the production of cytokines, chemokines and growth factors that support proliferation [Fausto, 1999]. In addition, activated immune cells secrete reactive oxygen species (ROS) and nitrogen oxide species (NOS) which increase mutagenesis and thereby can lead to the activation of oncogenes and/or inactivation of tumour suppressor genes [Sakurai et al., 2008].

Primary liver cancer is the fifth most common cancer, causing approximately 600,000 deaths each year, and is the third most common cause of cancer-related death worldwide [El-Serag and Rudolph, 2007, Parkin, 2001]. The vast majority (85% to 90%) of primary liver cancers are HCCs which preferentially develop within an inflammatory microenvironment [El-Serag and Rudolph, 2007]. The observation that chronic inflammation drives cancer development and progression dates back to 1863 where Rudolf Virchow observed that cancer predominantly develops at sites of inflammation (reviewed in [Balkwill and Mantovani, 2001, Mantovani et al., 2008]. 150 years later, 15% of all cancers are attributed to chronic infection and inflammation while tumour-promoting inflammation is now considered a hallmark of cancer [Hanahan and Weinberg, 2011, Kuper et al., 2000].

While numerous signalling cascades are described to be involved in HCC development and

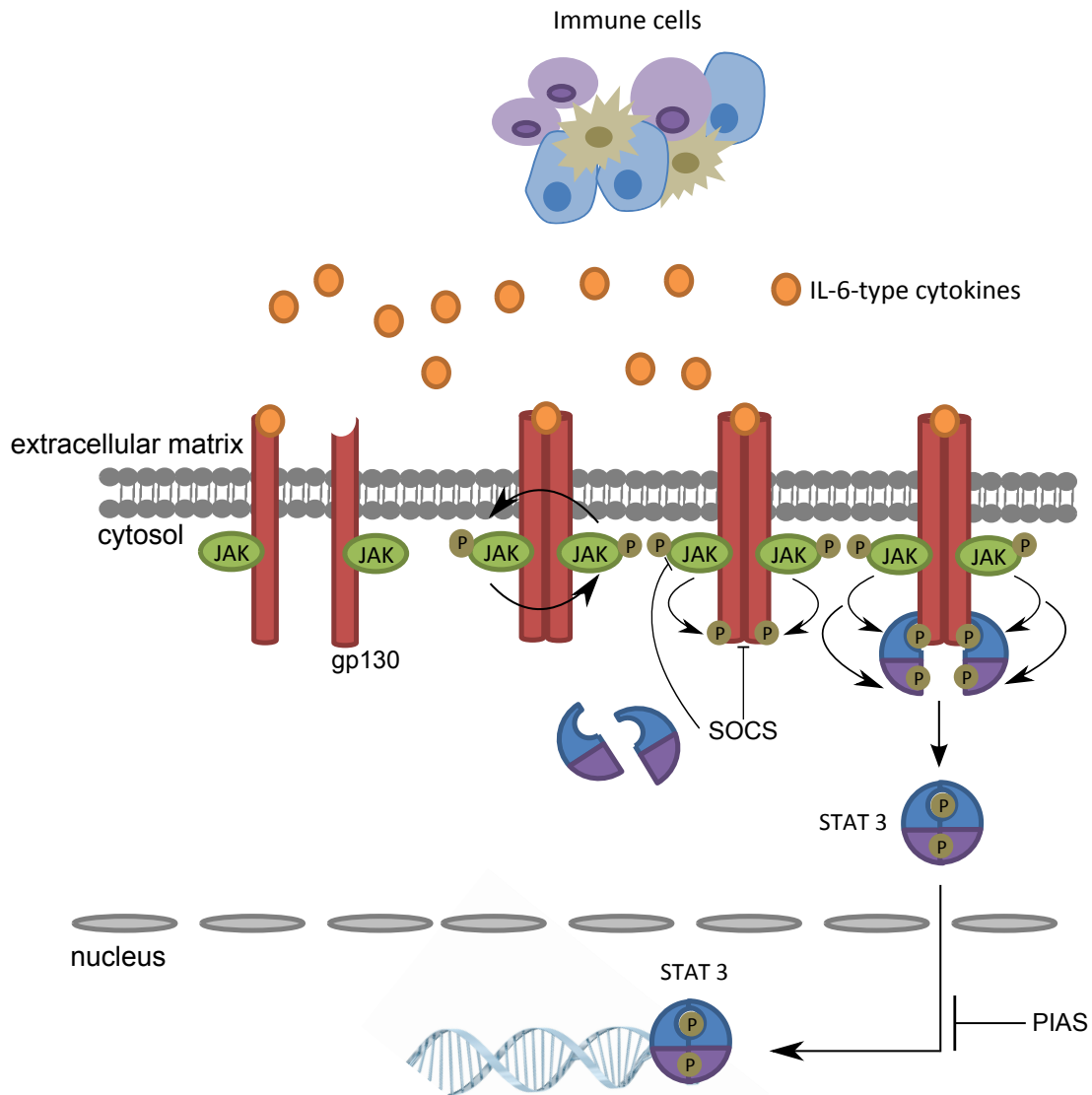
progression, an important role has been attributed to the signal transducer and activator of transcription 3 (STAT3) (reviewed in [Aravalli et al., 2008]) (Section 1.2).

## 1.2 The implication of STAT3 in cancer development

The transcription factor STAT3 is activated in 50-90% of primary human tumours and in numerous cancer cell lines [Garcia et al., 2001, Ma et al., 2004, Mora Linda et al., 2002, Xu et al., 2005]. Growing evidence indicates that STAT3-induced gene transcription plays a key role in inflammation-mediated tumorigenesis and inflammation-stimulated tumour progression [Bollrath et al., 2009, Catlett-Falcone et al., 1999, Grivennikov et al., 2009, Kortylewski et al., 2009, Kujawski et al., 2008, Mantovani et al., 2008]. Constitutive STAT3 activation results either from genetic alterations or extrinsic stimuli such as chemicals, carcinogens and infection [Arredondo et al., 2006, Bronte-Tinkew et al., 2009, Chan et al., 2004, Ernst et al., 2008, Gao et al., 2007, Gu et al., 2007, Olcaydu et al., 2009, Samavati et al., 2009, Sano et al., 2005, Spannauer and Trautwein, 2009]. Since STAT3 oncogenic mutations are rare in malignant liver cancer, it is most probable that growth factors and cytokines within the inflammatory microenvironment are responsible for aberrant STAT3 activation [He and Karin, 2011] (Section 1.3).

## 1.3 STAT3 activation by IL-6-type cytokines

STAT3-mediated transcription is commonly induced by cytokines, growth factors and carcinogens (reviewed in [Aggarwal et al., 2009]). Cytokines that activate STAT3 include the family of Interleukin-6 (IL-6)-type cytokines which is composed of IL-6, interleukin-11 (IL-11), leukaemia inhibitory factor (LIF), oncostatin M (OSM), ciliary neurotrophic factor (CNPF), cardiotrophin 1 (CT-1) and cardiotrophin-like cytokine (CLCF-1) (reviewed in [Heinrich et al., 1998]). IL-6-type cytokines initiate the Janus kinase (JAK)-STAT3 signalling cascade through ligand-induced membrane receptor homo- or heterodimerization (Figure 1.1). Dimeric IL-6-type cytokine receptors are composed of glycoprotein 130 (gp130) and a ligand specific subunit (reviewed in [Heinrich et al., 1998]) (Figure 1.1). IL-6 signals via a gp130 homodimer while CNPF, LIF and CT-1 recruit gp130-LIF receptor (LIFR) heterodimers and OSM requires gp130-LIFR or gp130-OSM receptor (OSMR) heterodimers [Davis et al., 1993, Gearing et al., 1992, Ichihara et al., 1997, Murakami et al., 1993, Pennica et al., 1995]. IL-11 signals via gp130-IL-11 receptor (IL11R) complexes [Robb et al., 1996]. Ligand-mediated receptor activation leads to the phosphorylation of receptor-associated JAKs (Figure 1.1). In turn, JAKs phosphorylate tyrosine residues on the cytoplasmic tail of the



| Survival  | Proliferation | Angiogenesis      | Inflammation | Cell Adhesion    |
|-----------|---------------|-------------------|--------------|------------------|
| BCL2L1    | MYC           | HIF-1             | IL6          | ICAM-1           |
| BCL2      | CCND1         | VEGF              | IL11         | TWIST1           |
| MCL1      | CCNB          | FGF2              | IL17         |                  |
| BIRC5     | CDC2          |                   | IL23         |                  |
| HSP 70/90 | JUN           | <b>Metastasis</b> | CXCL12       | <b>Signaling</b> |
|           | FOS           | MMP2              | IL10         | STAT3            |
|           | p21           | MMP9              | Cox2         | SOCS3            |
|           |               |                   |              | LIN28A           |

FIGURE 1.1: **IL-6-type cytokine-mediated JAK/STAT3 signalling.** Immune cells secrete IL-6-type cytokines which bind their surface receptors on target cells. As a consequence, the receptors homo- or heterodimerize which brings the JAKs bound to the receptor in close proximity and leads to their transphosphorylation. In turn, activated JAKs phosphorylate the cytosolic part of the receptor which leads to the docking and subsequent phosphorylation of STAT3. Phosphorylated STAT3 molecules dimerize and translocate to the nucleus where they act as transcriptional regulators. A subset of STAT3 target genes and their respective functions are listed (adapted from [Yu et al., 2009]). JAK-STAT3 signalling is negatively regulated by SOCS and PIAS which respectively interfere with signal transduction and transcriptional activity of STAT3. **JAK** Janus kinase, **STAT3** signal transducer and activator of transcription 3, **SOCS** suppressor of cytokine signaling, **PIAS** protein inhibitor of activated STAT.

receptor and thereby recruit STAT3. Consequently, STAT3 is phosphorylated and thereby activated [Hemmann et al., 1996, Stahl et al., 1995]. Phosphorylated STAT3 molecules dimerize and translocate to the nucleus where they regulate the expression of genes involved in cellular survival, proliferation, invasion, angiogenesis and metastasis (reviewed in [Aggarwal et al., 2009, Frank, 2007]) (Figure 1.1). Canonical IL-6-type cytokine signalling occurs via STAT3, however, in parallel other signalling cascades such as the mitogen-activated protein kinase (MAPK) pathway and the phosphatidylinositide 3-kinase (PI3K)/protein kinase B (PKB)/mechanistic target of rapamycin (mTOR) pathways are also induced (reviewed in [Dey et al., 2013, Hermanns, 2015]).

STAT3 signalling is tightly regulated by protein tyrosine phosphatases (PTPs), the protein inhibitor of activated STAT (PIAS) and the suppressor of cytokine signalling (SOCS) (reviewed in [Shuai and Liu, 2003] (Figure 1.1). PTPs carry out tyrosine dephosphorylations within the components of the JAK/STAT3 signalling pathway and thereby regulate its activity (reviewed in [Yang et al., 2004]. SOCS binds JAKs and the cytokine receptor and compete with STAT signalling while PIAS interferes with the capacity of STAT to bind DNA (reviewed in [Carow and Rottenberg, 2014, Shuai and Liu, 2005]). In addition, cytokine signalling is inhibited by receptor internalization [Wang and Fuller, 1994].

### 1.3.1 The IL-6-type cytokine Oncostatin M

Activated monocytes and macrophages are the primary source of OSM *in vivo*: it is released upon stimulation with Toll-like-receptor ligands or prostaglandins while T-cells and dendritic cells also secrete OSM [Ganesh et al., 2012, Zarling et al., 1986]. OSM primarily activates STAT3 signalling and in parallel induces PI3K, STAT1, extracellular signal-regulated kinase (ERK) and Jun amino-terminal kinase (JNK) pathways [Faris et al., 1996]. In the liver, Kupfer cells secrete OSM along with other IL-6-type cytokines and thereby initiate the secretion of acute phase proteins which are part of the innate non-specific immune response [Richards et al., 1992]. Furthermore, OSM regulates fetal liver development, liver regeneration, hepatic cell differentiation and hematopoiesis [Kamiya et al., 1999, Miyajima et al., 2000, Nakamura et al., 2004].

OSM was considered as an anticancer drug because it inhibits the proliferation of various cancer cell lines including melanoma, glioma, hepatoma, neuroblastoma, lung and breast cancer [Halfter et al., 1998, Horn et al., 1990, Klausen et al., 2000, Zarling et al., 1986]. However, preclinical studies were not completed, most probably due to OSM-induced side effects [Richards, 2013]. Moreover, the effects of OSM on proliferation are pleiotropic, while it inhibits growth in some cell lines it stimulates proliferation in others such as in Kaposi's

sarcoma cells [Nair et al., 1992].

## 1.4 The implication of STAT3 in HCC

Aberrant STAT3 activation occurs in 60% of HCCs and is associated with aggressive cancer and a poor prognosis [Calvisi et al., 2006, He et al., 2010]. Although it is clear that constitutive STAT3 activation is involved in HCC, the exact mechanisms remain to be elucidated. 60% of benign liver adenomas harbour small in-frame deletions within the gp130 subunit of the IL-6-type cytokine receptor that lead to constitutive STAT3 activation. HCC, however, only develops when the gp130 deletion is combined with an activating mutation in  $\beta$ -catenin [Spannbauer and Trautwein, 2009]. Since STAT3 oncogenic mutations are rare in HCC, it is most probable that growth factors and cytokines within the inflammatory microenvironment are responsible for STAT3 activation [He and Karin, 2011].

Pro-inflammatory cytokines, such as IL-6 and OSM, can establish a pro-carcinogenic microenvironment by activating STAT3 [Mantovani et al., 2008]. Indeed, cirrhotic liver tissue contains high levels of OSM while high IL-6 concentrations in serum promote the development of hepatocellular carcinoma in patients with hepatitis B [Wong et al., 2009, Znoyko et al., 2005]. Moreover, patients with HCC have increased IL-6 and OSM serum levels [Gianitrapani et al., 2006, Liang et al., 2012]. According to data from the *Human Proteome Atlas*, OSM is not present in healthy liver tissue, while moderate levels are detected in HCC tissue slices [Uhlén et al., 2015]. Mouse models also point towards STAT3 and IL-6 as important mediators in HCC development. In mice, HCC can be induced by diethylnitrosamine (DEN). DEN-induced HCC is characterized by IL-6-mediated persistent STAT3 activation [Naugler et al., 2007]. However, when HCC is induced by DEN in STAT3 deficient mice, less mice developed the disease and tumours are generally smaller [He et al., 2010]. Interestingly, DEN-induced liver damage can be dampened by OSM [Hamada et al., 2007]. Furthermore, inhibition of STAT3 in HCC cells impairs cell proliferation and induces apoptosis *in vitro* and in xenograft models [Sun et al., 2008].

Cellular transformation is a multi-step process that drives progressive malignant transformation described as hallmarks of cancer. These hallmarks include sustained proliferative signalling, the evasion of growth suppressors, resistance to cell death, replicative immortality, induction of angiogenesis, activation of invasion and metastasis, evading immune destruction and reprogramming of energy metabolism [Hanahan and Weinberg, 2000, 2011]. The effect of STAT3 on most hallmarks of cancer has been intensively studied over the last years, however little is known so far about STAT3-mediated effects on cellular metabolism.

## 1.5 The metabolic effects of STAT3

STAT3 regulates the expression of genes that are involved in cellular metabolism. STAT3 suppresses gluconeogenesis by blocking the transcription of phosphoenolpyruvate carboxykinase 1 (PEPCK) and the catalytic subunit of glucose-6-phosphatase (G6PC) [Inoue et al., 2004, Ramadoss et al., 2009]. Furthermore, STAT3 upregulates miR-23a which targets G6PC and thereby further reduces gluconeogenic rates [Bo Wang, Shuhao Hsu, Wendy Frankel and Jacob, 2013]. While STAT3 downregulates gluconeogenesis it enhances glycolysis by up-regulating hexokinase 2 (HK2) and phosphofructokinase 1 (PFK-1) [Ando et al., 2010]. Apart from its impact on glycolysis, STAT3 also interferes with mitochondrial respiration. While transcriptionally active STAT3 is phosphorylated on tyrosine 705, mitochondrial STAT3 is phosphorylated on serine 727 and regulates the activity of complexes I and II within the electron transport chain [Wegrzyn et al., 2009]. Mitochondrial STAT3 is furthermore thought to support oncogenic transformation and promote cancer growth [Gough et al., 2009, Zhang et al., 2013].

Little is known about the effects of OSM on cellular metabolism. OSM was described to up-regulate the expression of the low density lipoprotein receptor (LDLR) in the liver, suggesting its potential involvement in cholesterol metabolism [Grove et al., 1991]. Another study describes the involvement of OSM in the regulation of fatty acid metabolism [Zhou et al., 2007]. OSM stimulation in HepG2 HCC cells results in the upregulation of acyl-CoA synthase long-chain family (ACSL) members 3 and 5 and thereby stimulates  $\beta$ -oxidation [Zhou et al., 2007]. However, the effect of OSM on fatty acid metabolism was mediated by OSM-induced ERK and not STAT3 signalling [Zhou et al., 2007].

Recent studies have revealed an interesting crosstalk between STAT3 and the metabolic key regulator hypoxia-inducible factor 1- $\alpha$  (HIF-1 $\alpha$ ) and indicate that IL-6-type cytokines might have unforeseen roles in the regulation of cellular metabolism (Section 1.6.2.1)

## 1.6 Hypoxia-inducible factor 1- $\alpha$

HIF-1 is a basic loop-helix-loop transcription factor that regulates the expression of hundreds of genes, many of which code for metabolic enzymes that play key roles in the adaptation of cellular metabolism to low oxygen tension (Figure 1.2)[Allen et al., 2006, Chi et al., 2006, Vengellur et al., 2003, Wang et al., 1995]. It is composed of  $\alpha$  and  $\beta$  subunits that regulate the transcription of genes containing the hypoxia response consensus sequences 5'-RCGTG-3' [Wenger et al., 2005]. The HIF- $\alpha$  subunit has three different isoforms: HIF-1 $\alpha$  [Semenza and Wang, 1992], HIF-2 $\alpha$  [Ema et al., 1997] and HIF-3 $\alpha$  [Gu et al., 1998]. The HIF- $\beta$  subunit exists as two isoforms: HIF-1 $\beta$  and HIF-2 $\beta$ . The best studied complex and the most relevant

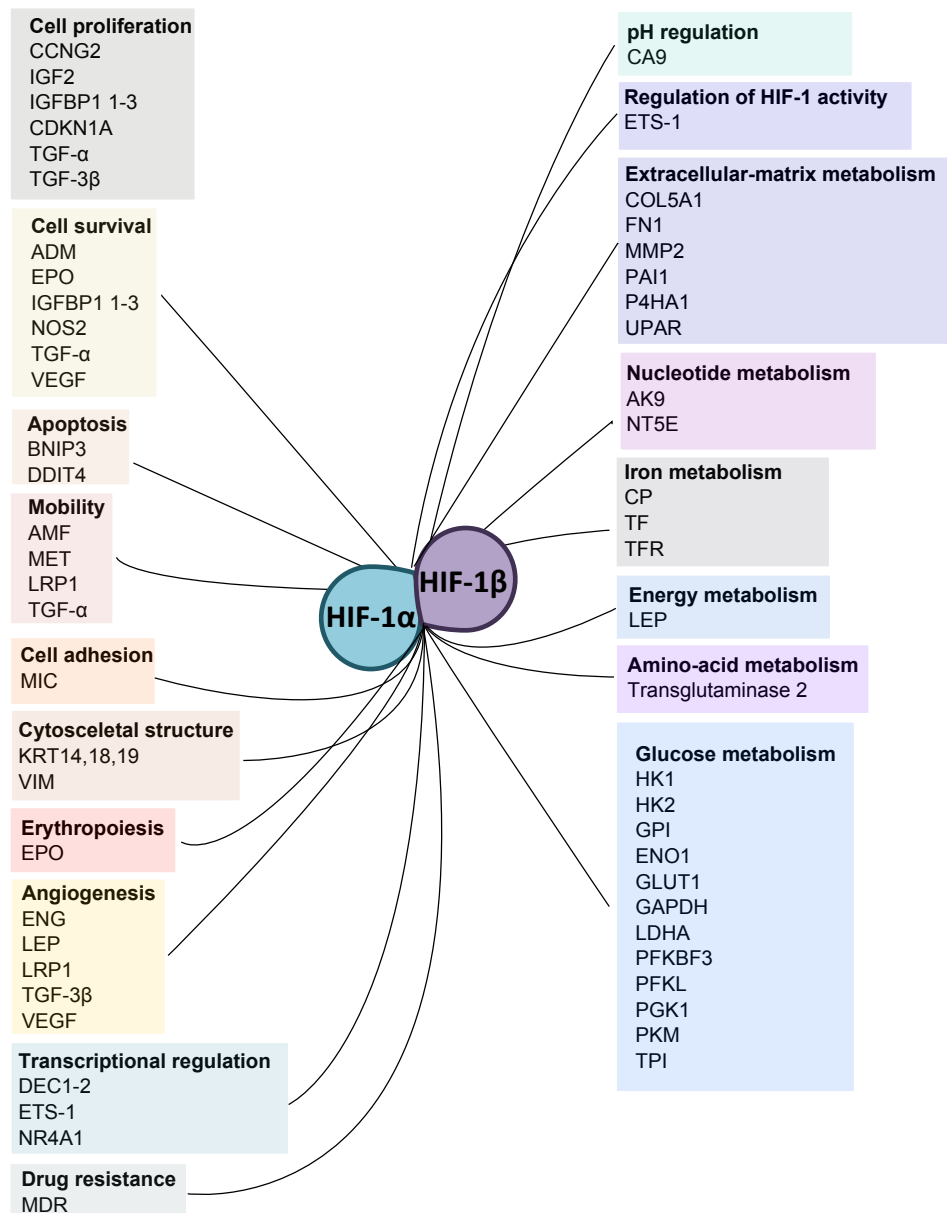


FIGURE 1.2: **HIF-1 target genes.** HIF-1 regulates to the expression of hundreds of target genes and thereby regulates various cellular processes. A subset of HIF-1 target genes is shown. **ADM** adrenomedullin, **AK9** adenylate kinase 9, **AMF** autocrine motility factor, **BNIP3** BCL2/adenovirus E1B 19kDa interacting protein 3, **CA9** carbonic anhydrase IX, **CDKN1A** cyclin-dependent kinase inhibitor 1A, **COL5A1** collagen, type V, alpha 1, **CP** ceruloplasmin, **DDIT4** DNA-damage-inducible transcript 4, **DEC** deleted in oesophageal cancer, **ENG** endoglin, **ENO1** enolase 1, **EPO** erythropoietin, **ETS-1** E26 transformation-specific 1, **FN1** fibronectin 1, **GAPDH** glyceraldehyde-3-phosphate dehydrogenase, **GLUT1** glucose transporter 1, **GPI** glucose-6-phosphate isomerase, **HK1** hexokinase 1, **HK2** hexokinase 2, **IGF2** insulin-like growth factor 2, **IGFBP1** insulin-like growth factor binding protein 1, **KRT** keratin, **LDHA** lactate dehydrogenase A, **LEP** leptin, **LRP1** low density lipoprotein receptor-related protein 1, **MDR** multi-drug resistant, **MET** MET proto-oncogene, receptor tyrosine kinase, **MIC2** CD99 molecule, **MMP2** matrix metalloproteinase 2, **NOS2** nitric oxide synthase 2, **NR4A1** nuclear receptor subfamily 4, group A, member 1, **NT5E** 5'-nucleotidase, ecto, **P4HA1** prolyl 4-hydroxylase, alpha polypeptide I, **PAI1** serpin peptidase inhibitor member 1, **PFKFB3** 6-phosphofructo-2-kinase/fructose-2,6-biphosphatase 3, **PFKL** phosphofructokinase, liver, **PGK1** phosphoglycerate kinase 1, **PKM** pyruvate kinase muscle isozyme, **TF** transferrin, **TFRC** transferrin receptor, **TGF** transforming growth factor, **TGM2** transglutaminase 2, **TPI** triosephosphate isomerase, **UPAR** urokinase plasminogen activator receptor, **VEGF** vascular endothelial growth factor A, **VIM** vimentin (adapted from [Semenza, 2003]).



to this work is HIF-1, composed of a HIF-1 $\alpha$  and a HIF-1 $\beta$  subunit.

HIF-1 activation contributes to a wide range of human cancers, where HIF-1 expression correlates with increased tumour aggressiveness, therapeutic resistance and mortality (reviewed in [Brahimi-Horn and Pouyssegur, 2004, Quintero et al., 2004, Semenza, 2003]). HIF-1 regulates angiogenesis, stem cell maintenance, metabolic reprogramming, autocrine growth factor signalling, epithelial to mesenchymal transition, invasion, metastasis and resistance to radiation and chemotherapy (reviewed in [Semenza, 2003, 2012, Sturek, 2011]).

### 1.6.1 Oxygen-dependent HIF-1 $\alpha$ induction

HIF-1 was first purified in 1995 and found to upregulate erythropoietin (EPO) production in response to low oxygen tension [Wang et al., 1995, Wang and Semenza, 1995]. The stability of the HIF-1 $\alpha$  subunit is tightly regulated by oxygen availability, while the HIF-1 $\beta$  subunit is continuously expressed. Under normoxia, the HIF-1 $\alpha$  protein has a half-life of only 5 minutes as it undergoes oxygen-dependent degradation via the ubiquitin-proteasome pathway [Huang et al., 1998, Moroz et al., 2009]. In the presence of oxygen, prolyl hydroxylase dioxygenases (PHDs) catalyse the hydroxylation of HIF-1 $\alpha$  on two proline residues (Pro402 and Pro564) (Figure 1.3) [Bruick and Mcknight, 2001, Epstein et al., 2001, Ivan et al., 2001, Jaakkola et al., 2001]. Mammalian cells express 4 PHD isoforms, out of which, PHD1, PHD2 and PHD3 hydroxylate the HIF $\alpha$  subunit (reviewed in [Fong and Takeda, 2008]). PHD2 has a higher affinity for HIF-1 $\alpha$  while PHD1 and PHD3 more efficiently hydroxylate HIF-2 $\alpha$  (reviewed in [Appelhoff et al., 2004]). Upon proline hydroxylation, HIF-1 $\alpha$  binds to the von Hippel-Lindau (VHL) tumour suppressor which is complexed to elongin B and C. VHL acts as an E3 ubiquitin ligase which adds ubiquitin residues to HIF-1 $\alpha$  and thereby tags it for proteasomal degradation (Figure 1.3) [Cockman et al., 2000, Maxwell et al., 1999, Stickle et al., 2004].

A second level of HIF-1 $\alpha$  regulation is managed by the factor inhibiting HIF (FIH). FIH hydroxylates HIF-1 $\alpha$  on an asparaginyl residue (Asp803) located within the carboxy-terminal transactivation domain (Figure 1.3). Thereby FIH prevents protein-protein interactions between the HIF-1 $\alpha$  transactivation domain and transcriptional co-regulators such as p300 and the CREB binding protein (CBP) (Figure 1.3) [Masson et al., 2012, Stolze et al., 2004]. Both PHDs and FIH are members of the iron- and  $\alpha$ -ketoglutarate-dependent family of dioxygenases, using oxygen to hydroxylate their substrates and, in parallel, oxidize and decarboxylate  $\alpha$ -ketoglutarate to succinate [Schofield and Zhang, 1999]. The Arrest-defective protein 1 (ARD1) acetylates HIF-1 $\alpha$  on lysine 532 and thereby enhances the interaction with VHL and thus supports HIF-1 $\alpha$  degradation [Jeong et al., 2002] (Figure 1.3).

Under hypoxic conditions, PHDs and FIH are inhibited by the lack of oxygen leading to HIF-1 $\alpha$  stabilization in the cytoplasm, dimerization with HIF-1 $\beta$  and translocation to the nucleus

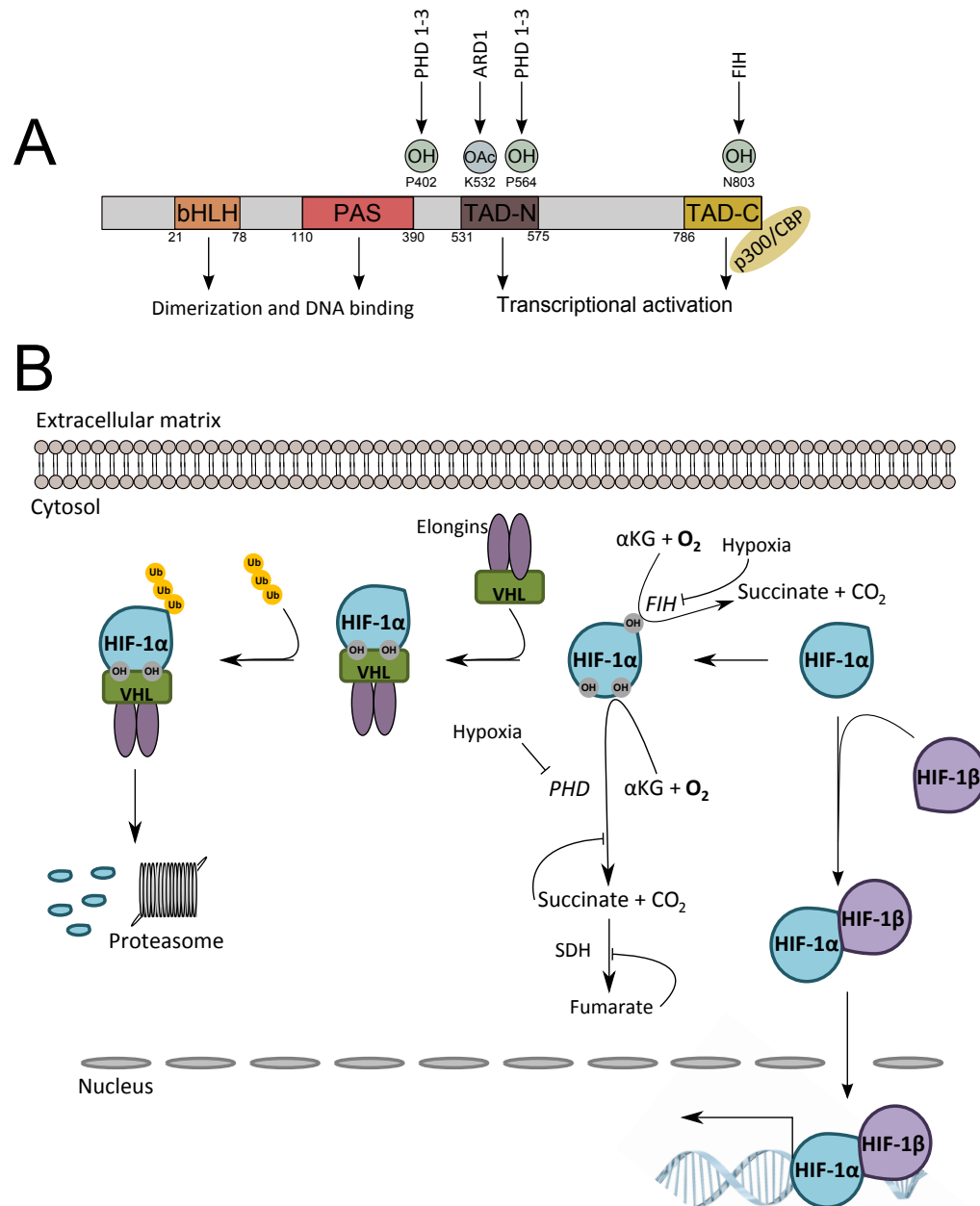


**FIGURE 1.3: Mechanisms of HIF-1 $\alpha$  stabilization.** (A) HIF-1 $\alpha$  is composed of 4 domains. The basic helix-loop-helix (**bHLH**) and the Per-Arnt-Sim (**PAS**) are involved in complex dimerization and DNA binding. The N- and C-terminal transactivation domains (**TAD-N**, **TAD-C**) regulate the transcriptional activity of HIF-1 $\alpha$ . O<sub>2</sub>-dependent HIF-1 $\alpha$  hydroxylation is regulated by PHDs (proline 402 and 564) and by FIH (asparagine 803). FIH-mediated hydroxylation prevents the interaction between HIF-1 $\alpha$  and transcriptional co-regulators p300 and CBP. ARD1 acetylates HIF-1 $\alpha$  on lysine 532 within the TAD-N domain and enhances the interaction with VHL and thus HIF-1 $\alpha$  degradation (adapted from [Semenza, 2012]). (B) Under normoxic conditions, PDHs and FIH catalyze HIF-1 $\alpha$  hydroxylation. Hydroxylation on prolines 402 and 564 lead to the binding of VHL and subsequent proteasomal degradation. PHDs can be inhibited by the TCA cycle intermediates fumarate and succinate and HIF-1 $\alpha$  can be stabilized. Low oxygen tension or high levels of succinate and fumarate result in HIF-1 $\alpha$  stabilization, dimerization with HIF- $\beta$  and translocation to the nucleus. **PHD** Prolyl hydroxylase, **SDH** succinate dehydrogenase,  **$\alpha$ -KG**  $\alpha$ -ketoglutarate, **VHL** von Hippel Lindau

where the assembled HIF-1 regulates the expression of numerous genetic targets [Jiang et al., 1996, Mole et al., 2009, Ortiz-Barahona et al., 2010, Semenza et al., 1994, Wang and Semenza, 1995, Xia et al., 2009] (Figure 1.2, 1.3). Another mode of PHD inactivation under hypoxia might be mediated by ROS generated by the mitochondria under oxygen limitation [Brunelle et al., 2005, Guzy et al., 2005, Mansfield et al., 2005].

## 1.6.2 Oxygen-independent HIF-1 $\alpha$ induction

HIF-1 $\alpha$  induction under normoxic conditions either results from genetic alterations or cytokine and growth factor signalling.

The tumor suppressor VHL is involved in the degradation process of HIF-1 $\alpha$  under normoxic conditions (Figure 1.3). Loss of expression or mutations in its binding domain lead to low-affinity interactions with HIF-1 $\alpha$  which consequently is stabilized [Clifford et al., 2001, Krieg et al., 2000]. Mutations within fumarate hydratase (FH) and succinate dehydrogenase (SDH) lead to accumulation of succinate and fumarate which consequently inhibit PHD-mediated HIF-1 $\alpha$  prolyl-hydroxylation. [Hewitson et al., 2007, Isaacs et al., 2005, Pollard et al., 2007, Selak et al., 2005] (Figure 1.3).

HIF-1 $\alpha$  expression can be induced by a variety of cytokines and growth factors (epidermal growth factor (EGF), fibroblast growth factor 2 (FGF2), hepatocyte growth factor (HGF), insulin-like growth factor 1 and 2 (IGF), interleukin-1 $\beta$  (IL-1 $\beta$ ), insulin, prostaglandin E2, transforming growth factor  $\alpha$  (TGF- $\alpha$ ), TGF- $\beta$ , thrombin, and tumor necrosis factor  $\alpha$  (TNF- $\alpha$ )) via MAPK and PI3K signal transduction pathways [Fukuda et al., 2002, Laughner et al., 2001, Treins et al., 2002].

In addition, STAT3 was shown to actively regulate HIF-1 $\alpha$  expression (Section 1.6.2.1).

### 1.6.2.1 Interactions between STAT3 and HIF-1 $\alpha$

Drastic evidence suggests that also STAT3-dependent signalling interferes with HIF-1 $\alpha$ . HIF-1 $\alpha$  is a direct STAT3 target gene [Vollmer et al., 2009] and IL-6-type cytokines (OSM, IL-6, IL-1 $\beta$ , TNF- $\alpha$ ) upregulate HIF-1 $\alpha$  which translates into increased HIF-1 $\alpha$  protein levels even under normoxic conditions in HCC cells and immortalized hepatocytes [Vollmer et al., 2009]. Among all IL-6-type cytokines, OSM induces the strongest HIF-1 $\alpha$  expression, which is the reason why we studied its role in this work. OSM-induced HIF-1 $\alpha$  is an active transcription factor that upregulates reporter genes and the endogenous target genes VEGF and serpin peptidase inhibitor member 1 (PAI) [Vollmer et al., 2009]. In contrast to hypoxia,

OSM-induced HIF-1 $\alpha$  is solely dependent on STAT3-mediated upregulation and not on mechanisms that interfere with HIF-1 $\alpha$  stability [Vollmer et al., 2009].

Demaria et al. showed that constitutive STAT3 activation in mouse embryonic fibroblasts (MEFs) induces HIF-1 $\alpha$  under normoxic conditions. In turn, HIF-1 $\alpha$  upregulates glycolytic genes and induces aerobic glycolysis [Demaria et al., 2012]. In response to constitutive STAT3 activation, complex IV and V within the electron transfer chain were downregulated, however in a HIF-1 $\alpha$  independent fashion [Demaria et al., 2010]. In further work, Demaria et al. show that constitutive STAT3 expression can serve as a first hit in carcinogenesis where STAT3-mediated HIF-1 $\alpha$  induction supports cellular proliferation by inducing high glycolytic rates [Demaria et al., 2012].

Furthermore, STAT3 is not only required for cytokine-induced HIF-1 $\alpha$  activity but is also essential for basal HIF-1 $\alpha$  expression under normoxia and under hypoxia [Niu et al., 2008, Xu et al., 2005]. In addition, STAT3 and HIF-1 $\alpha$  can interact on protein level, where STAT3 binds the C-terminal domain of HIF-1 $\alpha$  and thereby stabilizes it [Jung et al., 2008, Niu et al., 2008]. STAT3 and HIF-1 $\alpha$  cooperatively act on gene transcription. STAT3 binds to HIF-1 target gene promoters where it interacts with HIF-1 $\alpha$  and helps to recruit transcriptional co-activators such as CBP, p300 and RNA polymerase II [Jung et al., 2005, Pawlus et al., 2014a].

### 1.6.3 The transcriptional and metabolic consequences of HIF-1 $\alpha$ stabilization under hypoxia

The transcription factor HIF-1 regulates the expression of a large variety of genes (Figure 1.2). Mole et al. have performed genome-wide chromatin immunoprecipitation (ChIP) of HIF-1 and correlated their results with transcript profiling. They identified 546 HIF-1 $\alpha$  binding sites in the genome that mapped 394 different gene loci in MCF-7 cells [Mole et al., 2009]. Xia et al. also identified several hundred direct HIF-1 target genes in HepG2 cells and described a high enrichment of genes that facilitate the metabolic adaptation to hypoxia [Xia et al., 2009]. Ortiz-Barahona et al. have combined phylogenetic footprinting with transcription profiling meta-analysis to identify HIF-1 target genes. In this work over 200 high confidence HIF-1 target genes are identified [Ortiz-Barahona et al., 2010]. Further investigations by Schödel et al. using high-resolution genome-wide mapping of HIF-1 binding sites lead to the identification of high-confidence binding sites [Schoedel et al., 2011]. Apart from direct gene regulation, HIF-1 also regulates microRNAs and chromatin modifying enzymes [Crosby et al., 2009, Wu et al., 2011, Xia et al., 2009].

HIF-1 targets a large group of genes that code for metabolic genes which play key roles in the adaptation of cellular metabolism to low oxygen tension [Allen et al., 2006, Chi et al.,

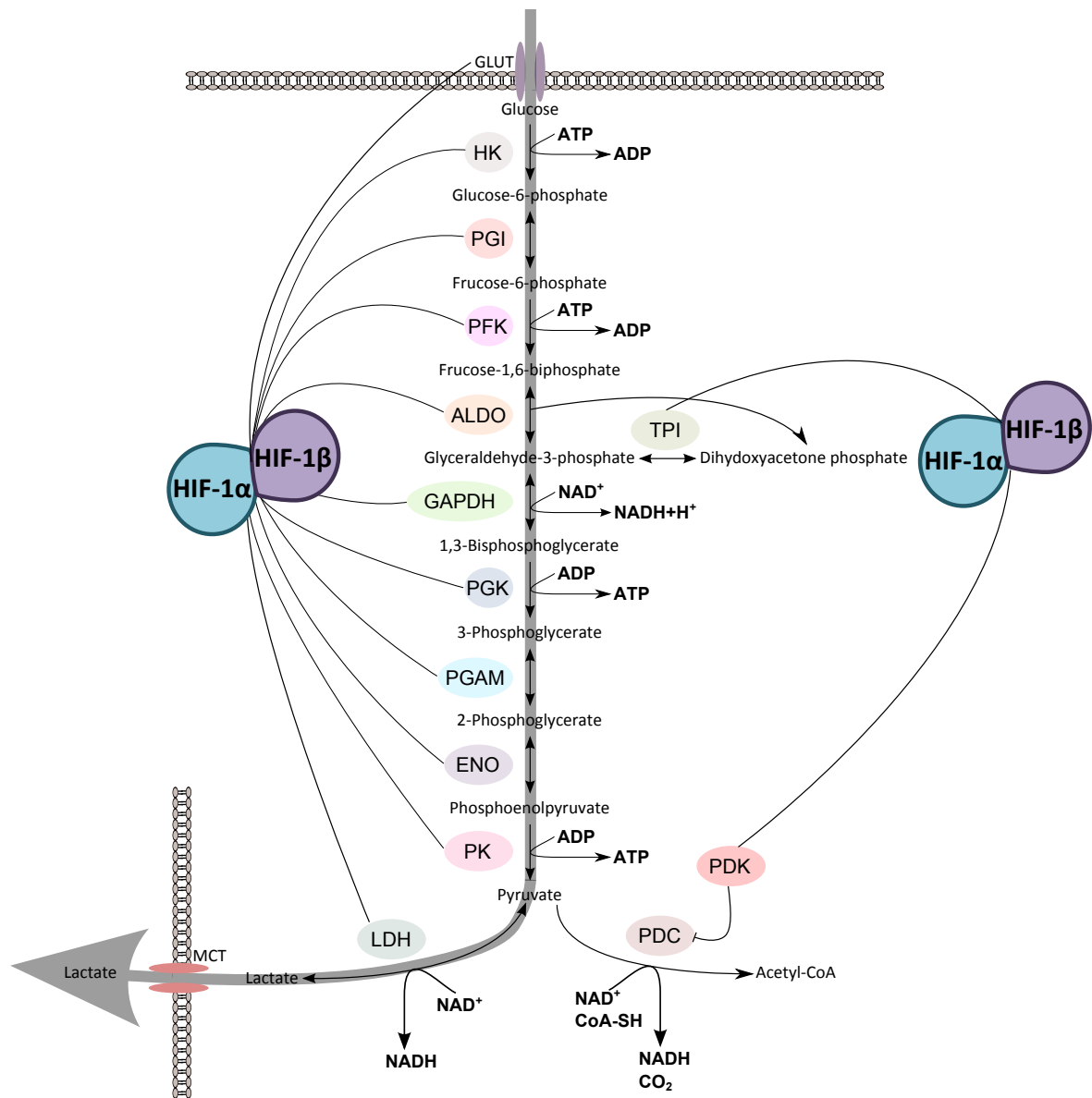


FIGURE 1.4: **The effects of HIF-1 $\alpha$  on glycolysis.** A large functional group of HIF-1 $\alpha$  regulated genes consist of glycolytic enzymes and metabolite transporters. HIF-1 $\alpha$  up-regulates the expression of glucose transporters ((GLUT) and thereby glucose uptake is increased. HIF-1 $\alpha$  induces the expression of all glycolytic genes and thereby enhances the breakdown of glucose to pyruvate. By upregulating the expression of lactate dehydrogenase (LDH) and pyruvate dehydrogenase kinase 1 (PDK1), the conversion of pyruvate to lactate is enhanced and the entry of pyruvate into the TCA cycle inhibited. **HK** hexokinase, **PGI** glucosephosphate isomerase, **PFK** phosphofructo kinase, **ALDO** aldolase, **TPI** triosephosphate isomerase, **GAPDH** glyceraldehyde-3-phosphate dehydrogenase, **PGK** phosphoglycerate kinase, **PGAM** phosphoglycerate mutase, **ENO** enolase, **PK** pyruvate kinase, **PDC** pyruvate dehydrogenase complex, **MCT** monocarboxylate transporter, **ATP** adenosine 5'-triphosphate, **ADP** adenosine diphosphate, **NAD** nicotinamide adenine dinucleotide, **NADH** reduced nicotinamide adenine dinucleotide.

2006, Vengellur et al., 2003]. HIF-1 $\alpha$  activation under hypoxic conditions serves two main metabolic purposes: the stimulation of energy production via glycolysis and the downregulation of mitochondrial respiration.

HIF-1 upregulates the expression of the glucose transporters 1 and 3 (GLUT1, GLUT3) and thereby increases cellular glucose uptake (Figure 1.4) [Maxwell et al., 1997, Wang et al., 2001]. Furthermore, HIF-1 upregulates all enzymes that concordantly break down glucose into pyruvate (Figure 1.4) [Iyer et al., 1998, Seagroves et al., 2001, Semenza et al., 1994]. Glycolytic rates are largely regulated by substrate and product availabilities where increased glucose availability leads to increased glucose breakdown.

Under normoxic conditions, pyruvate enters the mitochondria while reduced nicotinamide adenine dinucleotide (NADH) is shuttle through the malate-aspartate or 3-phosphoglycerate shuttle into the mitochondria. Pyruvate is converted to acetyl-coA by the pyruvate dehydrogenase complex (PDC) and further oxidized to generate NADH and reduced flavin adenine dinucleotide (FADH<sub>2</sub>), both of which finally donate electrons to the electron transfer chain. The electrons are then transferred to molecular oxygen to generate water and a proton gradient that serves the generation of adenosine 5'-triphosphate (ATP). Under hypoxia, however, mitochondria cannot function properly due to a lack of oxygen and therefore NADH and pyruvate accumulate. HIF-1 upregulates the expression of lactate dehydrogenase (LDH) that converts pyruvate and NADH into lactate and NAD<sup>+</sup> (Figure 1.4). The resulting lactate can then be secreted from the cells via the HIF-1 induced monocarboxylate transporter 4 (MCT4) [Firth et al., 1995]. This mechanism removes the excess of lactate from the cell and regenerates NAD<sup>+</sup> which is required for further glycolytic activities (Figure 1.4).

Furthermore, HIF-1 $\alpha$  prevents the entry of pyruvate into the tricarboxylic acid (TCA) cycle and thereby reduces cellular respiration. HIF-1 $\alpha$  upregulates pyruvate dehydrogenase kinase 1 (PDK1) which phosphorylates and thereby inactivates PDC and thus prevents the decarboxylation of pyruvate to acetyl-coA (Figure 1.4). PDC inactivation reduces cellular oxygen consumption and decreases ROS generation [Kim et al., 2006, Papandreou et al., 2006, Roche et al., 2001].

Under hypoxia, the deviation of the glycolytic flux towards lactate production results in a depleted mitochondrial citrate pool. Citrate, however, is an indispensable precursor for fatty acid synthesis. Under hypoxic conditions, cells use glutamine to replenish the intracellular citrate pool and thereby sustain fatty acid synthesis (Figure 1.5). In cells, where HIF-1 is stabilized, the vast majority of citrate is generated using reductive glutamine metabolism [Metallo et al., 2011, Wise et al., 2011]. For this type of metabolism, glutamine is converted to  $\alpha$ -ketoglutarate which is carboxylated to isocitrate by isocitrate dehydrogenase 2 (IDH) and then converted to citrate (Figure 1.5) [Des Rosiers et al., 1995, Metallo et al., 2011,

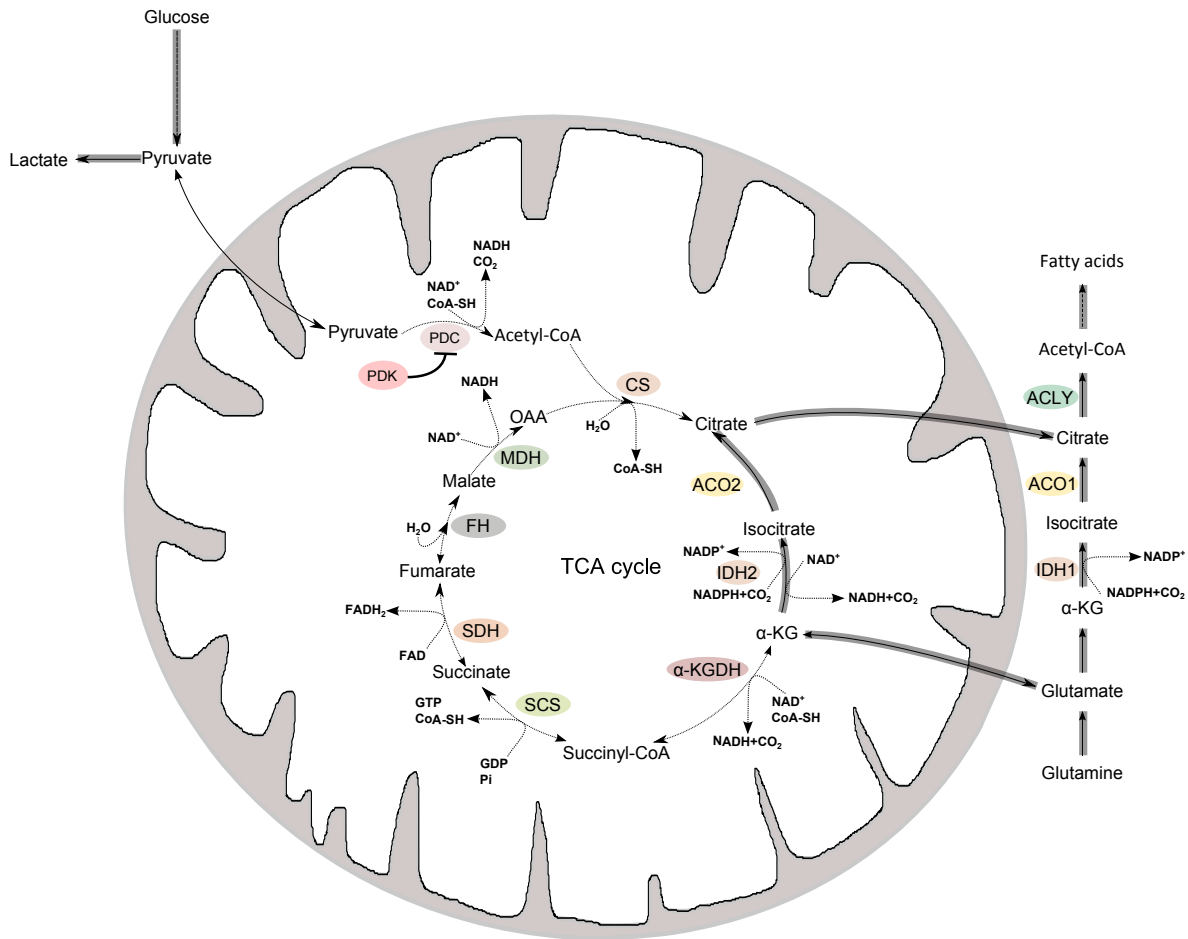


FIGURE 1.5: **The effects of HIF-1 $\alpha$  on the TCA cycle.** HIF-1 $\alpha$  induction results in reduced mitochondrial respiration. HIF-1 $\alpha$  upregulates PDK1 which in turn phosphorylates and thereby inactivates PDC, the enzyme that regulates the entry of pyruvate into the TCA cycle. Under hypoxia, reduced carbon entry into the TCA cycle results in drastically decreased citrate levels. Citrate consist in an important precursor for fatty acid synthesis. Glutamine-derived carbon serves to replenish the mitochondrial citrate pool under hypoxic conditions. **PDK** Pyruvate dehydrogenase kinase, **PDC** Pyruvate dehydrogenase complex, **CS** Citrate snythase, **ACO** Aconitase, **IDH** Isocitrate dehydrogenase,  **$\alpha$ -KGDH**  $\alpha$ -Ketoglutarate dehydrogenase, **SCS** Succinate synthase, **SDH** Succinate dehydrogenase, **FH** Fumarate hydratase, **MDH** Malate dehydrogenase.

Yoo et al., 2008]. Glutamine-derived citrate can then serve as carbon source for fatty acid synthesis and thereby ensure cellular proliferation under hypoxic condition [Gameiro et al., 2013, Metallo et al., 2011]. A study has recently identified a mechanism by which HIF-1 actively participates in the shift from oxidative to reductive glutamine metabolism [Sun and Denko, 2014]. They show that HIF-1 activation results in a drastically reduced activity of  $\alpha$ -ketoglutarate dehydrogenase ( $\alpha$ -KGDH) [Sun and Denko, 2014]. HIF-1 seems to induce ubiquitinylation and subsequent proteolysis of the E1 subunit of  $\alpha$ -KGDH and thereby inactivating this enzyme [Sun and Denko, 2014]. Increased  $\alpha$ -ketoglutarate to citrate ratios under hypoxia trigger reductive glutamine metabolism by mass action [Fendt et al., 2013].

## 1.7 The metabolism of proliferating cells

Proliferating cells largely depend on a glycolytic metabolism even under normoxic conditions and in absence of HIF-1 activation. In the 1920s, Otto Warburg discovered that cancer cells consume higher amounts of glucose and secrete more lactate when compared to normal cells. This phenomena is known as the "Warburg effect" or "aerobic glycolysis". Aerobic glycolysis describes the fact that cancer cells have high glycolytic rates and secrete most of the glucose derived-carbon as lactate despite the fact that oxygen is present and oxidative phosphorylation would be an option (Figure 1.6) [Warburg, 1928, 1956]. In normal tissues approximately 10% of the ATP is generated by glycolysis while 90% of the ATP is generated via oxidative phosphorylation within the mitochondria (Figure 1.6). In tumour sections, however, 50% of the cellular energy is produced by glycolysis with the remaining being generated by oxidative phosphorylation [Warburg, 1956]. This is one of the reasons why Otto Warburg hypothesized that cancer cells harbour defects in their mitochondrial metabolism which are compensated by aerobic glycolysis [Warburg, 1956]. Later, it was discovered that not only cancer cells but proliferating cells in general depend on aerobic glycolysis (Figure 1.6). In proliferating lymphocytes, for example, about 90% of glucose-derived carbon is converted to lactate [Wang et al., 1976]. Numerous cancer cell lines have now been investigated in detail and no defects within oxidative phosphorylation were identified (reviewed in [Moreno-Sánchez et al., 2007]). This observation shows that aerobic glycolysis is not a result of a defective mitochondrial metabolism but a metabolic feature of proliferating cells [Brand et al., 1992, Fabiano and Qiu, 2015, Hedekov, 1968, Wang et al., 1976]. In rare cases, however, mutations in the TCA cycle enzymes SDH and FH indeed can lead to severe metabolic consequences and tumour development. Mutations in SDH lead to the development of familial paraganglioma and can cause pheochromocytoma [Astuti et al., 2001, Baysal, 2000, Niemann and Müller, 2000] while mutations in FH lead to papillary renal cancer [Tomlinson et al., 2002].

## 1.8 The Warburg effect

The reason behind aerobic glycolysis in proliferating cells is still not fully elucidated, but widely discussed and an intense field of investigation. It is hypothesized that high glycolytic rates provide advantages required for cellular proliferation (Figure 1.6). While high glycolytic rates produce more ATP than oxidative phosphorylation, it is thought that the requirements of proliferating cells go beyond high ATP production, as these cells strongly depend on biosynthetic precursors to support high proliferation rates (Figure 1.6) [Pfeiffer et al., 2001]. Glucose-derived carbon serves as precursor for the generation of intermediates that can be used in biosynthetic pathways including ribose sugars for nucleotide synthesis, glycerol and



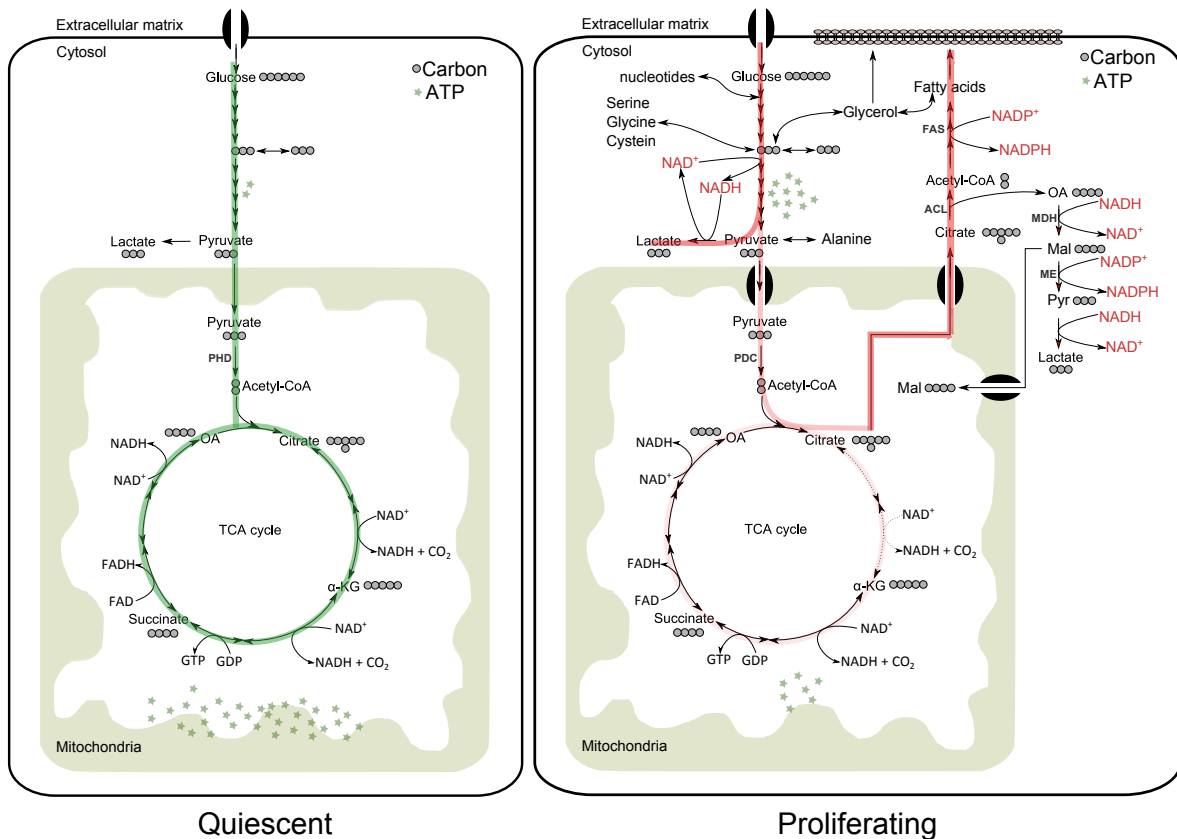


FIGURE 1.6: Glucose metabolism in resting and proliferating cells. Quiescent cells (left) have basal level of glycolysis. Glucose is converted to pyruvate, which is then oxidized within the TCA cycle. The majority of the ATP (green stars) in resting cells is generated by oxidative phosphorylation. In proliferating cells, the high influx of glucose results in high levels of ATP generated by glycolysis and decreased  $\text{NAD}^+/\text{NADH}$  ratios. Most of the pyruvate is converted by to lactate by lactate dehydrogenase (**LDH**) which is subsequently secreted. The conversion of pyruvate to lactate regenerates  $\text{NAD}^+$  and thereby keeps glycolysis running. Some pyruvate enters the TCA cycle where it is used for fatty acid synthesis to support proliferation rather than for oxidative phosphorylation. Citrate is exported into the cytoplasm and is cleaved by ATP citrate lyase (**ACL**) to form acetyl-CoA. In turn acetyl-coA is used by fatty acid synthase (**FAS**) to generate fatty acids while oxaloacetate (**OA**) is converted to malate (**Mal**) and pyruvate (adapted from [DeBerardinis et al., 2008]. **MDH** malate dehydrogenase, **ME** malic enzyme. Green lines represent the glucose flux in resting cells and red lines represent the glucose flux in proliferating cells

citrate for lipogenesis and non-essential amino-acids (Figure 1.6) [DeBerardinis et al., 2008]. It is however surprising that so much glucose-derived carbon is discarded by generating high amounts of lactate although it could be further oxidized and increase ATP yields [DeBerardinis et al., 2008]. Possibly, under aerobic glycolysis, the velocity of glycolysis outpaces the maximal velocity of oxidative phosphorylation so that pyruvate must be eliminated using a high flux mechanism [Curi et al., 1988]. While the velocity of the oxidation of pyruvate and its subsequent entry into the TCA cycle seems outpaced by high glycolytic rates, the velocity of biosynthetic pathways could be maximized [DeBerardinis et al., 2008]: high-flux metabolic pathways, such as glycolysis, branch into low flux metabolic pathways such as

pathways involved in macromolecule synthesis. By increasing the flux through glycolysis the entry of glucose-derived carbon into low flux metabolic pathways could be optimized and thereby push the synthesis of molecular precursors for macromolecule synthesis [Newsholme et al., 1985].

Glycolytic genes are frequently upregulated in cancer [Altenberg and Greulich, 2004]. In particular a specific isoform of pyruvate kinase (PK) regulates the metabolic switch from oxidative phosphorylation to aerobic glycolysis in proliferating cells. PK regulates the last step in glycolysis by converting phosphoenolpyruvate and ADP to pyruvate and ATP. PK exists in four isoforms: the L and the R isoforms are expressed in the liver and in red blood cells, the M1 isoform is expressed in most adult tissues and the M2 isoform is expressed during embryonic development [Jurica et al., 1998]. Many tumour cells exclusively express pyruvate kinase muscle isozyme 2 (PKM2) [Dombrauckas et al., 2005, Mazurek et al., 2005]. While the PKM1 isoform is constitutively active, the PKM2 isoform relies on the allosteric regulation by the upstream metabolite fructose-1,6-bisphosphate: low levels of fructose-1,6-bisphosphate render PKM2 inactive while high levels of fructose-1,6-bisphosphate activate PKM2 [Jurica et al., 1998]. This particular allosteric regulation of the PKM2 isoform allows the accumulation of glycolytic intermediates and their channelling into biosynthetic pathways which branch off from glycolysis. Switching PK expression from the M2 back to the M1 isoform was shown to reverse the Warburg effect and correlate with reduced ability to form tumours *in vivo* [Christofk et al., 2008]. A recent study uncovered the importance of PKM2 in normal proliferating cells; in MEFs loss of PKM2 results in PKM1 expression and proliferation arrest [Lunt et al., 2015]. The expression of PKM1 leads to impaired nucleic acid biosynthesis and thereby hinders cell proliferation [Lunt et al., 2015].

PKM2 can form tetramers, which are enzymatically active, or dimers which are enzymatically inactive. While tumours show high levels of PKM2 dimers, normal proliferating cells mainly express PKM2 tetramers [Mazurek, 2011]. Destabilization of PKM2 tetramers can occur upon growth factor signalling, the interaction with oncoproteins and in the presence of ROS via a number of mechanisms including tyrosine phosphorylation, association with tyrosine phosphopeptides or oxidation [Anastasiou et al., 2011, Christofk et al., 2008, Hitosugi et al., 2009]. As a consequence of decreased PKM2 enzymatic activity, cell proliferation is enhanced. This can be partly explained by the diversion of glycolytic intermediates from catabolic to anabolic processes [Anastasiou et al., 2011, Vander Heiden et al., 2009]. Apart from the metabolic consequences of PKM2 expression, PKM2 dimers seem to have independent roles in the nucleus. Among other examples, PKM2 dimers were shown to interact with STAT3 in the nucleus. PKM2 can phosphorylate STAT3 on tyrosine 705 and thereby induces the transcription of STAT3 target genes [Gao et al., 2012].

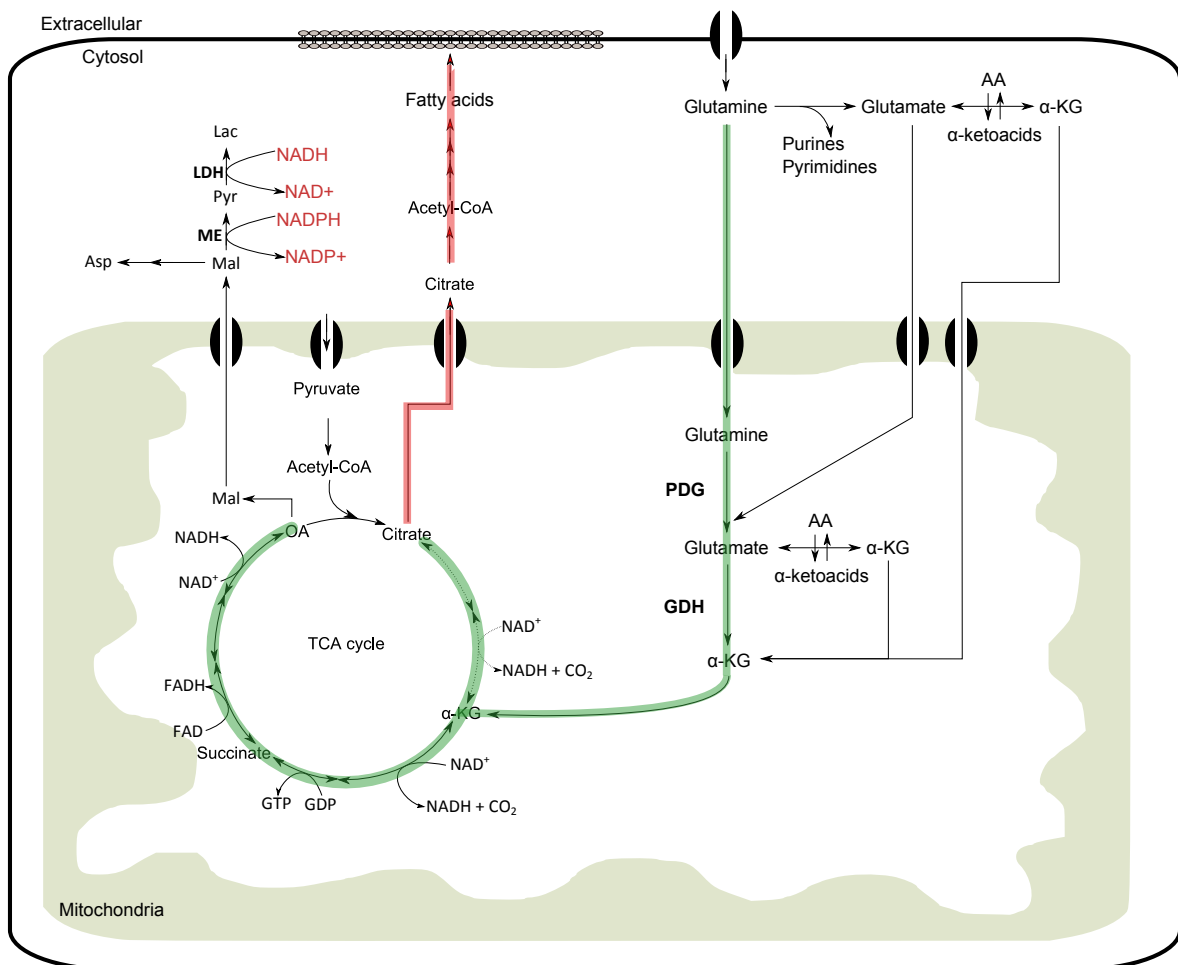


FIGURE 1.7: **Glutamine metabolism in proliferating cells.** In proliferating cells, citrate is used to generate fatty acids. The efflux of citrate from the TCA cycle results in the loss of oxaloacetate (OA). OA anaplerosis is governed by the complex glutamine metabolism. In the cytosol, glutamine donates nitrogen to purines and pyrimidines, which result in the formation of glutamate. In turn, glutamate donates its amino groups to  $\alpha$ -ketoacids and  $\alpha$ -ketoglutarate ( $\alpha$ -KG) which can enter the mitochondria. Glutamine can also be directly converted to glutamate in the mitochondria by phosphate-dependent glutaminase (PDG) and mitochondrial glutamate is converted to  $\alpha$ -KG by glutamate dehydrogenase (GDH) or aminotransferases. For TCA cycle anaplerosis,  $\alpha$ -KG enters the TCA cycle and forms OA. On the other hand, glutamine-derived  $\alpha$ -KG can be converted to citrate and fuel fatty acid synthesis (adapted from [DeBerardinis et al., 2008]). LDH lactate dehydrogenase, ME malic enzyme.

The TCA cycle is a hub for biosynthesis and plays key roles in providing proliferating cells with biosynthetic precursors. While in resting cells most of the carbon entering the TCA cycle yields in ATP production, in proliferating cells most of the carbon is used for biosynthesis rather than ATP production. In proliferating cells, this results in an efflux of carbon from the TCA towards biosynthetic pathways. One example consists in the generation of fatty acids and cholesterol from mitochondrial citrate to meet the high demand for the generation of membranes (Figure 1.6). In the TCA cycle citrate is generated from oxaloacetate that is condensed with acetyl-coA by CS. Mitochondrial citrate is then shuttled from the mitochondria to the cytoplasm. In the cytoplasm, citrate is cleaved to oxaloacetate and acetyl-coA which is used by fatty acid synthase (FAS) to synthesize lipids. The remaining oxaloacetate is then reduced to malate by malate dehydrogenase (MDH), utilizing the low cytosolic  $\text{NAD}^+/\text{NADH}$  ratio. Malate can either be transported back into the mitochondria via the malate/citrate antiport or converted to pyruvate by malic enzyme (ME), generating NADPH that further supports fatty acid synthesis (reviewed in [DeBerardinis et al., 2008]). The export of mitochondrial citrate to synthesize fatty acids is crucial to sustain cellular proliferation. The two enzymes, ATP citrate lyase (ACL) and FAS, which are involved in this process, are induced in proliferating cells where their activity is required for proliferation [Bauer et al., 2005, Hatzivassiliou et al., 2005, Kuhajda et al., 1994, Pizer et al., 1996]. The depletion of the mitochondrial citrate pool results in a truncated TCA cycle [Hatzivassiliou et al., 2005, Parlo and Coleman, 1984a]. Despite the drastic efflux of glucose-derived carbon from the TCA cycle into fatty-acid synthesis and other biosynthetic precursor pathways, cells must sustain an equal influx to resupply the TCA cycle with oxaloacetate. One enzyme that can refuel the TCA cycle is pyruvate carboxylase (PC). PC generates oxaloacetate directly from pyruvate in an ATP dependent reaction. PC activity is of substantial importance in cells with a truncated TCA cycle. In SDH-deficient cells, PC replenishes the TCA cycle with oxaloacetate which keeps the TCA cycle running but also ensures the synthesis of aspartate which is an indispensable precursor for the synthesis of proteins, nucleotides and the amino acids arginine and asparagine [Lussey-Lepoutre et al., 2015]. Another alternative of TCA cycle anaplerosis is to use amino acids, in particular glutamine. Replenishment of oxaloacetate in the TCA cycle can be assured by glutaminolysis. For this, glutamine is taken up by the cell and converted to glutamate. Glutamate is then further oxidized to  $\alpha$ -ketoglutarate which is fuelled into the TCA cycle and thereby produces oxaloacetate. In recent years, however it has become more and more clear that glutamine can also be used to generate citrate via a mechanism that is known as "reductive glutamine metabolism" [Holleran et al., 1995]. Under reductive conditions,  $\alpha$ -ketoglutarate is carboxylated to isocitrate by isocitrate dehydrogenase 1 (IDH1) and converted to citrate [Des Rosiers et al., 1995, Yoo et al., 2008]. Glutamine derived citrate can then serve as carbon source for fatty acid synthesis [Holleran et al., 1995]. Reductive glutamine metabolism is essential for tumour cells with defective mitochondria as they count on this mechanism as a major pathway to generate citrate which

provides the carbon necessary for acetyl-CoA synthesis [Mullen et al., 2011]. Reductive glutamine metabolism is IDH1 dependent and is active in most cell lines under normal culturing condition, and required for cell proliferation under hypoxic conditions [Gameiro et al., 2013, Metallo et al., 2011].

## 1.9 Metabolomics

The knowledge about signal transduction, gene transcription and protein induction and protein-protein interaction is getting more detailed and complex while databases that document findings are growing. Transcriptomic and proteomic approaches deliver valuable information on gene and protein expression under certain experimental conditions. Metabolomic approaches help to define if the observed changes in expression levels also translate into a metabolic phenotype. mRNA levels do not necessarily correlate with increased protein abundance [Gygi et al., 1999], translated proteins might or might not be active, such as for example PKM2 (Section 1.8) [Schwab, 2003]. Consequently, drawing conclusions about metabolic changes from transcriptomic and proteomic datasets alone might result in incorrect assumptions and conclusions.

Originally metabolomics was used to identify and quantify metabolites while the application of  $^{13}\text{C}$ -labelled tracers now also allows to study metabolic fluxes through networks (Section 1.9.3) [Haverkorn van Rijsewijk et al., 2011, Noguchi et al., 2009]. Metabolomics is a high-throughput technique and can be applied to various sample types including cells, tissues and body fluids. The field of metabolomics can be separated into targeted and non-targeted metabolomics (reviewed in [Hiller et al., 2010]). Targeted metabolomics concentrates on a set of known metabolites while non-targeted metabolomics tries to derive information about all detectable, known and unknown metabolites.

### 1.9.1 Metabolomics workflow

The study of cellular metabolism is generally composed of three steps that include (1) sample preparation, (2) analytical metabolite detection and (3) computational data analysis. The first step in a metabolomics experiment is the preparation of the sample. The turnover rate of metabolites is very high thus the first step in sample processing includes quenching of cellular metabolism with ice-cold methanol:water mixtures [Spura et al., 2009]. Thereby the tertiary structures of enzymes is disrupted and heat-sensitive metabolites are stabilized [Villas-Bôas et al., 2005]. The next step consists in a liquid-liquid extraction, generally using chloroform/methanol/water mixtures to separate polar and non-polar metabolites and clear the sample from DNA, RNA and proteins (reviewed in [Sapcariu et al., 2014]).

Extracted metabolites can then be separated by chromatography, including gas- or liquid

[Koek et al., 2006] chromatography and identified by mass spectrometry (reviewed in [Lei et al., 2011, Want et al., 2005]) or NMR [Holmes et al., 1998]. In this thesis, we used gas chromatography (GC) couple to mass spectrometry (MS) and thus I will briefly introduce these two techniques. To make a sample suitable for separation by GC it needs to be volatile. Therefore polar hydrogen groups within metabolites such as hydroxyl (-OH), primary amine(-NH<sub>2</sub>), carboxyl (-COOH) or carbonyl(-CO-) groups are chemically substituted by derivatization agents [Kanani et al., 2008].

Once derivatized, metabolites are separated by gas chromatography and subsequently ionized by electron impact ionization under vacuum to form positive radicals. Formed radicals are highly unstable and further fragment. The fragmentation of metabolites results in a characteristic pattern that is recorded by MS.

### 1.9.2 Mass isotopomer distribution

In MS, fragment ions are separated according to their mass over charge ratios. The mass spectrum of each metabolite is composed of different fragment ions each of which is composed of an isotopomer cluster [Wegner et al., 2013]. An isotopomer cluster results from the natural occurrence of stable isotopes and in the context of stable-isotope assisted metabolomics from the incorporation of labelled carbon sources. An example is depicted in figure 1.8. This metabolite is composed of two carbon atoms and concordantly results in three mass isotopomers: the mass isotopomer M0 is only composed of unlabelled carbon; the mass isotopomer M1 contains one <sup>13</sup>C atom at either position; M2 is in this case the heaviest mass isotopomer and only contains <sup>13</sup>C carbon atoms (Figure 1.8 A). The mass spectrum of a given fragment always reflects the complex mixture of all mass isotopomers, those that occur naturally and those introduced with tracers (Figure 1.8 B). The relative abundance of each mass isotopomer within a mass spectrum is termed mass isotopomer distribution (MID) and can be calculated by solving the following linear equation systems:

$$A \cdot f = I$$

where A is the matrix to correct for the natural abundance of heavy isotopes, f is the vector containing the fractional abundance of each mass isotopomer and I is the vector that contains the signal intensities for each isotopomer measured by GC-MS [Hiller et al., 2011] (Figure 1.8 B).

### 1.9.3 Metabolic flux analysis

Using metabolic flux analysis, intracellular metabolic fluxes can be quantified under the assumption that the system is in a metabolic steady-state. To resolve changes in intracellular fluxes  $^{13}\text{C}$ -labelled tracers are introduced into the system. Various  $^{13}\text{C}$ -labelled tracers exist and their application largely depends on which metabolic pathway is targeted [Metallo et al., 2009]. In stable-isotope assisted metabolomics experiments,  $^{13}\text{C}$ -labelled carbon sources are fed into the system and the labelled carbon atoms are redistributed to other metabolites within a metabolic network. Once the system has reached an isotopic and metabolic steady-state, which assumes constant intracellular fluxes and labelling patterns, the distribution of the labelled carbons within metabolites can be measured by MS or NMR.

Changes in intracellular fluxes can then be estimated based on the mass isotopomer distribution (MID). Here I give two examples. One of the tracers that we used throughout this project is  $^{13}\text{C}_6$ glucose (Figure 1.9). Besides others, we used this tracer to study the entry of glucose-derived carbon into the TCA cycle.  $^{13}\text{C}_6$ glucose is metabolized through glycolysis and generates  $^{13}\text{C}_3$ pyruvate.  $^{13}\text{C}_3$ pyruvate can enter the TCA cycle via PDC activity which oxidatively decarboxylates  $^{13}\text{C}_3$ pyruvate and thereby generates  $^{13}\text{C}_2$ acetyl-coA and NADH.  $^{13}\text{C}_2$ acetyl-coA is then condensed with unlabelled oxaloacetate to form  $^{13}\text{C}_2$ citrate. The relative abundance of  $^{13}\text{C}_2$ citrate or M2 citrate directly reflects PDC activity.  $^{13}\text{C}_3$ pyruvate can also be fuelled into the TCA cycle via the anaplerotic reaction mediated by PC. PC activity carboxylates  $^{13}\text{C}_3$ pyruvate and thereby generates  $^{13}\text{C}_3$ oxaloacetate. Due to its chemical instability, oxaloacetate is not detectable in most metabolomics experiments while the MID of aspartate can serve as a surrogate for oxaloacetate in aspartate free medium [Buescher et al., 2015, Zimmermann et al., 2014]. Further, if  $^{13}\text{C}_3$ oxaloacetate is used within the TCA cycle it will combine with unlabelled (coming from fatty acid degradation) or labelled (coming from PDC activity) acetyl-coA to generate  $^{13}\text{C}_3$ citrate and  $^{13}\text{C}_5$ citrate, respectively. Thus  $^{13}\text{C}_5$ citrate or M5 citrate reflects the combined activity of PDC and PC (Figure 1.9). PC activity can also be inferred from M3 malate, M3 aspartate and M3 fumarate. Since the before mentioned mass isotopomers can also result from cycling through the TCA, it is recommended to compare M3 malate, M3 aspartate and M3 fumarate to M3 succinate [Buescher et al., 2015]. This comparison allows to infer the proportion of carbon within the TCA cycle that results from TCA cycle anaplerosis by PC [Buescher et al., 2015].

Apart from stable-isotope assisted metabolomics, other methods exist to measure PDC and PC activities [Kerr et al., 1987, Sheu et al., 1981]. A commonly used diagnostic method to determine PDC activity is to measure the production of  $^{14}\text{CO}_2$  from 1- $^{14}\text{C}$ -pyruvate [Kerr

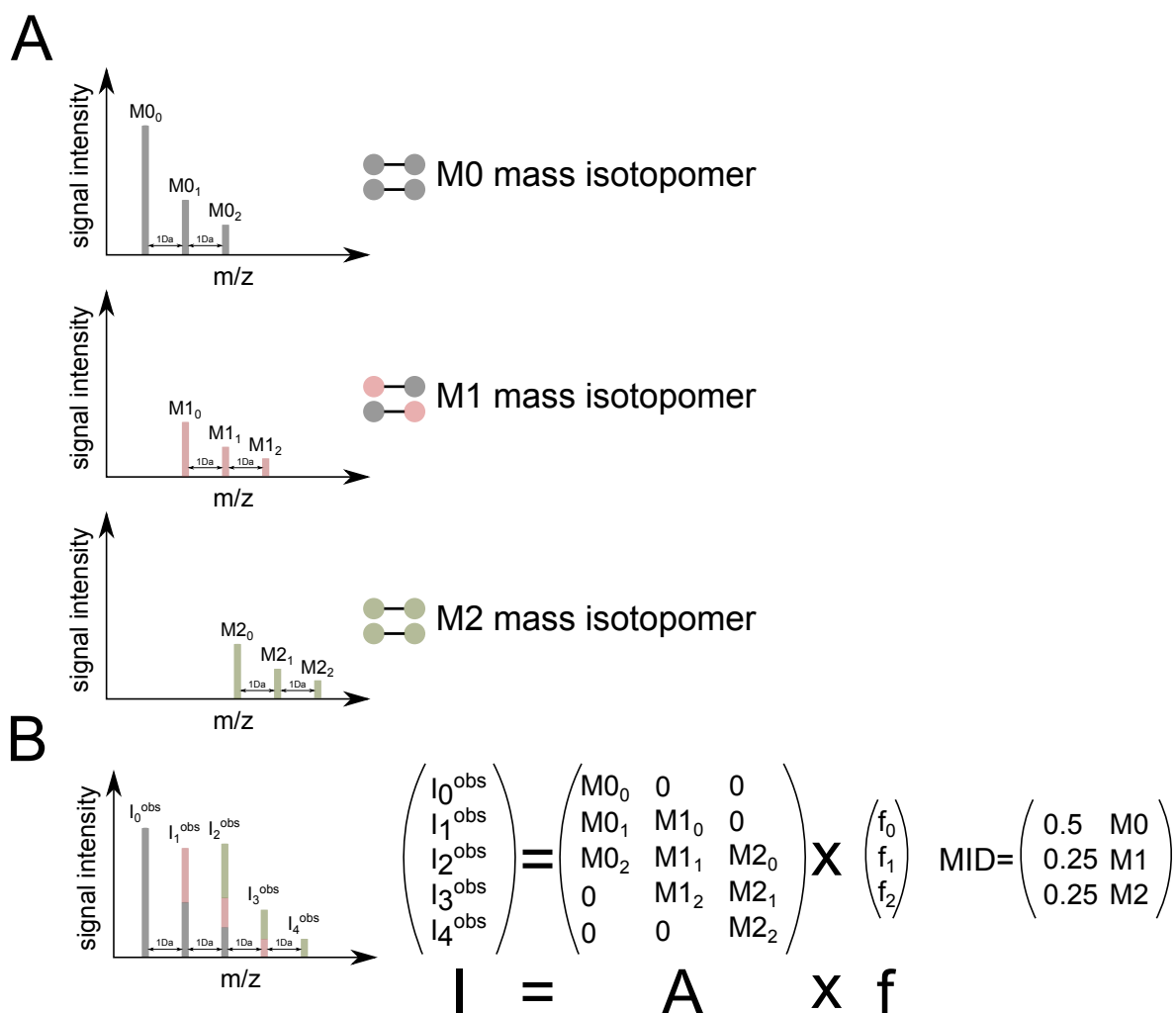


FIGURE 1.8: **Mass isotopomer distribution.** (A) A molecule composed of two carbon atoms give rise to different mass isotopomers. Mass isotopomers result from the natural occurrence of  $^{13}\text{C}$  and, in the case of stable-isotope assisted metabolomics, from the incorporation of  $^{13}\text{C}$  from labelled tracers. The mass spectra is depicted along with the corresponding mass isotopomer (grey circles =  $^{12}\text{C}$ , red/green circles =  $^{13}\text{C}$ ). (B) Only one mass spectrum is measured for a complex mixture of mass isotopomers and the relative abundance of each mass isotopomer can be calculated by solving a linear equation system. In this example 50% of the molecule contains unlabelled carbon (M0), 25% contains one  $^{13}\text{C}$  atom (M1) and the remaining 25% is labelled on two carbon atoms (M2) (adapted from [Hiller et al., 2011]).

et al., 2012]. While this assay is relatively time consuming, it does not require enzyme purification nor mitochondrial extracts, thus crude cell or tissue samples are suitable for this method [Kerr et al., 2012]. The first step in this assay is the optional activation of PDC by incubating cells or tissues with dichloroacetate or phosphatases, respectively, leading to the dephosphorylation and thus full activation of PDC. The second step consists in the incubation of the crude cell or tissue extracts with  $1\text{-}^{14}\text{C}$ -pyruvate in the presence of pyrophosphate and coenzyme A [Kerr et al., 2012]. The activity of PDC can then be derived from the production of  $^{14}\text{CO}_2$  which is measured using a liquid scintillation counter [Kerr et al., 2012]. As an alternative, a variety of manufactures now offer kits to determine PDC activity which



consist of enzyme-linked immunosorbent assays and subsequent colorimetric detection. A frequently used diagnostic method to determine the activity of PC in crude cell extracts is based on the carboxylation of pyruvate with  $^{14}\text{CO}_2$ . This reaction leads to the formation of oxaloacetate and subsequently citrate when CS and acetyl-coA are present [Atkin et al., 1979]. This method is insensitive towards interfering reactions that compete for pyruvate, while it has the disadvantage to be based on the usage of radioactive and volatile  $^{14}\text{CO}_2$  [Kerr et al., 2012]. PC activity is calculated based on the fixation of  $^{14}\text{CO}_2$  measured using a liquid scintillation counter [Kerr et al., 2012]. Furthermore the activity of PC in crude extracts can be assayed using spectrophotometric techniques. Various ready-to-use reagents are commercially available or can be prepared in-house [Scrutton and White, 1974, Warren and Tipton, 1974].

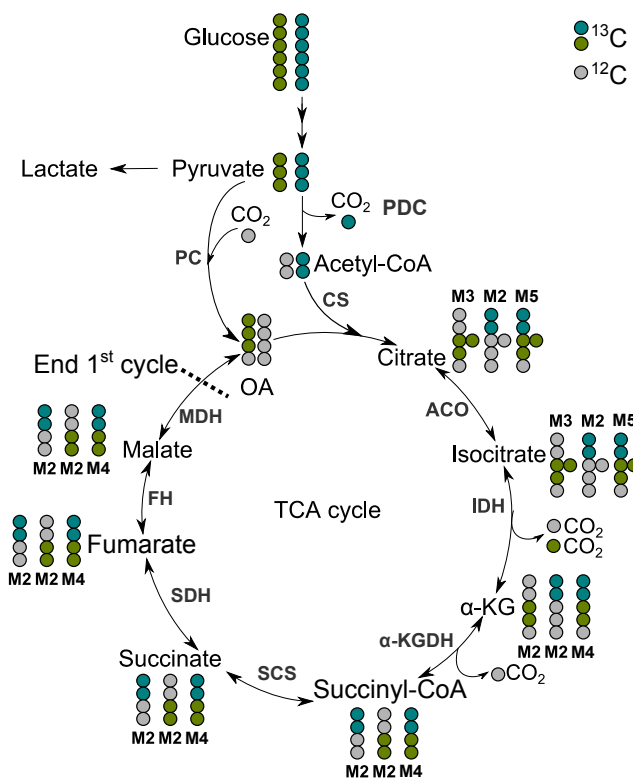


FIGURE 1.9: Mass isotopomer distributions from  $[^{13}\text{C}_6]$ glucose. MIDs resulting from PC (in green) and PDC (in blue) activities are depicted for all TCA cycle intermediates. **PDC** Pyruvate dehydrogenase complex, **CS** Citrate synthase, **ACO** Aconitase, **IDH** Isocitrate dehydrogenase,  **$\alpha$ -KGDH**  $\alpha$ -Ketoglutarate dehydrogenase, **SCS** Succinate synthase, **SDH** Succinate dehydrogenase, **FH** Fumarate hydratase, **MDH** Malate dehydrogenase, **OA** Oxaloacetate

The other tracer that we used throughout this study is  $[^{13}\text{C}_5]$ glutamine by which oxidative and reductive glutamine metabolism can be profiled. In both cases,  $[^{13}\text{C}_5]$ glutamine is converted to  $\alpha$ - $[^{13}\text{C}_5]$ ketoglutarate. Under oxidative conditions  $\alpha$ - $[^{13}\text{C}_5]$ ketoglutarate undergoes

decarboxylation within the TCA cycle and thereby generates  $[^{13}\text{C}_4]$ succinyl-CoA which is further metabolized through the TCA cycle resulting in  $[^{13}\text{C}_4]$ oxaloacetate.  $[^{13}\text{C}_4]$ oxaloacetate then condenses with unlabelled acetyl-coA to form  $[^{13}\text{C}_4]$ citrate. When glutamine is metabolized in a reductive manner  $[^{13}\text{C}_5]$  $\alpha$ -ketoglutarate is carboxylated to form  $[^{13}\text{C}_5]$ isocitrate and subsequently  $[^{13}\text{C}_5]$ citrate (Figure 1.10).

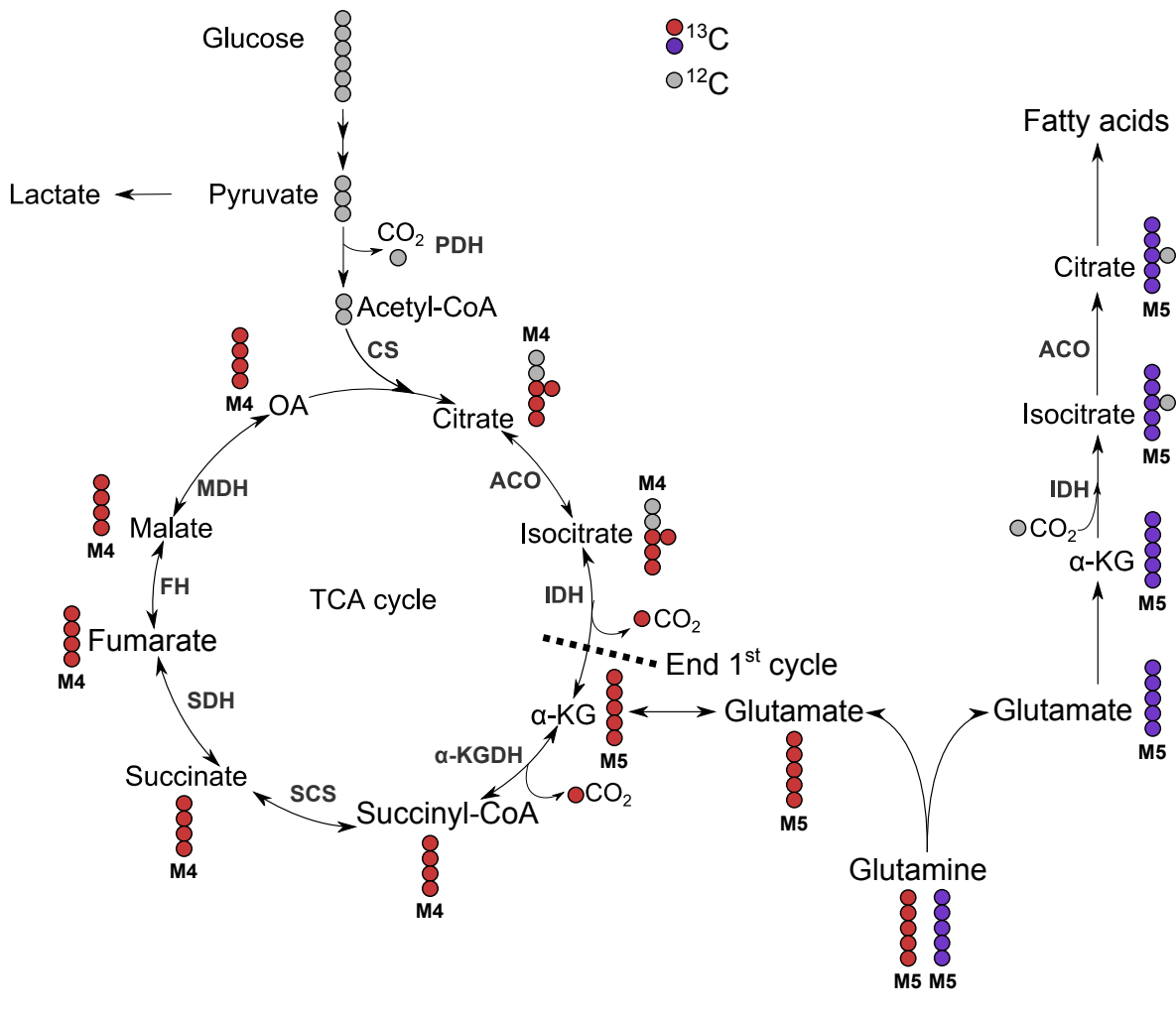


FIGURE 1.10: Mass isotopomer distributions from  $[^{13}\text{C}_5]$ glutamine. MID's resulting from oxidative (in red) and reductive (in purple) glutamine metabolism are depicted for all TCA cycle intermediates. **PDC** Pyruvate dehydrogenase complex, **CS** Citrate synthase, **ACO** Aconitase, **IDH** Isocitrate dehydrogenase,  **$\alpha$ -KGDH**  $\alpha$ -Ketoglutarate dehydrogenase, **SCS** Succinate synthase, **SDH** Succinate dehydrogenase, **FH** Fumarate hydratase, **MDH** Malate dehydrogenase, **OA** Oxaloacetate

## 1.10 Aims and scope of the thesis

The fact that inflammation promotes neoplastic growth is known since Rudolf Virchow made this observation in 1863. While numerous cancers develop in an inflammatory microenvironment, liver cancer is one of the most striking examples. Virtually all HCCs are preceded and

accompanied by chronic inflammatory conditions that promote its development and support its progression. A large body of evidence shows that the combination of ROS, cytokines and growth factors, released by immune cells within the inflammatory microenvironment, drive neoplastic growth by increasing mutagenesis rates and by supporting cellular survival and proliferation. In conjunction with growth-promoting stimuli, proliferating cells have a high demand of biomass precursors such as: amino acids for protein synthesis, nucleotides for DNA replication and fatty acids for the generation of cellular membranes.

This study was designed based on the observation that IL-6-type cytokines increase the expression of the metabolic key regulator HIF-1 $\alpha$  on mRNA and protein level in a STAT3-dependent manner. While the metabolic consequences of HIF-1 $\alpha$  stabilization under hypoxic conditions were well understood, the particular impact of cytokine-mediated HIF-1 $\alpha$  induction under normoxic growth conditions remained to be elucidated. IL-6-type cytokines such as IL-6 and OSM were shown to be implicated into HCC development and progression while the observation that these cytokines can upregulate HIF-1 $\alpha$  suggested an interesting and so far unstudied interplay with cellular metabolism.

The aim of this thesis was to elucidate whether the induction of HIF-1 $\alpha$  by IL-6-type cytokines results in similar changes within central carbon metabolism than hypoxia itself. While numerous studies showed that growth factors and cytokines can upregulate HIF-1 $\alpha$  under normoxic conditions, it remained to be studied whether this also results in a metabolic phenotype. In the larger context, our findings should show how inflammatory conditions, such as present during HCC development and progression modulate cellular metabolism and determine whether cytokine-mediated HIF-1 $\alpha$  induction plays a crucial role in this context. To simulate an inflammatory environment, we used the IL-6-cytokine OSM which plays an important role during HCC promotion and development while it also induced a strong response in terms of HIF-1 $\alpha$  induction *in vitro*. To study whether OSM stimulation in HCC cells promotes a hypoxia-like metabolic phenotype in cells we treated different HCC cells and immortalized hepatocytes with OSM, cultured them under hypoxia and subjected them to a combinatorial treatment. We studied the metabolic consequences of these treatments on the cellular metabolome using a targeted stable-isotope assisted metabolomics approach.

## Chapter 2

# Material and Methods

Unless specified differently, buffers and dilutions were prepared in water.

Only ultrapure water was used (resistivity (25°C) > 18.18 MΩcm).

All solvents were of the highest purity grade available.

Technical details on experiments done by our collaborator Dr. Andreas Zimmer can be found in [[Battello et al., 2016](#)].

### 2.1 Cell culture and reagents

HCC cells and immortalized hepatocytes were maintained in Dulbecco's Modified Eagle Medium (DMEM) (D5796, Sigma Aldrich) supplemented with 10% fetal bovine serum (FBS) (PAA or Invitrogen). Cells were cultured at 37 °C in a humidified atmosphere at 5% CO<sub>2</sub> (Sanyo). Detailed information on the cell lines is given in table 2.1. For routine culture, cells were maintained in cell culture flasks (Thermo Fisher Scientific) and grown to 90% confluency before splitting. To do this, old cell culture medium was gently removed and cells washed with 1x Dulbecco's phosphate-buffered saline (DPBS) (Gibco). Trypsin (Life Technologies) was added to fully cover cell monolayers and flasks were incubated for 5-10 min at 37 °C in a humidified atmosphere at 5% CO<sub>2</sub>. Trypsin was inactivated with complete cell culture medium and cells were resuspended to get a single cell suspension. An adequate volume of the cell suspension was transferred into a new cell culture flask and supplemented with fresh growth medium (splitting ratios are depicted in table 2.1).

Human OSM M (227 a. a., Peprotech) was reconstituted in 1x DPBS containing 0.1% bovine serum albumin (Sigma Aldrich) to a concentration of 100 ng/μl and stored at -80°C.

Hypoxia treatments were carried in a hypoxia chamber (Jacomex) at 1% O<sub>2</sub> and 37 °C in a humidified atmosphere at 5% CO<sub>2</sub>. Cell culture media was incubated under hypoxia 24 h

prior to each experiment.

TABLE 2.1: Overview on HCC cell lines and immortalized hepatocytes.

| Name      | Tumour / Stage                | Morphology      | Age | Gender | Ethnicity     | Splitting ratio | Supplier             | Catalog No. |
|-----------|-------------------------------|-----------------|-----|--------|---------------|-----------------|----------------------|-------------|
| HepG2/C3A | HCC                           | epithelial      | 15  | male   | Caucasian     | 1:3             | ATCC                 | CRL-10741   |
| Hep-3B    | HCC                           | epithelial      | 8   | male   | Afro-american | 1:3             | DSMZ                 | ACC 93      |
| HepG2     | HCC                           | epithelial      | 15  | male   | Caucasian     | 1:3             | ATCC                 | HB-8065     |
| HLE       | undifferentiated HCC          | -               | 68  | male   | -             | 1:8             | JCRB                 | JCRB0404    |
| HLF       | undifferentiated HCC          | -               | 68  | male   | -             | 1:8             | JCRB                 | JCRB0405    |
| HuH-7     | well differentiated HCC       | epithelial-like | 57  | male   | Asian         | 1:4             | JCRB                 | JCRB0403    |
| JHH-4     | HCC                           | epithelial-like | 51  | male   | Asian         | 1:4             | JCRB                 | JCRB0435    |
| PH5CH1    | immortalized hepatocytes      | epithelial      | -   | -      | Asian         | 1:3             | [Ikeda et al., 1998] | -           |
| PH5CH7    | immortalized hepatocytes      | epithelial      | -   | -      | Asian         | 1:3             | [Ikeda et al., 1998] | -           |
| PH5CH8    | immortalized hepatocytes      | epithelial      | -   | -      | Asian         | 1:3             | [Ikeda et al., 1998] | -           |
| PLC/PRF/5 | hepatoma                      | epithelial      | -   | -      | -             | 1:3             | ATCC                 | CRL-8024    |
| SK-HEP-1  | adenocarcinoma                | epithelial      | 52  | male   | Caucasian     | 1:4             | ATCC                 | HTB-52      |
| SNU-387   | pleomorphic HCC, grade IV/V   | epithelial      | 41  | female | Asian         | 1:6             | ATCC                 | CRL-2237    |
| SNU-423   | pleomorphic HCC, grade III/IV | epithelial      | 40  | male   | Asian         | 1:6             | ATCC                 | CRL-2238    |
| SNU-449   | HCC , grade II-III/IV         | epithelial      | 52  | male   | Asian         | 1:6             | ATCC                 | CRL-2234    |
| SNU-475   | HCC , grade II-IV/V           | epithelial      | 43  | male   | Asian         | 1:6             | ATCC                 | CRL-2236    |

## 2.2 Stable isotope labelling experiments

One vial of DMEM 5030 (Sigma Aldrich) and 3.7 g of sodium bicarbonate were reconstituted 1 l of water. The pH was adjusted to 7.4 with 5 M hydrogen chloride (Sigma Aldrich), the medium was sterile filtered through a Millex-GV 0.22  $\mu\text{m}$  filter unit (Merck Millipore) and stored at 4 °C.

This basic labelling medium was supplemented with 10% dialysed FBS (Invitrogen). For stable isotope labelling experiments with a uniformly labelled glucose tracer, the labelling medium was supplemented with 25 mM [ $^{13}\text{C}_6$ ]glucose (Campro Scientific) and 4 mM glutamine (Sigma Aldrich). For isotope labelling experiments with uniformly labelled glutamine, basic labelling medium was supplemented with 25 mM glucose (Sigma Aldrich) and 4 mM [ $^{13}\text{C}_5$ ] glutamine (Campro Scientific). The pH was adjusted to 7.4 with 1 M hydrogen chloride and the complete labelling medium was sterile filtered through a 0.22  $\mu\text{m}$  Steriflip GP filter unit (Merck Millipore) and stored at 4 °C.

## 2.3 siRNA-mediated silencing of PDK1 and HIF-1 $\alpha$

Small interfering RNA (siRNA)-mediated silencing of PDK1 and HIF-1 $\alpha$  was performed by reverse transfection and was based on the recommended RNAiMAX protocol from the manufacturer (Invitrogen). siRNA sequences, suppliers and catalogue numbers are depicted in table 2.2. 5 nmol of the PDK1 and non-targeting control siRNA were reconstituted in 250  $\mu\text{l}$  of RNase free water (Santa Cruz) to create a stock solution of 20  $\mu\text{M}$ . The HIF-1 $\alpha$  siRNA was reconstituted in 330  $\mu\text{l}$  of RNase free water to create a stock solution of 10  $\mu\text{M}$ . SiRNAs

were stored in aliquots at  $-80^{\circ}\text{C}$ .

For the siRNA-mediated HIF-1 $\alpha$  knockdown, 2  $\mu\text{l}$  of 10  $\mu\text{M}$  siRNA was diluted in 200  $\mu\text{l}$  1x Opti-MEM I (Gibco by Life Technologies) and gently mixed by inversion. 3  $\mu\text{l}$  of Lipofectamine RNAiMAX (Invitrogen) were added and the solution was mixed by inverting the tube. For siRNA-mediated PDK1 knockdown, 1  $\mu\text{L}$  of 20  $\mu\text{M}$  siRNA was diluted in 200  $\mu\text{l}$  1x Opti-MEM I (Gibco, Thermo Scientific) and gently mixed by inversion. 2.5  $\mu\text{l}$  of Lipofectamine RNAiMAX (Invitrogen) were added and the solution was mixed by inversion. The transfection solution was incubated for 20 min at room temperature and transferred into a 12-well cell culture plate (Thermo Fisher Scientific). The 12-well cell culture plate was gently agitated back and forth until the entire growth surface was covered with transfection solution and incubated for another 5 min at room temperature. PH5CH clones were seeded at a density of 95 000 cells/well in a volume of 800  $\mu\text{l}$  directly onto the transfection mix. A pool of non-targeting siRNAs was used as control (table 2.2). The final concentration of all siRNAs was 20 nM. Cells were grown for 6-24 h at  $37^{\circ}\text{C}$  in a humidified atmosphere at 5%  $\text{CO}_2$  and the medium was replaced with fresh growth medium.

TABLE 2.2: siRNA sequences

| Gene                 | Target sequence(s)              | Supplier   | Catalogue Number |
|----------------------|---------------------------------|------------|------------------|
| Human HIF-1 $\alpha$ | 5'-CUG AUG ACC AGC AAC UUG A-3' | Santa Cruz | sc-35561         |
| Human PDK1           | 5'-GAU CAG AAA CCG ACA CAA U-3' | Dharmacon  | D-001810-10-20   |
|                      | 5'-GCC AGA AUG UUC AGU ACU U-3' |            |                  |
|                      | 5'-GCA UAA AUC CAA ACU GCA A-3' |            |                  |
|                      | 5'-CAA AGG AAG UCC AUC UCA U-3' |            |                  |
| non-targeting siRNA  | 5'-UGG UUU ACA UGU CGA CUA A-3' | Dharmacon  | L-005019-00-0005 |
|                      | 5'-UGG UUU ACA UGU UGU GUG A-3' |            |                  |
|                      | 5'-UGG UUU ACA UGU UUU CUG A-3' |            |                  |
|                      | 5'-UGG UUU ACA UGU UUU CCU A-3' |            |                  |

### 2.3.1 OSM stimulation

### 2.3.2 Short-term OSM stimulation

All experiments were carried out in 12-well cell culture plates. Cells were seeded in a volume of 750  $\mu\text{l}$  at the seeding densities indicated in table 2.3 and grown for 24 h at  $37^{\circ}\text{C}$  in a humidified atmosphere at 5%  $\text{CO}_2$ . Normal growth medium was gently removed and cells were washed once with 1 ml 1x DPBS. 750  $\mu\text{l}$  of labelling medium was added per well. Cells were either left untreated or stimulated with 50 ng/ml OSM for the indicated periods of time.

TABLE 2.3: Cell seeding densities for stable isotope labelling experiments

| Cell line    | Seeding density (cells/cm <sup>2</sup> ) |
|--------------|--|
| PH5CH clones | 25 000                                   |
| HepG2        | 50 000                                   |
| HepG2/C3A    | 50 000                                   |
| JHH-4        | 15 000                                   |
| Sk-Hep1      | 25 000                                   |

### 2.3.3 Long-term OSM stimulation

On day one PH5CH8 and JHH-4 cells were plated at 60 000 cells/well and 45 000 cells/well respectively, in 12-well cell culture plates. Cells were grown for 8 h at 37 °C in a humidified atmosphere at 5% CO<sub>2</sub>. Cell culture media was replaced with fresh cell culture medium with or without 25 ng/ml OSM and cells were grown for 24 h. On the subsequent days, cell culture medium was replaced and the OSM stimulation refreshed. On day four, the cell culture medium was replaced with labelling medium with or without 25 ng/ml OSM. 24 hours later, intracellular metabolites and proteins were extracted. Cells were furthermore transferred into a T25 cell culture flasks and grown over the weekend. Control cells were left untreated and stimulated cells were grown in the presence of 25 ng/ml OSM. On day seven of the experiment, cells were reseeded as previously described. The experimental scheme is depicted in Figure 2.1

## 2.4 Extraction of intracellular metabolites

The extraction of intracellular metabolites was performed on cells grown in 12-well cell culture plates. The cell culture media was gently removed and cells were washed once with 1 ml 0.9% NaCl (w/v) (Sigma Aldrich). Cellular metabolism was quenched with 200  $\mu$ L of -20 °C 100% methanol (Sigma Aldrich). 200  $\mu$ L of 4 °C water was added containing 1  $\mu$ g/ml pentanedioic-d<sup>6</sup> acid (C/D/N Isotopes Inc.) as an internal standard. The cells were scraped off the plate and transferred into 1.5 ml reaction tubes containing 200  $\mu$ L -20 °C 100% chloroform (Sigma Aldrich). Extracts were incubated in a Thermomixer for 20 min at 4 °C and under continuous shaking at 1400 rpm (Eppendorf). Cell extracts were centrifuged for 5 min at 4 °C and 21 000 xg in a benchtop centrifuge (Eppendorf 5424R or 5415R). Centrifugation resulted in phase separation, where the upper phase contains polar metabolites, the interphase is composed of DNA, RNA and proteins and the lower phase contains non-polar metabolites. 200  $\mu$ L of the polar phase were transferred into GC glass vials (Chromatographie Zubehr Trott) and dried in a refrigerated rotary vacuum evaporator (Labconco). Dried metabolite extracts were stored at -80 °C until further processing.

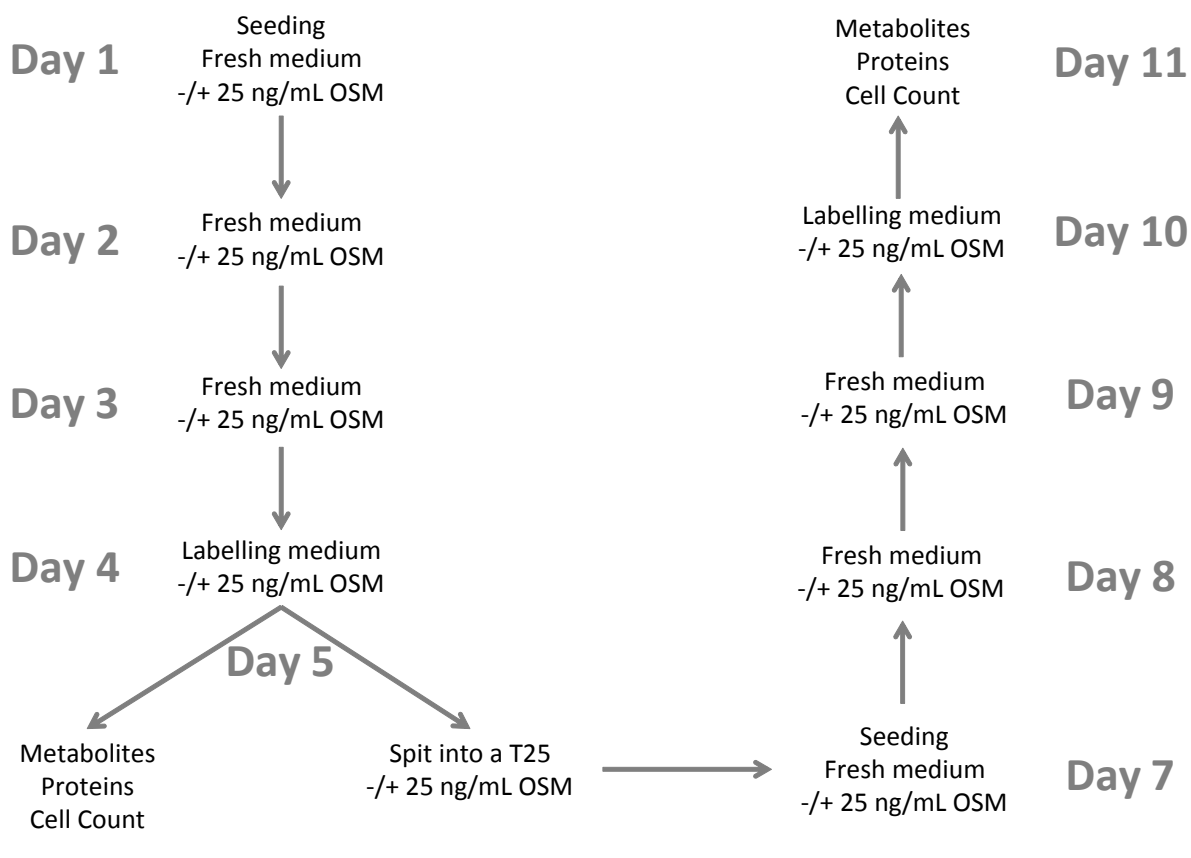


FIGURE 2.1: Experimental scheme of the long-term OSM stimulation.

For hypoxia experiments, the first two extraction steps were carried out inside the hypoxia chamber. Cells were washed with hypoxic 0.9% NaCl (w/v), quenched then taken out of the hypoxia chamber and intracellular metabolites extracted as described below.

## 2.5 Medium preparation for GC-MS analysis

The cell culture medium was transferred into a 1.5 ml reaction tube and centrifuged at 300 xg for 5 min at room temperature in a benchtop centrifuge. The supernatant was transferred into a fresh 1.5 ml reaction tube and stored at -80 °C until further processing. For the calibration curve, cell culture medium (D5796, Sigma Aldrich) was spiked with 8 mM lactic acid (Sigma Aldrich) and 0.4 mM glutamate and diluted to 1:32 in serial dilution steps of 1:2. Extracellular metabolites from medium samples were extracted using ice-cold extraction fluid (8+1 methanol/water) containing the internal standard [<sup>13</sup>C<sub>5</sub>]ribitol (Omicron Biochemicals, Inc.) at a concentration of 1 µg/ml. 20 µl of medium was mixed with 180 µl ice-cold extraction fluid, vortexed for 10 s and centrifuged at 21 000 xg for 5 min at 4 °C in a benchtop centrifuge. 50 µl of medium extracts were transferred to GC glass vials and dried in a refrigerated rotary vacuum evaporator.



## 2.6 Cell counting

Cell culture medium was gently removed from cells grown in 12-well cell culture plates. Cells were washed once with 1 ml 1x DPBS and 200  $\mu\text{L}$  of trypsin was added into each well to disperse the cells. Cell culture plates were incubated for 7 min at 37 °C in a humidified atmosphere at 5%  $\text{CO}_2$ . Trypsin was inactivated with 400  $\mu\text{L}$  of complete cell culture medium. Cells were resuspended to single cell suspension and transferred into sample cups (Vi-Cell, Beckman Coulter). Cell viability and count was determined on a cell viability analyser (Vi-Cell, Beckman Coulter).

## 2.7 GC-MS analysis

Metabolite derivatization was performed using a Multi Purpose Sampler (Gerstel).

Dried polar intracellular metabolites were dissolved in 15  $\mu\text{l}$  of 2% methoxyamine hydrochloride (w/v)(Sigma Aldrich) in pyridine (Sigma Aldrich) and incubated 60 min at 55 °C under continuous shaking. An equal volume of N-tert-butyldimethylsilyl-N-methyltriuroacetamide (Restek) was added and incubated for 60 min at 55 °C under continuous shaking.

GC-MS analysis was carried out on a Agilent 7890A gas chromatograph coupled to an Agilent 5975C inert XL mass selective detector (Agilent Technologies). 1  $\mu\text{l}$  sample was injected into a split/splitless inlet, operating in splitless mode at 270 °C . The GC was equipped with a 5 m DuraGuard capillary column and a 30 m (I.D. 250  $\mu\text{m}$ , film 0.25  $\mu\text{m}$ ) DB-35MS analytical column (Agilent J&W GC Column). Helium was used as carrier gas at a constant flow rate of 1 ml/min. The GC oven temperature was held at 100 °C for 2 min and increased to 300 °C at 10 °C/min and held for 4 min. The total run time of one sample was 26 min. The transfer line temperature was set to 280 °C. The MS was operating under electron ionization at 70 eV. The MS source was held at 230 °C and the quadrupole at 150 °C. The detector was operated in selected ion mode (SIM) and details on SIM parameters can be found in table 2.4.

Dried extracellular metabolites were dissolved in 15  $\mu\text{l}$  of 2% methoxyamine hydrochloride (w/v) in pyridine and incubated 60 min at 40 °C under continuous shaking. An equal volume of N-Methyl-N-(trimethylsilyl)trifluoroacetamide (Sigma Aldrich) was added and the samples were incubated at 40 °C for 30 min under continuous shaking. 1  $\mu\text{L}$  of sample was injected into a split/splitless inlet, operating in splitless mode at 270 °C. GC oven temperature was held at 90 °C for 1 min and increased to 300 °C by 15 °C/min for 8 min to 320 °C. The total run time of one sample was 24.3 min.

TABLE 2.4: GC-MS analysis: Details on the SIM method

| Comound                         | Sum Formula   | Ions    | Exact ion | Dwell time (ms) | RT (min) | Carbon atoms | MID size |
|---------------------------------|---------------|---------|-----------|-----------------|----------|--------------|----------|
| Pyruvic acid 1MeOX 1TBDMS       | C6H12O3NSi    | 174-180 | 0         | 15              | 6.82     | 3            | 4        |
| Lactic acid 2TBDMS              | C11H25O3Si2   | 261-267 | 0.1       | 15              | 8.99     | 3            | 4        |
| Alanine 2TBDMS                  | C11H26NO2Si2  | 260-266 | 0.1       | 15              | 9.51     | 3            | 4        |
| Glycine 2TBDMS                  | C10H24NO2Si2  | 246-252 | 0.1       | 15              | 10.02    | 2            | 3        |
| Succinic acid 2TBDMS            | C12H25O4Si2   | 289-296 | 0.1       | 15              | 12.66    | 4            | 5        |
| Fumaric acid 2TBDMS             | C12H23O4Si2   | 287-294 | 0.1       | 15              | 12.79    | 4            | 5        |
| Serine 3TBDMS                   | C17H40NO3Si3  | 390-396 | 0.2       | 15              | 14.18    | 3            | 4        |
| Methionine 2TBDMS               | C13H30NO2SSi2 | 320-328 | 0.2       | 10              | 14.8     | 5            | 6        |
| 2-Oxoglutaric acid 1MeOX 2TBDMS | C14H28NO5Si2  | 346-354 | 0.2       | 10              | 15.47    | 5            | 6        |
| Malic acid 3TBDMS               | C18H39O5Si3   | 419-426 | 0.2       | 15              | 15.69    | 4            | 5        |
| Aspartic acid 3TBDMS            | C18H40NO4Si3  | 418-425 | 0.2       | 15              | 16.1     | 4            | 5        |
| Glutamic acid 3TBDMS            | C19H42NO4Si3  | 432-440 | 0.3       | 10              | 17.19    | 5            | 6        |
| Glutamine 3TBDMS                | C19H43N2O3Si3 | 431-439 | 0.3       | 10              | 18.85    | 5            | 6        |
| Citric acid 4TBDMS              | C26H55O7Si4   | 591-600 | 0.3       | 10              | 19.81    | 6            | 7        |

## 2.8 GC-MS data analysis

All GC-MS chromatograms were processed using the MetaboliteDetector software [Hiller et al., 2009]

### 2.8.1 Mass isotopomer distribution analysis

MIDs were determined from samples measured in SIM. The monitored fragments contained the full carbon backbone of the respective metabolite and the provided sum formula was used to correct for natural isotope abundance. GC-MS raw data files were converted to netCDF format (GC/MSD ChemStation Software, Agilent) and imported into MetaboliteDetector. The retention time was used for chromatogram alignment and metabolites were identified using an in-house library. Software settings for compound identification and MID calculation are depicted in supplemental tables B.1 and B.2. Chemical formulas for MID determination are given in table 2.4 and were taken from [Wegner et al., 2014].

Weighted carbon contribution was calculated with the following formula:

$$\frac{1}{n} \cdot \sum_{i=1}^n M_i \cdot i$$

where  $n$  is the number of carbons of the molecule of interest and  $M_i$  the  $i^{th}$  mass isotopomer.

### 2.8.2 Relative quantification of metabolites

Chromatograms were processed as described in 2.8.1 and metabolites were quantified using the batch quantification wizard (Supplemental table B.2).

For relative quantification of intracellular metabolites from samples measured in SIM, the signal intensities of metabolites were divided by the signal intensity of the internal standard

pentanedioic-d<sub>6</sub> acid, which accounts for variations during metabolite extraction and GC-MS measurements. Furthermore, signal intensities were divided by cell count, to account for variations in the cell number.

For relative quantification of extracellular metabolites, signal intensities were normalized to the cell number.

## 2.9 Reverse transcription and quantitative PCR procedure

Total RNA was extracted using the RNeasy Mini Kit (QIAGEN) according to the manufacturer's instructions. 500 ng of total RNA were reverse transcribed using SuperScript III reverse transcriptase (Invitrogen) in a final volume of 20  $\mu$ l according to manufacturer's recommendations and diluted with 180  $\mu$ l PCR-grade water (Sigma Aldrich). qPCR was performed on a LightCycler 480 (Roche) in a total volume of 20  $\mu$ l containing 1  $\mu$ l cDNA, 5 pmol of each forward and reverse primer (Eurogentec), 10  $\mu$ l iTaq Universal SYBR Green Supermix (Bio-Rad) and PCR-grade water. qPCRs were performed on samples from biological triplicates and each sample was measured in technical duplicates. Primer sequences are depicted in table 2.5. Thermal cycling conditions for all qPCR assays consisted of an initial enzyme activation step at 95 °C for 15 min, followed by 40 cycles of 30 s of denaturation at 95 °C, annealing at 60 °C and elongation at 72 °C. The threshold crossing value of each transcript was normalized to the housekeeping gene L27 and relative quantification was performed using the comparative Ct method.

TABLE 2.5: Primer sequences

| Gene Symbol                           |                | Primer Sequence                   |
|---------------------------------------|----------------|-----------------------------------|
| <i>Human HIF-1<math>\alpha</math></i> | <i>Forward</i> | 5'-CGT TCC TTC GAT CAG TTG TC-3'  |
|                                       | <i>Reverse</i> | 5'-TCA GTG GTG GCA GTG GTA GT-3'  |
| <i>Human PDK1</i>                     | <i>Forward</i> | 5'-GCA CTC TTT ATT GTT TGG TGG-3' |
|                                       | <i>Reverse</i> | 5'-ACG CCT AGC ATT TTC ATA GC-3'  |
| <i>Human L27</i>                      | <i>Forward</i> | 5'-CTG GTG GCT GGA ATT GAC-3'     |
|                                       | <i>Reverse</i> | 5'-ACA GAG TAC CTT GTG GGC-3'     |

## 2.10 Western blots

Protein extraction was performed on cells grown in 12-well cell culture plates. Cells were washed once with 1 ml 1x DPBS and lysed with 60  $\mu$ l M-PER lysis buffer (Thermo Scientific) supplemented with 1 x protease inhibitors (Roche). Cells were scraped off the plate

and transferred into 1.5 ml reaction tubes. Protein extracts were incubated 30 min at 4°C under continuous shaking at 1400 rpm. Protein extracts were centrifuged at 21 000 xg for 5 min at 4°C in a benchtop centrifuge and the supernatant was used for western blot analysis. Protein extracts were quantified on a Nanodrop spectrophotometer (Thermo Scientific) and protein extracts containing 10 µg of protein were diluted 1:3 with 4 x Laemmli sample buffer (Thermo Scientific) supplemented with 10% β-mercaptoethanol (v/v) (Sigma Aldrich). Proteins were denatured for 5 min at 95 °C, centrifuged down at 21 000 xg and at 4°C in a benchtop centrifuge and kept on ice.

Sodium dodecyl sulfate polyacrylamide gels were pored in-house and were composed of a 3% acrylamide stacking and 10% acrylamide separating gel. 5 mL stacking gel solution contained 500 µl acrylamide/bis-acrylamide (29:1) (Sigma Aldrich), 1.25 ml 0.5 M tris-hydrogen chloride (Sigma Aldrich) at pH 6.8, 50 µl 10 % sodium dodecyl sulfate (w/v) (Sigma Aldrich), 3.15 ml water, 50 µl freshly prepared 10 % ammonium persulfate (w/v) (Sigma Aldrich) and 7 µl tetramethylethylenediamine (Sigma Aldrich). 10 mL separating gel solution was composed of 3.3 µl acrylamide/bis-acrylamide (29:1), 2.5 ml 1.5 M tris-hydrogen chloride at pH 8.8, 100 µl 10 % sodium dodecyl sulfate (w/v), 4 ml water, 100 µl freshly prepared 10 % ammonium persulfate (w/v) and 14 µl tetramethylethylenediamine (Sigma Aldrich).

Protein extracts and 5 µl Precision Plus Kaleidoscope protein standard were loaded on the gel. Proteins were separated for 15 min at 90 V and then for 60 min at 120 V in a Mini-Protean Tetra System (Biorad) electrophoresis chamber filled with a running buffer composed of 25 mM tris-base at pH 8.3 (Sigma Aldrich), 0.2 M glycine (Sigma Aldrich), 0.1% sodium dodecyl sulfate (w/v).

Gels were washed once for 5 min in water and proteins were transferred on a polyvinylidene fluoride membrane with a pore size of 0.45 µm (Merck). Therefore, the membrane was activated for 1 min with 100% methanol. All components of the western blot stack *i.e.* the gel, the membrane, the Whatman paper (GE Healthcare Life Sciences ) were wet in transfer buffer composed of 25 mM tris-base at pH 8.3 (Sigma Aldrich), 0.2 M glycine (Sigma Aldrich) and 20% methanol (Sigma Aldrich) before being assembled. Proteins were transferred onto the membrane in a Criterion Blotter (Biorad) filled with transfer buffer for 1 h at 90 V.

Membranes were washed once in tris-buffered saline-tween (TBS-T) (20 mM tris-hydrochloride, 0.4 mM sodium chloride (Sigma Aldrich), 0.1% Tween (v/v) (Sigma Aldrich), pH 7.6) and blocked in 10% BSA (w/v) (Sigma Aldrich) in TBS-T for 1 h at room temperature and 50 rpm. Primary antibodies were diluted in 5% BSA (w/v) in TBS-T (refer to table 2.6) and blots were incubated with the primary antibody over night at 4 °C under continuous rotation at 50 rpm. Blots were washed three times for 5 min with TBS-T. The secondary horse reddish peroxidase-coupled antibodies (Cell signalling) were diluted 1:5000 in TBS-T containing 5% skim milk (w/v) (Sigma Aldrich) and the membranes were incubated at room temperature for 1 h under continuous rotation at 50 rpm. Blots were washed three times for 5 min with

TBS-T and ECL signals were detected on a Odyssey imaging system (LI-COR Biosciences) as previously described [[Haan and Behrmann, 2007](#)]

TABLE 2.6: Antibody dilutions and suppliers

| Primary antibody       | Supplier                     | Catalogue Number | Species | Dilution |
|------------------------|------------------------------|------------------|---------|----------|
| HIF-1 $\alpha$         | BD Transduction Laboratories | 610958           | mouse   | 1:500    |
| PDK1                   | Enzo                         | ADI-KAP-PK112    | rabbit  | 1:1000   |
| pSTAT3 (pTyr705)       | Cell signaling               | D3A7             | rabbit  | 1:1000   |
| STAT3                  | Cell signaling               | 12640            | rabbit  | 1:1000   |
| pPDH-E1alpha (pSer232) | Millipore                    | AP1063           | rabbit  | 1:1000   |
| pPDH-E1alpha (pSer300) | Millipore                    | ABS194           | rabbit  | 1:1000   |
| pPDH-E1alpha (pSer293) | Millipore                    | ABS204           | rabbit  | 1:10000  |
| alpha-tubulin          | ThermoFisher scientific      | PA1-38814        | rabbit  | 1:5000   |

## 2.11 Statistical analysis

Each experiment was done in biological triplicates and each triplicate consisted of three wells per condition. Statistical significance was determined using two-tailed Student's t-test where \* denotes  $P \leq 0.05$ , \*\* denotes  $P \leq 0.01$ , and \*\*\* denotes  $P \leq 0.001$ . Error bars represent the standard deviation.

## Chapter 3

# Results

This study was based on the observation that the IL-6 type cytokine OSM upregulates HIF-1 $\alpha$  on mRNA and protein level under normoxic conditions in HCC cell lines and in immortalized hepatocytes [Vollmer et al., 2009]. While HIF-1 $\alpha$  is known to orchestrate the metabolic response to hypoxia, the metabolic consequences of HIF-1 $\alpha$  induction by the inflammatory cytokine OSM under normoxia remained to be elucidated. Thus, we investigated whether OSM can induce a hypoxia-like metabolic phenotype via HIF-1 $\alpha$  upregulation under normoxic conditions.

First, we studied hypoxia-mediated metabolic effects in two HCC cell lines (HepG2 and JHH-4) and in immortalized hepatocytes (PH5CH8). Next, we studied the metabolic effects of OSM under normoxic conditions and compared hypoxia-mediated metabolic changes with those induced by OSM. Based on the observation that OSM treatment can further increase HIF-1 $\alpha$  levels under hypoxia, we investigated whether a combinatorial treatment can also boost metabolic effects [Vollmer et al., 2009].

We found that OSM can indeed induce hypoxia-like metabolic changes in immortalized hepatocytes, while cellular metabolism of HCC cells remained unaffected although HIF-1 $\alpha$  was upregulated. OSM-mediated metabolic effects in PH5CH8 cells were less pronounced than those observed under hypoxia, despite the fact that HIF-1 $\alpha$  protein levels were similar. Furthermore, a combined treatment of OSM and hypoxia did not result in a stronger metabolic phenotype. Then we validated, that OSM-mediated metabolic reprogramming is mediated via HIF-1 $\alpha$  and showed that the HIF-1 $\alpha$  target gene PDK1 plays a crucial role in this context.

In order to simulate chronic exposure to inflammatory cytokines in PH5CH8 and JHH-4 cell lines, we performed long-term OSM stimulations. Chronic OSM treatment strengthened OSM-induced metabolic reprogramming of PH5CH8 cells and induced HIF-1 $\alpha$  independent metabolic effects in the HCC cell line JHH-4.

These results consist of our contribution to the TANDEM project entitled: "Effects of inflammatory cytokines and hypoxia on cancer metabolism in a systems approach". This project was carried out in collaboration with Dr. Claude Haan and Dr. Andreas Zimmer (Signal transduction group, Life Science Research Unit, University of Luxembourg). While we conducted the metabolic profiling, our collaborators contributed valuable information on gene and protein regulation. Wherever appropriate, I will state our collaborators contributions to the figures and findings. While the majority of the results was published recently [Battello et al., 2016] (supplements C), I will describe and discuss our results in more detail and elaborate on findings from unpublished experiments.

### 3.1 Effects of hypoxia on cellular metabolism of HCC cells and immortalized hepatocytes

HIF-1 $\alpha$  is the key regulator of the cell's response to hypoxia. HIF-1 $\alpha$  stabilization under hypoxic conditions results in the transcription of numerous target genes, a multitude of which code for metabolic enzymes [Mole et al., 2009, Ortiz-Barahona et al., 2010]. To study the metabolic effects of HIF-1 $\alpha$  stabilization under hypoxia we performed stable-isotope assisted metabolomics. We cultured HepG2, JHH-4 and PH5CH8 cell lines for 36 h under normoxia (18.6% O<sub>2</sub>) or hypoxia (1%O<sub>2</sub>) and used uniformly labelled glucose ([<sup>13</sup>C<sub>6</sub>]glucose) and uniformly labelled glutamine ([<sup>13</sup>C<sub>5</sub>]glutamine) to profile central carbon metabolism.

#### 3.1.1 Hypoxia reduces glucose-derived carbon entry into the TCA cycle

The majority of carbon within central metabolism is derived from glucose and glutamine. Glucose is metabolized through glycolysis to generate pyruvate. Pyruvate can be decarboxylated to acetyl-coA to be further oxidized within the TCA cycle or converted to lactate and excreted from the cell. Glutamine is converted to  $\alpha$ -ketoglutarate which undergoes oxidative decarboxylation within the TCA cycle or reductive carboxylation to generate lipogenic citrate. Other carbon sources that contribute to the carbon pool are degradation products from fatty, amino and nucleic acids. By using [<sup>13</sup>C<sub>6</sub>]glucose and [<sup>13</sup>C<sub>5</sub>]glutamine, we can calculate relative carbon contributions to the metabolites of central carbon metabolism which reflect the relative proportion of glucose- or glutamine-derived carbon within a given metabolite.

First, we were interested to acquire a general overview of glucose- and glutamine-derived carbon contributions to central carbon metabolism in HepG2 and JHH-4 HCC cell lines and in PH5CH8 immortalized hepatocytes grown under control conditions (18.6% O<sub>2</sub>). Therefore, we analysed glucose- and glutamine-derived carbon contribution to (1) pyruvate and lactate

as representatives for glycolysis, (2) the amino acids serine and glycine and (3) the TCA cycle intermediates: citrate,  $\alpha$ -ketoglutarate, succinate, fumarate, malate and aspartate.

Glucose-derived carbon accounts for the majority (70-90%) of carbon within glycolysis as could be derived from pyruvate and lactate (Figure 3.1 A-C). Glutamine-derived carbon and carbon derived from unlabelled sources contributed to glycolysis to lesser extent (Figure 3.1 A-C). Within the TCA cycle, glucose-derived carbon contributed 25-50% of the carbon in citrate (Figure 3.1 A-C) and 5-25% of the carbon in the other intermediates. Furthermore, 35-50% of the carbon within the TCA cycle was derived from glutamine while 10-15% came from other carbon sources (Figure 3.1 A-C).

The general distribution of glucose- and glutamine-derived carbon in HCC cell lines and immortalized hepatocytes might reflect the typical metabolic features of proliferating cells. The contribution of glucose-derived carbon to the TCA cycle metabolites is relatively low, while compensated by carbon coming from glutamine. However, it remains difficult to draw final conclusions as we did not profile the metabolism of non-proliferating hepatocytes. Nevertheless, our observations underlined the importance of glutamine as carbon source in proliferating hepatocytes and HCC cell lines which is the case for proliferating cells in general [DeBerardinis et al., 2008].

Although the distribution of glucose- and glutamine-derived carbon within central carbon metabolism was comparable, cell lines exhibited differences. In HepG2 cells, for example, we measured that glucose- and glutamine-derived carbon contributed equally to serine while in JHH-4 and PH5CH8 cell lines, glucose-derived carbon contribution to serine was only 10%. This suggests differences, either in serine uptake rates from the cell culture medium or a different influx of glucose-derived carbon into serine and glycine synthesis. Furthermore, we observed that in HepG2 cells, the contribution of glucose-derived carbon to citrate and other TCA cycle intermediates was much higher when compared to JHH-4 and PH5CH8 cells. This observation might be explained by their high PC activity (Figure 3.2 E).

Under hypoxia, we observed that cellular metabolism undergoes drastic changes in terms of glucose- and glutamine-derived carbon contributions to TCA cycle metabolites. We observed that the relative contribution of glucose-derived carbon to TCA cycle drops drastically while the contribution of glutamine-derived carbon, and other unlabelled sources, increased (Figure 3.1 A-C). Under low oxygen tension and for all cell lines, the synthesis of citrate,  $\alpha$ -ketoglutarate and succinate became almost entirely independent of carbon coming from glucose, providing evidence for that glucose-derived carbon entry into the TCA cycle is drastically altered.

Taken together we observed that in immortalized hepatocytes and HCC cells the metabolic adaptation to hypoxia goes hand in hand with a drastic decrease in glucose-derived carbon to the TCA cycle while glutamine-derived carbon is used as a substitute to synthesize



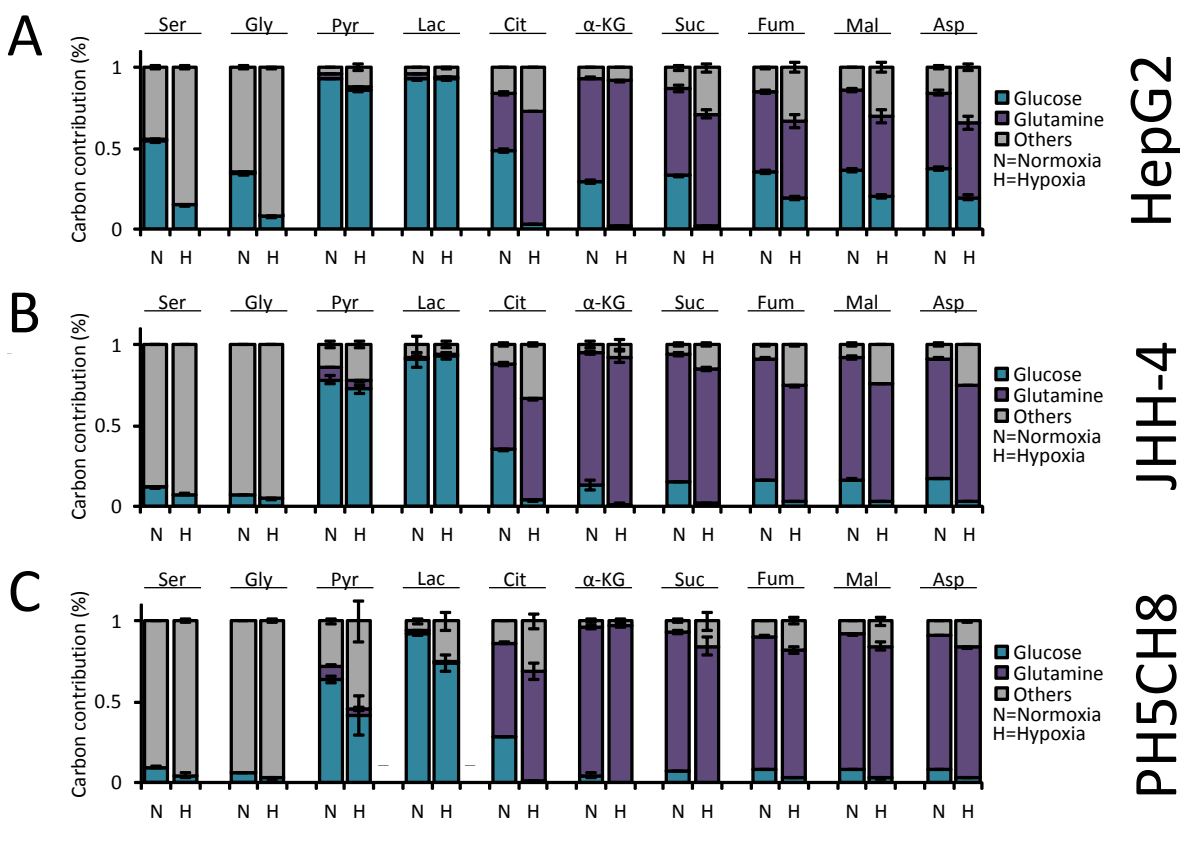


FIGURE 3.1: **Hypoxia-mediated changes in glucose- and glutamine-derived carbon contributions.** HCC cell lines (HepG2, JHH-4) and immortalized hepatocytes (PH5CH8) were grown for 36 h under normoxia (N) (18.6% O<sub>2</sub>) or under hypoxia (H) (1% O<sub>2</sub>) in presence of [<sup>13</sup>C<sub>6</sub>]glucose or [<sup>13</sup>C<sub>5</sub>]glutamine. Relative carbon contributions from glucose, glutamine and other (unlabelled) carbon sources to serine (Ser), glycine (Gly), pyruvate (Pyr), lactate (Lac), citrate (Cit), α-ketoglutarate (α-KG), succinate (Suc), fumarate (Fum), malate (Mal) and aspartate (Asp) were calculated for (A) HepG2, (B) JHH-4 and (C) PH5CH8.

TCA cycle metabolites. These results demonstrate that the entry of pyruvate into the TCA cycle is prohibited while glutamine ensures the generation of numerous metabolites under hypoxic conditions. Our results are in agreement with the classical hypoxia-mediated metabolic changes that have been described in numerous cell lines [Fendt et al., 2013, Filipp et al., 2012, Metallo et al., 2011, Scott et al., 2011].

### 3.1.2 Metabolic consequences of hypoxia on glucose and glutamine metabolism

To profile the activity of PDC and PC, the two enzymes that link glycolysis and the TCA cycle, we applied [<sup>13</sup>C<sub>6</sub>]glucose. When [<sup>13</sup>C<sub>6</sub>]glucose is metabolized via glycolysis, [<sup>13</sup>C<sub>3</sub>]pyruvate is generated. By oxidative decarboxylation, PDC generates [<sup>13</sup>C<sub>2</sub>]acetyl-CoA (Figure 3.2 A). Then, CS catalyzes the condensation of [<sup>13</sup>C<sub>2</sub>]acetyl-CoA and unlabelled oxaloacetate and

thereby generates [ $^{13}\text{C}_2$ ]citrate (Figure 3.2 A). Thus, the abundance of M2 citrate mass isotopologues represents PDC activity (Figure 3.2 A). Pyruvate can also enter the TCA cycle via PC which regulates TCA cycle anaplerosis and is implicated into gluconeogenesis. Further, PC catalyzes the carboxylation of [ $^{13}\text{C}_3$ ]pyruvate and generates [ $^{13}\text{C}_3$ ]oxaloacetate (Figure 3.2 B). CS condenses [ $^{13}\text{C}_3$ ]oxaloacetate with unlabelled acetyl-CoA derived from  $\beta$ -oxidation of fatty acid, or with [ $^{13}\text{C}_2$ ]acetyl-CoA derived from PDC activity and generates [ $^{13}\text{C}_3$ ]- or [ $^{13}\text{C}_5$ ]citrate, respectively (Figure 3.2 B,C). Thus, the relative abundance of M3 citrate mass isotopologues reflects PC activity while the fraction of M5 citrate mass isotopologues represents the combined activity of PC and PDC (Figure 3.2 B, C). By analysing the relative fractions of M2, M3 and M5 isotopologues of citrate we can distinguish PDC and PC mediated reactions and draw conclusions about their respective activities. To avoid bias from general mass isotopomer enrichment, we normalized the abundance of citrate isotopologues to the abundance of M3 lactate isotopologues.

In line with the differential contribution of glucose-derived carbon to citrate (Figure 3.1 A-C), we detected different PDC and PC activities in the cell lines (Figure 3.2 D-F). We found that PDC activity was lowest in HepG2 cells, while it was similar in PH5CH8 and JHH-4 cells (Figure 3.2 D). This suggests that the relative pyruvate flux through PDC was lower in HepG2 cells when compared to JHH-4 and PH5CH8 (Figure 3.2 D). Furthermore, we observed that the relative activity of PC was variable between cell lines, where HepG2 cells exposed the highest and PH5CH8 the lowest fraction of M3 citrate mass isotopologues (Figure 3.2 E). This suggested that TCA cycle anaplerosis, which is regulated by PC, was differently regulated in the cell lines. Together, our data indicated that the three cell lines have different relative PDC and PC activities, which might be explained by different expressions levels, distinct activation states and/or allosteric regulation (Figure 3.2 D-E). Despite different PDC and PC activities, the majority of pyruvate entered the TCA cycle via PDC as reflected by a 6 to 30 times higher abundance of M2 citrate isotopologues as compared to M3 citrate.

Under hypoxia, we found that in all cell lines the fraction of M2, M3 and M5 citrate isotopologues strongly decreased. This shows that PDC and PC were less active and that the glucose flux into the TCA cycle was drastically dampened (Figure 3.2 D-F). Inhibited glucose-derived carbon entry into the TCA cycle is a metabolic consequence of hypoxia and is mediated by HIF-1 $\alpha$ . HIF-1 $\alpha$  upregulates the protein kinase PDK1 and downregulates the pyruvate dehydrogenase phosphatase catalytic subunit 2 (PDP2) thereby leading to PDC phosphorylation and consequently inhibition [Kim et al., 2006, Liou et al., 2001]. We measured significant PDK1 upregulation and PDP2 downregulation under hypoxia in all cell lines (Supplemental figure A.2 A-F and A.3 A-C). PDK1 upregulation translated in PDC phosphorylation on all three serine residues (Supplemental figure A.2 A-F and A.3 A-C). Furthermore, under hypoxia, we detected significantly decreased PC activity which might be due to reduced PC expression or allosteric regulation. HIF-1 can indeed bind the promoter region of PC while it remains elusive if this stimulates or represses PC expression [Schoedel et al., 2011]. Moreover,

PC is allosterically regulated by acetyl-coA. Since acetyl-coA synthesis is drastically inhibited under hypoxia, PC activity might consequently be dampened.

To study glutamine metabolism, we employed a [ $^{13}\text{C}_5$ ]glutamine tracer. By applying this tracer we can distinguish oxidative and reductive glutamine metabolism. Under oxidative conditions, [ $^{13}\text{C}_5$ ]glutamine undergoes oxidation within the TCA cycle and [ $^{13}\text{C}_4$ ]citrate is generated (Figure 3.2 C). However, if glutamine is metabolized in a reductive manner, [ $^{13}\text{C}_5$ ]glutamine generates [ $^{13}\text{C}_5$ ]citrate (Figure 3.2 C). Therefore, M4 and M5 citrate isotopologues represent the oxidative and reductive glutamine metabolism, respectively. To avoid bias from a different glutamine influx into the TCA cycle, the relative abundance of M4 and M5 citrate isotopologues was normalized to the abundance of the M5 glutamate isotopologues.

Similar to our observation for glucose metabolism, the different cell lines exhibit differences in the relative fractions of the M4 and M5 citrate isotopologues under normoxia suggesting a cell line to cell line specific distribution of glutamine within central carbon metabolism (Figure 3.2 F-G). We found that the fraction of M5 citrate was almost equal in HepG2 and PH5CH8 cells, while JHH-4 cells metabolized much less glutamine in a reductive manner (Figure 3.2 F-G). Concerning the oxidative metabolism of glutamine, we detected the highest fraction of M4 citrate in JHH-4 cells, an intermediate fraction in PH5CH8 cells and the lowest abundance of M4 citrate isotopologues in HepG2 (Figure 3.2 F-G). This suggested that the relative proportion of glutamine that was either used for decarboxylation within the TCA cycle or the generation of lipogenic citrate varied between the cell lines. However, we observed that in all cell lines, the majority of glutamine was metabolized oxidatively, as reflected by the abundance of the M4 citrate isotopologues that was 2 to 7 times higher than the abundance of the M5 citrate isotopologues (Figure 3.2 F-G).

Under hypoxia, the fraction of the M5 citrate isotopologues increased while the abundance of the M4 citrate isotopologues decreased in all cell lines (Figure 3.2 F-G). This suggests that under hypoxia, reductive carboxylation of  $\alpha$ -ketoglutarate increases while oxidative  $\alpha$ -ketoglutarate decarboxylation decreases. Under hypoxic conditions, the majority of glutamine was metabolized in a reductive manner as reflected by a 6 to 8 times higher fraction of the M5 citrate isotopologues as compared to abundance of the M4 citrate isotopologues (Figure 3.2 F-G).

In the HCC cells lines HepG2 and JHH-4 and in the immortalized hepatocytes PH5CH8, hypoxia reduced oxidation of glucose- and glutamine-derived carbon within the TCA cycle while reductive glutamine metabolism was increased. These observations are in-line with other studies that investigated the metabolic consequences of hypoxia and show that HIF-1 $\alpha$  stabilization results in the upregulation of PDK1 which consequently inhibits PDC by phosphorylation [Kim et al., 2006]. As a result, the entry of pyruvate into the TCA cycle

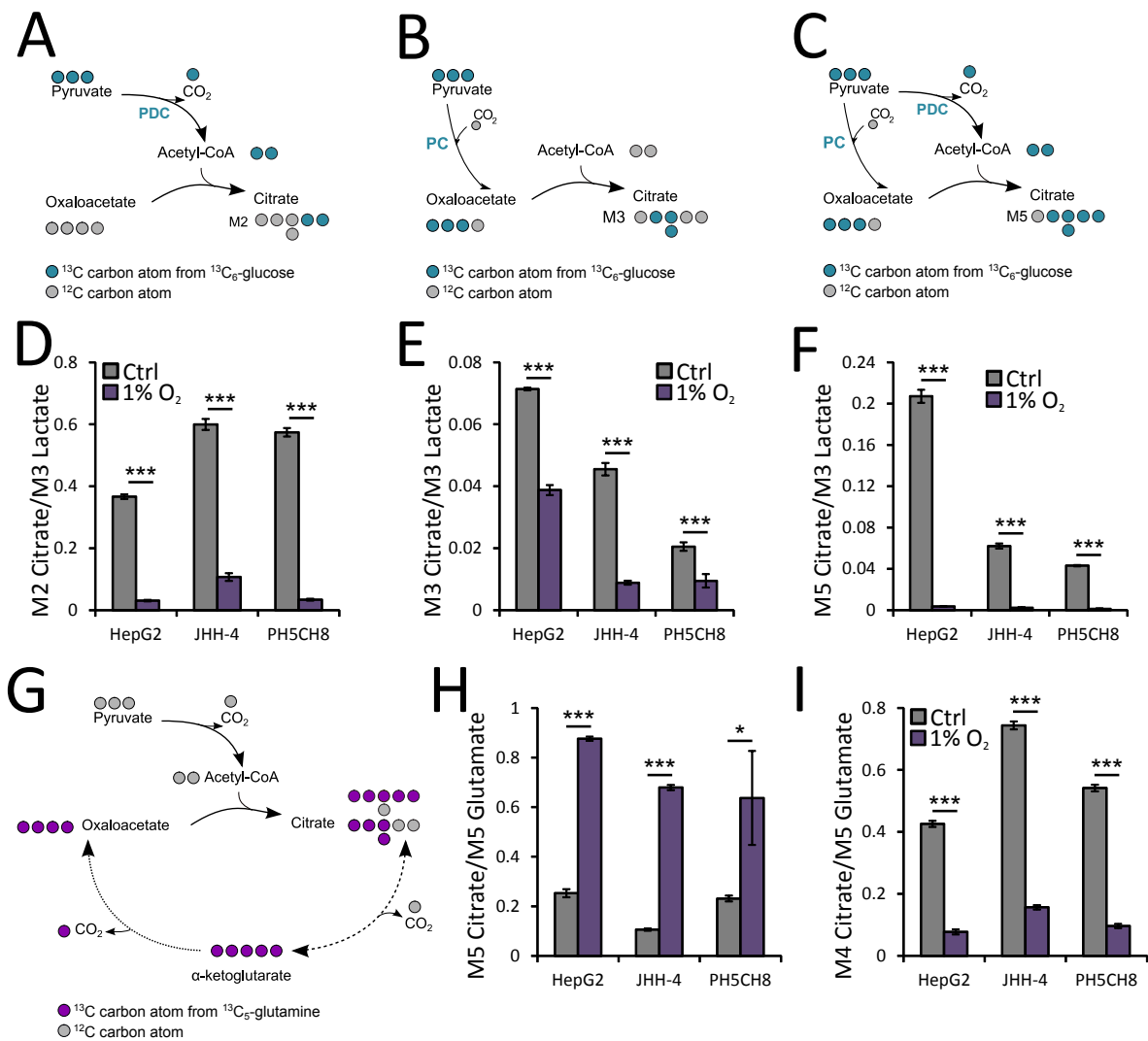


**FIGURE 3.2: Hypoxia-mediated changes in glucose and glutamine metabolism in HCC cell lines and immortalized hepatocytes.** HepG2 and JHH-4 HCC cell lines and PH5CH8 immortalized hepatocytes were grown for 36 h under normoxia (18.6%  $\text{O}_2$ ) (Ctrl) or under hypoxia (1%  $\text{O}_2$ ) in the presence of [ $^{13}\text{C}_6$ ]glucose or [ $^{13}\text{C}_5$ ]glutamine. **(A-C)** Carbon atom transitions for pyruvate carboxylase (PC) and pyruvate dehydrogenase complex (PDC) activities, from a [ $^{13}\text{C}_6$ ]glucose tracer. **(D)** PDC activity determined from the M2 citrate isotopologues normalized to the M3 lactate isotopologues, from [ $^{13}\text{C}_6$ ]glucose. **(E)** PC activity determined from the M3 citrate isotopologues normalized to the M3 lactate isotopologues, from [ $^{13}\text{C}_6$ ]glucose. **(F)** M5 isotopologues of citrate reflecting the combined carbon contribution of PC and PDC normalized to the M3 lactate isotopologues, from [ $^{13}\text{C}_6$ ]glucose. **(G)** Carbon atom transitions for oxidative and reductive glutamine metabolism, from [ $^{13}\text{C}_5$ ]glutamine. **(H)** Reductive glutamine contribution to citrate, determined by the ratio of the M5 isotopologues of citrate to M5 isotopologues of glutamate, from [ $^{13}\text{C}_5$ ]glutamine. **(I)** Oxidative glutamine contribution to citrate, determined by the ratio of the M4 isotopologues of citrate to the M5 isotopologues of glutamate, from [ $^{13}\text{C}_5$ ]glutamine. Error bars indicate the standard deviation and are calculated from at least two independent replicates. Statistical significance between control and the treatment was determined by a two-tailed t-test where \* denotes  $P \leq 0.05$ , \*\* denotes  $P \leq 0.01$ , and \*\*\* denotes  $P \leq 0.001$ .

is prohibited and consequently less citrate is generated from glucose while the generation of lipogenic citrate becomes dependent on reductive carboxylation of glutamine [Fendt et al., 2013, Metallo et al., 2011].

## 3.2 OSM-mediated metabolic effects in HCC cell lines and immortalized hepatocytes

In the previous section, I have presented HIF-1 $\alpha$ -mediated metabolic effects under hypoxia in HCC cell lines and in immortalized hepatocytes. As expected, HIF-1 $\alpha$  stabilization under hypoxic conditions results in metabolic reprogramming of cellular metabolism. Since the pro-inflammatory cytokine OSM induces HIF-1 $\alpha$  upregulation on mRNA and protein level under normoxia, we hypothesized that OSM will induce a hypoxia-like metabolic phenotype under normoxic conditions [Vollmer et al., 2009]. To investigate the metabolic effects of OSM-mediated HIF-1 $\alpha$  induction under normoxic conditions in hepatocellular carcinoma cells and immortalized hepatocytes we performed stable-isotope assisted metabolomics. We stimulated HepG2, JHH-4 and PH5CH8 for 36 h with 50 ng/mL OSM or left the cells untreated and incubated them under normoxia (18.6% O<sub>2</sub>). To profile central carbon metabolism, we employed [<sup>13</sup>C<sub>6</sub>]glucose and [<sup>13</sup>C<sub>5</sub>]glutamine.

### 3.2.1 Effects of OSM on glucose- and glutamine-derived carbon contribution to central carbon metabolism

Unlike hypoxia, OSM-stimulation did not effect glucose- nor glutamine-derived carbon contributions to citrate in the HCC cell lines HepG2 and JHH-4 (Figure 3.3 A, B). Solely in HepG2 cells, glucose-derived carbon contribution to serine and glycine was mildly reduced suggesting a decreased glucose flux to one-carbon metabolism or an increased uptake of serine from cell culture medium (Figure 3.3 A). Interestingly, in HepG2 cells a reduction of glucose-derived carbon to serine and glycine was also observed under hypoxia (Figure 3.1 A). Whereas OSM treatment had no typical hypoxia-like metabolic effects in HCC cells, we detected a significant decrease in glucose-derived carbon contribution to citrate in OSM-stimulated PH5CH8 cells (Figure 3.3 C). In line with this result, we observed an increased contribution of glutamine-derived carbon to citrate (Figure 3.3 C).

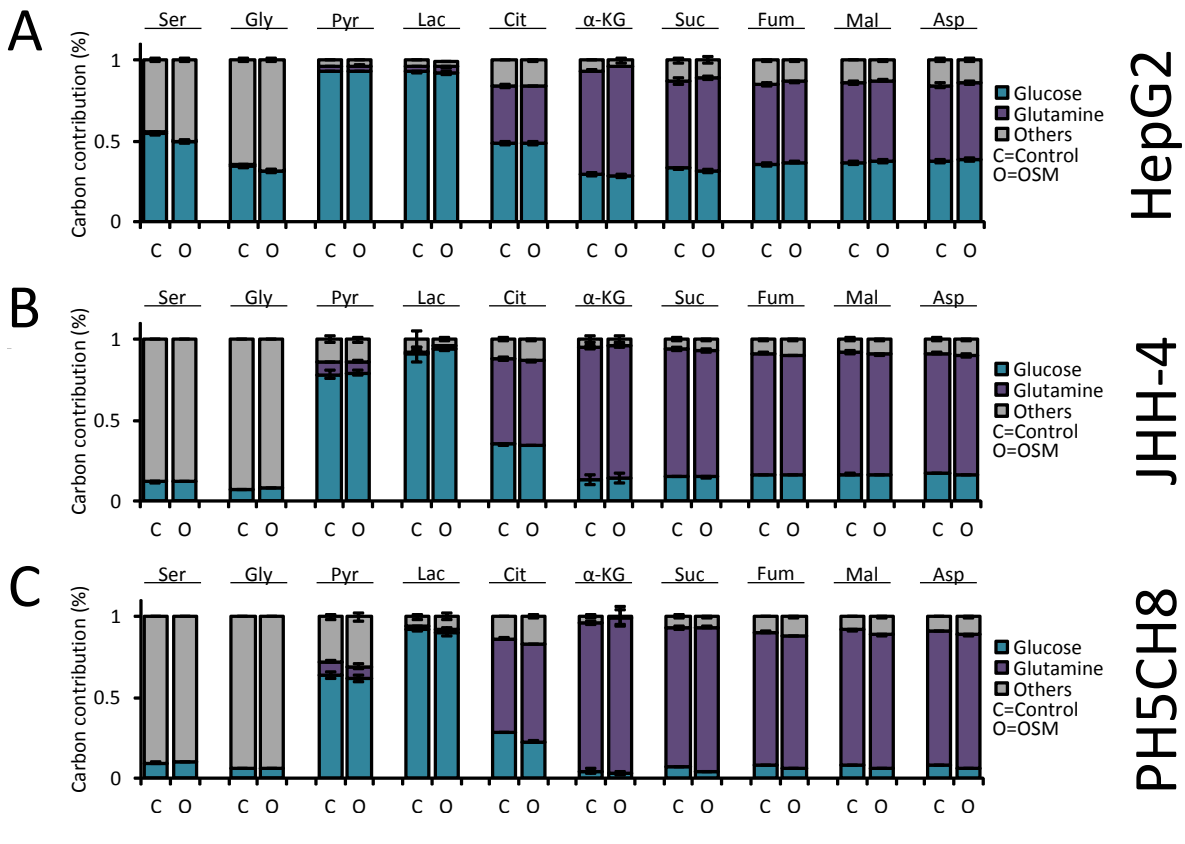


FIGURE 3.3: **OSM-mediated changes in carbon contributions in HCC cells and immortalized hepatocytes.** HepG2, JHH-4 hepatocellular carcinoma cells and PH5CH8 immortalized hepatocytes were left untreated (C) or stimulated with 50 ng/mL OSM (O) for 36 h under normoxia in presence of [ $^{13}\text{C}_6$ ]glucose or [ $^{13}\text{C}_5$ ]glutamine. Relative carbon contributions from glucose, glutamine and other (unlabelled) carbon sources to serine (Ser), glycine (Gly), pyruvate (Pyr), lactate (Lac), citrate (Cit),  $\alpha$ -ketoglutarate ( $\alpha$ -KG), succinate (Suc), fumarate (Fum), malate (Mal) and aspartate (Asp) were calculated for (A) HepG2, (B) JHH-4 and (C) PH5CH8 cells. Error bars represent the standard deviation.

### 3.2.2 Effects of OSM on glucose and glutamine metabolism

Next, we studied the entry of glucose-derived carbon into the TCA cycle. Therefore we analysed the abundance of the M2 and M3 mass isotopologues of citrate, reflecting PDC and PC activity, respectively (Figure 3.4 A-B). Correlating with our finding that OSM had no effect on the glucose-derived carbon contribution to citrate in HepG2 and JHH-4 HCC cell lines, the fraction of the M2 and M3 citrate isotopologues remained unaffected (Figure 3.4 D-E). Furthermore, we studied oxidative and reductive glutamine metabolism which is reflected by the fraction of the M4 and M5 citrate isotopologues generated from [ $^{13}\text{C}_5$ ]glutamine (Figure 3.4 C). As illustrated by unchanged fractions of M4 and M5 citrate isotopologues in these cells, OSM treatment did not effect glutamine metabolism (Figure 3.4 F-G).

However in PH5CH8 cells, we detected a significant decrease in the abundance of the M2 citrate isotopologues pointing towards decreased PDC activity (Figure 3.4 D). In conjunction

with decreased PDC activity, PH5CH8 cells secreted significantly more lactate when compared to untreated cells (Supplemental figure A.1). Furthermore, we observed a significantly decreased oxidative glutamine metabolism while reductive glutamine metabolism through IDH1 was increased by OSM stimulation (Figure 3.4 F-G).

Based on the fact that under hypoxia HIF-1 $\alpha$  mediates metabolic reprogramming via PDK1 up- and PDP2 downregulation, we analysed the expression of these two genes after OSM treatment in PH5CH8 cells. We detected a significant upregulation of PDK1 on mRNA and protein level while PDP2 expression remained unaffected (Supplemental figure A.3 A-C). Although hypoxia and OSM treatment induced similar levels of PDK1 mRNA expression, PDK1 protein expression was stronger after hypoxia (Supplemental figure A.3 A-C). Intriguingly, OSM-induced PDK1 upregulation did not translate into enhanced PDC phosphorylation which might be explained by the fact that PDP2 is not downregulated (Supplemental figure A.3 A-C).

To conclude, we observed that OSM stimulation did not induce hypoxia-like metabolic changes in the HCC cell lines HepG2 and JHH-4. In PH5CH8 immortalized hepatocytes, however, the stimulation triggered a hypoxia-like metabolic phenotype which was way less pronounced than the one induced by hypoxia. Moreover when we applied a combinatorial treatment of OSM and hypoxia in PH5CH8 cells, we did not observe further hypoxia-mediated metabolic effects (Supplemental figure A.4).

### 3.2.3 OSM-mediated HIF-1 $\alpha$ upregulation in hepatoma and hepatic cells

Based on our observation that OSM induced a hypoxia-like metabolic phenotype in immortalized hepatocytes but not in HCC cell lines, we studied HIF-1 $\alpha$  mRNA and protein expression upon OSM treatment in HepG2 and JHH-4 hepatocellular carcinoma cells and compared those to the expression in PH5CH8<sup>1</sup>. Therefore, we analysed HIF-1 $\alpha$  mRNA and protein expression levels after 8, 12, 24 and 36 h of OSM treatment, hypoxia (1% O<sub>2</sub>) or a combinatorial treatment.

In PH5CH8 cells, HIF-1 $\alpha$  mRNA and protein expression was upregulated after OSM treatment over the full length of the timecourse (Figure 3.5 A-C). 36 h after the treatment, OSM- and hypoxia-induced HIF-1 $\alpha$  protein expression reached equal levels (Figure 3.5 B-C). Despite the fact that hypoxia- and OSM-induced HIF-1 $\alpha$  protein expression was similar, hypoxia-mediated effects on cellular metabolism were much stronger than those mediated by OSM under normoxia (Figure 3.2 and figure 3.4). This suggests that in PH5CH8 cells, OSM-induced HIF-1 $\alpha$  is either less active or that other factors influence metabolism under hypoxic conditions.

---

<sup>1</sup>The data in this section has been generated by our collaborator Dr. Andreas Zimmer

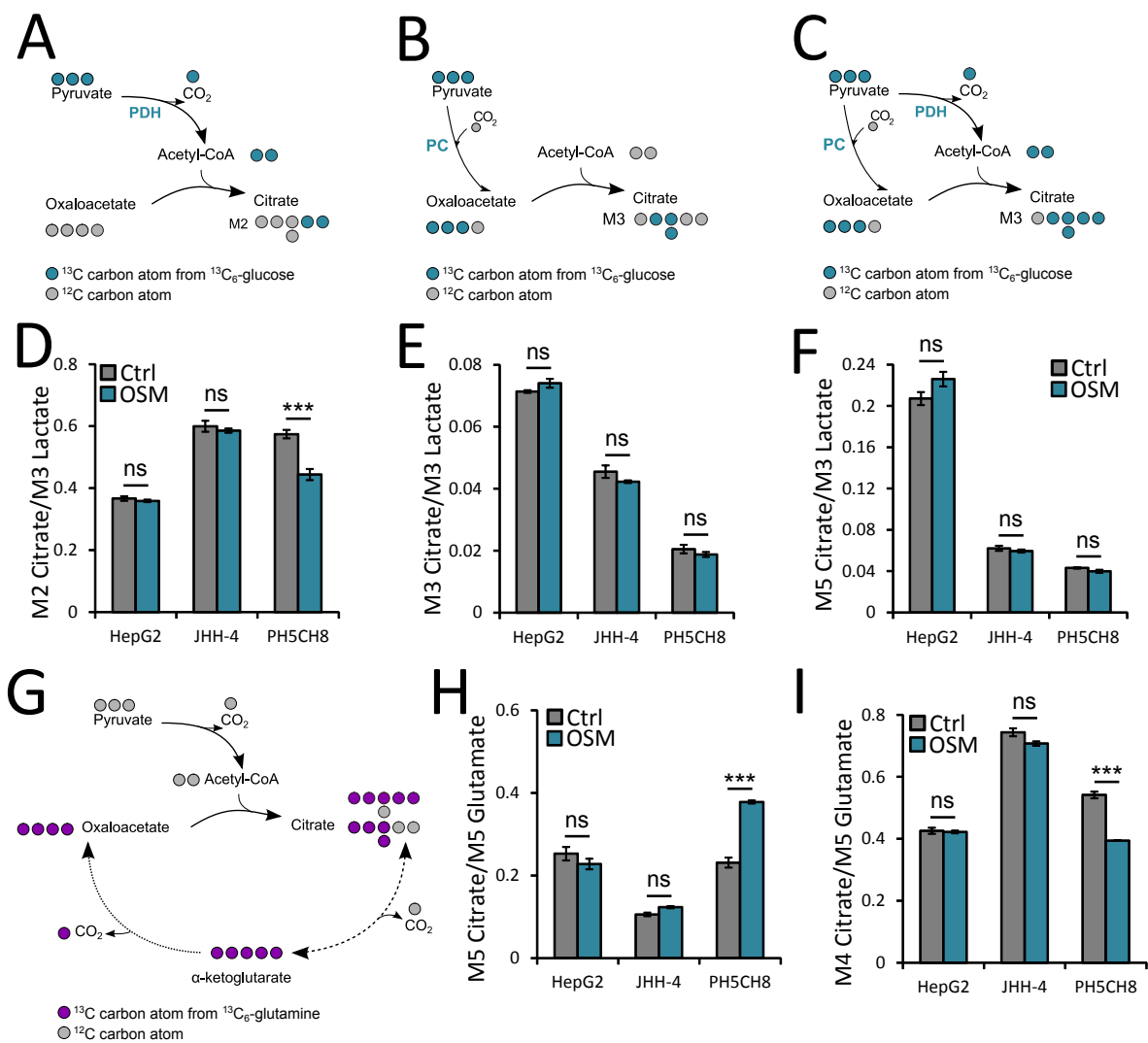


**FIGURE 3.4: OSM-mediated changes in glucose and glutamine metabolism in hepatoma cells and immortalized hepatocytes.** HepG2 and JHH-4 HCC cell lines and PH5CH8 immortalized hepatocytes were treated for 36 h with 50 ng/mL OSM under normoxia (18.6% O<sub>2</sub>) (OSM) or left untreated and grown in the presence of [<sup>13</sup>C<sub>6</sub>]glucose or [<sup>13</sup>C<sub>5</sub>]glutamine. **(A-C)** Carbon atom transitions for pyruvate carboxylase (PC) and pyruvate dehydrogenase complex (PDC) activities, [<sup>13</sup>C<sub>6</sub>]glucose. **(D)** PDC activity determined from the M2 citrate isotopologues normalized to the M3 lactate isotopologues, from [<sup>13</sup>C<sub>6</sub>]glucose. **(E)** PC activity determined from the M3 citrate isotopologues normalized to the M3 lactate isotopologues, from [<sup>13</sup>C<sub>6</sub>]glucose. **(F)** M5 isotopologues of citrate reflecting the combined carbon contribution of PC and PDC normalized to the M3 lactate isotopologues, from [<sup>13</sup>C<sub>6</sub>]glucose. **(G)** Carbon atom transitions for oxidative and reductive glutamine metabolism, [<sup>13</sup>C<sub>5</sub>]glutamine. **(H)** Reductive glutamine contribution to citrate, determined by the ratio of the M5 isotopologues of citrate to the M5 isotopologues of glutamate, from [<sup>13</sup>C<sub>5</sub>]glutamine. **(I)** Oxidative glutamine contribution to citrate, determined by the ratio of the M4 isotopologues of citrate to the M5 isotopologues of glutamate, from [<sup>13</sup>C<sub>5</sub>]glutamine. Error bars indicate the standard deviation and are calculated from at least two independent replicates. Statistical significance between control and the treatment was determined by a two-tailed t-test where \* denotes P ≤ 0.05, \*\* denotes P ≤ 0.01, and \*\*\* denotes P ≤ 0.001.



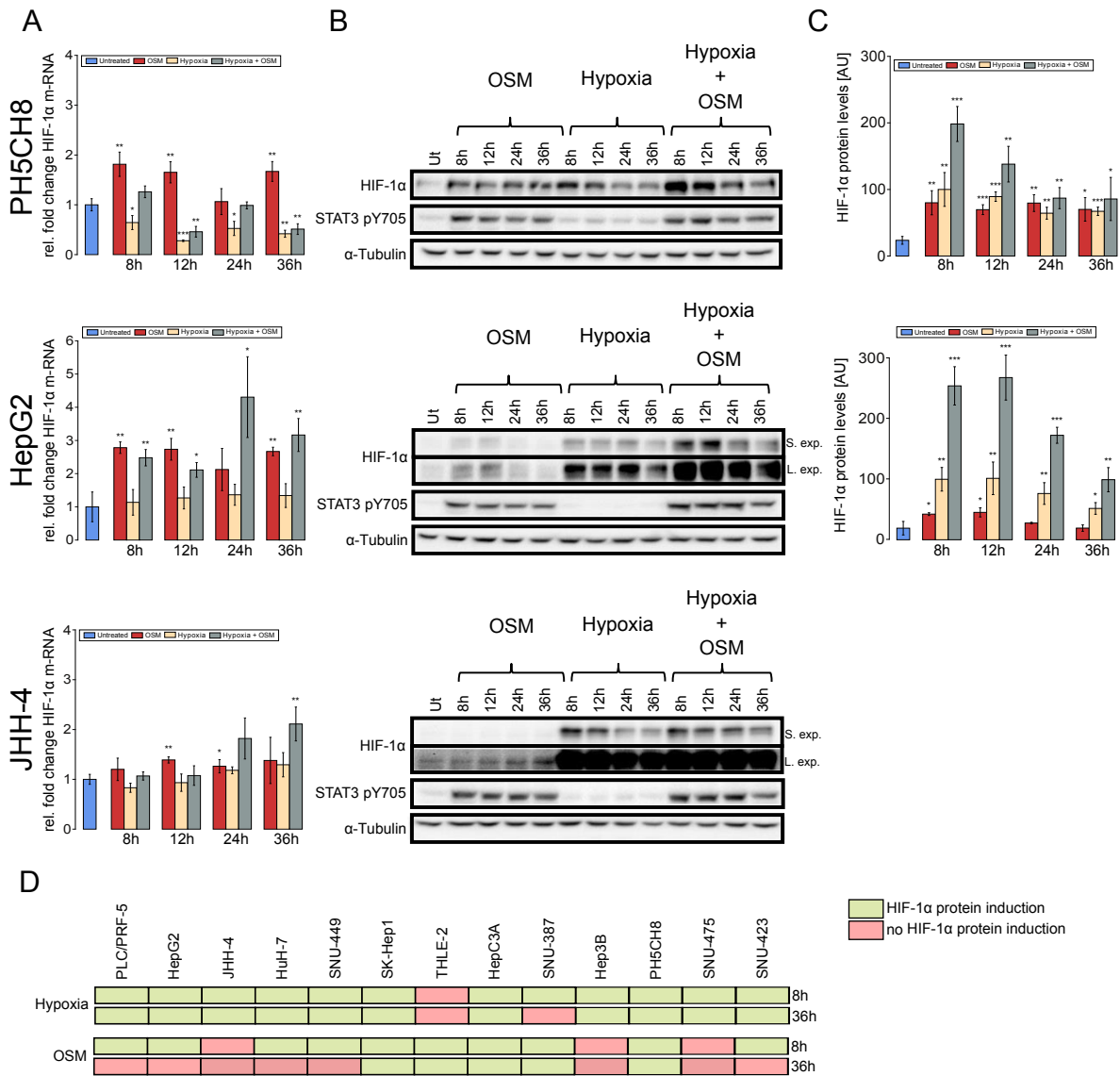


**FIGURE 3.5: The effect of OSM on HIF-1 $\alpha$  expression in PH5CH8 immortalized hepatocytes and HepG2 and JHH-4 hepatoma cells.** HepG2, JHH-4 and PH5CH8 cells were treated with 50 ng/ml OSM, hypoxia (1% O<sub>2</sub>), or a combinatorial treatment for 8, 12, 24 and 36 h. **(A)** qPCR on HIF-1 $\alpha$  mRNA expression. The fold change was calculated relative to the untreated control. Error bars represent the standard deviation of three biological replicates. **(B)** Western Blot on HIF-1 $\alpha$ .  $\alpha$ -Tubulin was used as a loading control, and one representative blot for  $\alpha$ -Tubulin is shown. S. Exp. = short exposure; L. Exp. = long exposure. **(C)** Quantification of HIF-1 $\alpha$  protein levels in HepG2 and PH5CH8 cells. Error bars indicate the standard deviation and are calculated from at least three independent replicates. Statistical significance between control and the treatment was determined by a two-tailed t-test where \* denotes  $P \leq 0.05$ , \*\* denotes  $P \leq 0.01$ , and \*\*\* denotes  $P \leq 0.001$ . Figure published in [Battello et al., 2016] This data was kindly provided by Dr. Andreas Zimmer.

In HepG2 cells, HIF-1 $\alpha$  mRNA was upregulated by OSM treatment under normoxia over the entire time course (Figure 3.5 A). However, increased mRNA levels did not translate into increased HIF-1 $\alpha$  protein levels at later stimulation time points. In HepG2 cells, OSM-mediated HIF-1 $\alpha$  protein induction peaks between 8 and 12 h and decreases between 24 and 36 h (Figure 3.5 B-C). This suggests that OSM-induced HIF-1 $\alpha$  proteins underwent degradation under normoxia at longer stimulation time points. Interestingly, we observed that a combinatorial treatment of OSM and hypoxia over 24 and 36 h led to higher HIF-1 $\alpha$  protein levels than hypoxia alone. Thus, OSM-induced HIF-1 $\alpha$  proteins probably underwent oxygen-dependent degradation, while they were stabilized under hypoxic conditions and thus further increased HIF-1 $\alpha$  protein levels. While OSM stimulation under hypoxia further increased HIF-1 $\alpha$  protein expression, we did not detect a more pronounced hypoxic metabolic phenotype (Supplemental figure A.4).

In JHH-4 cells, OSM-mediated HIF-1 $\alpha$  mRNA upregulation was transient and very mild, reaching a maximum between 8 and 12 h (Figure 3.5 A) while HIF-1 $\alpha$  protein levels were barely detectable and remained unaffected by OSM treatment (Figure 3.5 B-C). This observation implied that in JHH-4 cells, HIF-1 $\alpha$  protein expression cannot be induced by OSM-mediated STAT3 activation.

Based on the finding that OSM-induced HIF-1 $\alpha$  upregulation is transient in HepG2 cells we screened 11 HCC cell lines and 2 non-neoplastic hepatocyte cell lines, 8 hours and 36 hours after OSM treatment or exposure to hypoxia (1% O<sub>2</sub>). In 10 out of 13 cell lines, we detected HIF-1 $\alpha$  protein induction within the first 8 hours after stimulation, whereas after 36 hours, we detected OSM-induced HIF-1 $\alpha$  in 5 out of 13 cell lines (Figure 3.5 D). In almost all cell lines we observed a continuous and strong HIF-1 $\alpha$  induction by hypoxia (Figure 3.5 D).

In summary, these data suggested that OSM-mediated HIF-1 $\alpha$  protein induction is transient and restricted to early stimulation time-points in many HCC cell lines. Based on this finding the question rises whether cytokine-induced HIF-1 $\alpha$  induction is required for metabolic reprogramming at early stimulation time points.

### **3.2.4 OSM does not induce metabolic changes in HepG2-C3A and SK-Hep1 HCC cells despite HIF-1 $\alpha$ induction**

Based on the previously described results, we aimed to study the effects of OSM on the metabolism of HepG2-C3A and SK-Hep1 HCC cell lines since we detected a strong induction of HIF-1 $\alpha$  protein over the whole period of OSM treatment (Figure 3.6 A, F ). Therefore, we stimulated HepG2-C3A and SK-Hep1 cells for 8 and 36 hours with 50 ng/mL OSM and conducted metabolic tracer experiments using [<sup>13</sup>C<sub>6</sub>]glucose and [<sup>13</sup>C<sub>5</sub>]glutamine. Our results show that, strong OSM-mediated HIF-1 $\alpha$  protein inductions did not result in drastic activity

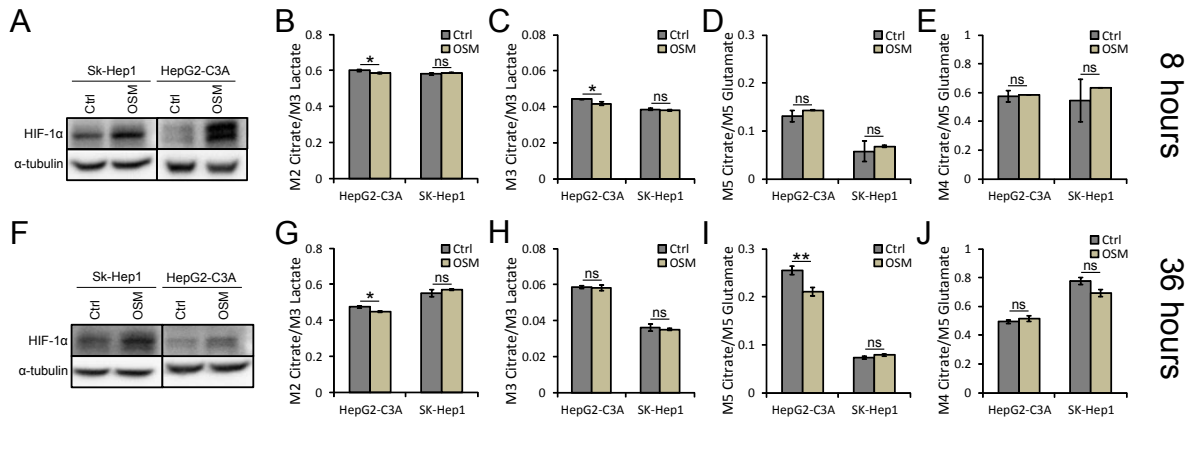


**FIGURE 3.6: OSM-mediated metabolic effects in Sk-Hep1 and HepG2-C3A HCC cell lines.** Sk-Hep1 and HepG2-C3A HCC cell lines were stimulated for 8 and 36 h with 50 ng/mL OSM or left untreated and grown in the presence of [ $^{13}\text{C}_6$ ]glucose or [ $^{13}\text{C}_5$ ]glutamine. (A) Westernblot on HIF-1 $\alpha$ . (B, G) PDC activity determined from the M2 citrate isotopologues normalized to the M3 lactate isotopologues, from [ $^{13}\text{C}_6$ ]glucose. (C, H) PC activity determined from the M3 citrate isotopologues normalized to the M3 lactate isotopologues, from [ $^{13}\text{C}_6$ ]glucose. (D, I) Reductive glutamine contribution to citrate, determined by the ratio of M5 isotopologues of citrate to M5 isotopologues of glutamate, from [ $^{13}\text{C}_5$ ]glutamine. (E, J) Oxidative glutamine contribution to citrate, determined by the ratio of the M4 isotopologues of citrate to M5 isotopologues of glutamate, from [ $^{13}\text{C}_5$ ]glutamine. Error bars indicate the standard deviation and are calculated from at least two independent replicates. Statistical significance was determined by a two-tailed t-test. \* denotes  $P \leq 0.05$ , \*\* denotes  $P \leq 0.01$ , and \*\*\* denotes  $P \leq 0.001$ . Westernblots were generated by our collaborator Dr. Andreas Zimmer

changes of PDC and PC (Figure 3.6 B-C, G-H). Furthermore, we did not observe hypoxia-like metabolic changes within glutamine metabolism (Figure 3.6 D-E, I-J). Solely in HepG2-C3A cells we detected a decreased abundance of M5 citrate isotopologues pointing towards a decreased reductive glutamine metabolism after a 36 h OSM treatment. This effect was the contrary to what we would have expected from HIF-1 $\alpha$  and furthermore was not observed after a 8 h OSM stimulation (Figure 3.6 D-E, I-J).

These results demonstrated that despite its induction, HIF-1 $\alpha$  did not induce hypoxia-like metabolic changes within central carbon metabolism in the HCC cell lines HepG2-C3A and Sk-Hep. These data suggest that OSM-induced HIF-1 $\alpha$  might either be fully inactive under the given conditions or participate in the regulation of cellular functions other than the metabolism.

### 3.2.5 OSM-mediated metabolic effects in PH5CH8 cells are concentration dependent

Based on our finding that OSM treatment leads to a hypoxia-like metabolic phenotype in PH5CH8 cells, we studied if these effects are concentration dependent. For that purpose,

we stimulated PH5CH8 cells with 10, 25 and 50 ng/mL OSM for 36 h. In line with a dose dependent increase of HIF-1 $\alpha$  protein levels (Figure 3.7 A), we observed that the strength of the metabolic effects is indeed dependent on the concentration (Figure 3.7 B-E). While OSM-mediated metabolic effects on PDC activity (Figure 3.7 B) and on glutamine metabolism (Figure 3.7 D-E) were strongest with the highest OSM concentration, significant changes in glucose and glutamine metabolism could already be detected with 10 ng/mL OSM.

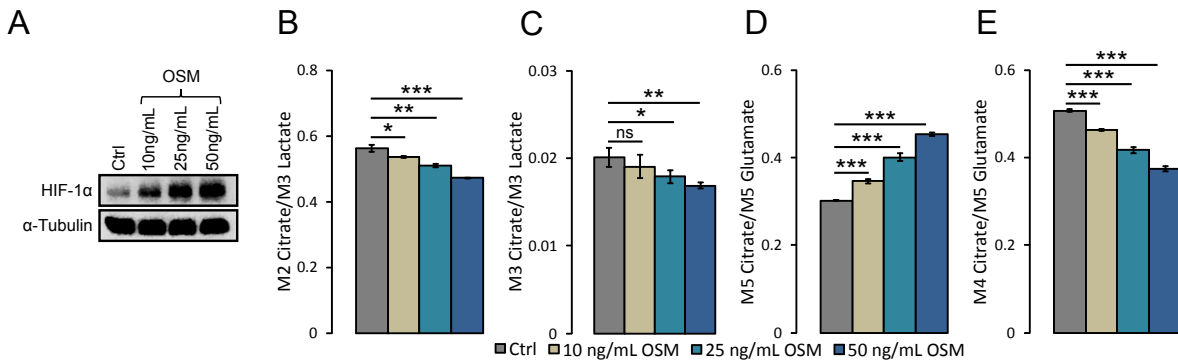


**FIGURE 3.7: OSM-mediated metabolic changes in PH5CH8 are concentration-dependent.** PH5CH8 immortalized hepatocytes were stimulated for 36 h with 10, 25 and 50 ng/mL OSM or left untreated and grown in the presence of [ $^{13}\text{C}_6$ ]glucose or [ $^{13}\text{C}_5$ ]glutamine. **(A)** Western blot on HIF-1 $\alpha$ . **(B)** PDC activity determined from the M2 citrate isotopologues normalized to the M3 lactate isotopologues, from [ $^{13}\text{C}_6$ ]glucose. **(C)** PC activity determined from the M3 citrate isotopologues normalized to the M3 lactate isotopologues, from [ $^{13}\text{C}_6$ ]glucose. **(D)** Reductive glutamine contribution to citrate, determined by the ratio of the M5 isotopologues of citrate to the M5 isotopologues of glutamate, from [ $^{13}\text{C}_5$ ]glutamine. **(E)** Oxidative glutamine contribution to citrate, determined by the ratio of the M4 isotopologues of citrate to the M5 isotopologues of glutamate, from [ $^{13}\text{C}_5$ ]glutamine. Error bars indicate the standard deviation and are calculated from at least two independent replicates. Statistical significance between control and the treatment was determined by a two-tailed t-test. \* denotes  $P \leq 0.05$ , \*\* denotes  $P \leq 0.01$ , and \*\*\* denotes  $P \leq 0.001$ .

### 3.2.6 OSM-mediated metabolic effects in PH5CH8 cells are HIF-1 $\alpha$ dependent

To verify that the hypoxia-like metabolic effects observed in OSM-stimulated PH5CH8 cells are indeed dependent on HIF-1 $\alpha$  we performed an siRNA-mediated HIF-1 $\alpha$  knockdown in OSM-treated PH5CH8 cells under normoxia and hypoxia and profiled central carbon metabolism with [ $^{13}\text{C}_6$ ]glucose and [ $^{13}\text{C}_5$ ]glutamine<sup>2</sup>.

Silencing HIF-1 $\alpha$  under normoxia already effected the metabolism of unstimulated PH5CH8 cells. We observed that upon HIF-1 $\alpha$  knockdown PC activity increased while PDC activity remained unaffected (Figure 3.8 A-B). At the same time we observed a very mild increase

<sup>2</sup>The data in this section was generated by Carole Goebel as part of her Master thesis

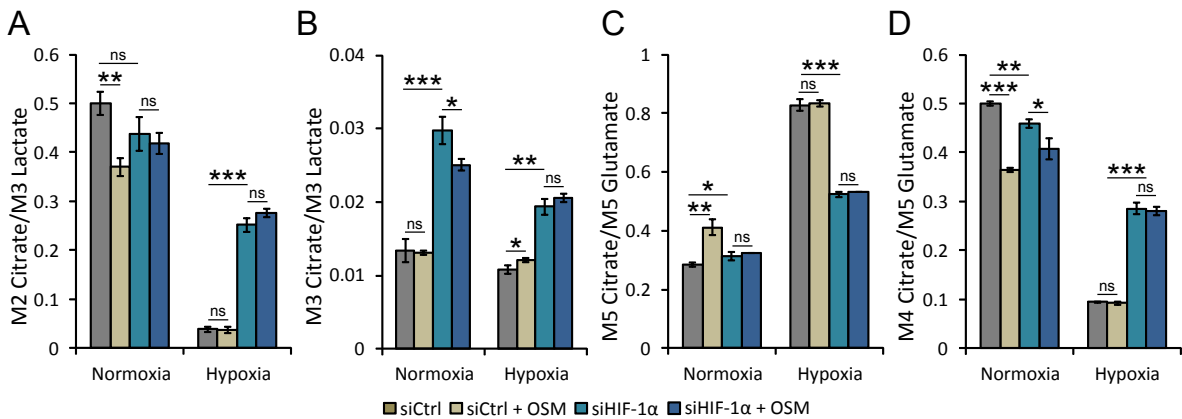


**FIGURE 3.8: The metabolic effects of HIF-1 $\alpha$  silencing on the OSM-induced hypoxia-like metabolic phenotype in PH5CH8.** A siRNA-mediated HIF-1 $\alpha$  knockdown (siHIF-1 $\alpha$ ) was performed in PH5CH8 cells grown under normoxia or hypoxia. A non-targeting siRNA (siCtrl) was used as control. PH5CH8 cells were stimulated for 36 h with 50 ng/mL OSM or left untreated and grown in the presence of [ $^{13}\text{C}_6$ ]glucose or [ $^{13}\text{C}_5$ ]glutamine. **(A)** The enzymatic activity of PDC determined from the M2 citrate isotopologues normalized to the M3 lactate isotopologues, from [ $^{13}\text{C}_6$ ]glucose. **(B)** PC activity determined from the M3 citrate isotopologues normalized to the M3 lactate isotopologues, from [ $^{13}\text{C}_6$ ]glucose. **(C)** Reductive glutamine metabolism, determined by the ratio of the M5 isotopologues of citrate to the M5 isotopologues of glutamate, from [ $^{13}\text{C}_5$ ]glutamine. **(D)** Oxidative glutamine metabolism, determined by the ratio of the M4 isotopologues of citrate to the M5 isotopologues of glutamate, from [ $^{13}\text{C}_5$ ]glutamine. Error bars indicate the standard deviation and are calculated from at least two independent replicates. Statistical significance between control and the treatment was determined by a two-tailed t-test. \* denotes  $P \leq 0.05$ , \*\* denotes  $P \leq 0.01$ , and \*\*\* denotes  $P \leq 0.001$ .

in reductive glutamine metabolism while oxidative glutamine metabolism was slightly decreased (Figure 3.8 C-D). These data suggest that HIF-1 $\alpha$  might have some metabolic effects, although HIF-1 $\alpha$  protein expression was low under normoxia and barely detectable on a Western blot.

Furthermore we found that HIF-1 $\alpha$  knockdown under hypoxic conditions results in a partial recovery of the typical hypoxia-mediated metabolic effects. We observed that the pyruvate flux through PDC was enhanced, the reductive glutamine metabolism was decreased while oxidative glutamine metabolism was increased (Figure 3.8 C-F). While HIF-1 $\alpha$  silencing under hypoxic conditions partially recovered the hypoxia-mediated phenotype, a normoxic metabolic phenotype could not be restored. While we cannot exclude that the HIF-1 $\alpha$  silencing efficiency was insufficient, it is more probably that other limiting factors, such as the oxygen availability itself prevent a full recovery. Unlike for hypoxia-mediated metabolic effects, we found that silencing HIF-1 $\alpha$  in OSM-treated PH5CH8 cells under normoxia led to an almost completely abolished OSM-mediated metabolic response (Figure 3.8 C-F).

Contrarily to our observations in HCC cell lines, these findings support the hypothesis that OSM induces hypoxia-like metabolic effects via HIF-1 $\alpha$  protein induction in immortalized hepatocytes. To this point, the exact difference between OSM-mediated HIF-1 $\alpha$  induction in

HCC cells and in immortalized hepatocytes remains to be clarified. Furthermore we showed that the mechanisms underlying OSM- and hypoxia-induced metabolic changes shared the common feature of HIF-1 $\alpha$  induction, while other factors might further contributed to the strong metabolic effects under hypoxia.

### 3.2.7 OSM-induced metabolic effects are partially dependent on PDK1

Under hypoxia, the HIF-1 $\alpha$  target gene PDK1 coordinates the metabolic switch from oxidative phosphorylation towards a more glycolytic metabolism. [Kim et al., 2006, Papandreou et al., 2006, Roche et al., 2001]. We were interested to validate whether PDK1 also plays a role in the mediation of the OSM-induced metabolic phenotype. As previously described, OSM-stimulation resulted in PDK1 upregulation which however did not translate into differential PDC phosphorylation in PH5CH8 cells (Section 3.2.3).

In PH5CH8 immortalized hepatocytes we showed that HIF-1 $\alpha$  silencing reduced PDK1 expression under normoxia and hypoxia and furthermore prevented OSM-mediated PDK1 upregulation (Figure 3.9 A). This proved that PDK1 expression is at least partially under the control of HIF-1 $\alpha$  in these cells. Furthermore, we observed that PDK1 silencing abolished both OSM- and hypoxia-mediated PDK1 upregulation on mRNA and protein level (Figure 3.9 B-C).

When we silenced PDK1 under normoxia, glucose-derived carbon contribution to citrate increased by 14%, underlining a high influx of glucose-derived carbon into the TCA cycle (Figure 3.9 G). In line, we observed that PDC activity was increased as reflected, in this particular case, by an increased fraction of M4 citrate isotopologues. The very high influx of fully labelled acetyl-coA into the TCA cycle consequently generated a high relative fraction of M2 oxaloacetate isotopologues which in turn were condensed with fully labelled acetyl-coA, thus increasing the abundance of M4 citrate isotopologues (Figure 3.9 G). As a consequence of increased isotopic enrichment of the TCA cycle intermediates and in particular oxaloacetate, the relative proportion of unlabelled oxaloacetate was diminished and thus the relative fraction of M2 citrate decreased (Figure 3.9 E, G). Furthermore, we measured an increased abundance of M3 citrate isotopologues when PDK1 was silenced which suggested that PC was allosterically regulated by increased acetyl-coA levels (Figure 3.9 E, G). Moreover, we observed that following PDK1 silencing the fraction of the M5 citrate isotopologues was increased thus further providing evidence for the increased influx of pyruvate into the TCA cycle (Figure 3.9 F). PDK1 silencing in HCC cell lines had similar effects on glucose metabolism (Supplemental figure A.5).

In addition to its effects on glucose metabolism, we observed that silencing PDK1 under normoxia had a impact on glutamine metabolism. We measured that reductive glutamine

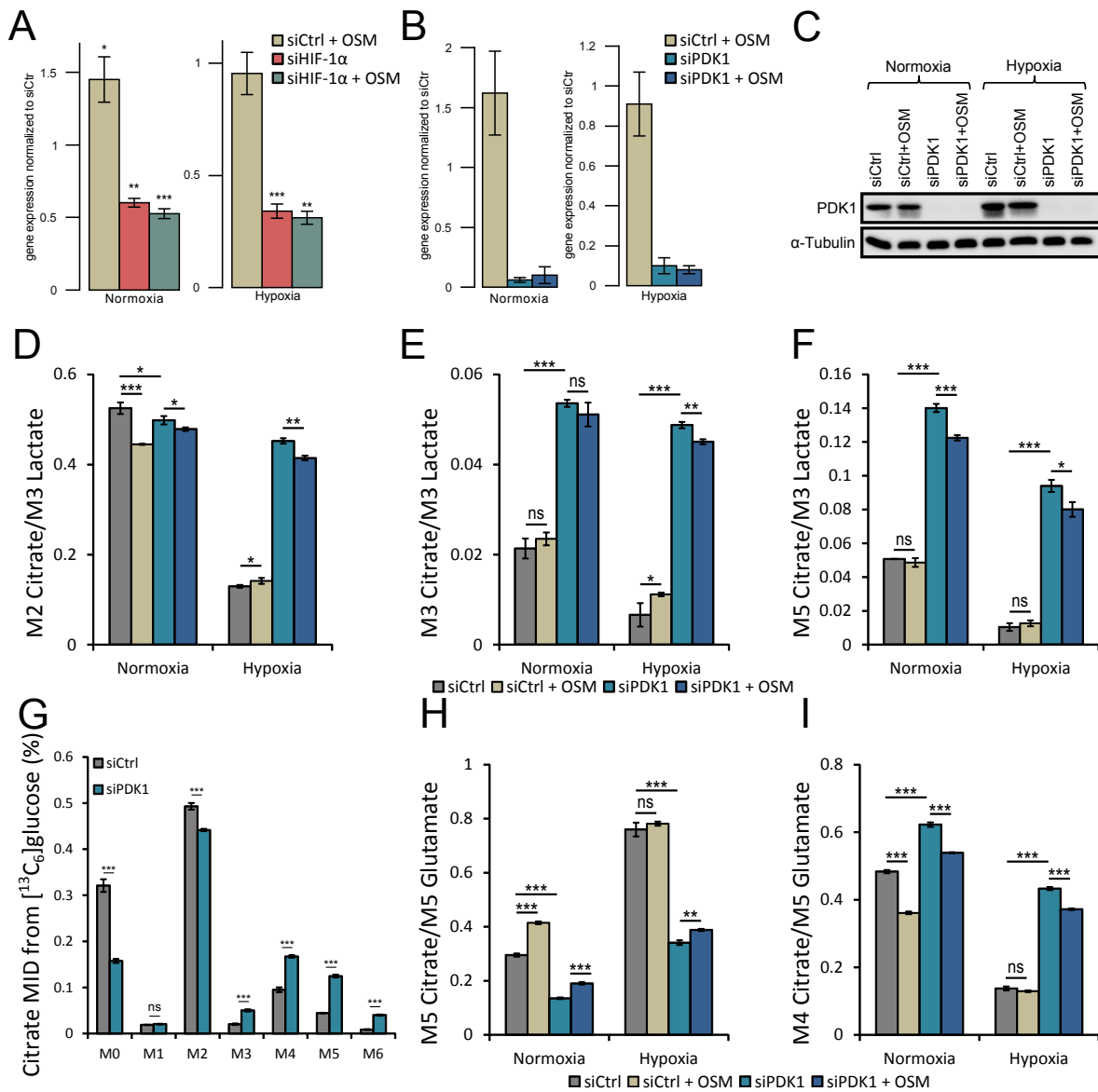
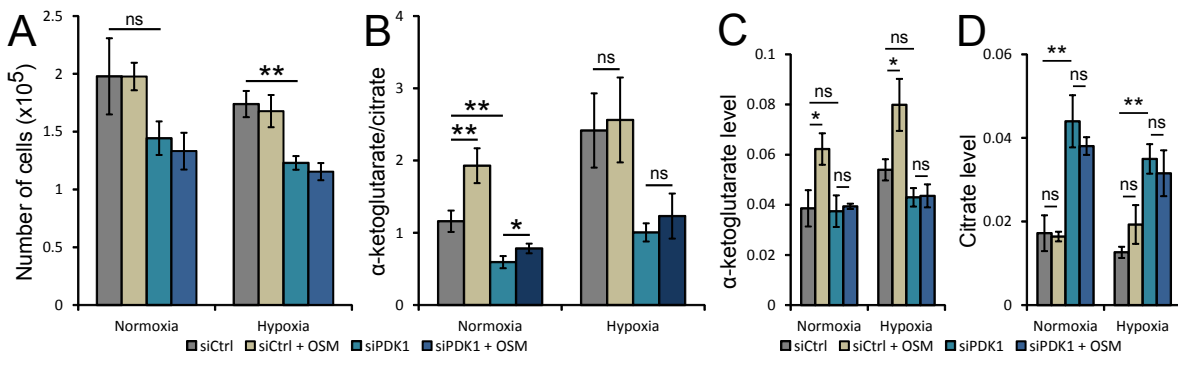


FIGURE 3.9: The metabolic effects of PDK1 silencing on the OSM-induced hypoxia-like metabolic phenotype in PH5CH8. SiRNA-mediated PDK1 knockdown (siPDK1) was performed on PH5CH8 cells grown under normoxia or hypoxia. A non-targeting siRNA (siCtrl) was used as control. PH5CH8 cells were stimulated for 36 h with 50 ng/mL OSM or left untreated and grown in the presence of [ $^{13}\text{C}_6$ ]glucose or [ $^{13}\text{C}_5$ ]glutamine. (A) qPCR on PDK1 under HIF-1 $\alpha$  knockdown conditions (B) qPCR on PDK1 under PDK1 knockdown conditions (C) Westernblot on PDK1 (D) The enzymatic activity of PDC determined from the M2 citrate isotopologues normalized to the M3 lactate isotopologues, from [ $^{13}\text{C}_6$ ]glucose. (E) PC activity determined from the M3 citrate isotopologues normalized to the M3 lactate isotopologues, from [ $^{13}\text{C}_6$ ]glucose. (F) Combined PDC and PC activities determined from the M5 citrate isotopologues normalized to the M3 lactate isotopologues, from [ $^{13}\text{C}_6$ ]glucose. (G) Citrate MID from [ $^{13}\text{C}_6$ ]glucose. (H) Reductive glutamine contribution to citrate, determined by the ratio of M5 isotopologues of citrate to M5 isotopologues of glutamate, from [ $^{13}\text{C}_5$ ]glutamine. (I) Oxidative glutamine contribution to citrate, determined by the ratio of M4 isotopologues of citrate to M5 isotopologues of glutamate, from [ $^{13}\text{C}_5$ ]glutamine. Error bars indicate the standard deviation and are calculated from at least two independent replicates. Statistical significance between control and the treatment was determined by a two-tailed t-test. \* denotes  $P \leq 0.05$ , \*\* denotes  $P \leq 0.01$ , and \*\*\* denotes  $P \leq 0.001$ .

metabolism has inhibited while oxidative glutamine metabolism was enhanced (Figure 3.9 H, I).

When we silenced PDK1 under hypoxic conditions, we observed drastic effects on cellular metabolism, underlining its strong regulatory potential. We measured a drastic increase of the glucose flux through PDC and PC (Figure 3.9 D-F) while reductive glutamine metabolism was inhibited and oxidative decarboxylation of glutamine increased (Figure 3.9 H-I).

As a consequence of PDK1 silencing in OSM-treated PH5CH8 cells, we attenuated OSM-mediated metabolic effects. While OSM-induced reduced PDC activity and OSM-mediated changes in glutamine metabolism were impaired when PDK1 was silenced, they were not fully abolished. This suggests that either the PDK1 knockdown was insufficient or that yet other regulators are involved (Figure 3.9 D-F). Taken together, our results show that PDK1 is necessary to mediate OSM-induced metabolic reprogramming, while we cannot exclude that yet other HIF-1 $\alpha$  target genes are involved.



**FIGURE 3.10: The metabolic effects of PDK1 silencing on cell proliferation and intracellular metabolite levels.** SiRNA-mediated PDK1 knockdown (siPDK1) was performed on PH5CH8 cells grown under normoxia or hypoxia. A non-targeting siRNA (siCtrl) was used as control. PH5CH8 cells were stimulated for 36 h with 50 ng/mL OSM or left untreated. **(A)** Effects of PDK1 silencing on the proliferation of PH5CH8 cells **(B)**  $\alpha$ -ketoglutarate to citrate ratio. Intracellular metabolite levels of **(C)**  $\alpha$ -ketoglutarate and **(D)** citrate. GC-MS derived signal intensities were normalized to the internal standard and to cell count. Error bars indicate the standard deviation and are calculated from at least two independent replicates. Statistical significance between control and the treatment was determined by a two-tailed t-test. \* denotes  $P \leq 0.05$ , \*\* denotes  $P \leq 0.01$ , and \*\*\* denotes  $P \leq 0.001$ .

Finally, we were interested if PDK1 silencing affects cell proliferation and intracellular metabolites levels. We observed that PDK1 silencing significantly affected cell proliferation under hypoxia underlying the importance of PDK1 under low oxygen tension (Figure 3.10 A). Next we analysed intracellular metabolite levels and were especially interested in the ratio between intracellular  $\alpha$ -ketoglutarate and citrate levels. The ratio between these two metabolites was shown to be determinative to induce reductive glutamine metabolism [Fendt et al., 2013] where an increase in  $\alpha$ -ketoglutarate to citrate ratios correlates with an increase in reductive



glutamine metabolism. First we considered intracellular  $\alpha$ -ketoglutarate and citrate levels individually. Both, hypoxia and OSM treatment led to increased intracellular  $\alpha$ -ketoglutarate levels while citrate levels remained unchanged (Figure 3.10 C). When we silenced PDK1, OSM and hypoxia induced increased  $\alpha$ -ketoglutarate levels dropped while intracellular citrate levels increased (Figure 3.10 C, D). Both, OSM stimulation and hypoxia led to increased  $\alpha$ -ketoglutarate to citrate ratios supporting our finding that reductive glutamine metabolism is induced (Figure 3.10 B). Silencing PDK1 abolished both the OSM- and the hypoxia-mediated increase in  $\alpha$ -ketoglutarate to citrate ratios (Figure 3.10 B). These results reinforce our finding that OSM induces reductive glutamine carboxylation and show that PDK1 is crucial regulator, both under normoxic and under hypoxic conditions.

### 3.2.8 Oncostatin-M induces a hypoxia-like metabolic phenotype in other PH5CH clones

Next, we aimed to validate that OSM-mediated hypoxia-like metabolic changes are not restricted to PH5CH8 cells. Therefore we performed OSM stimulation and PDK1 silencing in conjunction with metabolic tracer analysis in the PH5CH clones PH5CH1 and PH5CH7 under normoxic conditions. We validated that HIF-1 $\alpha$  and PDK1 expressions were increased in response to OSM treatment in both PH5CH clones (Supplemental figure A.6 A, B and supplemental figure A.7 A, B ) and validated the efficiency of the PDK1 knockdown on protein level (Figure 3.11 A).

We observed in both PH5CH clones, that OSM stimulation decreased glucose-derived carbon contribution to citrate due to a reduced activity of PDC (Figure 3.11 B,C and Figure 3.11 D,E). PDK1 silencing in PH5CH1 and PH5CH7 immortalized hepatocytes abolished OSM-mediated effects on PDC activity (Figure 3.11 D-E). Comparable to PH5CH8 cells, PH5CH1 and PH5CH7 cell lines reacted to OSM treatment with a decrease in oxidative glutamine metabolism while a higher proportion of glutamine undergoes reductive carboxylation. By silencing PDK1, OSM-mediated metabolic effects on glutamine metabolism were dampened but not fully abolished (Figure 3.11 G-F). Similar to PH5CH8, OSM stimulation led to increased  $\alpha$ -ketoglutarate to citrate ratios in PH5CH1 and PH5CH7 immortalized hepatocytes, while this effect could be abolished when PDK1 was silenced (Figure 3.11 H). We can conclude that OSM-mediated metabolic reprogramming is a more common feature and can be observed in all tested PH5CH clones.

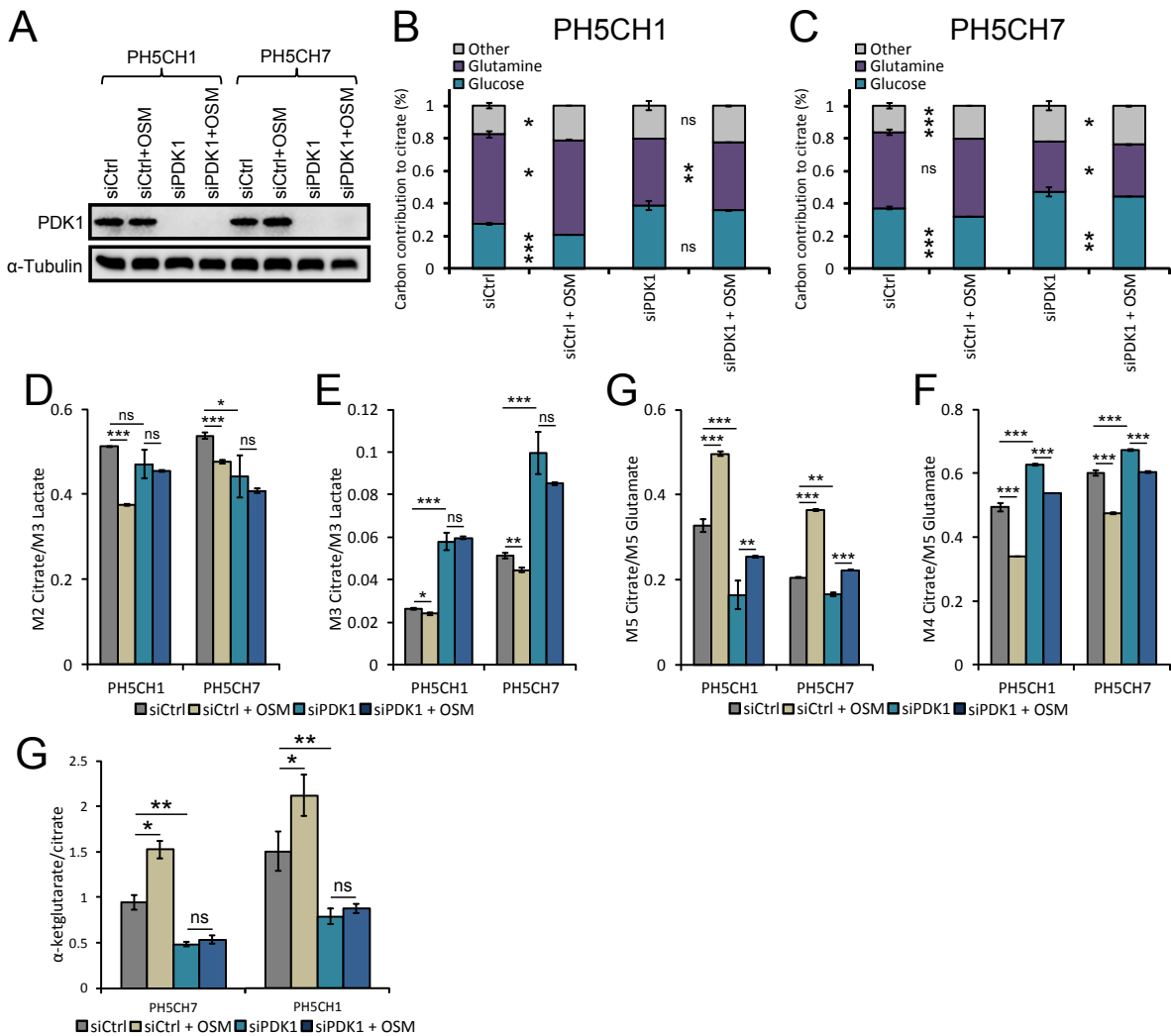


**FIGURE 3.11: The metabolic effects of PDK1 silencing on the OSM-induced hypoxia-like metabolic phenotype in PH5CH1 and PH5CH7 cells.** PH5CH1 and PH5CH7 immortalized hepatocytes were stimulated for 36 h with 50 ng/mL OSM or left untreated in the presence of  $[^{13}\text{C}_6]$ glucose or  $[^{13}\text{C}_5]$ glutamine. PDK1 was knocked down using siRNA (siPDK1) while non-targeting siRNA was used as control (siCtrl). **(A)** qPCR on PDK1. **(B)** PDK1 Westernblot. **(C)** The enzymatic activity of PDC determined from the M2 citrate isotopologues normalized to the M3 lactate isotopologues, from  $[^{13}\text{C}_6]$ glucose. **(D)** PC activity determined from the M3 citrate isotopologues normalized to the M3 lactate isotopologues, from  $[^{13}\text{C}_6]$ glucose. **(E)** Reductive glutamine contribution to citrate, determined by the ratio of the M5 isotopologues of citrate to the M5 isotopologues of glutamate, from  $[^{13}\text{C}_5]$ glutamine. **(F)** Oxidative glutamine contribution to citrate, determined by the ratio of the M4 isotopologues of citrate to M5 isotopologues of glutamate, from  $[^{13}\text{C}_5]$ glutamine. **(G)**  $\alpha$ -ketoglutarate to citrate ratio. Error bars indicate the standard deviation and are calculated from at least two independent replicates. Statistical significance between control and the treatment was determined by a two-tailed t-test. \* denotes  $P \leq 0.05$ , \*\* denotes  $P \leq 0.01$ , and \*\*\* denotes  $P \leq 0.001$ .

### 3.2.9 Long-term OSM treatment effects cellular metabolism in hepatocellular carcinoma cells and immortalized hepatocytes

Our previous experiments were based on acute OSM treatments (36 h). However, we aimed to study the effect of long-term OSM treatment which better simulates inflammation. For this purpose, we continuously exposed PH5CH8 immortalized hepatocytes and JHH-4 HCC cells to 25 ng/mL OSM for up to 11 days.

Surprisingly, chronic OSM treatment led to metabolic changes not only in PH5CH8 but also in JHH-4 HCC cells. After 5 and 11 days of treatment, we detected a decrease in glucose-derived carbon contribution to citrate while glutamine-derived carbon was increased (Figure 3.12 B,I).

In PH5CH8 cells, the metabolic effects of long-term OSM stimulation were stronger than those observed by acute treatment. In PH5CH8 cells, we observed reduced PDC and PC activities. Furthermore, reductive glutamine carboxylation was increased while oxidative glutamine decarboxylation was decreased (Figure 3.12 C-G, J-M).

Unlike in PH5CH8 cells, chronic OSM treatment did not effect PDC activity in JHH-4 cells (Figure 3.12 C), while we measured reduced PC activity and an increased reductive glutamine metabolism while oxidative glutamine metabolism was decreased (Figure 3.12 F-G, L-M). Interestingly, long-term OSM treatments did not induce HIF-1 $\alpha$  in JHH-4 cells, suggesting that metabolic effects are HIF-1 $\alpha$  independent (Figure 3.12 A, H).

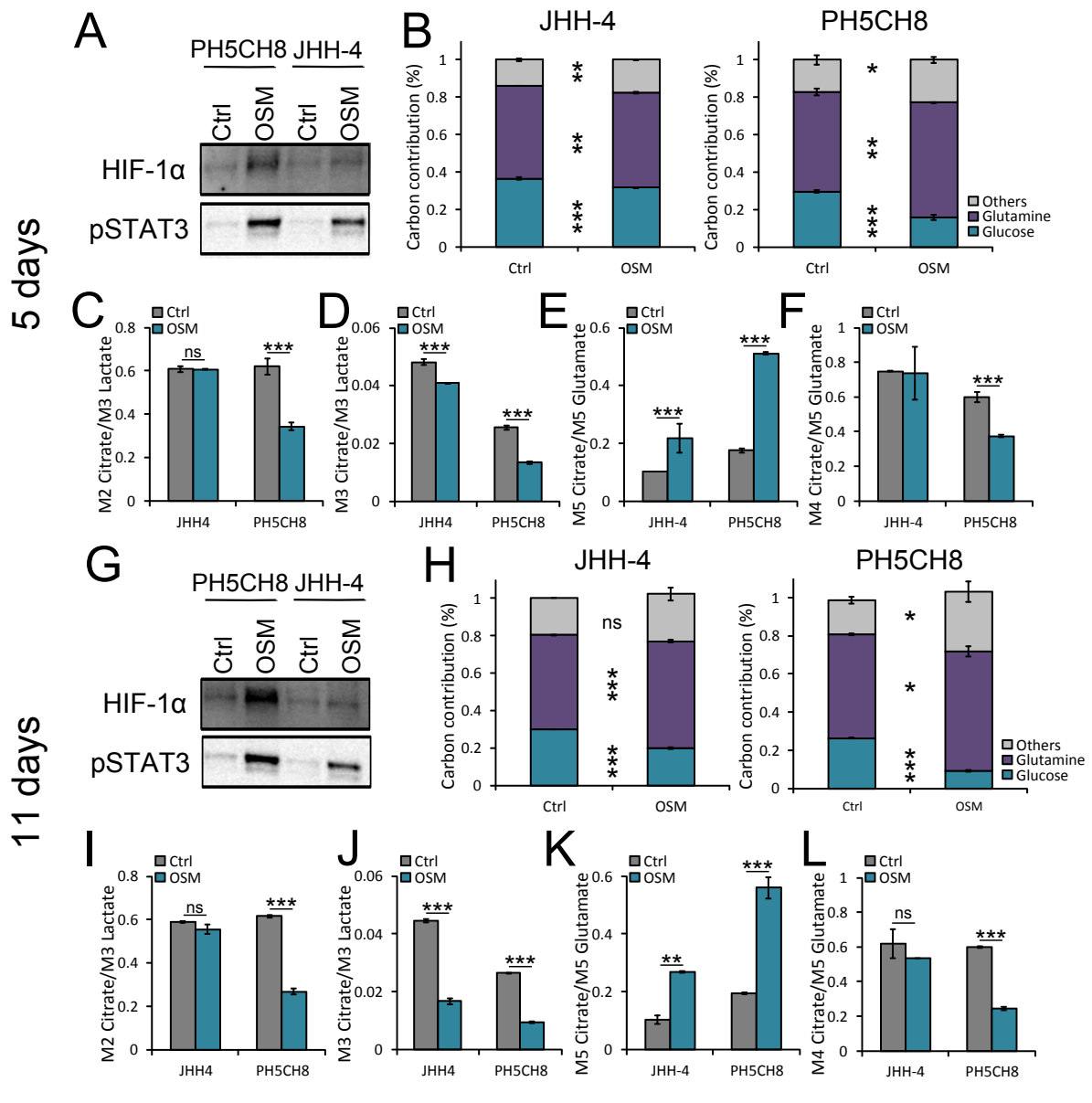


**FIGURE 3.12: Long-term OSM stimulation in PH5CH8 and JHH-4 cells.** PH5CH8 and JHH-4 cells were treated with 25 ng/mL OSM over 11 days. Metabolites were extracted after 5 days (**A-G**) and 11 days (**H-M**) of chronic treatment. (**A,G**) HIF-1 $\alpha$  Western blot. (**B,H**) Glucose- and glutamine-derived carbon contribution to citrate. (**C,K**) PDC activity determined from the M2 citrate isotopologues normalized to the M3 lactate isotopologues, from [ $^{13}\text{C}_6$ ]glucose. (**D, J**) PC activity determined from the M3 citrate isotopologues normalized to the M3 lactate isotopologues, from [ $^{13}\text{C}_6$ ]glucose. (**E,K**) Oxidative glutamine contribution to citrate, determined by the ratio of M4 isotopologues of citrate to M5 isotopologues of glutamate, from [ $^{13}\text{C}_5$ ]glutamine. (**F,L**) Reductive glutamine metabolism, determined by the ratio of M5 isotopologues of citrate to M5 isotopologues of glutamate, from [ $^{13}\text{C}_5$ ]glutamine. Error bars indicate the standard deviation and are calculated from at least two independent replicates. Statistical significance between control and the treatment was determined by a two-tailed t-test. \* denotes  $P \leq 0.05$ , \*\* denotes  $P \leq 0.01$ , and \*\*\* denotes  $P \leq 0.001$ .

### 3.3 Results summary

In summary, we showed that:

- OSM mediated HIF-1 $\alpha$  protein induction in various HCC cell lines and in immortalized hepatocytes under normoxia. In most of the tested HCC cell lines OSM-induced HIF-1 $\alpha$  upregulation was transient and restricted to early stimulation time points. Few HCC cell lines and in particular immortalized hepatocytes displayed continuous HIF-1 $\alpha$  expression over 36 h.
- OSM induced hypoxia-like metabolic effects in immortalized hepatocytes which were characterized by a reduced entry of glucose-derived carbon into the TCA cycle and the induction of reductive glutamine metabolism.
- In immortalized hepatocytes, OSM-mediated metabolic effects were coordinated by HIF-1 $\alpha$  and partially dependent on the HIF-1 $\alpha$  target gene PDK1. Silencing HIF-1 $\alpha$  abolished OSM-induced effects on central carbon metabolism, while under PDK1 silencing conditions, OSM-dependent effects were dampened.
- OSM did not exert metabolic effects on central carbon metabolism in any of the tested HCC cell lines, despite the fact that HIF-1 $\alpha$  was induced.
- Chronic OSM treatment in the HCC cell line JHH-4 resulted in HIF-1 $\alpha$ -independent metabolic effects. As a consequence of chronic exposure to OSM these cells exposed an increased reductive glutamine metabolism while the entry of glucose-derived carbon via PDC remained unaffected.

## Chapter 4

# Discussion and Perspectives

### 4.1 Discussion

The fact that HCC development and progression are frequently accompanied by chronic inflammation suggests that this microenvironment favours malignant transformation and supports uncontrolled growth [Fausto, 1999]. In HCC, constitutive STAT3 activation is common, despite the absence of genetic alterations [Calvisi et al., 2006, He et al., 2010, Spannbauer and Trautwein, 2009]. This suggests that external stimuli, such as cytokines, present within the inflammatory microenvironment lead to aberrant STAT3 activity [He and Karin, 2011]. While STAT3 activation by inflammatory mediators protects cells during inflammation, the exact same pathways might drive neoplastic growth [Hodge et al., 2005]. In this context, the cytokines IL-6 and OSM seem to play an important role and thus levels are increased in the serum and in liver tissue of patients with cirrhosis and HCC [Giannitrapani et al., 2006, Liang et al., 2012, Mantovani et al., 2008, Uhlén et al., 2015, Wong et al., 2009, Znoyko et al., 2005]. Neoplastic growth generally goes hand in hand with changes in cellular metabolism that support high proliferation rates [DeBerardinis et al., 2008].

Based on the finding that IL-6 type cytokines induce the expression of the key metabolic regulator HIF-1 $\alpha$  [Vollmer et al., 2009], we hypothesized that the activation of STAT3 by inflammatory cytokines redirects cellular metabolism towards a more proliferative phenotype. A multitude of studies describe that cytokines and growth factors upregulate HIF-1 $\alpha$  under normoxia [Fukuda et al., 2002, Laughner et al., 2001, Treins et al., 2002, Vollmer et al., 2009]. While the metabolic consequences of HIF-1 $\alpha$  stabilization under hypoxia are well understood, we aimed to elucidate the metabolic effects of cytokine-induced HIF-1 $\alpha$  upregulation under normoxic conditions using stable-isotope assisted metabolomics. The use of uniformly labelled [ $^{13}\text{C}_6$ ]glucose and [ $^{13}\text{C}_5$ ]glutamine is a very robust and sensitive method that allows to trace changes in metabolic states and permits to unravel both changes in

enzyme activities and alterations in the usage of carbon sources [Liu et al., 2014, Roberts et al., 2012, Zamboni and Sauer, 2009]. The direct interpretation of  $^{13}\text{C}$  labelling patterns in metabolites confers a straightforward method that allows to monitor enzymatic activities, qualitative changes occurring in metabolic pathways and the contribution of various nutrients to metabolite synthesis [Buescher et al., 2015]. Using this method we were able to profile central carbon metabolism and determine global metabolic changes occurring under hypoxia and OSM treatment in immortalized hepatocytes and HCC cell lines. In line with numerous other metabolomics studies we derived the relative activity of PDC from the relative proportion of the M2 citrate mass isotopologues when using a  $^{13}\text{C}_6$ glucose tracer [Aguilar et al., 2016, Grassian et al., 2011, Meiser et al., 2016]. This method has numerous advantages when compared to other methods used to determine PDC activity: (1) it allows to profile the metabolism on -omics level, (2) does not require the usage of radioactive  $^{14}\text{C}$  and (3) is a high throughput and quick technique. However, it should be noted that results from stable-isotope assisted metabolomics, at least in what concerns PDC activity, could be validated using a different method such as PDC specific enzymatic assays [Scrutton and White, 1974, Warren and Tipton, 1974]. While we put our major emphasis on the determination of PDC activity under the various experimental conditions, TCA cycle anaplerosis via PC was also accessed. With our extraction method, oxaloacetate cannot be measured as a consequence of its chemical instability [Zimmermann et al., 2014]. Thus we used the relative abundance of M3 citrate mass isotopologues to access PC activity in this study. While this method is less biased by TCA cycle cycling products, such as the case when using M3 malate, M3 aspartate and M3 fumarate, it has to be noted that this mass isotopomer is generated by the condensation of  $^{13}\text{C}_3$ oxaloacetate with unlabelled acetyl-coA and thus might be biased by drastically changed unlabelled acetyl-coA pools. Other tracers can be used to complement the information derived from a  $^{13}\text{C}_6$ glucose tracer in order to further investigate PC in a more targeted manner. Additional tracers, such as a  $[1-^{13}\text{C}_1]$ pyruvate tracer or a  $[3,4-^{13}\text{C}_2]$ glucose tracer can be used which loose their  $^{13}\text{C}$  atom when metabolized via PDC while it is retained when undergoing PC activity. Subsequent metabolization through the TCA cycle will lead to the loss of the  $^{13}\text{C}$  atom allowing the unbiased determination of PC activity [Cheng et al., 2011, Niklas et al., 2011].

#### 4.1.1 The metabolic phenotype of HCC cell lines and immortalized hepatocytes

The HCC cell lines and the immortalized hepatocytes that we used in this study were proliferating cells. The contribution of glucose-derived carbon to citrate accounted for less than 50% (Figure 3.1 A-C). This might imply that the influx of pyruvate into the TCA cycle is

relatively low and that a high proportion of glucose-derived carbon fuels other biosynthetic pathways and/or is secreted after conversion to lactate. The relatively low contribution of glucose-derived carbon to citrate might furthermore be explained by the fact that a substantial fraction of citrate is generated from glutamine in these cells (Figure 3.1 A-C). Furthermore, the proportion of glutamine-derived carbon into the TCA cycle intermediates downstream of citrate was higher than that observed for citrate itself. This could be explained by glutaminolysis where glutamine-derived  $\alpha$ -ketoglutarate enters the TCA cycle and is metabolized oxidatively, and thereby diluting the contribution of glucose-derived carbon to the TCA cycle intermediates (Figure 3.1 A-C).

While nutrient uptake is tightly regulated in quiescent cells, proliferating cells adapt metabolic features that support the synthesis of anabolic precursors to sustain unlimited growth [Hsu and Sabatini, 2008, Vander Heiden et al., 2009]. Cell proliferation is controlled by signal transduction pathways that can be activated by growth factors and cytokines, and tumour cells often acquire oncogenic mutations that render growth-stimulating pathways constitutively active [Edinger and Thompson, 2002]. When cellular metabolism switches to aerobic glycolysis, proliferating cells take up more glucose and convert it to lactate at near stoichiometric levels, and consequently deviate the glycolytic flux away from oxidative phosphorylation [Metallo et al., 2011, Semenza, 2011, Warburg, 1928, 1956]. Moreover, in proliferating cells, TCA cycle intermediates, such as citrate serve as biosynthetic precursors that support high proliferation rates, resulting in an efflux of carbon from the TCA cycle [DeBerardinis et al., 2008]. The low contribution of glucose-derived carbon to the TCA cycle intermediates in the cell lines used in this study, might reflect their proliferative nature (Figure 3.1 A-C). We furthermore found that glutamine-derived carbon is an essential component of the TCA cycle intermediates in HCC cells and immortalized hepatocytes. Glutamine was preferentially metabolized in an oxidative rather than a reductive manner and thus might compensate for the efflux towards biosynthetic pathways (Figure 3.1 A-C, and Figure 3.2 H-I). This underlines the importance of glutamine as carbon source for TCA cycle intermediates in proliferating cells [DeBerardinis et al., 2007].

Interestingly, we detected differences in glucose and glutamine metabolism between the cell lines. How far these differences correlate with phenotypic features such as proliferation was beyond the scope of this work. However, it is becoming more and more clear that each tumour has an individual molecular signature which is accompanied by specific metabolic alterations [Galluzzi et al., 2013, Halama et al., 2015, Mishra and Ambs, 2015]. In HCC cells, for example, a high efflux of citrate from the TCA cycle towards cholesterol synthesis is proportional to their proliferation rate [Parlo and Coleman, 1984b, 1986].



### 4.1.2 Hypoxia inhibits glucose-derived carbon entry into the TCA cycle and induces reductive glutamine metabolism

First we studied the metabolic consequences of hypoxia-mediated HIF-1 $\alpha$  stabilization in HCC cell lines and in immortalized hepatocytes. As expected, we found that hypoxia induced HIF-1 $\alpha$  stabilization in all cell lines (Figure 3.5 B, C) and consequently led to the upregulation of the HIF-1 $\alpha$  target gene PDK1 while PDP2 was downregulated (Supplemental figure A.2 A-C and supplemental figure A.3 A-C). As a consequence of this, we observed that PDC phosphorylation on all three serine residues was enhanced (Supplemental figure A.2 B, E and supplemental figure A.3 B). In line with PDC inactivation under hypoxia, we found that the pyruvate flux through PDC was decreased and that glucose- and glutamine-derived carbon oxidation within the TCA cycle was drastically reduced (Figure 3.1 A-C and Figure 3.2 D-F, H-I). Reduced glucose-derived carbon entry into the TCA cycle was compensated by an increased contribution of carbon derived from glutamine where glutamine was preferentially metabolized reductively and used to generate lipogenic citrate (Figure 3.2 H-I). The molecular mechanisms by which hypoxia reduces respiration are well understood and support our findings in HCC cell lines and immortalized hepatocytes. Under hypoxic conditions, HIF-1 $\alpha$  is stabilized and upregulates PDK1 expression [Kim et al., 2006, Papandreou et al., 2006, Roche et al., 2001]. In turn, PDK1 phosphorylates and thereby inactivates PDC which results in a decreased entry of glucose-derived carbon into the TCA cycle [Kim et al., 2006, Papandreou et al., 2006, Roche et al., 2001]. Consequently, the mitochondrial citrate pool is depleted and glutamine-derived  $\alpha$ -ketoglutarate is carboxylated to generate lipogenic citrate [Fendt et al., 2013, Metallo et al., 2011, Wise et al., 2011]. We furthermore showed that PC activity was reduced under hypoxia which might be a consequence of low acetyl-coA levels that in turn allosterically regulated PC activity [Jitrapakdee et al., 2008] (Figure 3.2 E).

### 4.1.3 OSM does not induce a hypoxia-like metabolic phenotype in HCC cell lines

While numerous cytokines and growth-factors can induce HIF-1 $\alpha$  upregulation under normoxic conditions, it remained to be elucidated if "normoxic HIF-1" has metabolic effects that are comparable to those observed under hypoxia. Thus, we investigated whether OSM-mediated HIF-1 $\alpha$  induction under normoxic conditions resulted in a hypoxia-like metabolic phenotype in HCC cells. Unlike under hypoxia, cytokine-mediated HIF-1 $\alpha$  induction results from STAT3-induced increased HIF-1 $\alpha$  transcription and not HIF-1 $\alpha$  stabilization [Vollmer et al., 2009]. Vollmer *et al.* described that several IL-6 type cytokines are potent inducers of HIF-1 $\alpha$  expression [Vollmer et al., 2009]. Among all tested cytokines, OSM-induced HIF-1 $\alpha$

induction was strongest, and thus it was the focus of this work. Despite continuous STAT3 activation, we found that OSM-mediated HIF-1 $\alpha$  induction was transient and restricted to early stimulation time-points in most HCC cell lines (Figure 3.5 A-D). This was in contrast to HIF-1 $\alpha$  stabilization under hypoxia which was a continuous and strong event. It is thus likely that cytokine-induced HIF-1 $\alpha$  proteins underwent oxygen-dependent degradation in the vast majority of the HCC cell lines. In HepG2 cells, for example, we detected continuous OSM-induced HIF-1 $\alpha$  upregulation on mRNA level over the full length of the time course, while HIF-1 $\alpha$  protein levels decreased after 24 h (Figure 3.5 A-C). However, when we stimulated HepG2 cells with OSM under hypoxia, HIF-1 $\alpha$  protein levels were more abundant than those induced by hypoxia alone and persisted until later stimulation time points (Figure 3.5 B-D). This suggested that, at least in HepG2 cells, OSM-induced HIF-1 $\alpha$  was indeed degraded in an oxygen-dependent fashion under normoxia, while under hypoxia OSM-induced HIF-1 $\alpha$  was stabilized and thereby further increased HIF-1 $\alpha$  protein levels. Our data suggests that, at early stimulation time-points, OSM indeed upregulated HIF-1 $\alpha$  on protein level, while degradation mechanisms caught up and cytokine-induced HIF-1 $\alpha$  proteins were degraded in an oxygen-dependent manner at later time points. Vollmer *et al.* described that in contrast to hypoxia-stabilized HIF-1 $\alpha$ , OSM-induced HIF-1 $\alpha$  proteins carried hydroxylations and ubiquitylations [Vollmer *et al.*, 2009]. This finding is in line with the hypothesis that OSM-induced HIF-1 $\alpha$  is targeted by VHL-mediated and oxygen-dependent degradation in many HCC cell lines [Cockman *et al.*, 2000, Maxwell *et al.*, 1999, Stickle *et al.*, 2004]. VHL is frequently mutated in renal clear cell carcinomas (RCC), consequently HIF-1 $\alpha$  and HIF-2 $\alpha$  are expressed under normoxia [Krieg *et al.*, 2000]. As a result, RCC cells express high levels of the HIF-1 target genes VEGF and GLUT1 [Krieg *et al.*, 2000]. Furthermore, RCC cells have high glucose uptake and lactate secretions rates and exhibit a decreased flux of pyruvate through PDC [Minton *et al.*, 2015]. These effects are directly attributed to HIF-1 $\alpha$  expression [Minton *et al.*, 2015]. These findings in RCC cells show that the interruption of VHL-mediated HIF-1 $\alpha$  degradation is sufficient to induce a hypoxia-like metabolic features under normoxic conditions.

In concordance with our finding that OSM-treatment led to a transient induction of HIF-1 $\alpha$  in HepG2 cells under normoxia, we consequently did not detect metabolic effects on cellular metabolism after a 36 h treatment (Figure 3.3 A-B and Figure 3.4 D-F, H-I). The HCC cell lines HepG2-C3A and SK-Hep1, however, showed HIF-1 $\alpha$  induction 8 h and 36 h post-OSM stimulation suggesting that in these cells OSM-induced HIF-1 $\alpha$  did not undergo oxygen-dependent degradation and thus might exert metabolic effects (Figure 3.5 A, F). Despite a strong induction of HIF-1 $\alpha$  under normoxic conditions, we did not detect changes in metabolism which suggested that OSM-induced HIF-1 $\alpha$  was an inactive transcription factor, at least in what concerns the regulation of metabolic genes (Figure 3.6 B-E, G-J). This observation suggests that oxygen-dependent mechanisms might render OSM-induced HIF-1 $\alpha$  inactive under normoxia (Figure 4.1). While the exact mechanisms remain to be elucidated

in further research, it is probable that post-translational modifications inactivate HIF-1 $\alpha$  under normoxia in the HCC cell lines Sk-Hep1 and HepG2-C3A: (1) Under normoxia, HIF-1 $\alpha$  can be hydroxylated by FIH on its carboxy-terminal transactivation domain which prevents the interaction of HIF-1 $\alpha$  with the transcriptional co-regulators such as p300 and the CREB binding protein and thus interferes with its transcriptional activity [Masson *et al.*, 2012, Stolze *et al.*, 2004]; (2) OSM-induced HIF-1 $\alpha$  is hydroxylated by PHDs and recognized by VHL which might interfere with HIF-1-mediated transcription; (3) ARD1 acetylates HIF-1 $\alpha$  on lysine 532, enhances the interaction with VHL and thus supports HIF-1 $\alpha$  degradation under normoxia [Jeong *et al.*, 2002]; (4) other posttranslational modifications of HIF-1 $\alpha$  include phosphorylations, S-nitrosylations and SUMOylation, all of which might play important roles for its activity under normoxic (reviewed in [Dimova and Kietzmann, 2010]). While we showed in this work that OSM-induced HIF-1 $\alpha$  induction does not have the expected effects on cellular metabolism in HCC cells, Vollmer *et al.* showed that OSM-induced HIF-1 $\alpha$  proteins are active transcription factors. They validated the transcriptional activity of OSM-induced HIF-1 $\alpha$  in reporter gene assays and based on the upregulation of the endogenous HIF-1 target genes VEGF and PAI [Vollmer *et al.*, 2009]. However, VEGF and PAI are not only HIF-1 but also STAT3 target genes, rising the question whether OSM-mediated upregulation was not rather directly regulated by STAT3 [Dauer *et al.*, 2005, Niu *et al.*, 2002, Vollmer *et al.*, 2009, Wei *et al.*, 2003].

Our observation that OSM stimulation under hypoxia led to higher HIF-1 $\alpha$  proteins levels than hypoxia alone suggested that OSM-induced HIF-1 $\alpha$  was stabilized by hypoxic conditions in HepG2 cells. Thus, we studied whether this also translates into a more pronounced hypoxic metabolic phenotype. However, our data showed that despite increased HIF-1 $\alpha$  protein levels, OSM-treatment did not further boost the metabolic effects under hypoxia (Supplemental figure A.4 D-G). It is possible that the metabolic effects under 1% hypoxia were so profound that OSM-induced HIF-1 $\alpha$  was insufficient to further enhance hypoxia-mediated effects. To validate this hypothesis, it would be of interest to study whether OSM-stimulation under milder hypoxic conditions results in more pronounced metabolic effects in HepG2 cells. Vollmer *et al.* described that a combinatorial treatment of hypoxia (5%) and OSM further increased the expression of the HIF-1 target genes VEGF and PAI when compared to hypoxia alone [Vollmer *et al.*, 2009]. However, as discussed above, it remains to be elucidated if this observation is not a consequence of both, STAT3 and HIF-1 dependent transcriptional regulation.

Based on our findings, we hypothesize that OSM-induced HIF-1 $\alpha$  in HCC cells (1) is targeted by oxygen-dependent degradation mechanisms under normoxia, thus is only transiently upregulated in the vast majority of the tested cell lines and (2) is an inactive transcription factor, at least in what concerns the regulation of metabolic genes. In this context, gene expression microarrays were carried out on the HCC cell lines HepG2, JHH-4 and Huh-7 stimulated with OSM, grown at 1% hypoxia and subjected to a combinatorial treatment for 24 h and

48 h [Zimmer, 2015]. As expected, hypoxia strongly effected the expression of genes coding for enzymes within central carbon metabolism, although to various degrees when comparing all three cell lines. OSM treatment, however, did not induce a clear HIF-1 $\alpha$ -dependent transcriptional signature [Zimmer, 2015]. Moreover, a combinatorial treatment of hypoxia and OSM did not further enhance the transcriptional regulation [Zimmer, 2015]. These observations further supported our finding that OSM-induced HIF-1 $\alpha$  upregulation under normoxic conditions in HCC cell lines does not induce hypoxia-like metabolic features.

Although it becomes clear from our data that OSM-induced HIF-1 $\alpha$  is not required for metabolic reprogramming in HCC cells under inflammatory conditions, other roles of HIF-1 $\alpha$  in this context remain to be studied.

#### 4.1.4 OSM induces hypoxia-like metabolic changes in immortalized hepatocytes

Contrarily to our findings in HCC cell lines, OSM induced significant metabolic effects in PH5CH8 immortalized hepatocytes. In these cells, OSM stimulation resulted in HIF-1 $\alpha$  upregulation on mRNA and protein level, where OSM and hypoxia-mediated HIF-1 $\alpha$  protein levels were comparable after a 36 h treatment (Figure 3.5 A-C). Consequently the HIF-1 $\alpha$  target gene PDK1 was upregulated on mRNA and protein level, although OSM-induced PDK1 upregulation was less strong when compared to hypoxia (Supplemental figure A.3 A-C). We did not detect a significant downregulation of PDP2 and consequently no pronounced changes on PDC phosphorylation while PDC phosphorylation under hypoxia was increased (Supplemental figure A.3 A-C). In line with increased HIF-1 $\alpha$  and PDK1 expression levels in OSM-stimulated PH5CH8 cells, we detected OSM-induced metabolic changes. We observed that OSM treatment reduced glucose-derived carbon entry into the TCA cycle and negatively impacted oxidative glutamine metabolism while reductive glutamine metabolism was induced (Figure 3.3 C and Figure 3.4 D-F, H-I) (Figure 4.1). These changes were similar to those induced by hypoxia, although weaker in magnitude (Figure 3.3 C and Figure 3.4 D-F, H-I). In the context of STAT3-mediated metabolic effects on cellular metabolism, Demaria *et al.* have reported similar findings. They showed that the expression of constitutively active STAT3 (STAT3<sup>C/C</sup>) in MEFs induced aerobic glycolysis [Demaria *et al.*, 2010]. The expression of STAT3<sup>C/C</sup> in these cells led to HIF-1 $\alpha$ -mediated upregulation of PDK1 and correlated with increased glucose uptake and lactate secretion under normoxia, while PDC activity was reduced. In subsequent work, the same group showed that STAT3<sup>C/C</sup> expressing MEFs were more prone to undergo spontaneous immortalization. Immortal STAT3<sup>C/C</sup> cells proliferated faster when compared to their wild type counterparts and were less sensitive to apoptotic stimuli [Demaria *et al.*, 2012]. When HIF-1 $\alpha$  was silenced in STAT3<sup>C/C</sup> expressing MEFs, their transformed phenotype was partially reversed *i.e.* cell proliferation and the ability of

cells to form colonies on soft agar was decreased but not abolished [Demaria et al., 2012]. The authors concluded that STAT3<sup>C/C</sup> can serve as first hit in carcinogenesis and that STAT3 induced HIF-1 $\alpha$  expression supports higher proliferation rates by inducing aerobic glycolysis [Demaria et al., 2012]. In contrast to these studies, we found that OSM stimulation did not effect cellular proliferation in PH5CH8 cells, which might be explained by different cellular origins and by the fact that we used OSM to activate STAT3 while Demaria *et al.* used cells that express STAT3<sup>C/C</sup> and thus specifically targeted STAT3 regulated mechanisms. Furthermore, the effects of OSM on cell proliferation were described to be cell-type dependent and to induce both stimulatory and inhibitory effects [Halfter et al., 1998, Horn et al., 1990, Klausen et al., 2000, Nair et al., 1992, Zarling et al., 1986]. In the HCC cell line HepG2, OSM was described to inhibit cell proliferation [Klausen et al., 2000]. The underlying mechanism, however, was found to be regulated by OSM-induced STAT5 and ERK activation [Klausen et al., 2000]. Based on our observations in OSM-treated PH5CH8 cells, we derived that OSM-induced HIF-1 $\alpha$  induction further enhanced aerobic glycolysis which however had no effect on proliferation although it probably could support higher proliferation rates [Vander Heiden et al., 2009]. It can be hypothesised that cytokine-mediated metabolic reprogramming plays a supportive role in the context of cancer-promoting inflammation by stimulating aerobic glycolysis in pre-malignant cells and thus might favour proliferation in conjunction with malignant genetic alterations.

Although hypoxia and OSM treatment induced comparable levels of HIF-1 $\alpha$  protein in PH5CH8 cells, the metabolic effects we observed under hypoxia were more pronounced. This suggests that yet other mechanisms contribute to the strong metabolic changes observed under hypoxia. The exact reasons behind this observation remain to be elucidated, however it is possible that the availability of oxygen by itself plays a role. While PDC activity is reduced in OSM-treated immortalized hepatocytes, the oxygen supply in these cells remains unaffected and oxidative phosphorylation keeps running. Under hypoxia and in addition to a decreased PDC activity, oxygen availability becomes scarce which might effect mitochondrial metabolism independently of HIF-1 $\alpha$ . Interestingly, it was shown that mitochondrial oxygen consumption is in part maintained under hypoxia, although to a much lesser extend than under normoxia, while NAD<sup>+</sup>/NADH ratios consequently are lowered [Frezza et al., 2011]. While it remains to be tested if OSM treatment effects NAD<sup>+</sup>/NADH ratios, it is possible that the altered redox-state in hypoxic cells further contributes to the strength of the hypoxia-induced metabolic phenotype in PH5CH8 cells. The fact that OSM stimulation under normoxia did not result in a more pronounced phosphorylation of PDC, despite the fact that PDK1 was upregulated, furthermore supported our observation that OSM-induced metabolic changes are less pronounced than those induced by hypoxia. Since PDK1 activity can be regulated by the cellular redox-state, low NAD<sup>+</sup>/NADH ratios under hypoxia might further increase PDK1 activity [Kerbey et al., 1976].

#### 4.1.5 OSM-induced metabolic reprogramming in immortalized hepatocytes is HIF-1 $\alpha$ -dependent

In line with the findings from Demaria *et al.* in STAT3<sup>C/C</sup> expressing MEFs [Demaria *et al.*, 2010], we found that silencing HIF-1 $\alpha$  in OSM-treated PH5CH8 cells led to a full abolishment of OSM-mediated metabolic effects, which shows that OSM-driven metabolic reprogramming is clearly HIF-1 $\alpha$ -dependent (Figure 3.8 A-D).

However, when HIF-1 $\alpha$  was silenced under hypoxic conditions, hypoxia-mediated metabolic effects were abolished, a normoxic metabolic state was however not resorted (Figure 3.8 A-D). The fact that PDK1 was not upregulated under hypoxic conditions when HIF-1 $\alpha$  was silenced showed that HIF-1 $\alpha$  silencing was efficient and that the metabolic effects resulted from HIF-1 $\alpha$ -independent mechanisms (Figure 3.9 A). The absence of HIF-1 $\alpha$  upregulation under hypoxia probably resulted in an unrestrained influx of glucose-derived carbon into the TCA cycle and as a consequence of hindered respiration in the accumulation of NADH and depletion of NAD<sup>+</sup>. Consequently, metabolic reactions that are NAD<sup>+</sup>-dependent might be thermodynamically inhibited while NADH-dependent enzymatic reactions might be favoured. Furthermore, it might be possible that HIF-2 $\alpha$  supports some of the metabolic adaptation under hypoxia when HIF-1 $\alpha$  is silenced, although it was shown that HIF-1 $\alpha$  and not HIF-2 $\alpha$  regulate the glycolytic pathway under hypoxia [Hu *et al.*, 2003].

#### 4.1.6 OSM-induced metabolic reprogramming in immortalized hepatocytes is partially dependent on PDK1

While the HIF-1 $\alpha$  target gene PDK1 is essential to regulated the metabolic switch from oxidative phosphorylation towards a glycolytic metabolism occurring under hypoxia, we investigated whether OSM-mediated metabolic reprogramming was also dependent on PDK1 and thus silenced PDK1 in OSM-treated PH5CH8 cells. When PDK1 was silenced we could dampen, however not fully abolish OSM-mediated metabolic effects, despite a high silencing efficiency and the absence of PDK1 upregulation after OSM treatment (Figure 3.9 B-E). This finding suggests that PDK1 is not the only regulator involved in OSM-mediated metabolic reprogramming. Although PDK1 is mostly discussed in terms of HIF-1 $\alpha$ -mediated inhibition of PDC under hypoxia, the regulation of PDC by PDKs is highly complex and not only dependent on PDK1. While PDKs exists under 4 isoforms they exhibit a tissue specific expression pattern and isoform-specific differences in their affinity for the different phosphorylation sides on PDC [Bowker-Kinley *et al.*, 1998]. It is thus possible that in the absence of PDK1, other PDK isoforms coordinate PDC phosphorylation which would explain why OSM-mediated metabolic effects are not fully abolished. Based on our observation that HIF-1 $\alpha$  silencing

fully abolished OSM-induced metabolic effects while PDK1 silencing only dampened these, it is fairly possible that yet other HIF-1 $\alpha$  target genes coordinate the effects of OSM on cellular metabolism. While HIF-1 diminishes the entry of glucose-derived carbon into the TCA cycle via PDK1 upregulation, it also exerts direct effects on the mitochondrial respiratory chain [Fukuda et al., 2007]. Fukuda *et al.* described that HIF-1 $\alpha$  regulates a switch in the composition of the cytochrome c oxidase (COX) subunit 4 [Fukuda et al., 2007]. HIF-1 was shown to upregulate the expression the COX4-2 isoform while inducing the degradation of the COX4-1 isoform via the protease LON. This change in subunit composition of COX4 is suggested to optimize the efficiency of oxygen utilization under hypoxic conditions [Fukuda et al., 2007]. The expression of the COX4 isoforms in the context of cytokine induced HIF-1 $\alpha$  was not yet investigated while this mechanism could explain our finding that PDK1 silencing is not sufficient to fully abrogate OSM-mediated metabolic effects.

We furthermore validated our finding that OSM induces metabolic reprogramming in additional cell lines. OSM stimulation in PH5CH1 and PH5CH7 cells resulted in HIF-1 $\alpha$  upregulation on mRNA and protein levels (Supplemental figure A.6 A-B and supplemental figure A.7 A-B). Furthermore, PDK1 was upregulated while PDP2 expression was not consistently downregulated (Supplemental figure A.6 A-B). In line with our findings in PH5CH8 cells, the phosphorylation status of PDC remained unaffected by OSM treatment (Supplemental figure A.7 A-B). As a consequence of OSM-mediated HIF-1 $\alpha$  and PDK1 induction in these cells, we detected a decreased pyruvate flux through PDC, a reduced oxidative glutamine metabolism, while reductive glutamine metabolism was enhanced (Figure 3.11 D-F). When we silenced PDK1 in PH5CH1 and PH5CH7 cells, we could reduce but not abolish OSM-mediated metabolic, furthermore suggesting that other regulators could be involved.

#### 4.1.7 Long-term OSM treatment results in HIF-1 $\alpha$ -independent metabolic changes in the HCC cell line JHH-4

To study the metabolic effects of OSM in this project, we generally used acute OSM stimulations although these do not reflect a chronic exposure to inflammatory mediators. In order to study the metabolic consequences of long-term OSM treatment, we performed a chronic OSM treatment in PH5CH8 and JHH-4 cells. As expected, we observed that chronic OSM treatment in PH5CH8 cells induced HIF-1 $\alpha$  and led to similar although more profound metabolic changes when compared with acute OSM treatments (Figure 3.4 D-F, H-I and Figure 3.12 C-F, I-L ). Interestingly, chronic OSM treatment induced a strong reduction in PC activity, this effect, however was not consistently observed under acute OSM stimulation. Since PC activity is allosterically regulated by acetyl-coA, the strongly reduced activity of PDC might result in lower intracellular acetyl-coA and consequently in a lowered PC activity.

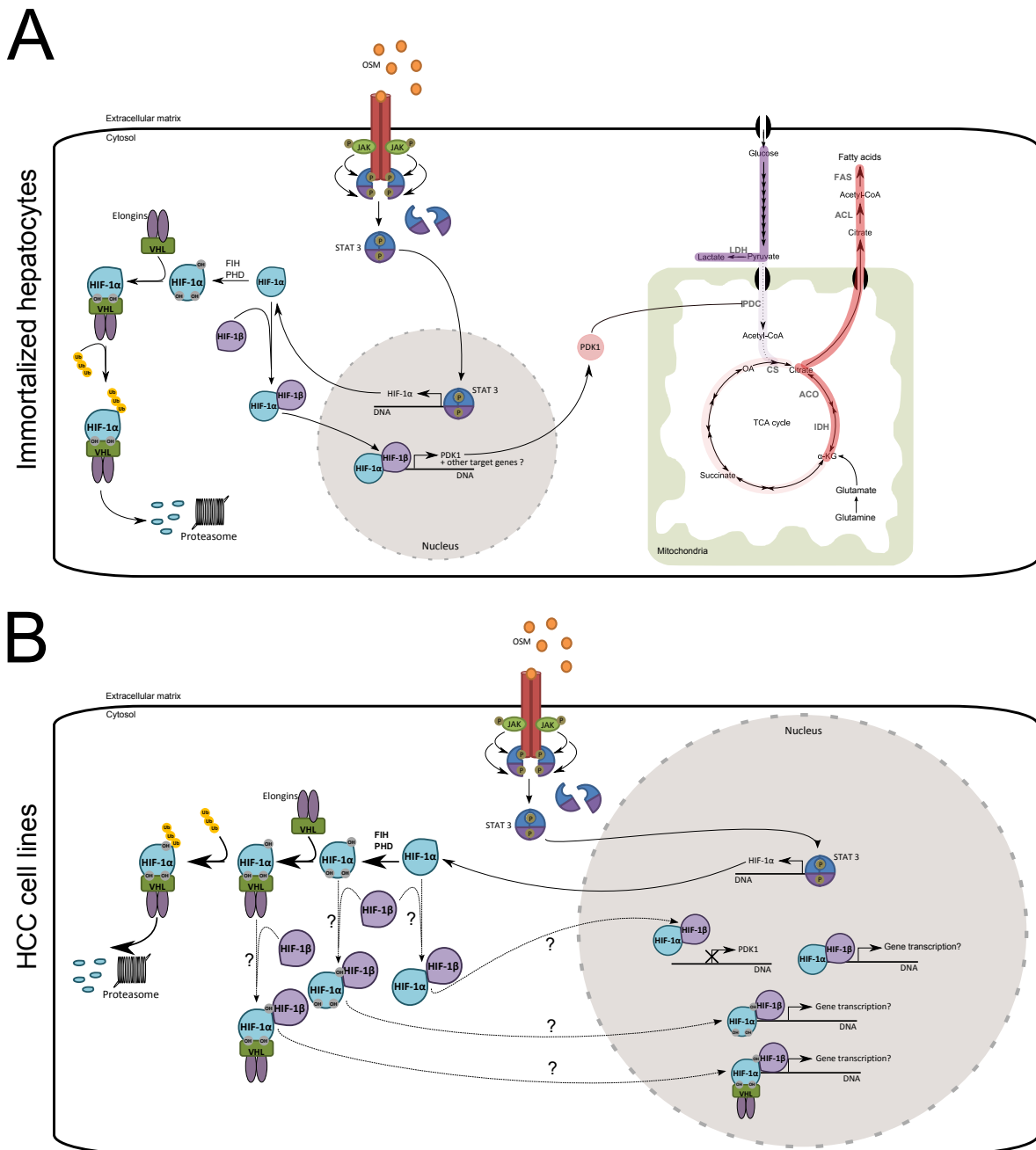


**FIGURE 4.1: Model of OSM-mediated HIF-1 $\alpha$  upregulation and effects on metabolism.** (A) In immortalized hepatocytes, OSM activates the transcription factor STAT3, which in turn upregulates HIF-1 $\alpha$ . Due to the presence of oxygen, PHDs and FIH remain active which results in the degradation of HIF-1 $\alpha$ . However, OSM-induced HIF-1 $\alpha$  upregulation seems sufficient to overwrite oxygen-dependent HIF-1 $\alpha$  degradation and results in the formation of transcriptionally active HIF-1 complexes. HIF-1 upregulates PDK1 and most probably other target genes and thereby mediates hypoxia-like metabolic changes under normoxia. The entry of glucose-derived carbon into the TCA cycle is reduced while reductive glutamine metabolism is enhanced. (B) In HCC cell lines, OSM-induced HIF-1 $\alpha$  is a "metabolically inactive" transcription factor. If OSM-induced HIF-1 $\alpha$  in HCC cells regulates other target genes remains to be elucidated. Furthermore it remains to be clarified which mechanisms render HIF-1 $\alpha$  inactive. Possible explanations are PHD and FIH regulated hydroxylations of HIF-1 $\alpha$  under normoxic conditions and HIF-1 $\alpha$  complexation with VHL.



While central carbon metabolism of JHH-4 cells remained unaffected by acute OSM stimulations, we showed that chronic OSM treatments indeed induced metabolic changes. Surprisingly, we did not detect HIF-1 $\alpha$  protein induction in JHH-4 cells which suggests that metabolic changes are HIF-1 $\alpha$  independent (Figure 3.12 A,G ). In line with absent HIF-1 $\alpha$  induction by chronic OSM treatment in JHH-4 cells, we did not detect an altered PDC activity. However, chronic OSM treatment drastically changed glutamine metabolism in JHH-4 cells (Figure 3.12 E-F, K-L ). We detected that reductive glutamine metabolism was increased, while less glutamine underwent oxidative decarboxylation (Figure 3.12 K-L). In line, the relative contribution of glutamine-derived carbon to citrate was increased, which suggests that more glutamine is used to generate lipogenic citrate (Figure 3.12 B, H). To this point, it remains unclear if OSM-mediated metabolic effects in JHH-4 cells are mediated by STAT3 or yet another OSM-induced signalling cascade such as MAPK or PI3P [Arita et al., 2008, Van Wagoner et al., 2000]. Few studies report on the effects of OSM on metabolism. OSM was described to upregulate the expression of the low density lipoprotein receptor (LDLR) in the liver, suggesting its potential involvement in cholesterol metabolism [Grove et al., 1991]. Another study describes the involvement of OSM in the regulation of fatty acid metabolism [Zhou et al., 2007]. Zhou *et al.* show that OSM stimulation in HepG2 cells results in the upregulation of ACSL 3 and 5 thereby stimulates  $\beta$ -oxidation [Zhou et al., 2007]. This effect was dependent on ERK and not on STAT3 signaling [Zhou et al., 2007]. Furthermore, OSM can downregulate the expression of the metabolic enzyme carnitine palmitoyltransferase (CPT1) which is involved in  $\beta$ -oxidation [Henkel et al., 2011]. In the liver, Kupffer cells secrete OSM and it is hypothesised that OSM then acts in a paracrine manner on hepatocytes and thereby increases lipid accumulation and decreases insulin sensitivity [Elks and Stephens, 2015].

#### 4.1.8 Conclusions

Inflammation plays an important role in HCC development and progression [Fausto, 1999]. Malignant transformation requires both, oncogenic mutations that favour uncontrolled growth and a metabolism that meets the requirements of proliferating cells [DeBerardinis et al., 2008, Edinger and Thompson, 2002]. Although it remains unclear if aerobic glycolysis is a cause or a consequence of proliferation, the metabolic switch observed in proliferating cells supports cellular proliferation by providing the necessary metabolic precursors to sustain unlimited growth [DeBerardinis et al., 2008, Edinger and Thompson, 2002]. In this work we showed that the inflammatory cytokine OSM induced metabolic changes that could support higher cellular proliferation in immortalized hepatocytes. Although OSM-induced metabolic changes did not correlate with increased proliferation rates, they might confer a metabolic advantage in conjunction with a second growth promoting event. Thus, the inflammatory

and pro-carcinogenic microenvironment driving HCC development, might assist carcinogenesis not only by promoting growth but also by regulating the appropriate switch in cellular metabolism. In this study we delineated OSM-induced HIF-1 $\alpha$  expression as trigger for a cytokine-dependent metabolic switch in immortalized hepatocytes under normoxic conditions and showed that the HIF-1 $\alpha$  target gene PDK1 is one of the regulators involved in this process. Since HIF-1 $\alpha$  is expressed in a large variety of cancers, we provide evidence for an interesting link between inflammation and malignant cellular transformation.

While cytokine-induced HIF-1 $\alpha$  induction resulted in hypoxia-like metabolic changes in immortalized hepatocytes, the metabolism of HCC cell remained unaffected, despite HIF-1 $\alpha$  induction. These observations show that HIF-1 $\alpha$  is necessary but not sufficient to induce cytokine-mediated metabolic reprogramming. Our findings suggest that the metabolic response to IL-6 type cytokines might be cell-type dependent and point towards the fact that cytokines rather exert HIF-1 $\alpha$ -mediated metabolic effects in hepatocyte cell lines than in cancerous HCC cells. To this point, it remains to be clarified why OSM-induced HIF-1 $\alpha$  induces metabolic reprogramming in immortalized hepatocytes while the metabolism of HCC cells remains unaffected.

While the metabolism of HCC cell lines remained unaffected by acute OSM treatments, we provide evidence for that long term OSM stimulation significantly alters the metabolism of JHH-4 cells. Unlike in immortalized hepatocytes, metabolic effects resulting from chronic OSM treatments in HCC cells seemed to be HIF-1 $\alpha$ -independent. While the exact mechanisms remain to be fully understood, our observations suggest that chronic OSM exposure stimulates fatty acid synthesis from glutamine. While acute OSM stimulations help to investigate early metabolic effects, long term treatments might better reflect chronic inflammatory conditions that promote cancer development and progression.

## 4.2 Perspectives

In this study we showed that OSM-induced HIF-1 is a "metabolically active" transcription factor in immortalized hepatocytes, while in all tested HCC cells, OSM-mediated HIF-1 $\alpha$  induction was mostly transient and did not have effects on cellular metabolism.

From these observations the questions rises whether OSM-mediated HIF-1 $\alpha$  induction is required as a regulator of cellular processes other than metabolism. Although OSM-induced HIF-1 $\alpha$  has no direct effects on central carbon metabolism at the time of extraction in HCC cells, it might nevertheless be required as transcription factor for the regulation of other genetic targets. Based on our observations we hypothesize that HIF-1 $\alpha$  might be required for a full transcriptional response to inflammatory stimuli. Interestingly, STAT3 and HIF-1 $\alpha$  can cooperatively act on gene expression, suggesting that HIF-1 $\alpha$  can interact with other

transcription factors [Pawlus et al., 2014b]. To tackle our question, gene expression profiling in OSM-treated and HIF-1 $\alpha$ -silenced HCC cells should be performed. Gene expression profiles would consequently reveal whether HIF-1 $\alpha$  expression is required for the response of HCC cells to OSM and more generally to IL-6 type cytokines. Depending on the results, chromatin-immunoprecipitation in combination with promoter-arrays or sequencing could be used to validate HIF-1 target genes in response to cytokine signalling.

While it remains to be clarified whether HIF-1 $\alpha$  induction is required for the full transcriptional response in OSM-treated cells under normoxia, we started to investigate the effect of OSM treatment under low oxygen tension, as these conditions might well reflect the pro-inflammatory and hypoxic microenvironment in solid tumours. In this context, we performed proteomics experiments in HepG2 cells and found that the stimulation of hypoxic HCC cells with OSM resulted in the regulation of a unique set of proteins suggesting that a hypoxic environment modulates the response to inflammatory mediators. Our collaborators carried out microarray experiments and validated our finding that OSM treatment in conjunction with hypoxia regulates a unique set of target genes which might point towards combinatorial effects of STAT3 and HIF-1 $\alpha$  [Zimmer, 2015].

Apart from the fact that HIF-1 $\alpha$  induction by OSM does not induce metabolic effects in HCC cells, we furthermore show that OSM-induced HIF-1 $\alpha$  expression is transient and restricted to early stimulation time points in many HCC cells. Based on these findings we hypothesise that OSM-induced HIF-1 $\alpha$  undergoes oxygen-dependent degradation. To this point, the exact mechanisms that regulate the degradation of OSM-induced HIF-1 $\alpha$  at later stimulation time points remain to be studied. It is possible that oxygen-dependent degradation mechanisms interfere with both, the stability of OSM-induced HIF-1 $\alpha$  and its transcriptional activity. We started to investigate into this direction and studied whether VHL silencing in HepG2 cells was sufficient to induce HIF-1 $\alpha$  under normoxic conditions, such as observed in RCC cells [Krieg et al., 2000]. Although VHL expression was reduced by 50%, we did not detect HIF-1 $\alpha$  stabilization under normoxia nor effects on cellular metabolism. Probably, siRNA-mediated VHL silencing was not powerful enough to sufficiently silence VHL expression. Thus it would be better in this context to create VHL-knockout HCC cells or use VHL inhibitors to fully abolish VHL-mediated HIF-1 $\alpha$  degradation.

Apart from VHL-mediated HIF-1 $\alpha$  degradation under normoxia, FIH-mediated HIF-1 $\alpha$  hydroxylation might interfere with the transcriptional activity of OSM-induced HIF-1 $\alpha$ . To verify whether FIH-mediated HIF-1 $\alpha$  hydroxylation interferes with the transcriptional activity of OSM-induced HIF-1 $\alpha$  under normoxia, we established HepG2 cells that constitutively express shRNA directed against FIH. Although FIH expression was reduced by 80% in HepG2 cells, no OSM-mediated metabolic changes were detected. This suggests that yet other mechanisms, eventually post-translational modification, might interfere with the transcriptional activity of OSM-induced HIF-1 $\alpha$ . A thorough investigation of the post-translational modifications of HIF-1 $\alpha$  under normoxic conditions might help to better understand its regulation.

While in this study we evaluated the metabolic effects of OSM on cellular metabolism of HCC cells and immortalized hepatocytes, it remains to be studied how OSM effects central carbon metabolism in primary hepatocytes. We focussed on proliferating cells, either derived from HCC or generated by hepatocyte immortalization, thus these cells expose the metabolic features of aerobic glycolysis. PH5CH cells were generated from primary hepatocytes immortalized with the Simian virus large T antigen, that consequently regulates immortalization by binding tumour suppressors such as p53 and retinoblastoma [Ikeda *et al.*, 1998]. Thus, it remains questionable how well PH5CH cells still reflect the phenotype of hepatocytes. Based on the observation from Nakamura *et al.* that OSM plays an important role in liver regeneration by inducing hepatocyte proliferation, it would be highly interesting to study whether OSM induces growth-promoting changes in cellular metabolism in hepatocytes and furthermore determine if HIF-1 $\alpha$  plays a key role in this context [Nakamura *et al.*, 2004]. We started to establish a protocol for the isolation of primary hepatocytes from mouse liver, however, due to the time limitation of the project did not yet finalize protocol optimization.

While acute OSM treatment in JHH-4 cells did not affect cellular metabolism, the increased reductive glutamine metabolism in JHH-4 cells subjected to chronic OSM-stimulation points towards increased fatty acid synthesis from glutamine. In this context, fatty acid metabolism should be more thoroughly investigated. This could be achieved by studying fatty acids as fatty acid methyl esters by GC-MS and determine whether changes occur in their abundance and in their MID in response to chronic OSM treatment.

While our metabolomics approach revealed that cytokine-induced HIF-1 $\alpha$  expression does not induce metabolic reprogramming in HCC cells, Demaria *et al.* described that the expression of STAT3<sup>C/C</sup> in MEFs confers a proliferative advantage. Thus it would be interesting to study whether the constitutive STAT3 activation, rather than the cytokine-induced STAT3, can further promote aerobic glycolysis in HCC cells [Demaria *et al.*, 2012]. We are currently generating HCC cell lines that express constitutively active STAT3 in an inducible fashion. This will help us to better understand the role of STAT3 in HCC and conduct long-term studies in more cell lines.

## Appendix A

### Supplemental figures

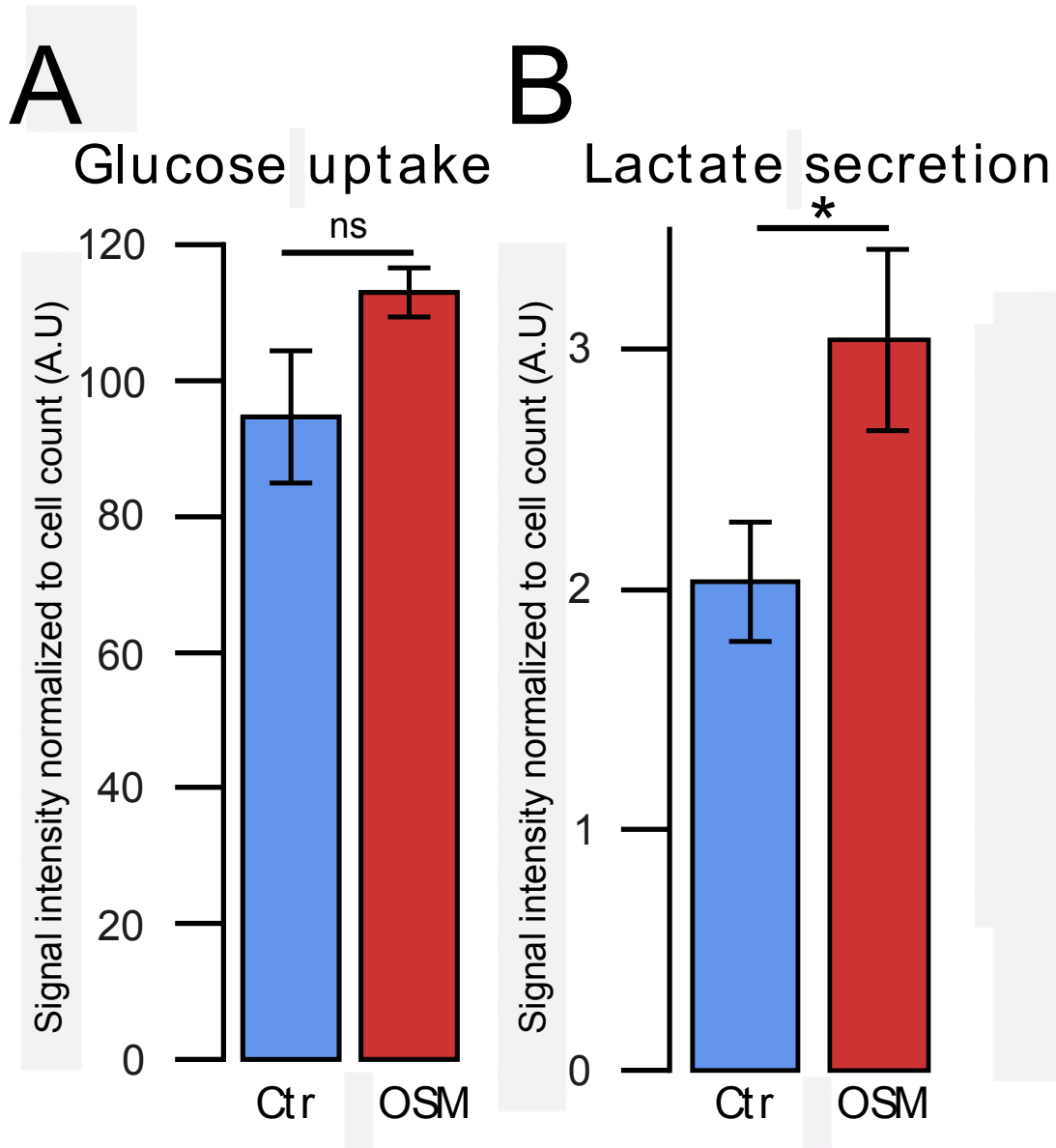
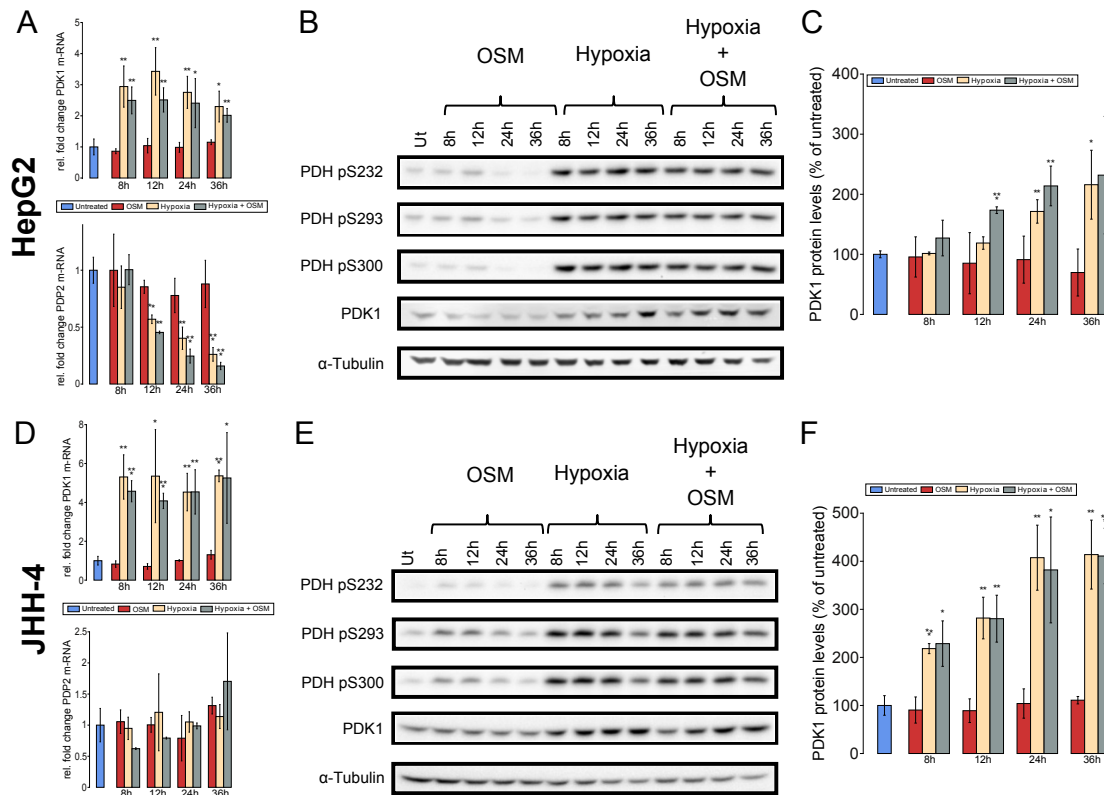


FIGURE A.1: **Glucose uptake and lactate secretion rates in PH5CH8.** PH5CH8 immortalized hepatocytes were treated with OSM (50 ng/ml) under normoxia for 36 h. (A) Glucose uptake rates. The signal intensity was normalized to cell count. (B) Lactate secretion rates. The signal intensity was normalized to cell count. Figure published in [Battello et al., 2016]



**FIGURE A.2: The effects of Hypoxia and OSM on PDK1 expression and PDC phosphorylation in HepG2 and JHH-4.** Cells were treated with OSM (50 ng/ml), hypoxia 1% O<sub>2</sub>, a combinatorial treatment for the given timepoints. (A & D) qRT-PCR of PDK1 and PDP2 after the indicated period of time and treatment, mRNA from three biological replicates in HepG2 (A) and JHH-4 (D) cells. Fold change was calculated to the untreated control. (B & E) Western Blot analysis of all three PDC phosphorylation sites (S232, S293, S300) and PDK1 in HepG2 (B) and JHH-4 (D) cells.  $\alpha$ -Tubulin was used as a loading control and one representative  $\alpha$ -Tubulin blot is shown. (C & F) PDK1 protein levels in HepG2 (C) and JHH-4 (F) cells after the indicated period of time and treatment, shown as percentage of the untreated control. All errorbars indicate the standard deviation calculated from three biological replicates. Figure published in [Battello et al., 2016] *This data was kindly provided by Dr. Andreas Zimmer.*

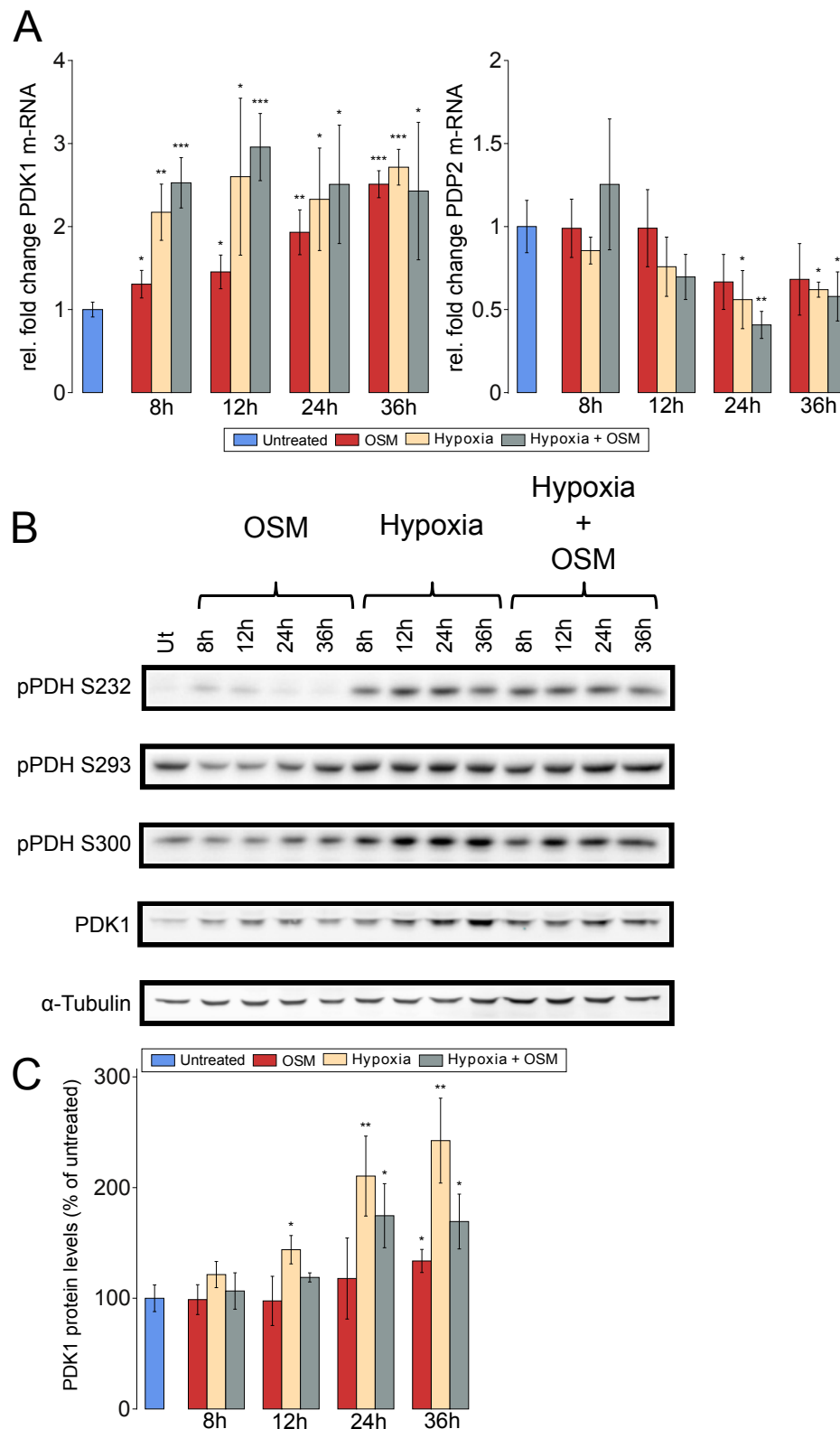
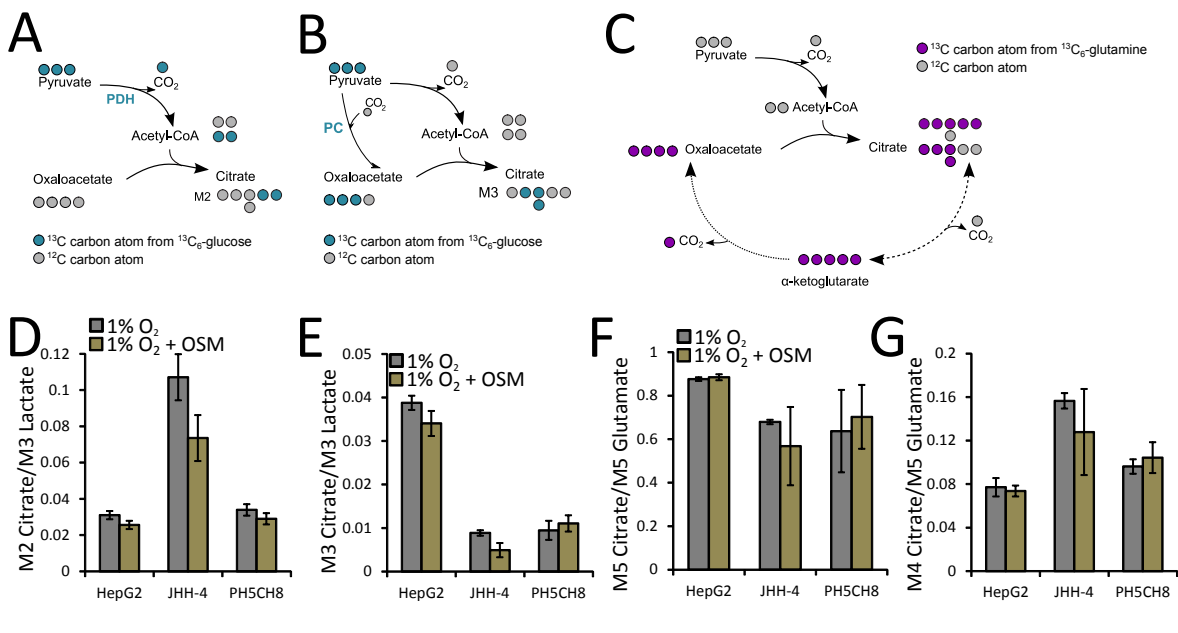


FIGURE A.3: **PDK1 expression and PDC phosphorylation in PH5CH8 cells.** PH5CH8 cells were treated with OSM (50 ng/ml), hypoxia (1% O<sub>2</sub>), or a combinatorial treatment for the indicated periods of time. (A) Quantitative RT-PCR of PDK1 and PDP2 mRNA. The fold change was calculated relative to the untreated control (B) Western Blot analysis for all three PDC phosphorylation sites (S232, S293, S300) and PDK1.  $\alpha$ -Tubulin was used as a loading control and one representative  $\alpha$ -tubulin blot is shown. (C) Quantification of PDK1 protein levels, shown as percentage of the untreated control. All error bars indicate the standard deviation from three biological replicates. Figure published in [Battello et al., 2016] This data was kindly provided by Dr. Andreas Zimmer.





**FIGURE A.4: Metabolic effects of OSM in combination with hypoxia in HepG2, JHH-4 and PH5CH8.** HepG2 and JHH-4 hepatocellular carcinoma cells and PH5CH8 immortalized hepatocytes were cultured under hypoxia (1%  $\text{O}_2$ ) for 36 h and left untreated or stimulated with 50 ng/mL OSM in the presence of [ $^{13}\text{C}_6$ ]glucose or [ $^{13}\text{C}_5$ ]glutamine. **(A,B)** Carbon atom transitions for pyruvate carboxylase (PC) and pyruvate dehydrogenase complex (PDC) activities, from a [ $^{13}\text{C}_6$ ]glucose tracer. **(C)** Carbon atom transitions for oxidative and reductive glutamine metabolism, from a [ $^{13}\text{C}_5$ ]glutamine tracer. **(D)** PDC activity determined from the M2 citrate isotopologue normalized to the M3 lactate isotopologue, from [ $^{13}\text{C}_6$ ]glucose. **(E)** PC activity determined from the M3 citrate isotopologue normalized to the M3 lactate isotopologue, from [ $^{13}\text{C}_6$ ]glucose. **(F)** Reductive glutamine contribution to citrate, determined by the ratio of M5 isotopologues of citrate to M5 isotopologues of glutamate, from [ $^{13}\text{C}_5$ ]glutamine. **(G)** Oxidative glutamine contribution to citrate, determined by the ratio of M4 isotopologues of citrate to M5 isotopologues of glutamate, from [ $^{13}\text{C}_5$ ]glutamine. Error bars indicate the standard deviation and are calculated from at least two independent replicates. Statistical significance was determined by a two-tailed t-test. \* denotes  $P \leq 0.05$ , \*\* denotes  $P \leq 0.01$ , and \*\*\* denotes  $P \leq 0.001$ .

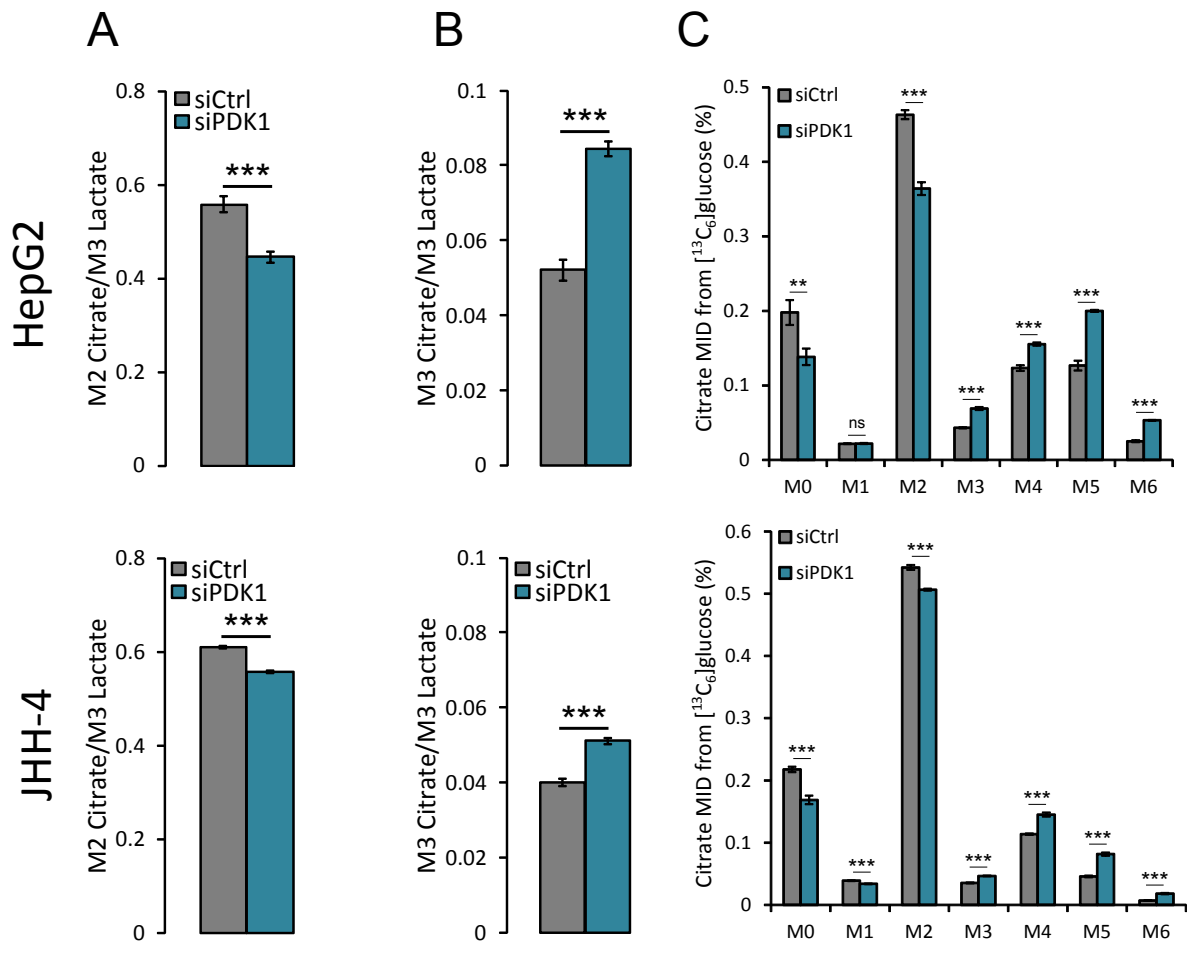


FIGURE A.5: **The metabolic effects of PDK1 silencing in HCC cell lines.** SiRNA-mediated PDK1 knockdown (siPDK1) was performed in HepG2 and JHH-4 cells grown under normoxia and grown in the presence of  $^{13}\text{C}_6$ glucose or  $^{13}\text{C}_5$ glutamine. A non-targeting siRNA (siCtrl) was used as control. **(A)** The enzymatic activity of PDC determined from the M2 citrate isotopologue normalized to the M3 lactate isotopologue, from  $^{13}\text{C}_6$ glucose. **(B)** PC activity determined from the M3 citrate isotopologue normalized to the M3 lactate isotopologue, from  $^{13}\text{C}_6$ glucose. **(C)** Citrate MID from  $^{13}\text{C}_6$ glucose. Error bars indicate the standard deviation and are calculated from at least two independent replicates. Statistical significance between control and the treatment was determined by a two-tailed t-test. \* denotes  $P \leq 0.05$ , \*\* denotes  $P \leq 0.01$ , and \*\*\* denotes  $P \leq 0.001$ .

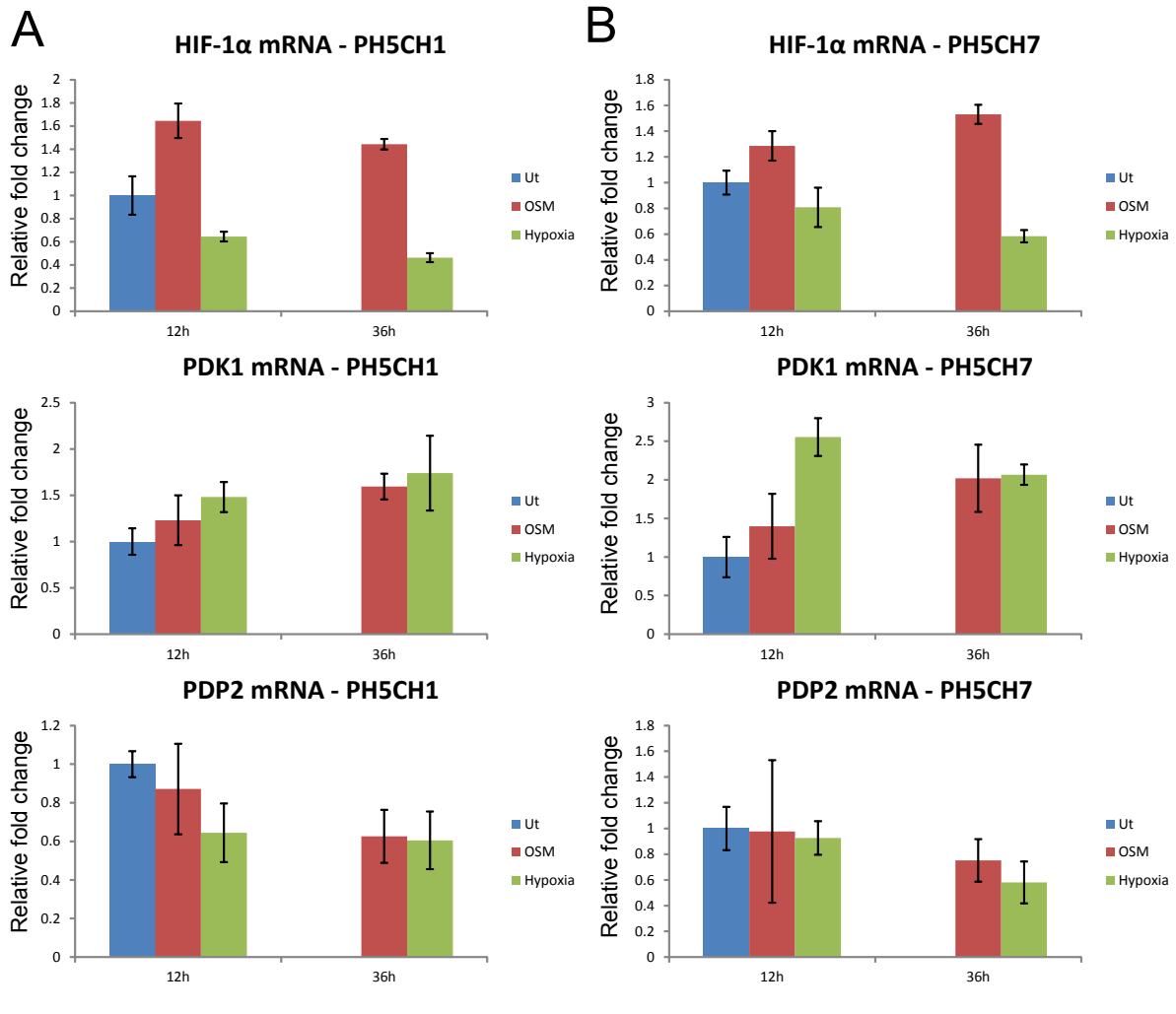


FIGURE A.6: **Response of PH5CH1 and PH5CH7 non-neoplastic hepatocytes to OSM, hypoxia and a combination of both stimuli.** PH5CH1 and PH5CH7 cells were treated with OSM (50 ng/ml), hypoxia (1% O<sub>2</sub>) or a combinatorial treatment for the indicated periods of time. Quantitative RT-PCR of PDP2, PDK1 and HIF-1 $\alpha$  mRNA in (A) PH5CH1 and (B) PH5CH7. Fold changes were calculated relative to the untreated control. Figure published in [Battello et al., 2016] *This data was kindly provided by Dr. Andreas Zimmer.*

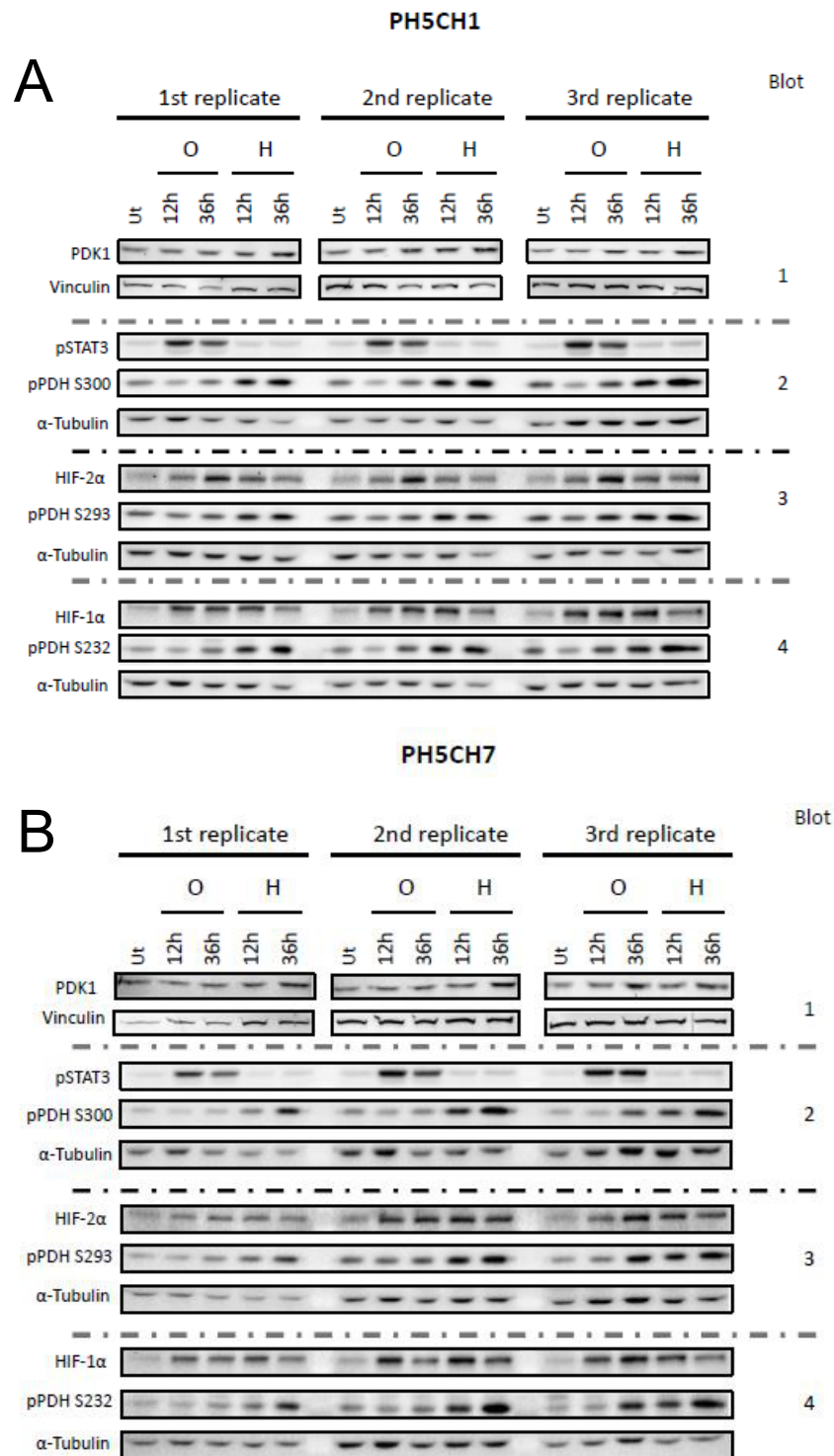


FIGURE A.7: **Response of PH5CH1 and PH5CH7 non-neoplastic hepatocytes to OSM, hypoxia and a combination of both stimuli.** PH5CH1 and PH5CH7 cells were treated with OSM (50 ng/ml), hypoxia (1% O<sub>2</sub>) or a combinatorial treatment for the indicated periods of time. Western Blot analysis for HIF-1 $\alpha$ , HIF-2 $\alpha$ , PDK1 and all three PDC phosphorylation sites (S232, S293, S300). Vinculin and  $\alpha$ -Tubulin were used as loading controls and one representative blot is shown. Figure published in [Battello et al., 2016] *This data was kindly provided by Dr. Andreas Zimmer.*

## Appendix B

# Supplemental Material and Methods

TABLE B.1: Metabolite Detector Settings

| MD Settings    |                                    |          |
|----------------|------------------------------------|----------|
| Centroid       | Peak threshold begin               | 10       |
|                | Peak threshold end                 | -5       |
|                | Max. baseline distance             | 30       |
|                | FWHM                               | 0.5      |
| Deconvolution  | Peak threshold                     | 5        |
|                | Max. peak height                   | 5        |
|                | Bins/Scan                          | 10 or 30 |
|                | Deconvolution width (scans)        | 10       |
|                | Required intensity                 | 0        |
| Identification | Required number of peaks           | 1        |
|                | Max. RI difference                 | 2        |
|                | Pure/Impure composition            | 0        |
|                | Number of fragments                | 3        |
|                | Min. number of identical fragments | 1        |
|                | Cutoff score                       | 0.5      |
|                | Similarity score                   | RI+Spec  |
| Quantification | Mass filter                        | 0-100    |
|                | Min. distance between subseq. Ions | 1        |
|                | Min. required quality index        | 0.6      |

TABLE B.2: MID Wizard settings

| MID Wizard settings |                             |         |
|---------------------|-----------------------------|---------|
|                     | Corrected using sum formula | Carbon  |
|                     | Individual MIDs             |         |
|                     | $\Delta$ RI                 | 2       |
|                     | Scoring method              | RI+Spec |
|                     | Pure/Impure                 | 0       |
|                     | Req. score                  | 0.5     |
|                     | Compound reproducibility    | 0.5     |
|                     | Max peak disc. Index        | 100     |
|                     | Req. S/N                    | 0       |
|                     | Min. # ions                 | 1       |

## Appendix C

# Publications

---

# The role of HIF-1 in oncostatin M-dependent metabolic reprogramming of hepatic cells

---

Nadia Battello<sup>1</sup>, Andreas David Zimmer<sup>2</sup>, Carole Goebel, Xiangyi Dong, Iris Behrmann, Claude Haan, Karsten Hiller and Andre Wegner

*Cancer & Metabolism*, February 2016, PMID: 26889381, DOI: 10.1186/s40170-016-0141-0

## Contributions

- Contribution to experimental design
- Conduction of experimental work
- Data analysis and creating figures
- Writing and revising the manuscript

---

<sup>1</sup>Equal contributors

<sup>2</sup>Equal contributors



RESEARCH

Open Access



# The role of HIF-1 in oncostatin M-dependent metabolic reprogramming of hepatic cells

Nadia Battello<sup>1†</sup>, Andreas David Zimmer<sup>2†</sup>, Carole Goebel<sup>1</sup>, Xiangyi Dong<sup>1</sup>, Iris Behrmann<sup>2</sup>, Claude Haan<sup>2</sup>, Karsten Hiller<sup>1</sup> and Andre Wegner<sup>1\*</sup>

## Abstract

**Background:** Hypoxia and inflammation have been identified as hallmarks of cancer. A majority of hepatocellular carcinomas are preceded by hepatitis B- or C-related chronic infections suggesting that liver cancer development is promoted by an inflammatory microenvironment. The inflammatory cytokine oncostatin M (OSM) was shown to induce the expression of hypoxia-inducible factor-1 $\alpha$  (HIF-1 $\alpha$ ) under normoxic conditions in hepatocytes and hepatoma cells. HIF-1 $\alpha$  is known to orchestrate the expression of numerous genes, many of which code for metabolic enzymes that play key roles in the adaptation of cellular metabolism to low oxygen tension.

**Results:** Here, we show that OSM-induced upregulation of HIF-1 $\alpha$  reprograms cellular metabolism in three clones of the human hepatocyte cell line PH5CH (PH5CH1, PH5CH7, and PH5CH8) towards a hypoxia-like metabolic phenotype but has no significant effect on cellular metabolism of HepG2 and JHH-4 hepatoma cells. Although we observed only minor changes in glucose uptake and lactate secretion in PH5CH8 upon OSM treatment, we identified more pronounced changes in intracellular fluxes based on stable isotope labeling experiments. In particular, glucose oxidation in the tricarboxylic acid (TCA) cycle is reduced through pyruvate dehydrogenase kinase 1 (PDK1)-mediated inhibition of the pyruvate dehydrogenase complex, thereby reducing the oxidative TCA cycle flux. As a result of the impaired mitochondrial glucose and glutamine oxidation, the reductive isocitrate dehydrogenase flux was increased.

**Conclusions:** We provide evidence that connects the inflammatory mediator OSM to a hypoxia-like metabolic phenotype. In the human hepatocyte cell line PH5CH, OSM-mediated upregulation of HIF-1 $\alpha$  and PDK1 can induce hypoxia-like metabolic changes, although to a lesser extent than hypoxia itself. Since PDK1 is overexpressed in several cancers, it might provide a causal link between chronic inflammation and malignant cellular transformation.

**Keywords:** Oncostatin M, Inflammation, Stable isotope labeling experiments, Hypoxia-inducible factor, Pyruvate dehydrogenase complex, Pyruvate dehydrogenase kinase

## Background

Interleukin 6 (IL6)-type cytokines such as oncostatin M (OSM) are key players in the regulation of the immune response, the immune surveillance of tumor cells, and in the development of cancer [1]. The main functions of IL6-type cytokines are the induction of the acute phase response by the liver, the stimulation of liver regeneration

(by inducing hepatocyte proliferation), and the shift from the innate to the adaptive immune response [2, 3]. Aberrant IL6 signaling is likewise able to induce a state of chronic inflammation, as observed in many cancer types and inflammatory diseases. Since hepatocellular carcinoma (HCC) development can be promoted by an inflammatory microenvironment, aberrant IL6 signaling is implicated in the onset of HCC [4, 5]. Elevated IL6 and OSM serum levels in HCC patients have been reported to negatively influence disease outcome [6, 7]. A direct link between IL6 and the onset of HCC was shown in a study by Naugler et al., where male IL6 knockout mice

\*Correspondence: andre.wegner@gmx.com

†Equal contributors

<sup>1</sup>Luxembourg Centre for Systems Biomedicine, University of Luxembourg, Avenue des Hauts-Fourneaux 7, L-4362 Esch-Belval, Luxembourg  
Full list of author information is available at the end of the article

showed a vastly reduced development of HCC, depicting IL6 as a key mediator in the onset of this cancer [4]. All IL6-type cytokines signal via a homodimer of the transmembrane receptor gp130 or a heterodimer of gp130 with a second receptor chain (e.g., the OSMR or LIFR for OSM), which bind and activate Janus kinases (JAKs) upon cytokine binding. In turn, JAKs activate multiple signaling cascades mainly including STAT3 but also MEK/Erk and the PI3K/Akt pathways [8]. Recently, we have shown in non-neoplastic hepatocytes and HCC cells that STAT3, activated by the IL6-type cytokine OSM, upregulates HIF-1 $\alpha$  expression under normoxic conditions, via a transcriptional mechanism, leading to the expression of vascular endothelial growth factor (VEGF) and plasminogen activator inhibitor 1 (PAI) [9]. HIF-1 $\alpha$  regulates the expression of numerous target genes, many of which code for metabolic enzymes that play key roles in the adaptation of cellular metabolism to low oxygen tension [10]. For example, HIF-1 $\alpha$  promotes high glycolytic rates by upregulating the expression of glucose transporters and many glycolytic enzymes [11]. In addition, pyruvate entry into the citric acid cycle is decreased by HIF-1 $\alpha$ -mediated upregulation of pyruvate dehydrogenase (PDH) kinase 1 (PDK1), leading to reduced pyruvate dehydrogenase complex (PDC) activity which results in reduced mitochondrial respiration and increased conversion of pyruvate to lactate [12–14]. Apart from its function in glucose metabolism, a strong impact of HIF-1 $\alpha$  on glutamine metabolism has been identified. Resulting from reduced PDC activity, the mitochondrial citrate pool is drastically depleted. Due to these concentration changes, the actual free energy change of the isocitrate dehydrogenase (IDH) reaction will become positive and thus, reversing the IDH flux towards isocitrate. Consequently, glutamine-derived  $\alpha$ -ketoglutarate is reductively carboxylated to isocitrate by IDH and eventually converted to citrate [15–17]. Malignant cellular transformation and proliferation goes hand-in-hand with reprogrammed cellular metabolism [18, 19], mainly characterized by an increased glucose uptake, a high glycolytic rate, and an increased conversion of pyruvate to lactate, even under normoxic conditions (Warburg effect). Most certainly, this hypoxia-like metabolic phenotype favors increased proliferation rates, as a high glucose turnover provides necessary intermediates such as ribose-5-phosphate, serine, and glycine for macromolecule synthesis. A link between inflammatory STAT3 activity, HIF-1 $\alpha$ , and the Warburg effect has been described recently. Demaria and coworkers showed that constitutively active STAT3 induces the Warburg effect in mouse embryonic fibroblasts [20] and renders the cells sensitive for malignant transformation [21]. Based on our previous finding that OSM mediates HIF-1 $\alpha$  upregulation through increased mRNA and protein levels in a STAT3-dependent manner,

we aimed to investigate the effects of OSM stimulation on central carbon metabolism in hepatocytes and hepatoma cells. Here, we (1) show that OSM induces the expression of HIF-1 $\alpha$  in several HCC cell lines and immortalized hepatocytes, (2) demonstrate that OSM stimulation leads to a hypoxia-like metabolic phenotype in three clones of the immortalized hepatocyte cell line PH5CH, (3) provide evidence that HIF-1 $\alpha$ -mediated PDK1 upregulation is necessary to induce OSM-dependent metabolic reprogramming in PH5CH cells, and (4) show that OSM-dependent HIF-1 $\alpha$  upregulation is not sufficient to induce metabolic reprogramming in the HCC cell lines HepG2 and JHH-4.

## Methods

### Cell culture and reagents

The hepatoma cell lines and the non-neoplastic, SV40 large T antigen-immortalized, hepatocyte lines, PH5CH1, PH5CH7, and PH5CH8 [22] were maintained in Dulbecco's modified Eagle's medium (DMEM) (AQMEDIA, Sigma-Aldrich) supplemented with 10% fetal calf serum (PAA), 100 mg/l streptomycin, 60 mg/l penicillin, and 25 mM HEPES (Lonza). The SV40 large T antigen-immortalized human liver epithelial cells (THLE-2) were cultured in LHC-8 medium supplemented with 70 ng/ml phosphoethanolamine, 5 ng/ml epidermal growth factor, 10% FBS, 100 mg/l streptomycin, and 60 mg/l penicillin. Cells were grown at 37°C in a water-saturated atmosphere at 5% CO<sub>2</sub>. Hypoxia treatment was performed at 37°C in a water-saturated atmosphere at 5% CO<sub>2</sub> in a hypoxia chamber (C-Chamber (C-274 & C-374) with a ProOx C21 Static O<sub>2</sub> & CO<sub>2</sub> Controller from BioSpherix) at the indicated oxygen percentage. HIF-1 $\alpha$  and HIF-2 $\alpha$  screening experiments were performed in an hypoxia incubator (Heracell) from Thermo Scientific at 37°C in a water-saturated atmosphere at 5% CO<sub>2</sub>. Human oncostatin M (227 a.a.) was from PeproTech. For all experiments, cells were seeded together, stimulated for the indicated periods of time, and harvested together at the latest time point.

### Western blot analysis and antibodies

Cells were lysed on the dish with ice-cold lysis buffer containing 30 mM Tris/HCl pH 6.7, 5% glycerol, 2.5% mercaptoethanol, and 1% SDS. Protein extracts were separated by SDS-PAGE and analyzed by Western blotting for the following proteins: HIF-1 $\alpha$  and STAT3 (BD Transduction Laboratories), phospho-STAT3, (Cell Signaling), PDH-E1 $\alpha$  (pSer232) and PDH-E1 $\alpha$  (pSer300) (Merck Millipore), HIF-2 $\alpha$  (Novus Biologicals), PDK1 (Enzo Life Sciences) and  $\alpha$ -tubulin (Thermo Fisher Scientific), and PDH-E1 $\alpha$  (pSer293) (Abcam). ECL signals were detected and membranes stripped before re-probing as previously described [23, 24]. The secondary antibodies

IRDye 800CW and 680LT (LI-COR Bioscience) were used for fluorescent Western blot detection with the Odyssey Infrared imaging system (LI-COR Biosciences) of PDK1. Quantification of PDK1 protein levels was done using Image Studio Lite version 4.0 (LI-COR Bioscience). For the evaluation the HIF-1 $\alpha$  protein levels, densitometric analysis was carried out using the Image-Lab software 4.0 (Bio-Rad Laboratories). The level of the target protein was normalized to the  $\alpha$ -tubulin protein level.

#### Quantitative PCR procedure

Total RNA was extracted using the NucleoSpin RNA II kit (Macherey-Nagel) according to the manufacturer's instructions. The concentration of isolated RNA was measured using a NanoDrop spectrophotometer. Five hundred nanograms of total RNA was reverse-transcribed with iScript (Bio-Rad Laboratories) in a final volume of 10  $\mu$ l, according to the manufacturer's instructions. Quantitative real-time PCR (qPCR) was carried out on an iQ5 Real-Time PCR detection system (Bio-Rad Laboratories). The reaction was performed in a total volume of 10  $\mu$ l containing cDNA corresponding to 5 ng RNA template, 10 pmol of each forward and reverse primer, and 5  $\mu$ l iTaq Universal SYBR Green Supermix (Bio-Rad Laboratories). Thermal cycling conditions for all qPCR assays consisted of an initial enzyme activation step at 95  $^{\circ}$ C for 15 min, followed by 40 cycles of denaturation at 95  $^{\circ}$ C, and annealing and elongation at 60  $^{\circ}$ C for 30 s. The housekeeping genes Cyclo A, HPRT, EEF1a, YWHAZ, and the target genes were assayed in parallel for each sample. All samples were run in triplicates. Gene-specific primers for Cyclo A, HPRT, EEF1a, YWHAZ, HIF-1 $\alpha$ , HIF-2 $\alpha$ , PDK1, and PDP2 were purchased from Eurogentec (Belgium). The geometric mean of three housekeeping genes was calculated, and a normalization factor for each sample was generated using geNorm (VBA add-in for Microsoft Excel). The normalization factor was used to calculate the relative amount of each target in each sample. Each sample was normalized to the untreated control.

Total RNA extraction in HIF-1 $\alpha$  silencing experiments was performed using the RNeasy mini kit (QIAGEN) according to the manufacturer's instructions. Six hundred nanograms of total RNA was reverse-transcribed using SuperScript III reverse transcriptase (Invitrogen) in a final volume of 20  $\mu$ l according to manufacturer's recommendations. qPCR was performed on a LightCycler 480 (Roche) in a total volume of 20  $\mu$ l containing cDNA corresponding to 6 ng RNA template, 5 pmol of each forward and reverse primer, and 10  $\mu$ l iTaq Universal SYBR Green Supermix (Bio-Rad Laboratories). Cycling conditions were identical to those described earlier. Target gene expression was normalized to the housekeeping gene L27.

#### siRNA-mediated silencing of HIF-1 $\alpha$ and PDK1

For the siRNA-mediated HIF-1 $\alpha$  knockdown, 3  $\mu$ l of Lipofectamine RNAiMAX (Invitrogen) was diluted in 150  $\mu$ l 1 $\times$  Opti-MEM I (Gibco by Life Technologies) and 1  $\mu$ l siRNA was added. The final concentration of non-targeting (Dharmacon, Inc.) and HIF-1 $\alpha$  siRNA (Santa Cruz) was 15 nM. For the siRNA-mediated PDK1 knockdown, 2.5  $\mu$ l of Lipofectamine RNAiMAX was diluted in 200  $\mu$ l 1 $\times$  Opti-MEM I and 1  $\mu$ l siRNA (Dharmacon, Inc.) was added. The final concentration of non-targeting and PDK1 siRNA was 20 nM. The Lipofectamine/siRNA mix was incubated for 20 min at room temperature, then transferred into a 12-well plate and incubated for another 5 min. PH5CH1, PH5CH7, and PH5CH8 cells were directly seeded onto the transfection mix. After 6 h, the medium was changed to complete culture media and cells were grown overnight.

#### Stable isotope labeling experiments

Cells were seeded and grown overnight. Complete cell culture medium was then replaced with labeling medium. For isotope labeling experiments using uniformly labeled glucose, cells were cultured in DMEM supplemented with 10% dialyzed FBS (Invitrogen), 25 mM [ $^{13}$ C<sub>6</sub>]glucose (Cambridge Isotope Laboratories), and 4 mM glutamine (Sigma-Aldrich). For isotope labeling experiments using uniformly labeled glutamine, cells were grown in DMEM supplemented with 10% dialyzed FBS (Invitrogen), 25 mM glucose (Sigma-Aldrich), and 4 mM [ $^{13}$ C<sub>5</sub>] glutamine (Cambridge Isotope Laboratories). Cells were stimulated with 50 ng/ml OSM (Pepro-Tech) and grown for 36 h under normoxia or hypoxia (1% O<sub>2</sub>) (Jacomex) at 37  $^{\circ}$ C, 5% CO<sub>2</sub> and humidified atmosphere. Metabolites were extracted as described previously [25].

#### Extraction of extracellular metabolites

Extracellular metabolites from medium samples were extracted using ice-cold extraction fluid (8:1 methanol/water) containing the internal standard [ $^{13}$ C<sub>5</sub>]ribitol (Omicron Biochemicals, Inc.) at a concentration of 10  $\mu$ g/ml. Twenty microliters of the medium was added to 180  $\mu$ l ice-cold extraction fluid, vortexed for 10 s, and centrifuged at maximum speed for 5 min at 4  $^{\circ}$ C. Fifty microliters of the medium extracts was transferred to GC-MS glass vials and evaporated under vacuum to dryness at -4  $^{\circ}$ C using the CentriVap Concentrator.

#### GC-MS analysis

Metabolite derivatization was performed using a Gerstel MPS. Dried polar metabolites were dissolved in 15  $\mu$ l of 2% methoxyamine hydrochloride in pyridine at 40  $^{\circ}$ C under shaking. After 60 min, an equal volume of MTBSTFA was added and held for 30 min at 40  $^{\circ}$ C under

continuous shaking. One microliter sample was injected into an SSL injector at 270 °C in splitless mode. GC-MS analysis was performed using an Agilent 7890A GC equipped with a 30-m DB-35MS + 5-m Duraguard capillary column. Helium was used as carrier gas at a flow rate of 1 ml/min. The GC oven temperature was held at 100 °C for 2 min and increased to 300 °C at 10 °C/min. After 3 min, the temperature was increased to 325 °C. The GC was connected to an Agilent 5975C inert XL MSD, operating under electron ionization at 70 eV. The MS source was held at 230 °C and the quadrupole at 150 °C. The detector was operated in single ion mode (see Additional file 1: Table S1 for details). The total run time of one sample was 25.00 min.

### Mass isotopomer distribution analysis

All GC-MS chromatograms were processed using MetaboliteDetector [26]. Chemical formulas for mass isotopomer distribution (MID) determination (Additional file 1: Table S1) were taken from [27]. Weighted carbon contribution was calculated with the following formula:

$$\frac{1}{n} * \sum_{i=1}^n M_i * i, \text{ where } n \text{ is the number of carbons of the molecule of interest and } M_i \text{ the } i\text{th mass isotopomer.}$$

### Statistical analysis

Error bars represent the standard deviation unless otherwise noted. Statistical significance was determined using two-tailed Student's *t* test. One asterisk denotes  $P < 0.05$ , two asterisks denote  $P < 0.01$ , and three asterisks denote  $P < 0.001$ .

## Results

### Oncostatin M mediates induction of HIF-1 $\alpha$ in hepatocytes and hepatoma cells

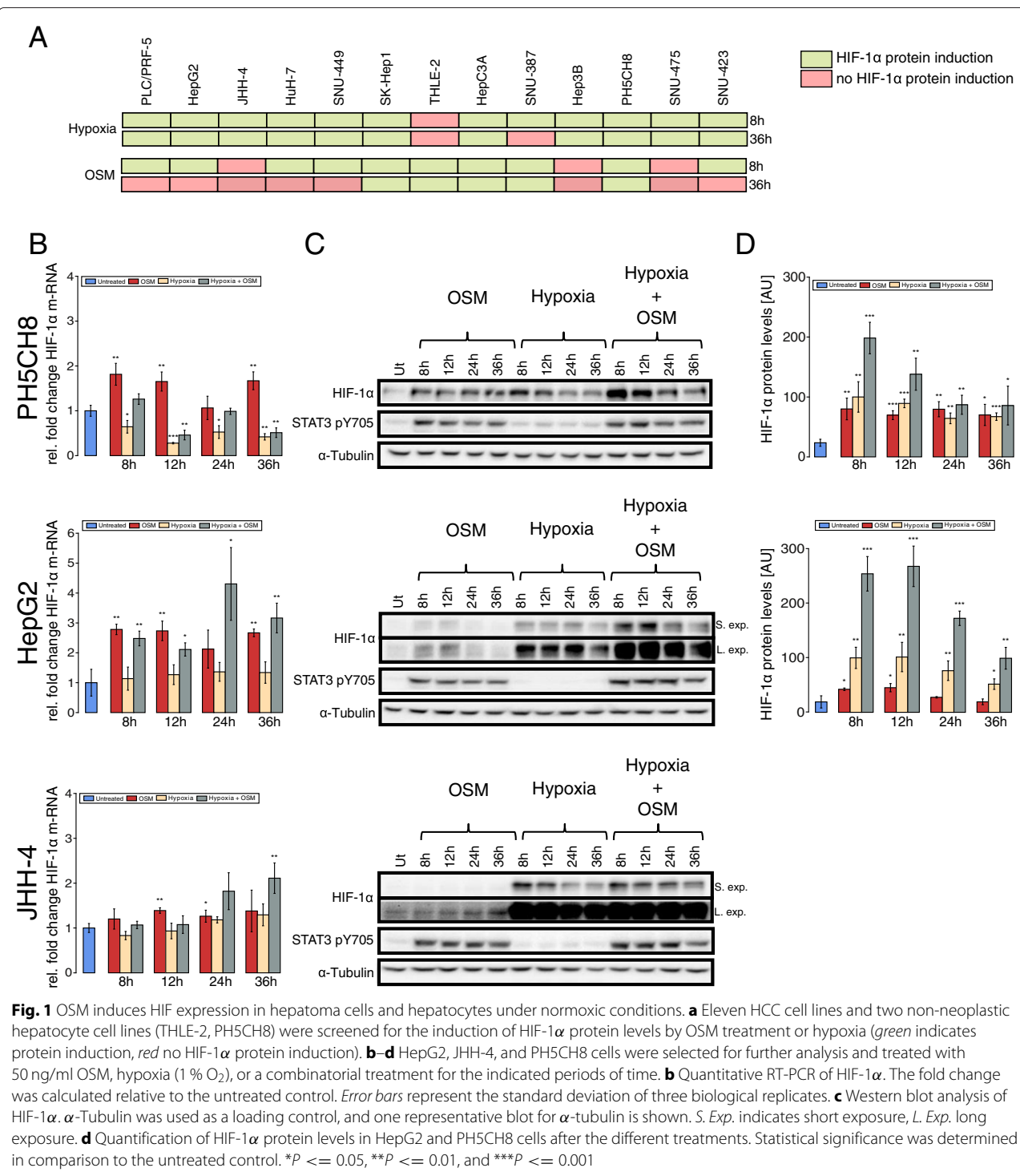
Based on our previous observation that oncostatin M (OSM) treatment induces HIF-1 $\alpha$  expression in hepatocytes under normoxia, we first investigated whether the OSM-mediated upregulation of HIF-1 $\alpha$  is a general effect for hepatocytes and hepatoma cells [9]. Therefore, we evaluated HIF-1 $\alpha$  protein levels after OSM stimulation and hypoxia in 11 HCC and two non-neoplastic hepatocyte cell lines 8 and 36 h after treatment (Additional file 2: Figure S1). After 8 h, we detected increased HIF-1 $\alpha$  protein levels following OSM treatment in eight out of 11 cell lines, whereas after 36 h only five cell lines showed an increase in HIF-1 $\alpha$  protein levels (Fig. 1a). Compared to OSM, the effect of hypoxia on HIF-1 $\alpha$  protein levels was generally more pronounced (Additional file 2: Figure S1). In ten cell lines, we detected hypoxia-mediated HIF-1 $\alpha$  protein induction after 8 h and in nine cell lines after 36 h (Fig. 1a).

We selected three of these cell lines for an in-depth study of OSM-induced effects on cellular metabolism.

HepG2 and JHH-4 are hepatocellular carcinoma cell lines, whereas PH5CH8 cells are immortalized hepatocytes. In PH5CH8 and HepG2 cells, we observed that OSM upregulates HIF-1 $\alpha$  mRNA expression over the entire time course, while we measured only a weak induction of HIF-1 $\alpha$  mRNA expression in JHH-4 cells (Fig. 1b). In non-neoplastic PH5CH8 cells, we observed continuous OSM-dependent induction of HIF-1 $\alpha$  protein levels, comparable to those observed under hypoxia (Fig. 1c, d). In HepG2 cells, we detected a transient induction of HIF-1 $\alpha$  protein levels, peaking around 12 h post-OSM treatment (Fig. 1c, d). Correlating with the weak induction on HIF-1 $\alpha$  mRNA, we did not observe an increase in HIF-1 $\alpha$  levels in JHH-4 cells (Fig. 1b, c).

### OSM stimulation reduces glucose oxidation via PDC inhibition under normoxia in non-transformed hepatocytes

Based on the observed OSM-induced upregulation of HIF-1 $\alpha$  under normoxia, we hypothesized that this would induce a pseudo-hypoxic metabolic phenotype. To investigate the effect of OSM stimulation on central carbon metabolism, we performed stable isotope labeling experiments using [ $^{13}\text{C}_6$ ]glucose and [ $^{13}\text{C}_5$ ]glutamine and quantified the isotopic enrichment in form of MIDs. Therefore, we cultured PH5CH8 cells under normoxia (18.6% O $_2$ ), hypoxia (1% O $_2$ ) either with or without 50 ng/ml OSM. We observed a significant decrease ( $P < 0.001$ ) in glucose carbon contribution to citrate in OSM-stimulated cells under normoxia as compared to the control (Fig. 2a), although glucose uptake was slightly increased (Additional file 3: Figure S2A). In line with a reduced glucose carbon contribution to the TCA cycle, we observed increased lactate secretion (Additional file 3: Figure S2A). We next investigated whether the decreased glucose contribution is a result of reduced anaplerosis via pyruvate carboxylase (PC) or reduced PDC activity. Using [ $^{13}\text{C}_6$ ]glucose as a tracer, the two pathways can be distinguished by analyzing the M2 and M3 isotopologues of citrate. Briefly, PDC activity generates [ $^{13}\text{C}_2$ ]acetyl-CoA from which M2 citrate is produced, whereas PC activity yields [ $^{13}\text{C}_3$ ]oxaloacetate leading to M3 citrate (Fig. 2b). M5 isotopologues of citrate reflect the combined carbon contribution of PC and PDC to citrate. To exclude bias from the overall enrichment, we normalized the abundance of the M2, M3, and M5 isotopologues of citrate to the abundance of the M3 isotopologue of lactate. While there was no difference in M3 and M5 isotopologues (data not shown), OSM-stimulated cells exhibited a significantly ( $P = 0.003$ ) reduced M2-citrate-to-M3-lactate ratio under normoxic conditions, pointing to reduced glucose catabolism via PDC (Fig. 2c) and thus a reduced oxidative TCA cycle flux. Reduced M2 isotopologues propagated to all analyzed downstream metabolites in the



TCA cycle (Additional file 4: Table S2). Although HIF-1α protein levels upon OSM treatment were comparable to those under hypoxic conditions (Fig. 1d), we observed a much stronger effect on cellular metabolism induced by hypoxia. Specifically, PDC activity and consequently glucose carbon contribution to citrate were almost reduced

to zero (Fig. 2a, c). OSM treatment did not further impact glucose oxidation under hypoxia (Fig. 2a, c).

Since PDC links glycolysis and TCA cycle, it is tightly regulated. Its activity is mainly controlled through reversible phosphorylation of the PDH-E1α subunit. An inhibition of the complex is mediated by its

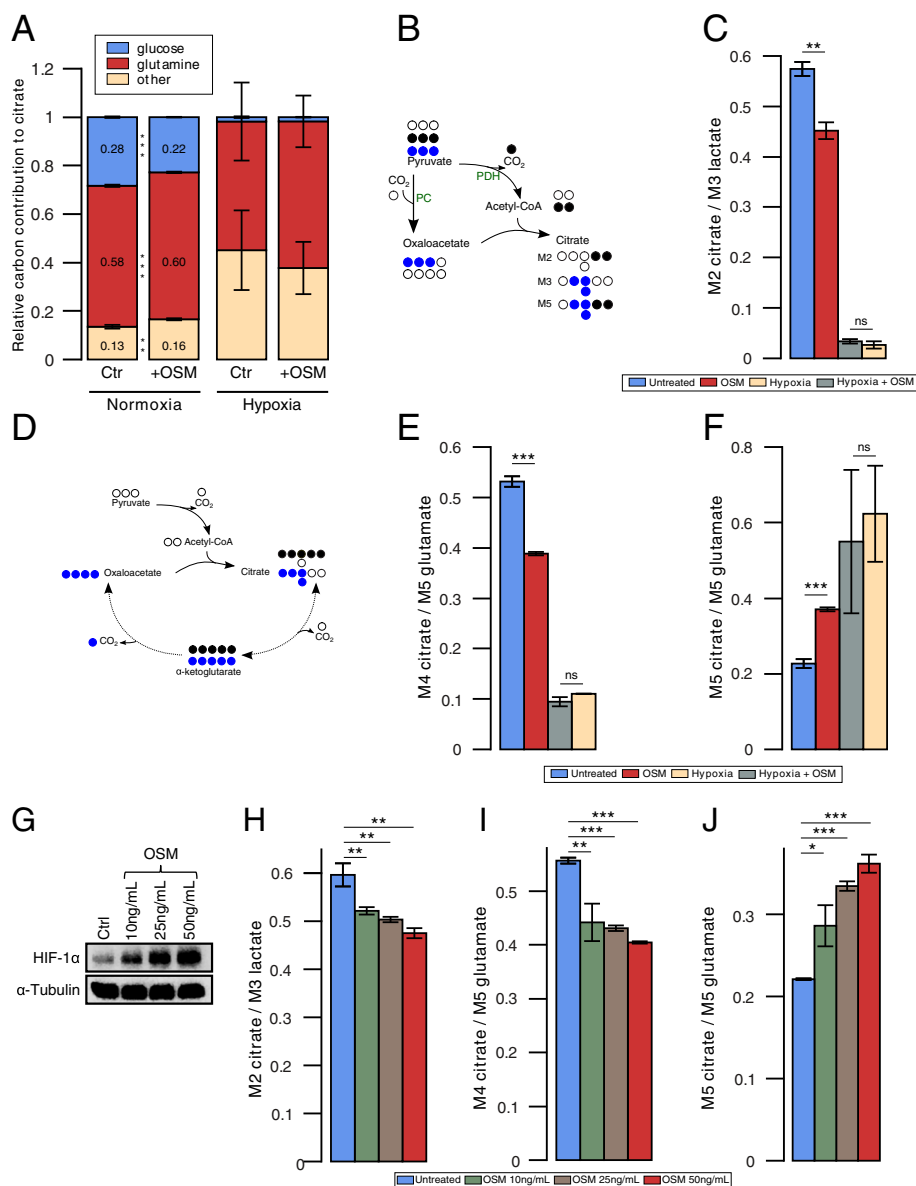


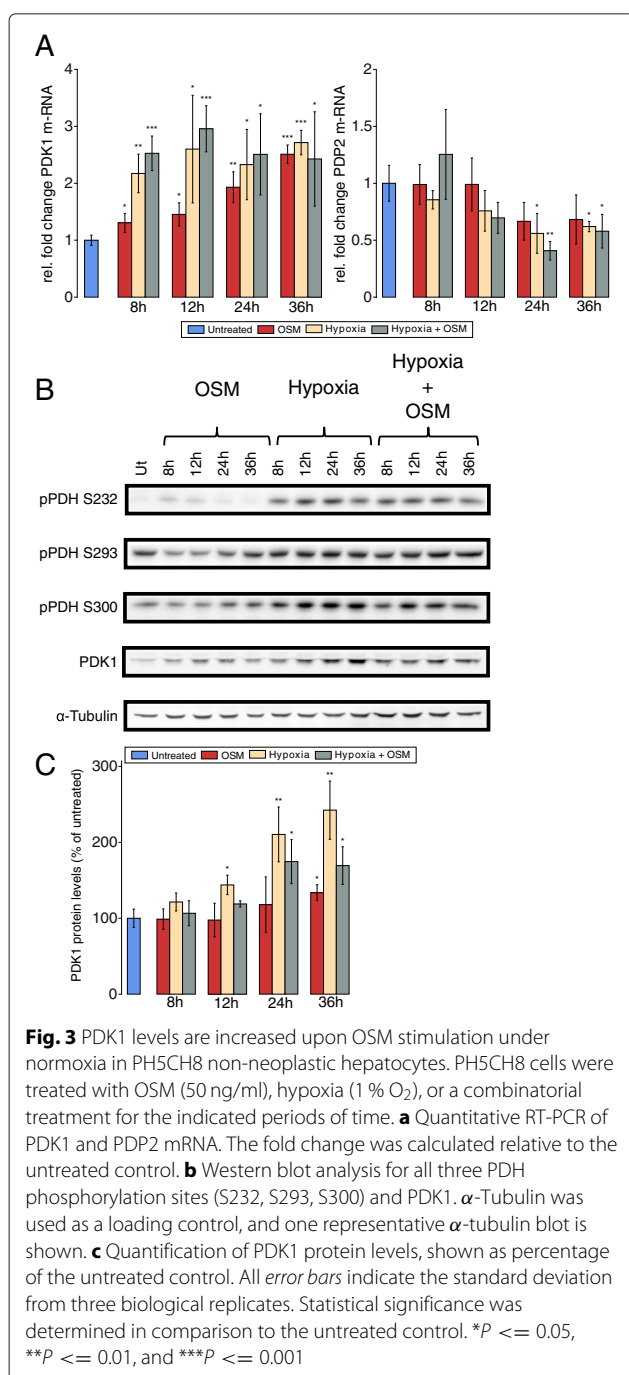
**Fig. 2** Effect of OSM on central carbon metabolism of PH5CH8 under normoxia and hypoxia. **a-f** PH5CH8 cells were treated with 50 ng/ml OSM, hypoxia (1% O<sub>2</sub>), or a combinatorial treatment, and metabolites were extracted after 36 h. **a** Relative glutamine and glucose carbon contribution to citrate. **b** Carbon atom transitions of pyruvate carboxylase (PC) and pyruvate dehydrogenase complex (PDC). **c** PDC activity determined by the ratio of M2 isotopologues of citrate to M3 isotopologues of lactate, from [<sup>13</sup>C<sub>6</sub>]glucose. **d** Atom transitions for reductive carboxylation and oxidative decarboxylation of α-ketoglutarate. **e** Oxidative glutamine contribution to citrate, determined by the ratio of M4 isotopologues of citrate to M5 isotopologues of glutamate, from [<sup>13</sup>C<sub>5</sub>]glutamine. **f** Reductive glutamine contribution to citrate, determined by the ratio of M5 isotopologues of citrate to M5 isotopologues of glutamate, from [<sup>13</sup>C<sub>5</sub>]glutamine. **g-j** PH5CH8 cells were treated with different concentrations of OSM. Metabolites and proteins were extracted after 36 h. **g** HIF-1α protein levels in PH5CH8 cells after treatment with the indicated OSM concentrations. **h** PDC activity determined by the ratio of M2 isotopologues of citrate to M3 isotopologues of lactate, from [<sup>13</sup>C<sub>6</sub>]glucose. **i** Oxidative glutamine contribution to citrate, determined by the ratio of M4 isotopologues of citrate to M5 isotopologues of glutamate, from [<sup>13</sup>C<sub>5</sub>]glutamine. **j** Reductive glutamine contribution to citrate, determined by the ratio of M5 isotopologues of citrate to M5 isotopologues of glutamate, from [<sup>13</sup>C<sub>5</sub>]glutamine. All error bars indicate the standard deviation. All *p* values and error bars are calculated from at least two independent replicates (*n* ≥ 2). Statistical significance was determined in comparison to the untreated control. \**P* ≤ 0.05, \*\**P* ≤ 0.01, and \*\*\**P* ≤ 0.001

phosphorylation via pyruvate dehydrogenase kinases (PDK1-4), whereas a dephosphorylation through pyruvate dehydrogenase phosphatases (PDP1-2) leads to an

increase in PDC activity. PDK1 is a direct HIF-1α target gene, and its upregulation has been implicated in the metabolic switch induced by HIF-1α [13]. For that

reason, we determined the effect of OSM treatment on PDK1 and PDP2 mRNA levels. Furthermore, we analyzed the degree of phosphorylation of all three serine phosphorylation sites of the PDH-E1 $\alpha$  subunit by Western blot. We observed an increase in the expression of PDK1 following OSM treatment, which was, however, weaker compared to hypoxia and hypoxia in combination with OSM treatment (Fig. 3a–c). The transcription of PDP2 was decreased under hypoxia at later time points but

remained unaffected by OSM (Fig. 3a). Moreover, hypoxia led to increased phosphorylation levels of the PDH-E1 $\alpha$  subunit at all three serine residues, whereas the results for OSM were not as unambiguous. We did not observe a clear effect on any of the three serine residues after OSM treatment (Fig. 3b). Hypoxia led to higher PDK1 protein levels than OSM, correlating with the weaker effect of OSM on PDC activity. Collectively, these data indicate that OSM treatment reduces PDC activity under normoxia in PH5CH8 cells but to a weaker extent than hypoxia.



### OSM stimulation increases reductive carboxylation of $\alpha$ -ketoglutarate

Because of the observed reduced glucose oxidation in the TCA cycle via PDC inhibition, we next sought to investigate whether this reduction is compensated by an increased glutamine contribution. To quantify the relative contribution of glutamine to the TCA cycle, we cultured PH5CH8 cells in the presence of [<sup>13</sup>C<sub>5</sub>]glutamine. We observed a modest increase of glutamine-derived carbon in citrate under OSM-stimulation (Fig. 2a). Using [<sup>13</sup>C<sub>5</sub>]glutamine as a tracer, the M4 isotopologue of citrate results from a condensation of [<sup>13</sup>C<sub>4</sub>]oxaloacetate and unlabeled acetyl-CoA (Fig. 2d), thereby providing a readout of relative glutamine oxidation in the TCA cycle. Although the fractional carbon contribution of glutamine to citrate was increased, we observed a decreased relative M4 isotopologue abundance when stimulating PH5CH8 cells with OSM under normoxic conditions (Fig. 2e), pointing to a decreased glutamine oxidation in the TCA cycle upon OSM stimulation. This result suggests that the glucose-derived acetyl-CoA pool is not fully replenished by an alternative acetyl-CoA source such as increased fatty acid oxidation or degradation of branched chain amino acids. We also observed reduced M4 isotopologues in downstream metabolites including malate, fumarate, and aspartate (Additional file 5: Table S3). Alternatively, citrate can be generated through reductive carboxylation of  $\alpha$ -ketoglutarate via IDH, eventually yielding M5 citrate (Fig. 2d). Reductive carboxylation was significantly increased ( $P < 0.001$ ) in OSM-stimulated cells compared to the control, as indicated by an increased M5 isotopologue abundance (Fig. 2f). In agreement with an increased relative reductive IDH flux, we observed increased  $\alpha$ -ketoglutarate levels together with decreased citrate levels in OSM-stimulated cells (see Additional file 3: Figure S2B). In line with the higher reduction of PDC activity under hypoxia (Fig. 2c), we observed a much stronger suppression of glutamine oxidation (Fig. 2e) and a higher induction of reductive IDH activity under hypoxia (Fig. 2f). However, OSM treatment did not have any effect on glutamine metabolism under hypoxia (Fig. 2e, f).

### OSM stimulation reduces glucose oxidation and increases reductive glutamine metabolism in a concentration-dependent manner

To investigate whether OSM affects cellular metabolism in a dose-dependent manner, we cultured PH5CH8 cells with 10, 25, and 50 ng/ml OSM. We found that OSM-mediated HIF-1 $\alpha$  protein induction steadily increased with the OSM concentration (Fig. 2g). While we observed the strongest effect on cellular metabolism with 50 ng/ml OSM, we observed a reduction of glucose and glutamine oxidation as well as increase of reductive glutamine metabolism already with 10 ng/ml OSM (Fig. 2h–j).

### HIF-1 $\alpha$ -mediated PDK1 upregulation is critical for OSM-induced metabolic reprogramming in PH5CH8 cells

To validate the hypothesis that OSM-induced metabolic reprogramming is caused by increased HIF-1 $\alpha$  activity,

we silenced HIF-1 $\alpha$  expression in PH5CH8 using siRNA (Fig. 4f). A scrambled siRNA was included as a control to exclude secondary effects of the transfection. Silencing of HIF-1 $\alpha$  almost completely prevented the metabolic reprogramming induced by OSM. Specifically, glucose-derived carbon in citrate increased under normoxia and hypoxia (Fig. 4a) and was comparable to levels of untreated cells (Fig. 2a). Glutamine carbon contribution to citrate decreased in HIF-1 $\alpha$ -silenced cells under normoxia and hypoxia (Fig. 4b). Moreover, silencing of HIF-1 $\alpha$  decreased PDK1 expression (Fig. 4e), increased PDC activity (Fig. 4c), and decreased reductive carboxylation (Fig. 4d). Overall, these data suggests that HIF-1 $\alpha$  is critical for OSM-dependent metabolic phenotype observed in PH5CH8 cells.

Based on the observation that PDK1 expression is increased by OSM treatment in an HIF-1 $\alpha$ -dependent

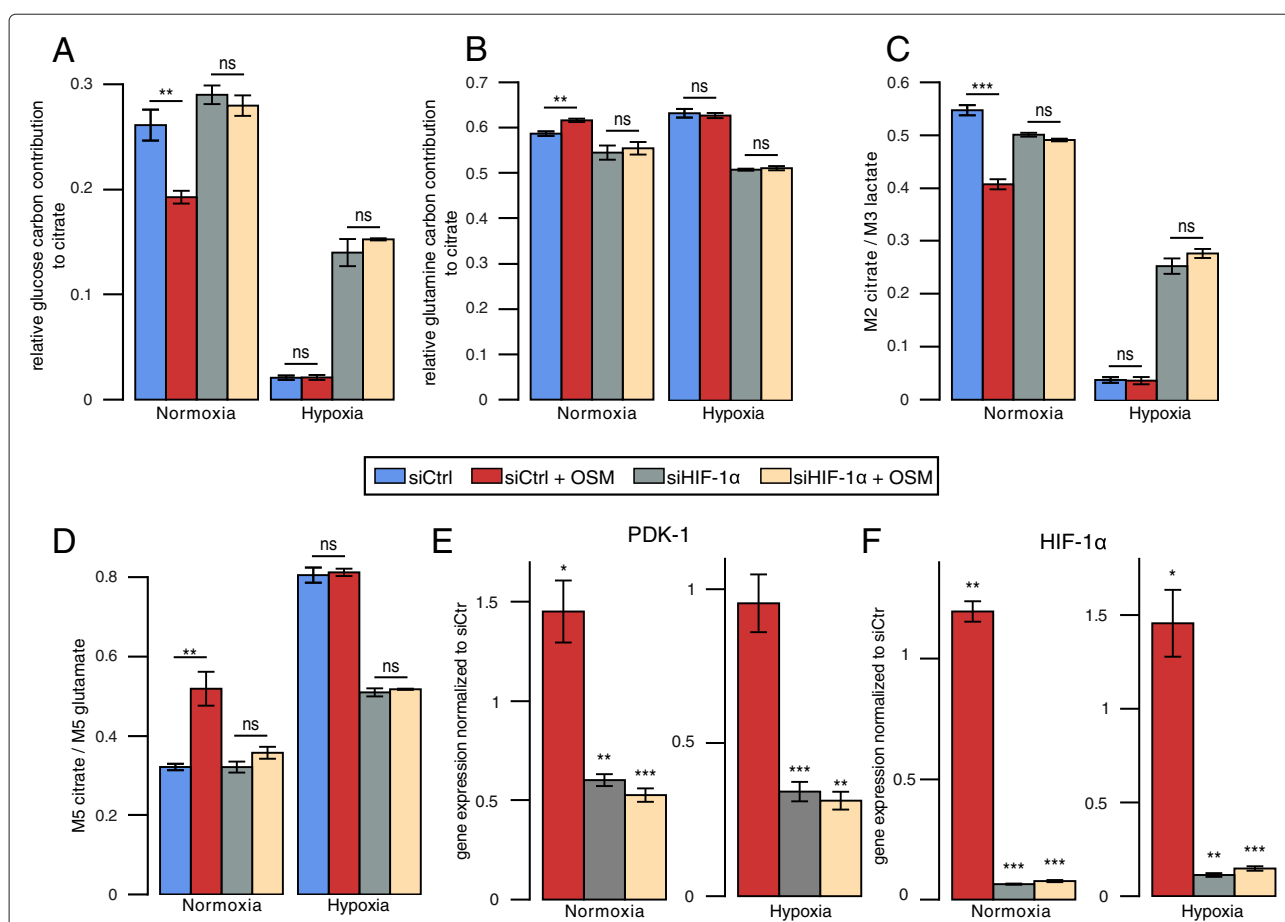


**Fig. 4** Metabolic effects of HIF-1 $\alpha$  silencing on the OSM-induced metabolic phenotype. **a** Relative glucose contribution to citrate. **b** Relative glutamine contribution to citrate. **c** PDH activity determined by the ratio of M2 isotopologues of citrate to M3 isotopologues of lactate, from [ $^{13}\text{C}_6$ ]glucose. **d** Reductive glutamine contribution to citrate, determined by the ratio of M5 isotopologues of citrate to M5 isotopologues of glutamate, from [ $^{13}\text{C}_5$ ]glutamine. **e** PDK1 gene expression. **f** HIF-1 $\alpha$  gene expression. Fold changes for qPCRs were calculated relative to the gene expression in control samples under normoxia or hypoxia, respectively. All error bars indicate the standard deviation. All *p* values and error bars are calculated from at least two independent replicates ( $n \geq 2$ ). Metabolites were extracted after 36 h of indicated treatment. Statistical significance was determined in comparison to the untreated control. \* $P \leq 0.05$ , \*\* $P \leq 0.01$ , and \*\*\* $P \leq 0.001$

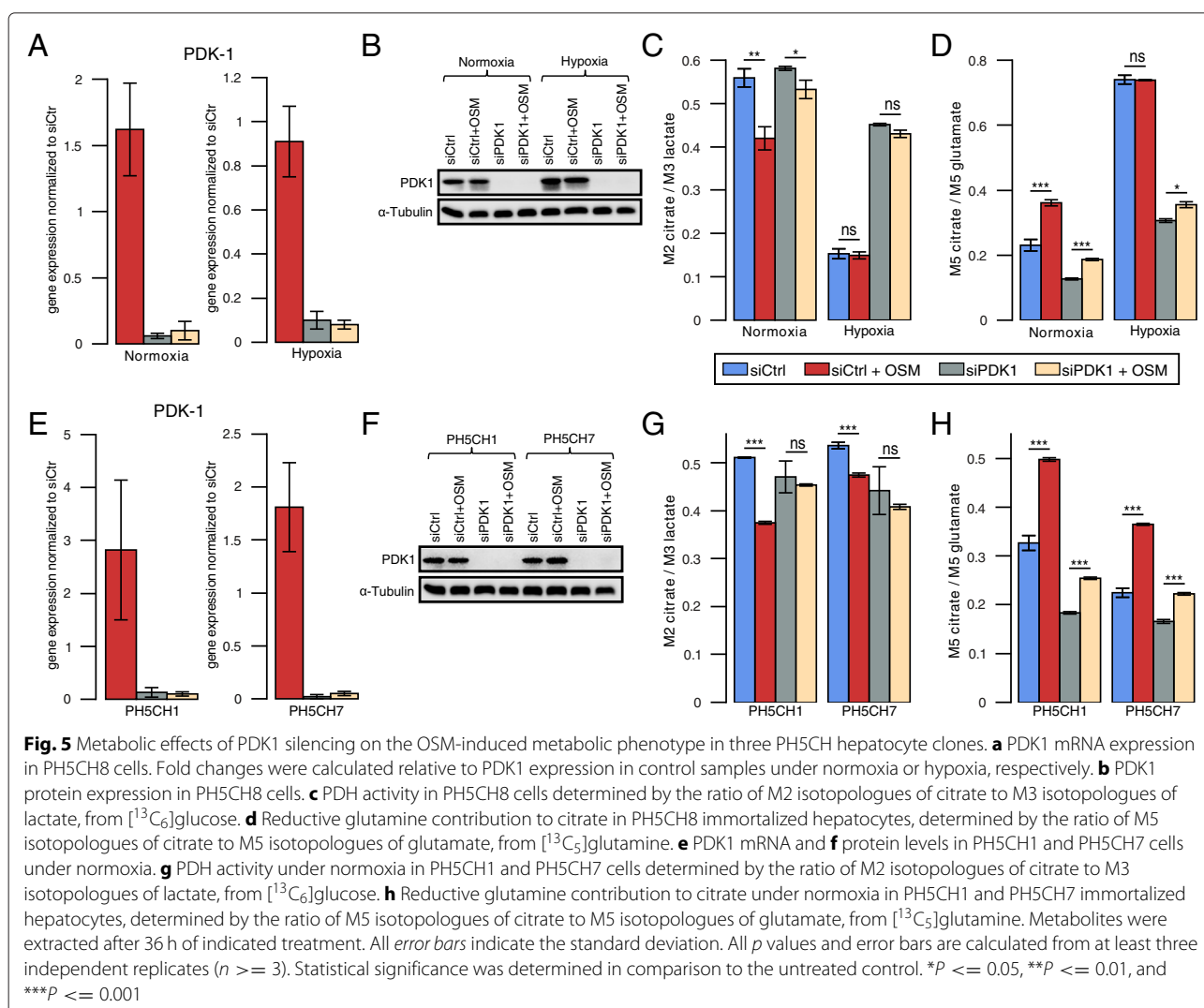


manner, we silenced PDK1 in PH5CH8 cells (Fig. 5a, b). As a consequence of suppressed PDK1 expression, previously observed OSM-mediated metabolic changes were attenuated. Both the OSM-induced changes in PDC activity and reductive carboxylation of  $\alpha$ -ketoglutarate were impaired when PDK1 was silenced (Fig. 5c, d). Under hypoxic conditions, we detected a pronounced increase in PDC activity and drastically reduced reductive glutamine metabolism (Fig. 5c, d). Taken together, our results show that the OSM-induced metabolic phenotype in PH5CH8 cells is mediated by HIF-1 $\alpha$ -dependent PDK1 upregulation.

### OSM induces PDK1-dependent metabolic reprogramming in other PH5CH clones

In order to show that OSM-mediated metabolic reprogramming is not a unique feature in PH5CH8 cells,

we aimed to validate our main findings in two other PH5CH clones PH5CH1 and PH5CH7. In line with our findings in PH5CH8, we detected continuous OSM-dependent HIF-1 $\alpha$  and PDK1 mRNA upregulation and protein induction (Additional file 6: Figure S3A and S3D), while PDP2 mRNA levels were downregulated. HIF-1 $\alpha$  protein levels were comparable to those found under hypoxia (Additional file 6: Figure S3B and S3E). Furthermore, OSM treatment reduced the entry of glucose-derived carbon into the TCA cycle and induced reductive glutamine metabolism (Fig. 5g, h). As already observed in PH5CH8, silencing of PDK1 attenuated the OSM-mediated metabolic changes in PH5CH1 and PH5CH7 cells (Fig. 5g, h). Taken together, these results confirm that PDK1 is required to induce a hypoxia-like metabolic phenotype in PH5CH1 and PH5CH7 cells.



### OSM-dependent HIF-1 $\alpha$ upregulation is not sufficient to induce a hypoxia-like metabolic phenotype in two hepatoma cell lines

Since aberrant IL6 signaling is implicated in the onset of HCC development, we next sought to investigate the effect of OSM on the two HCC cell lines HepG2 and JHH-4. Although HIF-1 $\alpha$  mRNA was increased in HepG2 (Fig. 1b) and HIF-1 $\alpha$  protein was transiently induced by OSM treatment (Fig. 1c, d), we did not observe changes in glucose and glutamine metabolism after 36 h of OSM stimulation (Fig. 6a–c). To verify that OSM has indeed no metabolic effect, we profiled cellular metabolism of HepG2 at 6 and 15 h post-OSM stimulation (Additional file 7: Figure S4). In line with HIF-1 $\alpha$  mRNA and protein expression levels in JHH-4 cells (Fig. 1b, c), we did not observe OSM-mediated metabolic changes (Fig. 6a–c). Under hypoxic conditions, however, glucose oxidation was suppressed, while glutamine carbon contribution was highly increased in both cell lines (Fig. 6a). In line with these data, we observed decreased PDC activity under hypoxia but no effect of OSM treatment under normoxia (Fig. 6b). We observed the same for reductive carboxylation of  $\alpha$ -ketoglutarate, which was increased under hypoxia but not significantly affected by OSM treatment under normoxia (Fig. 6c). In agreement with the MID

data, we did not observe an induction of PDK1 (Fig. 7a, c, d, f). Concordantly, phosphorylation at any of the three serine residues of PDH was not induced after OSM stimulation under normoxia in these two cell lines (Fig. 7b, e). Taken together, these data show that, in HepG2 and JHH-4, OSM did not induce the metabolic changes observed in the three clones of the human hepatocyte cell line PH5CH.

### Discussion

Along with others, we reported that transcription of HIF-1 $\alpha$ , one of the master regulators of the cellular response to hypoxia, is upregulated through IL6-type cytokine (e.g., IL6 and OSM) signaling or other activators of the JAK/STAT3 signaling pathway [9, 20]. Because HIF-1 $\alpha$  is heavily induced by hypoxia, we hypothesized that OSM induces a hypoxia-like metabolic phenotype under normoxic conditions. In this study, we provide insights in how OSM affects transcriptional regulation of central metabolism and how the transcriptional changes propagate to redirect intracellular metabolic fluxes. First, we demonstrated that OSM treatment under normoxia leads to an upregulation of PDK1 in three clones of the immortalized hepatocyte cell line PH5CH. Increased mRNA levels of PDK1 translated to increased protein

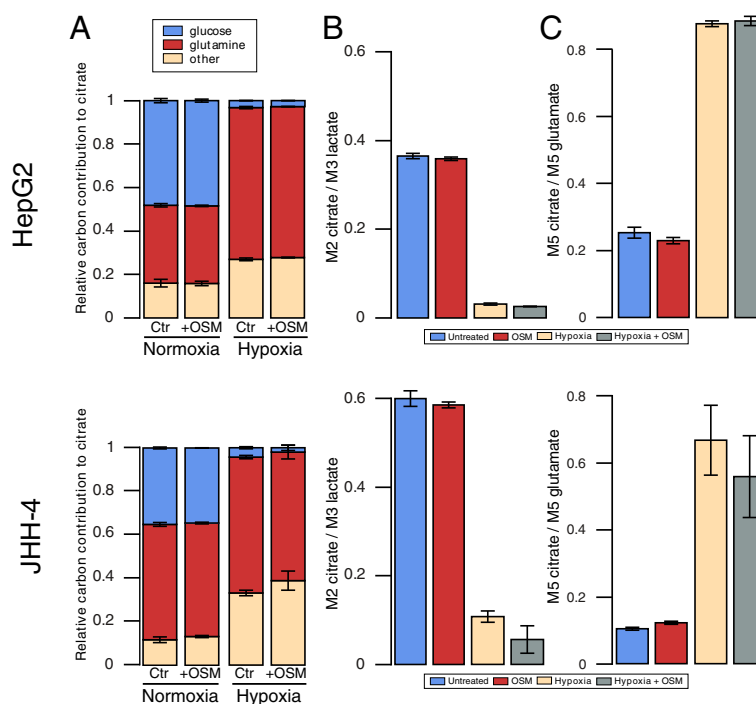


**Fig. 6** Effect of OSM treatment on central carbon metabolism of HepG2 and JHH-4. **a** Relative carbon contribution to citrate. **b** PDC activity determined by the ratio of M2 isotopologues of citrate to M3 isotopologues of lactate, from [ $^{13}\text{C}_6$ ]glucose. **c** Reductive glutamine contribution to citrate, determined by the ratio of M5 isotopologues of citrate to M5 isotopologues of glutamate, from [ $^{13}\text{C}_5$ ]glutamine. All error bars indicate the standard deviation. All error bars are calculated from at least two independent replicates ( $n \geq 2$ ). Metabolites were extracted after 36 h of indicated treatment

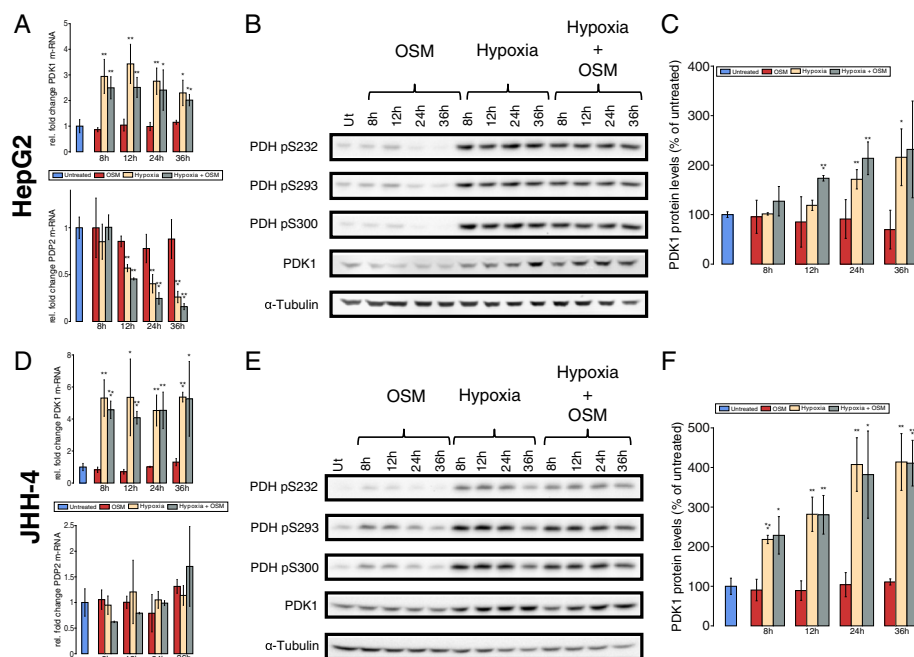


**Fig. 7** OSM does not influence PDK1 levels in the two HCC cell lines. Cells were treated with OSM (50 ng/ml), hypoxia 1 % O<sub>2</sub>, a combinatorial treatment for the given time points. **a, d** qRT-PCR of PDK1 and PDP2 after the indicated period of time and treatment, mRNA from three biological replicates in HepG2 (**a**) and JHH-4 (**d**) cells. Fold change was calculated to the untreated control. **b, e** Western blot analysis of all three PDH phosphorylation sites (S232, S293, S300) and PDK1 in HepG2 (**b**) and JHH-4 (**d**) cells.  $\alpha$ -Tubulin was used as a loading control and one representative  $\alpha$ -tubulin blot is shown. **c, f** PDK1 protein levels in HepG2 (**c**) and JHH-4 (**f**) cells after the indicated period of time and treatment, shown as percentage of the untreated control. All error bars indicate the standard deviation calculated from three biological replicates. Statistical significance was determined in comparison to the untreated control. \* $P \leq 0.05$ , \*\* $P \leq 0.01$ , and \*\*\* $P \leq 0.001$

levels (Fig. 3a, c; Additional file 6: Figure S3C), which correlated with reduced PDC activity (Fig. 2c, Fig. 5g) and therefore reduced glucose oxidation in the TCA cycle. Reduced glucose-derived acetyl-CoA was not compensated by an alternative acetyl-CoA source such as fatty acid oxidation or degradation of branched chain amino acids, leading to reduced glutamine oxidation (Fig. 2e, Fig. 5h). As a result of the reduced glucose and glutamine oxidation, the intracellular citrate levels decreased, triggering reductive  $\alpha$ -ketoglutarate carboxylation by mass action [15, 28]. This is in line with a previous study by Gameiro et al., showing that reductive carboxylation is triggered by a deficient mitochondrial pyruvate oxidation [16]. These results indicate that PDK1 plays an important role in the OSM-induced metabolic phenotype. Together, our current work shows that OSM treatment under normoxic conditions induces an intermediate metabolic phenotype between hypoxia (1 % O<sub>2</sub>) and normoxia (18.6 % O<sub>2</sub>) in PH5CH8 cells. This metabolic phenotype can support high proliferation rates. Although OSM was implicated in increased hepatocyte proliferation in vivo after partial hepatectomy (Nakamura et al. 2004), we did not observe an effect on the growth rate of PH5CH8 cells (data not shown).

Second, to confirm our hypothesis that the OSM-induced metabolic changes are HIF-1 $\alpha$ -dependent, we demonstrated that silencing of HIF-1 $\alpha$  almost completely attenuated the OSM-dependent metabolic effects under normoxia, showing that HIF-1 $\alpha$  expression is critical for OSM-dependent metabolic reprogramming. This dependency on HIF-1 $\alpha$  activity explains why although OSM leads to increased HIF-1 $\alpha$  protein levels under hypoxia, it does not have any additional effect, as with 1 % oxygen, the amount of transcriptionally active HIF-1 $\alpha$  cannot be further induced through OSM. Interestingly, silencing of HIF-1 $\alpha$  under hypoxia increased glucose-derived pyruvate oxidation, suggesting that glucose-derived acetyl-CoA and thus downregulated PDC activity is the limiting factor and not only reduced O<sub>2</sub> availability for respiration under hypoxia.

Third, we identified PDK1 as a critical HIF-1 $\alpha$  downstream regulator of the OSM-induced metabolic changes. PDK1 knockdown, however, did not fully abolish OSM-mediated effects on intracellular metabolic fluxes (Fig. 5c, d, g, h). Possibly, our siRNA-mediated PDK1 silencing was not sufficiently strong to fully abolish PDK1 activity, although PDK1 protein levels were not detectable by Western blot anymore (Fig. 5b, f). Furthermore, it cannot

be excluded that yet another regulator is involved in the mediation of OSM-dependent metabolic reprogramming.

Finally, we demonstrated that in HepG2 and JHH-4, OSM did not induce the metabolic changes we observed in the PH5CH clones (Figs. 6 and 7). This is potentially explained by the fact that OSM did not induce HIF-1 $\alpha$  in JHH-4 or solely in a transient way in HepG2. Even in the PH5CH clones, where OSM-induced HIF-1 $\alpha$  protein levels are similar to those induced by hypoxia, the impact on PDK1 expression was less pronounced. In addition, the metabolic effect observed upon OSM in the PH5CH clones was lower compared to the metabolic changes induced by hypoxia. Taken together, these data raise the hypothesis that OSM-induced HIF-1 $\alpha$  is not as potent in activating HIF downstream responses as hypoxic HIF. This might be due to the fact that HIF-1 $\alpha$  is post-translationally regulated by the following mechanisms: (1) Under normoxia, OSM-induced HIF-1 $\alpha$  might still be hydroxylated by PHDs on proline and asparagine residues. Hence, VHL binds HIF-1 $\alpha$  and tags it for proteasomal degradation leading to a faster degradation as compared to stabilized HIF-1 $\alpha$  under hypoxia. VHL binding complexes might also interfere with HIF-mediated transcription or lead to a reduced binding time of HIF on promoters. In addition, factor-inhibiting HIF (FIH)-mediated asparagine hydroxylation in the trans-activation domain of HIF-1 $\alpha$  prevents cofactor binding (CEBP) and might thereby reduce effective transcription [29, 30]. (2) HIF-1 $\alpha$  might be modified by other post-translational modifications upon hypoxia compared to OSM-induced HIF-1 $\alpha$  under normoxia and thus altering its function. In addition to hydroxylation, HIF1 $\alpha$  is known to undergo acetylation, phosphorylation, S-nitrosylation, and SUMOylation [31]. (3) Known cofactors of HIF-1 $\alpha$  (e.g., TAZ) found under hypoxia might not be present in normoxic conditions [32].

We have previously shown, however, that at least the HIF-1 $\alpha$  target genes VEGF and PAI as well as HIF-1 $\alpha$ -dependent reporter gene constructs under the control of the VEGF or the PAI promoter or of HRE elements are upregulated upon OSM stimulation [9]. Hence, OSM-induced HIF-1 $\alpha$  can be an active transcription factor in HepG2 cells. However, it remains unclear why we were not able to detect HIF-1 $\alpha$ -induced metabolic changes in HepG2 cells in this study. VEGF was discussed to be not only a HIF-1 $\alpha$  but also a STAT3 target gene [33]. Therefore, it is possible that VEGF and PAI are regulated by both transcription factors. In contrast to HIF, STAT3 might be able to recruit cofactors under normoxia that HIF cannot, as it remains hydroxylated at asparagine. For many metabolic genes (which are not STAT3 responsive or mainly rely on HIF-1 $\alpha$  for transcriptional regulation), asparagine hydroxylation might prevent HIF from being fully active.

Collectively, our data shows that HIF-1 $\alpha$  is necessary but not sufficient to induce OSM-dependent metabolic reprogramming of hepatic cells.

## Conclusions

Hypoxia and inflammation have been recognized as conditions favoring carcinogenesis [18]. Both microenvironments induce profound changes in cellular metabolism towards a more glycolytic phenotype [34], and it is assumed that high rates of glycolysis provide a selective growth advantage that promotes tumor progression [35]. However, it is still debated whether these metabolic changes are a consequence or a cause of carcinogenesis [35]. The OSM-induced metabolic changes described in this study would support increased proliferation rates and are similar to the metabolic adaptations described in tumors [19]. Hence, OSM-dependent metabolic reprogramming might serve as a first hit in carcinogenesis, which connects chronic infections to increased risks of tumor development. On the other hand, our experiments only applied acute treatments (50 ng/ml OSM, 18.6 % O<sub>2</sub>, and 1 % O<sub>2</sub>) and certainly do not reflect chronic conditions as encountered in a tumor. It will be interesting to investigate whether long-term activity of the JAK/STAT3 pathway affects hepatocyte/hepatoma cell metabolism in a different way.

## Additional files

**Additional file 1: Table S1.** For GC/MS measurements, the detector was operated in single ion mode (SIM). Metabolite specific parameters (selected ions, dwell time, retention time) are described. (PDF 66.8 kb)

**Additional file 2: Figure S1.** Effects of OSM and hypoxia on HIF-1 $\alpha$  and HIF-2 $\alpha$  protein expression in hepatoma cells and hepatocytes. Eleven hepatoma cell lines and two immortalized hepatocyte cell lines (PH5CH8 and THLE-2) were treated with 20 ng/ml OSM (O) or grown at 1 % O<sub>2</sub> (H) over 8 and 36 h. (A) HIF-1 $\alpha$  protein expression after OSM treatment represented in comparison to untreated cells (Ut). (B) HIF-1 $\alpha$  protein expression after OSM treatment represented in comparison to cells grown under hypoxia. (C) HIF-2 $\alpha$  protein expression after OSM treatment represented in comparison to untreated cells. (D) HIF-2 $\alpha$  protein expression after OSM treatment represented in comparison to cells grown under hypoxia. (E) HIF-1 $\alpha$  and HIF-2 $\alpha$  protein induction in non-neoplastic THLE-2 hepatocytes after OSM or hypoxia or a combinatorial treatment. (PDF 655 kb)

**Additional file 3: Figure S2.** (A) Glucose uptake and lactate secretion rates in PH5CH8 immortalized hepatocytes in response to a 36 h treatment with 50 ng/mL OSM. Uptake and secretion rates were determined by GC/MS. (B)  $\alpha$ -ketoglutarate to citrate ratios in PH5CH8 cells treated with 50ng/mL of OSM for 36 h in comparison to the respective untreated control. (PDF 42.2 kb)

**Additional file 4: Table S2.** Mass isotopomer distributions (MIDs) from [<sup>13</sup>C<sub>6</sub>]glucose in PH5CH8 immortalized human hepatocytes treated for 36 h with 50 ng/mL OSM or left untreated. MIDs were corrected for natural isotope abundance. (PDF 94.2 kb)

**Additional file 5: Table S3.** Mass isotopomer distributions (MIDs) from [<sup>13</sup>C<sub>5</sub>]glutamine in PH5CH8 immortalized human hepatocytes treated for 36 h with 50 ng/mL OSM or left untreated. MIDs were corrected for natural isotope abundance. (PDF 94.2 kb)

**Additional file 6: Figure S3.** Response of PH5CH1 and PH5CH7 non-neoplastic hepatocytes to OSM, hypoxia, and a combination of both stimuli. PH5CH1 and PH5CH7 cells were treated with OSM (50 ng/ml), hypoxia (1 % O<sub>2</sub>), or a combinatorial treatment for the indicated periods of time. (A, D) Quantitative RT-PCR of PDP2, PDK1, and HIF-1 $\alpha$  mRNA. Fold changes were calculated relative to the untreated control. (B, E) Western blot analysis for HIF-1 $\alpha$ , HIF-2 $\alpha$ , PDK1, and all three PDH phosphorylation sites (S232, S293, S300). Vinculin and  $\alpha$ -tubulin were used as loading controls, and one representative blot is shown. (C, F) Quantification of PDK1 protein levels. (PDF 428 kb)

**Additional file 7: Figure S4.** Mass isotopomer distributions (MIDs) from [<sup>13</sup>C<sub>6</sub>]glucose in HepG2 human hepatoma cells treated for 6 and 15 h with 50 ng/mL OSM or left untreated. MIDs were corrected for natural isotope abundance. (PNG 14.8 kb)

### Competing interests

The authors declare that they have no competing interests.

### Authors' contributions

CH, KH, IB, and AW designed the experiments; NB and XD performed the stable isotope labeling experiments; CG performed the HIF-1 $\alpha$  silencing experiments; NB performed the PDK1 silencing experiments; AZ performed the Western blots for HIF-1 $\alpha$ , STAT3, phospho-STAT3, PDK1, PDH-E1 $\alpha$  (pSer232), and PDH-E1 $\alpha$  (pSer300); AZ performed the qPCR for HIF-1 $\alpha$  and PDK1; and NB, AZ, CH, and AW wrote the manuscript. IB and KH critically revised the manuscript. All authors read and approved the final manuscript.

### Acknowledgements

We thank our collaborator Prof. Nobuyuki Kato (Okayama University) for providing the PH5CH1, PH5CH7, and PH5CH8 cells. We thank Annegrät Daujeumont for her technical support. The authors acknowledge the financial support from the University of Luxembourg Tandem project "Meta-IL6".

### Author details

<sup>1</sup>Luxembourg Centre for Systems Biomedicine, University of Luxembourg, Avenue des Hauts-Fourneaux 7, L-4362 Esch-Belval, Luxembourg. <sup>2</sup>Life Sciences Research Unit, University of Luxembourg, Avenue de la Faïencerie 162a, 1511 Luxembourg, Luxembourg.

Received: 30 July 2015 Accepted: 17 January 2016

Published online: 17 February 2016

### References

- Grivnenkov SI, Greten FR, Karin M. Immunity, inflammation, and cancer. *Cell*. 2010;140(6):883–99. doi:10.1016/j.cell.2010.01.025.
- Bode JG, Albrecht U, Häussinger D, Heinrich PC, Schaper F. Hepatic acute phase proteins—regulation by IL-6- and IL-1-type cytokines involving STAT3 and its crosstalk with NF- $\kappa$ B-dependent signaling. *European Journal of Cell Biology*. 2012;91(6-7):496–505. doi:10.1016/j.ejcb.2011.09.008.
- Hodge DR, Hurt EM, Farrar WL. The role of IL-6 and STAT3 in inflammation and cancer. *European journal of cancer (Oxford, England : 1990)*. 2005;41(16):2502–12. doi:10.1016/j.ejca.2005.08.016.
- Naugler WE, Sakurai T, Kim S, Maeda S, Kim K, Elsharkawy AM, et al. Gender disparity in liver cancer due to sex differences in MyD88-dependent IL-6 production. *Science (New York, N.Y.)*. 2007;317(5834):121–4. doi:10.1126/science.1140485.
- Wong VW-S, Yu J, Cheng AS-L, Wong GL-H, Chan HY, Chu ES-H, et al. High serum interleukin-6 level predicts future hepatocellular carcinoma development in patients with chronic hepatitis B. *International journal of cancer. Journal international du cancer*. 2009;124(12):2766–70. doi:10.1002/ijc.24281.
- Liang H, Block TM, Wang M, Nefsky B, Long R, Hafner J, et al. Interleukin-6 and oncostatin M are elevated in liver disease in conjunction with candidate hepatocellular carcinoma biomarker GP73. *Cancer Biomarkers*. 2012;11(4):161–71. doi:10.3233/CBM-2012-00276.
- Ohishi W, Cologne JB, Fujiwara S, Suzuki G, Hayashi T, Niwa Y, et al. Serum interleukin-6 associated with hepatocellular carcinoma risk: a nested case-control study. *International Journal of Cancer*. 2014;134(1):154–63. doi:10.1002/ijc.28337.
- Heinrich PC, Behrmann I, Haan S, Hermanns HM, Müller-Newen G, Schaper F. Principles of interleukin (IL)-6-type cytokine signalling and its regulation. *The Biochemical journal*. 2003;374(Pt 1):1–20. doi:10.1042/BJ20030407.
- Vollmer S, Kappler V, Kaczor J, Flügel D, Rolvering C, Kato N, et al. Hypoxia-inducible factor 1 $\alpha$  is up-regulated by oncostatin M and participates in oncostatin M signaling. *Hepatology*. 2009;50(1):253–60. doi:10.1002/hep.22928.
- Mole DR, Blancher C, Copley RR, Pollard PJ, Gleadle JM, Ragoussis J, et al. Genome-wide association of hypoxia-inducible factor (HIF)-1 $\alpha$  and HIF-2 $\alpha$  DNA binding with expression profiling of hypoxia-inducible transcripts. *Journal of Biological Chemistry*. 2009;284(25):16767–75. doi:10.1074/jbc.M901790200.
- Semenza GL, Roth PH, Fang HM, Wang GL. Transcriptional regulation of genes encoding glycolytic enzymes by hypoxia-inducible factor 1. *The Journal of biological chemistry*. 1994;269(38):23757–63.
- Holness MJ, Sugden MC. Regulation of pyruvate dehydrogenase complex activity by reversible phosphorylation. *Biochemical Society transactions*. 2003;31:1143–51. doi:10.1042/.
- Kim J-w, Tchernyshyov I, Semenza GL, Dang CV. HIF-1-mediated expression of pyruvate dehydrogenase kinase: a metabolic switch required for cellular adaptation to hypoxia. *Cell Metabolism*. 2006;3(3):177–85. doi:10.1016/j.cmet.2006.02.002.
- Papandreou I, Cairns RA, Fontana L, Lim AL, Denko NC. HIF-1 mediates adaptation to hypoxia by actively downregulating mitochondrial oxygen consumption. *Cell Metabolism*. 2006;3(3):187–97. doi:10.1016/j.cmet.2006.01.012.
- Fendt SM, Bell EL, Keibler MA, Olenchock BA, Mayers JR, Wasylenko TM, et al. Reductive glutamine metabolism is a function of the  $\alpha$ -ketoglutarate to citrate ratio in cells. *Nature Communications*. 2013;4:2236. doi:10.1038/ncomms3236.
- Gameiro PA, Yang J, Metelo AM, Pérez-Carro R, Baker R, Wang Z, et al. In vivo HIF-mediated reductive carboxylation is regulated by citrate levels and sensitizes VHL-deficient cells to glutamine deprivation. *Cell Metabolism*;17(3):372–85. doi:10.1016/j.cmet.2013.02.002.
- Metallo CM, Gameiro PA, Bell EL, Mattaini KR, Yang J, Hiller K, et al. Reductive glutamine metabolism by IDH1 mediates lipogenesis under hypoxia. *Nature*. 2011;481(7381):380–4. doi:10.1038/nature10602.
- Hanahan D, Weinberg RA. Hallmarks of cancer: the next generation. *Cell*. 144(5):646–74. doi:10.1016/j.cell.2011.02.013.
- Vander Heiden MG, Cantley LC, Thompson CB. Understanding the Warburg effect: the metabolic requirements of cell proliferation. *Science*. 2009;324(5930):1029–33. doi:10.1126/science.1160809.
- Demaria M, Giorgi C, Lebedzinska M, Esposito G, D'Angeli L, Bartoli A, et al. A STAT3-mediated metabolic switch is involved in tumour transformation and STAT3 addiction. *Aging (Albany NY)*. 2010;2(11):823–42.
- Demaria M, Misale S, Giorgi C, Miano V, Camporeale A, Campisi J, et al. STAT3 can serve as a hit in the process of malignant transformation of primary cells. *Cell Death Differ*. 2012;19(8):1390–7. doi:10.1038/cdd.2012.20.
- Ikeda M, Sugiyama K, Tanaka T, Tanaka K, Sekihara H, Shimotohno K, et al. Lactoferrin markedly inhibits hepatitis C virus infection in cultured human hepatocytes. *Biochemical and biophysical research communications*. 1998;254:9–53. doi:10.1006/bbrc.1998.8481.
- Haan C, Behrmann I. A cost effective non-commercial ECL-solution for Western blot detections yielding strong signals and low background. *Journal of Immunological Methods*. 2007;318(1-2):11–19. doi:10.1016/j.jim.2006.07.027.
- Böing I, Stross C, Radtke S, Lippok BE, Heinrich PC, Hermanns HM. Oncostatin M-induced activation of stress-activated MAP kinases depends on tyrosine 861 in the OSM receptor and requires JAK1 but not SRC kinases. 2006. 18(1):50–61. doi:10.1016/j.cellsig.2005.03.015.
- Wegner A, Sapcaric SC, Weindl D, Hiller K. Isotope cluster-based compound matching in gas chromatography/mass spectrometry for non-targeted metabolomics. *Analytical Chemistry*. 2013;85(8):4030–7. doi:10.1021/ac303774z.
- Hiller K, Hangebrauk J, Jäger C, Spura J, Schreiber K, Schomburg D. MetaboliteDetector: comprehensive analysis tool for targeted and

- nontargeted GC-MS based metabolome analysis. *Analytical Chemistry*. 2009;81(9):3429–39. doi:10.1021/ac802689c.
27. Wegner A, Weindl D, Jäger C, Sapcariu SC, Dong X, Stephanopoulos G, et al. Fragment formula calculator (FFC): determination of chemical formulas for fragment ions in mass spectrometric data. *Analytical Chemistry*. 2014;86(4):2221–8. doi:10.1021/ac403879d.
  28. Wegner A, Meiser J, Weindl D, Hiller K. How metabolites modulate metabolic flux. *Current Opinion in Biotechnology*. 2015;34:16–22. doi:10.1016/j.copbio.2014.11.008.
  29. Stolze IP, Tian YM, Appelhoff RJ, Turley H, Wykoff CC, Gleadle JM, et al. Genetic analysis of the role of the asparaginyl hydroxylase factor inhibiting hypoxia-inducible factor (HIF) in regulating HIF transcriptional target genes. *J Biol Chem*. 2004;279(41):42719–25. doi:10.1074/jbc.M406713200.
  30. Masson N, Singleton RS, Sekirnik R, Trudgian DC, Ambrose LJ, Miranda MX, et al. The FIH hydroxylase is a cellular peroxide sensor that modulates HIF transcriptional activity. 2012;13(3):251–7. doi:10.1038/embor.2012.9.
  31. Dimova EY, Kietzmann T. Hypoxia-inducible factors: post-translational crosstalk of signaling pathways. *Transcription Factors: Methods and Protocols*. 2010;647:215–36. doi:10.1007/978-1-60761-738-9.
  32. Xiang L, Gilkes DM, Hu H, Takano N, Lu H, Bullen JW, et al. Hypoxia-inducible factor 1 mediates TAZ expression and nuclear localization to induce the breast cancer stem cell phenotype. *Oncotarget*. 2014;5(24):12509–27.
  33. Wei LH, Kuo ML, Chen CA, Chou CH, Lai KB, Lee CN, et al. Interleukin-6 promotes cervical tumor growth by VEGF-dependent angiogenesis via a STAT3 pathway. *Oncogene*. 2003;22(10):1517–27. doi:10.1038/sj.onc.1206226.
  34. Palsson-McDermott EM, O'Neill LAJ. The Warburg effect then and now: from cancer to inflammatory diseases. *BioEssays*. 2013;35(11):965–73. doi:10.1002/bies.201300084.
  35. Jones RG, Thompson CB. Tumor suppressors and cell metabolism: a recipe for cancer growth. *Genes & Development*. 2009;23(5):537–48. doi:10.1101/gad.1756509.

Submit your next manuscript to BioMed Central  
and we will help you at every step:

- We accept pre-submission inquiries
- Our selector tool helps you to find the most relevant journal
- We provide round the clock customer support
- Convenient online submission
- Thorough peer review
- Inclusion in PubMed and all major indexing services
- Maximum visibility for your research

Submit your manuscript at  
[www.biomedcentral.com/submit](http://www.biomedcentral.com/submit)



---

# Pro-inflammatory Macrophages Sustain Pyruvate Oxidation through Pyruvate Dehydrogenase for the Synthesis of Itaconate and to Enable Cytokine Expression

---

Johannes Meiser, Lisa Krämer, Sean C. Sapcariu, Nadia Battello, Jenny Ghelfi, Aymeric Fouquier D'Herouel, Alexander Skupin, Karsten Hiller

*Journal of Biological Chemistry*, February 2016, PMID: 26679997, DOI: 10.1074/jbc.M115.676817

## Contributions

- Conduction of experimental work and analysis of the data underlying figure 3D-H

# Pro-inflammatory Macrophages Sustain Pyruvate Oxidation through Pyruvate Dehydrogenase for the Synthesis of Itaconate and to Enable Cytokine Expression\*

Received for publication, July 22, 2015, and in revised form, December 11, 2015. Published, JBC Papers in Press, December 17, 2015, DOI 10.1074/jbc.M115.676817

Johannes Meiser, Lisa Krämer, Sean C. Sapcariu<sup>1</sup>, Nadia Battello, Jenny Ghelfi, Aymeric Fouquier D'Herouel, Alexander Skupin, and Karsten Hiller<sup>2</sup>

From the Luxembourg Centre for Systems Biomedicine, University of Luxembourg, 6 Avenue de Swing, L-4367 Belvaux, Luxembourg

Upon stimulation with Th1 cytokines or bacterial lipopolysaccharides, resting macrophages shift their phenotype toward a pro-inflammatory state as part of the innate immune response. LPS-activated macrophages undergo profound metabolic changes to adapt to these new physiological requirements. One key step to mediate this metabolic adaptation is the stabilization of HIF1 $\alpha$ , which leads to increased glycolysis and lactate release, as well as decreased oxygen consumption. HIF1 abundance can result in the induction of the gene encoding pyruvate dehydrogenase kinase 1 (PDK1), which inhibits pyruvate dehydrogenase (PDH) via phosphorylation. Therefore, it has been speculated that pyruvate oxidation through PDH is decreased in pro-inflammatory macrophages. However, to answer this open question, an in-depth analysis of this metabolic branching point was so far lacking. In this work, we applied stable isotope-assisted metabolomics techniques and demonstrate that pyruvate oxidation is maintained in mature pro-inflammatory macrophages. Glucose-derived pyruvate is oxidized via PDH to generate citrate in the mitochondria. Citrate is used for the synthesis of the antimicrobial metabolite itaconate and for lipogenesis. An increased demand for these metabolites decreases citrate oxidation through the tricarboxylic acid cycle, whereas increased glutamine uptake serves to replenish the TCA cycle. Furthermore, we found that the PDH flux is maintained by unchanged PDK1 abundance, despite the presence of HIF1. By pharmacological intervention, we demonstrate that the PDH flux is an important node for M(LPS) macrophage activation. Therefore, PDH represents a metabolic intervention point that might become a research target for translational medicine to treat chronic inflammatory diseases.

Macrophages are innate immune cells that differentiate from monocytes, which circulate in the bloodstream. Upon differentiation, they invade the surrounding tissue and become resident

macrophages (1). Macrophages can be activated by cytokines or toll-like receptor agonists, e.g. lipopolysaccharide (LPS). In very general terms, macrophage activation can result in rather pro-inflammatory responses, serving as host defense mechanisms or in wound healing responses and aiding in tissue repair and remodeling. However, depending on the type of activation, very different subtypes of activation occur (2). Upon activation with LPS (M(LPS)) or the cytokine interferon- $\gamma$  (M(INF $\gamma$ )), macrophages undergo profound metabolic reprogramming, necessary to activate cellular defense mechanisms as well as to cope with different micro-environments in the inflamed tissue (3). A marker for pro-inflammatory activation is high expression of *Irg1* (4, 5). We recently showed that *Irg1* codes for the enzyme *cis*-aconitate decarboxylase (IRG1/CAD) that catalyzes the synthesis of the antimicrobial metabolite itaconate from *cis*-aconitate (6). Therefore, metabolic reprogramming due to these adaptations could affect the availability of substrate needed for the synthesis of itaconate during host defense.

The reprogramming during macrophage activation shows overlapping features with cancer cells; both have increased glycolytic rates and increased lactate release, known as aerobic glycolysis or the Warburg effect (7, 8). Increased glycolytic rates are observed in any cell type that exceeds the energy demand derived from oxidative phosphorylation (9). In macrophages, it has been revealed that this metabolic rewiring is mediated by stabilization of HIF1 $\alpha$  (10). A well described HIF1 target is the gene encoding pyruvate dehydrogenase kinase 1 (PDK1), an inhibitor of Pyruvate dehydrogenase (PDH)<sup>3</sup> (11). When HIF1 is stabilized, the PDH flux can be inhibited by PDK1-mediated phosphorylation, resulting in decreased pyruvate-derived acetyl-CoA levels. In this case, reductive carboxylation of  $\alpha$ -ketoglutarate ( $\alpha$ KG) increases to provide sufficient acetyl-CoA for lipogenesis, needed for cell proliferation (12–15). Increased glycolytic rates, decreased PDH flux, and increased reductive carboxylation can also be induced in any cell type when oxygen tension is decreased or when oxidative phosphorylation is impaired. In this case, NADH oxidation is compromised, and citrate levels decrease. This decrease in citrate is linked to an increase in NADH, which thermodynamically promotes the metabolic adaptation to hypoxia by increasing reductive carboxylation of  $\alpha$ KG (13, 16, 17). However, it is currently unclear

\* This work was supported in part by the Fonds National de la Recherche Luxembourg Grant ATTRACT A10/03 (to K. H.) and AFR-Postdoc-3973022 (to J. M.). The authors declare that they have no conflicts of interest with the contents of this article.

Author's Choice—Final version free via Creative Commons CC-BY license.

<sup>1</sup> Recipient of financial support from the Helmholtz Virtual Institute of Complex Molecular Systems in Environmental Health.

<sup>2</sup> To whom correspondence should be addressed: Metabolomics Group, University of Luxembourg, Luxembourg Centre for Systems Biomedicine, 6 Avenue de Swing, L-4367 Belvaux, Luxembourg. Tel.: 352-46-66-44-6136; E-mail: karsten.hiller@uni.lu.

<sup>3</sup> The abbreviations used are: PDH, pyruvate dehydrogenase;  $\alpha$ KG,  $\alpha$ -ketoglutarate; MDS, mass isotopomer distribution.



whether this full panel of metabolic consequences upon HIF1 stabilization is also true for pro-inflammatory macrophages. Although it has been demonstrated that HIF1 $\alpha$  can be stabilized and activated by cytokines, e.g. TNF $\alpha$  and IL1 $\beta$  (18, 19), the detailed metabolic consequences are still uncertain.

HIF1 can bind to the promoter of the *Tlr4* gene, thereby acting through a positive feedback loop on the TLR4 defense axis (20). Reactive oxygen species were shown to inhibit proteasomal degradation of HIF1 $\alpha$  (21), and recently, increased succinate levels in pro-inflammatory macrophages have also been described to stabilize HIF1 $\alpha$ , by inhibiting prolyl hydroxylase-mediated hydroxylation of HIF1 $\alpha$  (10).

In this study, we asked whether the stabilization of HIF1 $\alpha$  in M(LPS) macrophages alters TCA cycle fluxes similarly to hypoxic cells. We show that LPS-activated macrophages exhibit a metabolic adaptation with overlapping features to hypoxic cells, but also distinct differences, resulting in a unique LPS-specific metabolic signature. The most striking difference to hypoxic cells with stabilized HIF1 $\alpha$  is that there is no decrease in relative glucose flux through PDH and no increase in reductive carboxylation of  $\alpha$ KG. The sustained PDH flux provides sufficient acetyl-CoA for citrate production, which keeps the rate of reductive carboxylation of  $\alpha$ KG at a low level, as well as providing citrate that is needed for the synthesis of fatty acids and itaconate. Upon LPS stimulation, high PDH activity is maintained by a repression of *Pdk1*. As a result PDH phosphorylation on Ser-232 and Ser-293 remains at a low level. Finally, we demonstrate that the PDH flux is indeed important to sustain M(LPS) activation in macrophages.

### Experimental Procedures

**Chemicals**—UK5099 (Sigma, PZ0160) was first diluted in DMSO and further diluted in medium to a working stock concentration of 10 mM and then added to the wells of the culture dish to a final concentration of 100  $\mu$ M. The final concentration of DMSO did not exceed 1%; LPS (*Escherichia coli*, Sigma L6529) was prepared as a working stock of 1  $\mu$ g/ml in glucose- and glutamine-free DMEM and added 1:100 into the wells of the culture dish for a final concentration of 10 ng/ml. Cells were stimulated for 6 h; interferon  $\gamma$  (mouse) (*E. coli*, Sigma I4777) was prepared as a working stock of 5 mg/ml in glucose- and glutamine-free DMEM and added 1:100 into the wells of the culture dish for a final concentration of 50 ng/ml. Cells were stimulated for 6 h.

**Stable Isotope Tracing**—<sup>13</sup>C stable isotope tracers were obtained from Eurisotop as follows: glucose, CLM-1396; glutamine, CLM-1822-H. The tracer medium was prepared in DMEM without glucose and glutamine. [<sup>13</sup>C]Glucose (final 25 mM) and [<sup>12</sup>C]glutamine (final 4 mM) (or vice versa) was added to the medium; pH was set to 7.3; 10% FBS and 1% penicillin/streptomycin were added, and finally, the medium was sterile-filtered. Tracer medium was prepared in advance and incubated in the hypoxia chamber overnight to remove excessive oxygen from the medium (only for hypoxia conditions). The next morning, medium was replaced by tracer medium, and cells were incubated for 24 h with the tracer medium to reach isotopic steady state. LPS was added after 24 h and left on the cells for an additional 6 h prior to extraction. For further infor-

TABLE 1

Primer sequences used for quantitative PCR

| Gene           | 5' to 3' sequence        |
|----------------|--------------------------|
| <i>L27_F</i>   | ACATTGACGATGGCACCTC      |
| <i>L27_R</i>   | GCTTGGCGATCTTCTTCTTG     |
| <i>Irg1_F</i>  | GCAACATGATGGCTCAAGTCTG   |
| <i>Irg1_R</i>  | TGTCCTCCGAATGATACCA      |
| <i>Tnfa_F</i>  | GGTCTGTCCCTTTCACCTCAC    |
| <i>Tnfa_R</i>  | TGCCCTCTTCTGCCAGTTCC     |
| <i>iNos_F</i>  | AGCCCTCACCTACTTCCTG      |
| <i>iNos_R</i>  | CAATCTCTGCCATATCCGTCTC   |
| <i>Pdk1_F</i>  | TGCAAAGTTGGTATATCCAAAGCC |
| <i>Pdk1_R</i>  | ACCCCGAAGCTCTCCTTGTA     |
| <i>Il1b_F</i>  | TGCCACCTTTTGACAGTGATG    |
| <i>Il1b_R</i>  | TGATGTGCTGCTGCGAGATT     |
| <i>Cpt1_F</i>  | TGGCAGTCGACTCACCTTTC     |
| <i>Cpt1_R</i>  | CAAACAGTTCACCTGCTGC      |
| <i>Hif1a_F</i> | TGACGGCGACATGGTTTACA     |
| <i>Hif1a_R</i> | AATATGGCCCGTGACGTGAA     |

mation regarding stable isotope-assisted metabolomics, see also Refs. 22, 23.

**Cell Culture**—RAW 264.7 cells (ATCC® TIB-71™) were obtained from ATCC and were cultivated according to the manufacturer's instructions. Briefly, cells were kept in DMEM5796 with 10% FBS and 1% penicillin/streptomycin at 37 °C and 5% CO<sub>2</sub> under atmospheric oxygen concentrations. In the case of hypoxia, cells were cultivated in an incubator at 37 °C and 5% CO<sub>2</sub> located in a closed hypoxia chamber with an oxygen concentration of 2%. Cells were simultaneously seeded in the afternoon at a density of 150,000 cells per well in 12-well plates (Thermo Scientific, Nunc Multidish 12 Nunclon Delta Si) and then either incubated either at 21 or 2% O<sub>2</sub> overnight. The next day, medium was replaced. In the case of hypoxia, medium was already incubated in the hypoxia chamber overnight to remove excessive oxygen from the medium. For comparison reasons, medium for normoxic conditions was also prepared the day before and incubated in a similar way under atmospheric oxygen conditions. For LPS activation, LPS was added 18 h after medium replacement. 24 h after medium replacement cells were harvested.

**Viability Assay**—To assess cell viability, cells were transferred into tubes and analyzed using a Vi-Cell™ XR (Beckman Coulter) automated cell counter. To determine viability, cells were incubated with trypan blue and number of stained cells was determined.

**cDNA Synthesis and Gene Expression Analysis**—cDNA synthesis and quantitative PCR was performed as described previously (6). Briefly, RNA was isolated from the interphase after extraction of metabolites, using the Qiagen RNeasy mini kit. 0.5–1  $\mu$ g of RNA was used for cDNA synthesis using SuperScript III (Invitrogen), following the manufacturer's instructions. Quantitative PCR was performed using iQ SYBR Green Supermix (Bio-Rad) as per the manufacturer's instructions. PCR was carried out on a Light Cycler 480 (Roche Applied Science). Data analysis was performed using the analysis software according to manufacturer's instructions (Roche Applied Science). Gene expression was normalized to the housekeeping gene *L27*. For primer sequences, see Table 1.

**Extraction of Intracellular Metabolites**—Extraction was according to Ref. 24. Briefly, cells were cultivated in 12-well plates and washed with 1 ml of 0.9% NaCl and quenched with

## PDH Flux Is Important for Activation of M(LPS) Macrophages

0.2 ml of  $-20^{\circ}\text{C}$  methanol. After adding an equal volume of  $4^{\circ}\text{C}$  cold water, cells were collected with a cell scraper and transferred to tubes containing 0.2 ml  $-20^{\circ}\text{C}$  chloroform. The extracts were shaken at 1400 rpm for 20 min at  $4^{\circ}\text{C}$  (Thermomixer Eppendorf) and centrifuged at  $16,000 \times g$  for 5 min at  $4^{\circ}\text{C}$ . 0.2 ml of the upper aqueous phase was collected in specific glass vials with micro inserts and evaporated under vacuum at  $-4^{\circ}\text{C}$  using a refrigerated CentriVap Concentrator (Labconco).

**Gas Chromatography-Mass Spectrometry**—Metabolite derivatization was performed using a Gerstel MPS. Dried polar metabolites were dissolved in  $15\ \mu\text{l}$  of 2% methoxyamine hydrochloride in pyridine at  $40^{\circ}\text{C}$  under shaking. After 60 min, an equal volume of MTBSTFA was added and held for 60 min at  $40^{\circ}\text{C}$ .  $1\ \mu\text{l}$  of sample was injected into an SSL injector at  $270^{\circ}\text{C}$  in splitless mode. GC/MS analysis was performed using an Agilent 7890A GC equipped with a 30-m DB-35MS + 5-m Duraguard capillary column. Helium was used as carrier gas at a flow rate of 1.0 ml/min. The GC oven temperature was held at  $100^{\circ}\text{C}$  for 2 min and increased to  $300^{\circ}\text{C}$  at  $10^{\circ}\text{C}/\text{min}$ . After 3 min, the temperature was increased to  $325^{\circ}\text{C}$ . The GC was connected to an Agilent 5975C inert XL MSD, operating under electron ionization at 70 eV. The MS source was held at  $230^{\circ}\text{C}$  and the quadrupole at  $150^{\circ}\text{C}$ . The MS was operated in selected ion monitoring. The total run time of one sample was 25.00 min. All GC/MS chromatograms were processed by using Metabolite Detector software (25). MIDs were determined and corrected for natural isotope abundance using Metabolite Detector software.

Measurement of glucose and lactate intensities was performed by derivatization with an equal volume of MSTFA (instead of MTBSTFA) and held for 30 min at  $40^{\circ}\text{C}$  under continuous shaking. A  $1\text{-}\mu\text{l}$  sample was injected into an SSL injector at  $270^{\circ}\text{C}$  in split 10 mode. GC oven temperature was held at  $90^{\circ}\text{C}$  for 1 min and increased to  $300^{\circ}\text{C}$  at  $15^{\circ}\text{C}/\text{min}$  for 8 min to  $320^{\circ}\text{C}$ . The total run time of one sample was 24.3 min. For absolute quantification of glucose and lactate, a dilution series of a standard mix was included in the sequence and measured in triplicate. For normalization, we used  $[\text{U-}^{13}\text{C}]$ glucose and  $[\text{U-}^{13}\text{C}]$ lactate as internal standards (in this case, medium samples contained only  $^{12}\text{C}$  carbon sources).

**Quantification of Amino Acids**—Quantification of amino acids was performed on an Agilent 1100 HPLC system equipped with a Diode Array Detector. Separation was carried out on a ZORBAX amino acid analysis column ( $150 \times 4.6\ \text{mm}$ ,  $5\ \mu\text{m}$ ) with a preceding ZORBAX amino acid analysis guard cartridge (Agilent Technologies, Santa Clara, CA) at  $40^{\circ}\text{C}$  in gradient mode (see Table 1). The eluents used were 40 mM  $\text{Na}_2\text{HPO}_4$  (pH 7.8, eluent A) and a mixture of acetonitrile, methanol, and water (45:45:10, eluent B). 0.02% sodium azide was added to eluent A to prevent microbial growth. Primary amines were automatically derivatized with *ortho*-phthalaldehyde in borate buffer (0.4 N in water, pH 10.2) and diluted in eluent A prior to injection. The resulting *ortho*-phthalaldehyde derivatives were subsequently detected at 338 nm (10-nm bandwidth; reference wavelength, 390 nm; 20-nm bandwidth). All medium samples were diluted 1:1 with the internal standard L-2-aminobutyric acid (final concentration,  $300\ \mu\text{M}$ ) to correct

for deviations resulting from the derivatization process. External calibration standards as well as reference media with known concentrations were measured with every run to determine sample concentrations and ensure stability of the analysis. Gradient profile: 1.9 min, 0% eluent B; 18.1 min, 57% eluent B; 18.6 min, 100% eluent B; 22.3 min, 100% eluent B; 23.2 min, 0% eluent B; 26 min, 0% eluent B.

**Western Blot**—For preparation of whole cell extract,  $1 \times 10^6$  cells were harvested, washed with ice-cold  $1 \times$  phosphate-buffered saline (PBS) (Invitrogen/Life Technologies, Inc., Europe BV Belgium), lysed in  $1 \times$  M-PER<sup>®</sup>, mammalian protein extraction Reagent (Thermo Scientific, Belgium) completed with  $1 \times$  protease inhibitor mixture (Complete<sup>®</sup>, Roche Applied Science, Luxembourg), and further processed according to the manufacturer's instructions. A nanodrop analyzer was used to measure the protein concentration. Proteins were separated by size using SDS-PAGE (12%) and transferred to an Immobilon-FL PVDF membrane (Merck Millipore) using the Mini-PROTEAN Tetra Cell and PowerPac Basic Power Supply (Bio-Rad, Belgium). The membrane was blocked in 5% nonfat milk powder in PBS/Tween for 1 h at room temperature or overnight at  $4^{\circ}\text{C}$ . The antibodies used were as follows: anti-IRG1 (Sigma, hpa040143) 1:750 in PBS-T 5% nonfat milk powder for 1 h at room temperature; anti-PDK1 (rabbit) (Enzo catalog no. ADI-KAP-PK112) 1:3000 in TBST 5% BSA, overnight at  $4^{\circ}\text{C}$ ; anti-PDH-E1 $\alpha$  (rabbit) (Ser(P)-232) (Millipore catalog no. AP1063) 1:1000 in TBST 5% BSA, overnight at  $4^{\circ}\text{C}$ ; anti-PDH-E1 $\alpha$  (rabbit) (Ser(P)-300) (Millipore catalog no. ABS194) 1:1000 in TBST 5% BSA, overnight at  $4^{\circ}\text{C}$ ; anti-PDH-E1 $\alpha$  (rabbit) (Ser(P)-293) (Millipore catalog no. ABS204) 1:10,000 in TBST 5% BSA, overnight at  $4^{\circ}\text{C}$ ; anti- $\alpha$ -tubulin (mouse) 1:5000 in TBST 5% BSA, overnight at  $4^{\circ}\text{C}$ ; anti-rabbit HRP 1:5000 in TBST 5% skim milk (Cell Signaling); anti-mouse HRP 1:5000 in TBST 5% skim milk (Cell Signaling). Visualization was done using the ECL Plus Western blotting detection system Kit (GE Healthcare, Netherlands). Signals were detected using the LICOR system. Quantification of band intensities was done using the ImageStudioLight Software package.

**Cell Imaging and Data Analysis**—Phase contrast images were acquired using a  $\times 10$  objective on a Nikon Ti Eclipse inverted microscope with motorized stage (Nikon Corp., Tokyo, Japan) enclosed in a bench top incubator. Automatic microscope control, stage programming, and acquisition were done using the OptoMorph version of MetaMorph 7.8.10 (Cairn Research, Kent, UK). LPS-treated and untreated RAW 264.7 cells growing in 12-well Nunc plates (50,000 cells per well) were imaged in positive phase contrast. Nine adjacent but non-overlapping images were automatically acquired in a  $3 \times 3$  grid around the center of each well. The entire imaging experiment was performed twice, resulting in 36 images acquired per condition. One out-of-focus image and five containing cell aggregates were excluded from further analysis. Surfaces of strongly attached cells were estimated by thresholding in ImageJ 2.0.0-rc-31/1.49v using the IJ\_IsoData algorithm. Congruence of thresholding results with cell contours was verified by visual inspection. Cell sizes were calculated using the particle analysis tool, allowing for areas from 50 to 5000 pixels and excluding particles on the image edges. Average sizes were reported for

each image. Halo and contrast effects resulting from the phase-contrast imaging were analyzed to discriminate between strongly and weakly attached cells. Strongly attached cells appeared darker than background with a weak halo, although weakly attached cells appeared brighter than background with a strong halo. Histograms of pixel intensities of the entire field of view were analyzed using custom software written in MATLAB R2014b. First, the intensity peak corresponding to the background signal (cell-free surface) was identified and approximated by a Gaussian function. The approximated peak was subtracted from the original histogram, and the weighted sum of intensities below (dark) and above (bright) the background peak was calculated, respectively. The ratio of dark-to-bright values informs on the ratio of strongly-to-weakly attached cells. Renormalization of this ratio by values obtained for individual strongly and weakly attached cells yielded an adhesion index with values from 0 (no cells attached) to 1 (all cells attached).

**Statistical Analyses**—To analyze a significant difference between two groups, unpaired Welch's *t* test was applied. *p* values are indicated in each panel (\*, *p* < 0.01; or as indicated) and was considered as significantly different with a *p* value < 0.05. The number of independent replicates is indicated in the figure legends. Each experiment was at least performed three times with cells of a different passage. Each individual experiment consisted of three wells per condition.

## Results

**M(LPS) Macrophages Show a Distinct Metabolite Signature**—The macrophage environment is likely to be hypoxic, as these cells infiltrate hypoxic tissues such as tumors, wounded regions, or sites of inflammation. At the site of inflammation, different oxygen tensions result from increased oxygen demand as well as swelling or vascular damage (26, 27). To physiologically meet these challenging conditions, macrophages are well adapted to hypoxia by their ability to adjust their gene expression profile and increase glycolytic activity (28). To study whether the activation of macrophages reprograms metabolism to a hypoxia-like phenotype, we cultivated the murine macrophage cell line RAW 264.7 under normoxia (21% oxygen) and hypoxia (2%) and activated it with LPS for 6 h. We selected this time point, because it reflects the highest expression level of *irg1/Cad*, the enzyme that catalyzes the synthesis of the antimicrobial metabolite itaconate (6).

We analyzed intracellular metabolite levels and revealed that LPS stimulation resulted in increased levels of itaconate, succinate, and lactate under normoxia (Fig. 1, A–C). These three metabolites are marker metabolites for M(LPS) activation, demonstrating a clear pro-inflammatory activation (6, 10, 29, 30). Moreover, we observed increased levels of the TCA cycle associated metabolites malate and glutamate, whereas aspartate and citrate levels remained unchanged (Fig. 1, D–G). The amino acids glycine, serine, and alanine were also elevated upon LPS stimulation (Fig. 1, H–J). Compared with normoxia, LPS treatment of hypoxic cells was unable to induce similar itaconate and succinate levels (Fig. 1, A and B). As expected, lactate levels further increased upon hypoxia as a result of reduced respiration and concomitant increased glycolysis, known as the Pasteur Effect. Non-activated hypoxic cells exhibited decreased

levels of the TCA cycle associated metabolites malate, aspartate, glutamate, and citrate. However, LPS stimulation under hypoxia resulted in increased levels of malate, aspartate, and glutamate but not citrate (Fig. 1, D–G). The amino acids glycine and serine were unchanged between hypoxia and normoxia. Upon LPS activation of hypoxic cells, serine and alanine were increased (Fig. 1, H–J). Interestingly, we also observed a trend of increased levels of the branched chain amino acids isoleucine, leucine, and valine under hypoxia for both non-stimulated and LPS stimulated conditions (Fig. 1K; *p* value > 0.05).

We concluded from these results that LPS affects the metabolite profile of macrophages independent of the oxygen supply and that this profile is clearly different from a pure hypoxic profile. Intriguingly, we observed decreased abundance of the antimicrobial metabolite itaconate under oxygen-limiting conditions, which could have direct effects on the immune response in tissues with low oxygen tension.

**Decreased Itaconate Levels under Hypoxia Are Not the Result of Decreased *Irg1* Expression or Lower IRG1/CAD Protein Abundance**—To investigate whether the reduced levels of itaconate are caused by transcriptional repression, post-transcriptional regulation, or post-translational regulation, we analyzed gene expression and protein levels of the catalyzing enzyme IRG1/CAD. We found that hypoxia does not significantly reduce the gene expression level or the protein abundance of IRG1/CAD, indicating a regulation at the post-translational level or a result of decreased substrate concentrations (Fig. 2, A and B). To confirm LPS activation of macrophages, we analyzed gene expression of the pro-inflammatory marker genes *Tnfa*, *iNos*, and *Il1β* (Fig. 2, C–E). We found clear up-regulation under both oxygen conditions when the cells were treated with LPS. However, hypoxia resulted in a 20% reduction of *Tnfa* expression and ~3-fold higher expression of *Il1β* and *iNos*.

It has been reported in several recent publications that HIF1 $\alpha$  gets stabilized in M(LPS) macrophages compared with resting macrophages (10, 21, 29, 31). Therefore, we also analyzed gene expression of *Hif1 $\alpha$* , and we observed increased expression of *Hif1 $\alpha$*  in response to LPS treatment under hypoxia (Fig. 2F), indicating that HIF1 $\alpha$  stabilization in hypoxic M(LPS) macrophages can be a combined effect of increased transcriptional expression and post-translational stabilization. Under normoxia, no difference in *Hif1 $\alpha$*  expression was detected.

Based on these results, we conclude that the reduction of itaconate under hypoxia is mostly a result of post-translational effects such as altered metabolic fluxes, either due to an enzyme modification that regulates its activity or by changing substrate concentrations. To that end, we were interested to compare cellular flux changes with LPS activation between hypoxia and normoxia.

**LPS Activation Promotes Pyruvate Oxidation via PDH by Preventing *Pdk1* Expression**—To monitor intracellular glucose-derived fluxes in M(LPS) macrophages, we incubated RAW 264 cells for 24 h in the presence of uniformly labeled [U-<sup>13</sup>C]glucose to reach isotopic steady state conditions. During these 24 h, labeled glucose is metabolized within the cells and is incorporated in cellular metabolites downstream of glucose. To obtain the specific labeling patterns, intracellular metabolites

## PDH Flux Is Important for Activation of M(LPS) Macrophages

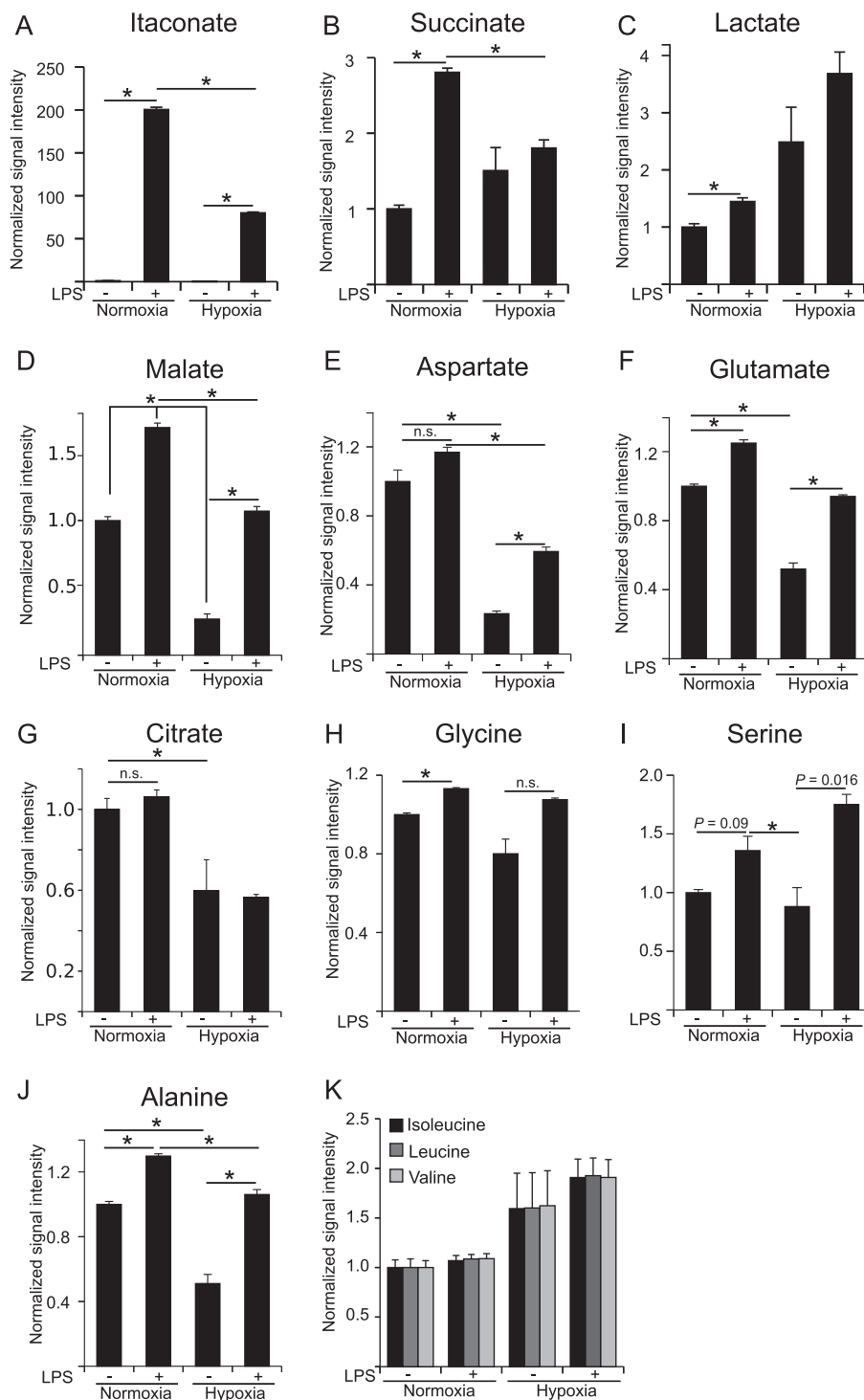


**FIGURE 1. Metabolome analysis of RAW 264 macrophages in the context of LPS activation and hypoxia.** Analysis of intracellular metabolite abundance in RAW 264 cells, cultivated under normoxia (21% O<sub>2</sub>) and hypoxia (2% O<sub>2</sub>), unstimulated or stimulated with LPS. Metabolites were extracted and analyzed by GC/MS. Signal intensities (peak area) are normalized to unstimulated cells under normoxia. Cells were treated with 10 ng/ml LPS for 6 h. Error bars indicate S.E. (Welsh's *t* test; \*, *p* < 0.01, *n* = 3 wells). *n.s.*, not statistically significant. One representative experiment with three individual wells per condition is presented. The experiment was performed three times.

were extracted and analyzed with gas chromatography/mass spectrometry to determine MIDs (corrected for natural isotope abundance), which reflect relative metabolic fluxes (Fig. 3A for atom transitions) (22, 23).

As expected, stable isotope labeling revealed that hypoxia resulted in decreased pyruvate flux through PDH, illustrated by

decreased M2 citrate isotopologues (Fig. 3B). Concomitant with decreasing citrate M2 isotopologues under hypoxia, we observed increased abundance of citrate M0 isotopologues, representing citrate molecules derived from carbon sources other than glucose (Fig. 3B). This decrease is a result of HIF1 $\alpha$  stabilization and *Pdk1* induction, where the PDK1 protein

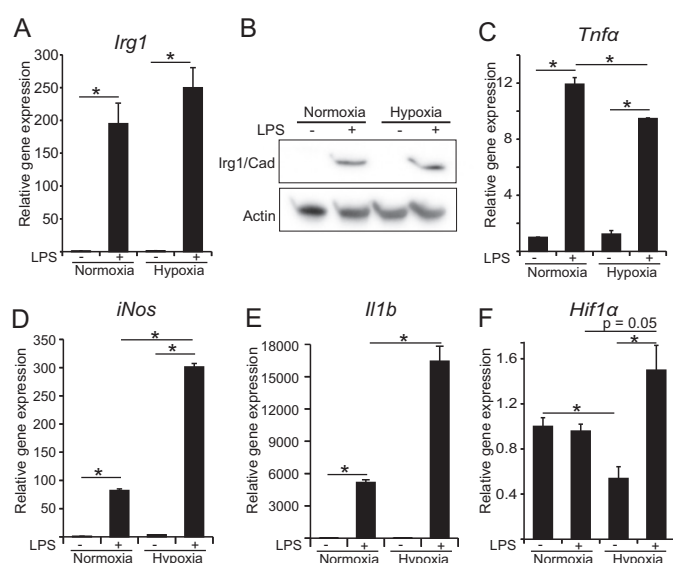


**FIGURE 2. Expression analysis of pro-inflammatory associated genes.** A, relative gene expression of *Irg1*. B, Western blot against IRG1/CAD, the protein that catalyzes the conversion of *cis*-aconitate to itaconate (no significant difference (data not shown)). C–F, relative gene expression of *Tnfa*, *iNos*, *Il1b*, and *Hif1a*, normalized to normoxia control (–LPS). Error bars indicate S.E. (Welsh’s *t* test, \*,  $p < 0.01$ ,  $n = 3$ ). Gene expression data represents the mean over three independent experiments.

inhibits PDH by phosphorylation (32, 33). Decreased pyruvate oxidation under hypoxia promotes decreasing downstream substrate levels, most probably resulting in the observed decreased itaconate levels (Fig. 1A). However, HIF1 $\alpha$  has also been shown to be stabilized in M(LPS) macrophages under normoxic conditions (10, 29). Therefore, it is speculated that pyruvate oxidation through PDH is decreased in M(LPS) macrophages, a similar phenotype to cancer cells with stabilized HIF1 $\alpha$  (3, 34). However, we did not observe decreased citrate M2 isotopologues in normoxic M(LPS) macrophages, raising the question whether PDH is inhibited under these conditions.

To analyze regulation of *Pdk1* in more detail, we investigated gene expression and protein abundance of PDK1 and phosphorylation status of PDH (Fig. 3, C–H). In line with current knowledge, hypoxia-mediated stabilization of HIF1 $\alpha$  resulted in increased *Pdk1* expression (Fig. 3C), which complements our observation of hypoxia-dependent, decreased glucose flux to citrate (Fig. 3B). Intriguingly, we observed that LPS stimulation resulted in a drastic reduction of *Pdk1* expression at both normoxia and hypoxia, indicating that PDK1-mediated inhibition of PDH is reduced in M(LPS) macrophages (Fig. 3C). Moreover, analysis of PDK1 protein abundance revealed similar PDK1 levels in non-activated or M(LPS)-activated macrophages. Only in hypoxia did we observe a significant increase of PDK1 abundance (Fig. 3, D and E). To investigate whether the low levels of PDK1 have an effect on PDH, we analyzed phosphorylation of PDH on serine 232, 293, and 300 (Fig. 3, D and F–H). Phosphorylation of these residues has been reported to result in an inhibition of PDH activity (33). As expected, hypoxia resulted in increased phosphorylation of the three analyzed serine residues (not significant in case of Ser-300). However, and in line with low PDK1 levels in normoxic M(LPS) macrophages, LPS activation did not increase phosphorylation levels of

Ser-232 and -293. Regarding Ser-300, we observed significantly increased phosphorylation upon LPS activation, although there was no further significantly increased phosphorylation due to hypoxia. Whether Ser-300 specifically has a unique function in the context of LPS activation in macrophages remains to be determined in future work. Our results from this part of the study reveal that HIF1-mediated induction of *Pdk1* can be attenuated by LPS stimulation, which is in line with increased citrate M2 isotopologues upon LPS activation (Fig. 3B).

In line with the results of PDK1 abundance and PDH phosphorylation status, our stable isotope analysis revealed that LPS stimulation did not result in a decreased relative pyruvate oxidation, both under hypoxia and normoxia (Fig. 3, B and I), indicating that HIF1 did not mediate PDH inhibition upon LPS stimulation. We observed increased citrate M2 isotopologue levels, reflecting even higher relative pyruvate flux through PDH (Fig. 3B). To normalize for upstream changes in glycolysis, we determined the ratio of M2 citrate/M3 pyruvate and observed an increase upon LPS stimulation, indicating increased pyruvate flux through PDH in M(LPS) macrophages (Fig. 3I). As a reduction of citrate M2 isotopologues was only observed under hypoxic conditions, HIF1-mediated inhibition of PDH depended only on the oxygen tension and not on the macrophage activation status. Indeed, LPS activation can even partially recover the HIF1-mediated PDH inhibition under hypoxia (Fig. 3, B and I).

The M2 abundance of  $\alpha$ KG and malate was significantly lower than in citrate (Fig. 3, J and K), suggesting that large amounts of citrate, *cis*-aconitate, or isocitrate are either used for pathways other than the oxidative TCA cycle or that other carbon sources (e.g. glutamine) increase their contribution to  $\alpha$ KG and malate. Stimulation with LPS as well as hypoxia further decreased glucose contribution to  $\alpha$ KG and malate, as can be seen by a decreasing abundance of  $\alpha$ KG and malate M2 isotopologues (Fig. 3, J and K).

Next, we analyzed glucose uptake from the medium and cellular lactate release, to evaluate whether M(LPS) macrophages increase their glycolytic rate. Under normoxia, LPS-stimulated macrophages increased glucose uptake and lactate release, and under hypoxia, glucose uptake and lactate release were exceeding the rate of M(LPS) macrophages under normoxia (Fig. 3L). This effect was further enhanced when hypoxic cells were additionally stimulated with LPS (Fig. 3L). Under normoxia, the lactate to glucose ratio was increased from 1.2 to 1.6 upon LPS stimulation, indicating increased activity of lactate dehydrogenase, which is in line with the Warburg-like phenotype of M(LPS) macrophages (3). However, 20% of the overall glucose carbon pool is still available for other metabolic pathways, indicating that M(LPS) macrophages still contain sufficient pyruvate to maintain oxidation through PDH.

It has been shown before that STAT3-specific signaling can inhibit PDH and thus block pyruvate oxidation through PDH in primary fibroblasts and cancer cell lines (35). Therefore, we investigated whether, and in contrast to LPS treatment, a STAT3-dependent activation with the cytokine INF $\gamma$  might inhibit PDH. To this end, we treated the cells with INF $\gamma$  or LPS and analyzed the isotope enrichment in citrate. We did not

## PDH Flux Is Important for Activation of M(LPS) Macrophages

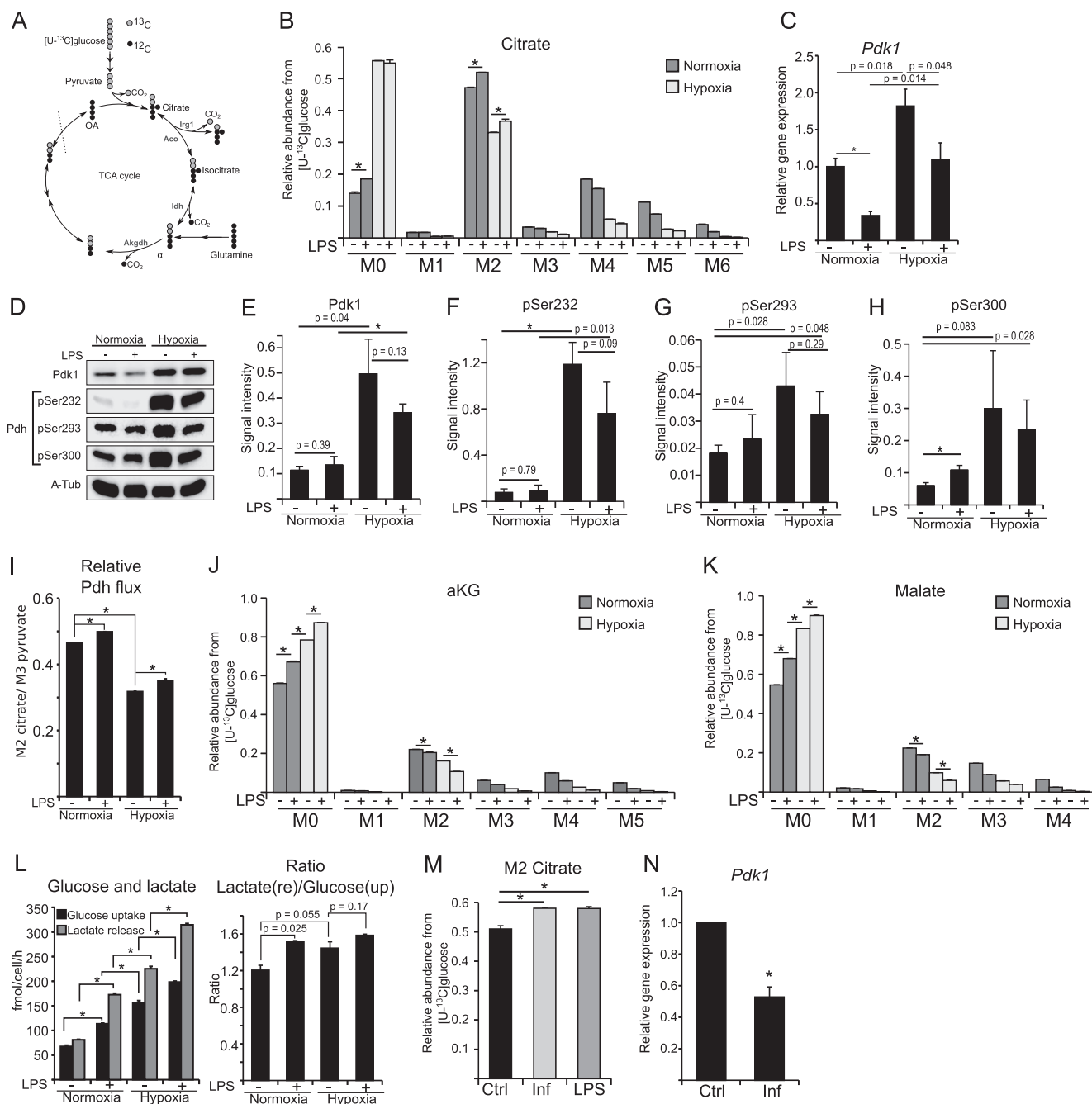


**FIGURE 3. PDH flux analysis in M(LPS) macrophages.** *A*, schematic of atom transitions in central metabolism using  $[U-^{13}C]$ glucose as a tracer for determination of MIDIs to infer relative intracellular fluxes.  $^{13}C$ -carbons are in gray and  $^{12}C$  in black. The dotted line indicates end of one route. Aco, aconitase; Idh, isocitrate dehydrogenase; Akgdh,  $\alpha$ KG dehydrogenase; OA, oxaloacetate. *B*, MID of citrate. M0 to M6 indicates the different mass isotopologues. *C*, gene expression analysis of *Pdk1*. *D–H*, Western blot analysis of PDK1 and PDH phosphorylation on Ser-232, -293, and -300.  $\alpha$ -Tubulin serves as loading control. *D* shows one representative Western blot of three independent experiments.  $\alpha$ -Tub,  $\alpha$ -tubulin. *E–H* shows quantification of three independent experiments. *I*, ratio of M2 citrate/M3 pyruvate indicating relative pyruvate oxidation through PDH. *J* and *K*, MID of  $\alpha$ KG and malate. *L*, absolute quantification of glucose uptake and lactate release, and ratio of lactate release/glucose uptake to infer fractional lactate formation per glucose. *M*, activation of RAW 264 cells with 10 ng/ml LPS or 50 ng/ml interferon- $\gamma$  (INF) in medium with  $[U-^{13}C]$ glucose. Presented are citrate M2 isotopologues as a readout for relative glucose flux through PDH. *N*, relative gene expression of *Pdk1* normalized to normoxia control (Ctrl) (–LPS). Error bars indicate S.E. (Welsh's *t* test, \*,  $p < 0.01$ ,  $n = 3$ ). One representative experiment with three individual wells per condition is presented. Each experiment was performed at least three times, except for *C*. Presented is the mean  $\pm$  S.E. over three independent experiments. (Welsh's *t* test, \*,  $p < 0.01$ ,  $n = 3$ ).

observe a difference between LPS and INF $\gamma$  treatment (Fig. 3M). In both cases, M2 citrate was significantly increased compared with untreated controls. In line with LPS activation, we also observed decreased expression of *Pdk1* in M(INF $\gamma$ ) macrophages (Fig. 3N), indicating no inhibition of pyruvate oxidation in M(INF $\gamma$ ) macrophages. In conclusion, sustained pyruvate

flux through PDH and its regulation by PDK1 seems to be independent of TLR4 signaling.

**LPS Activation Increases Glutamine Uptake but Does Not Induce Reductive Carboxylation of  $\alpha$ KG**—It has been demonstrated that hypoxic cells metabolize increased amounts of glutamine via reverse IDH activity to generate citrate by reductive

## PDH Flux Is Important for Activation of M(LPS) Macrophages

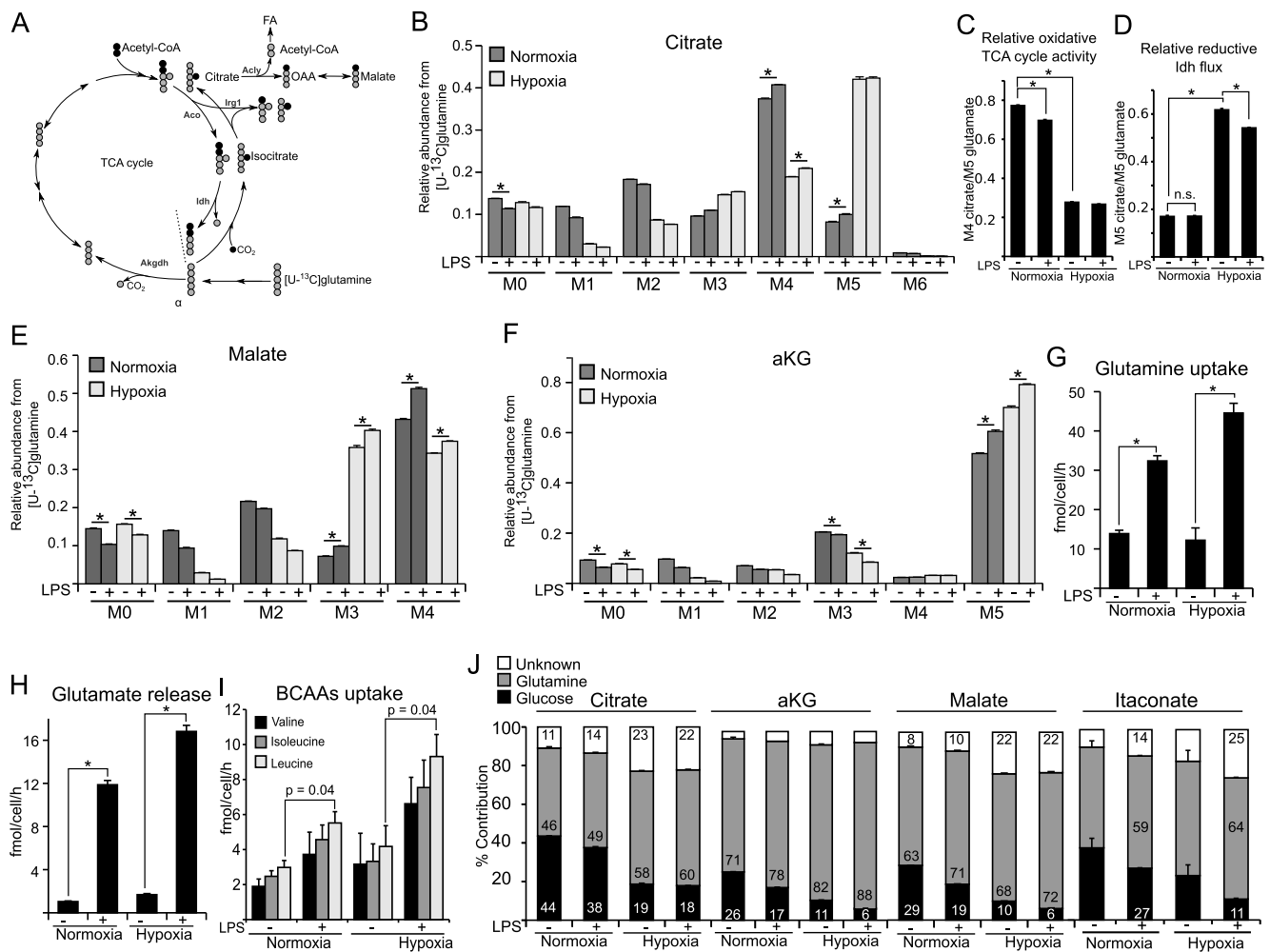


**FIGURE 4. Contribution of glutamine to central metabolism in M(LPS) macrophages.** *A*, schematic of atom transitions in central metabolism using [U-<sup>13</sup>C]glutamine as a tracer. <sup>13</sup>C-carbons are in gray, <sup>12</sup>C in black. Citrate molecules derived from reductive carboxylation of αKG are M5 isotopologues, whereas citrate molecules from the oxidative route of the TCA cycle are M4 isotopologues. The dotted line indicates end of one route. *Aco*, aconitase; *Idh*, isocitrate dehydrogenase; *Akgdh*, αKG dehydrogenase; *Acly*, ATP-dependent citrate lyase; *FA*, fatty acid. *B*, MID of citrate. *M0* to *M6* indicates the different mass isotopologues. *C* and *D*, determination of oxidative TCA cycle activity: ratio of M4 citrate/M5 glutamate and ratio of M5 citrate/M5 glutamate indicating relative reductive *Idh* flux. *E* and *F*, MID of malate and αKG. *G–I*, absolute quantification of glutamine uptake, glutamate release, and uptake of the branched chain amino acids (valine, isoleucine, and leucine). *J*, carbon contribution (%) of glucose, glutamine, and other carbon sources to citrate, αKG, malate, and itaconate. Carbon contributions are based on MIDs from [U-<sup>13</sup>C]glucose labeling (Fig. 3) and [U-<sup>13</sup>C]glutamine labeling. Carbon contribution to itaconate under non-LPS conditions should not be considered because itaconate levels are negligibly low under these non-stimulated conditions (Fig. 1A). Error bars indicate S.E. (Welsh's *t* test, \*, *p* < 0.01, *n* = 3). One representative experiment with three individual wells per condition is presented. Each experiment was performed at least three times.

carboxylation of αKG (12–15). This pathway fuels the citrate pool to provide sufficient acetyl-CoA for lipogenesis. Because M(LPS) activation also results in a stabilization of HIF1α (10, 19, 21, 29) and increased glycolytic flux (see Fig. 3, *I* and *L*), we investigated whether these cells exhibit increased reductive carboxylation of αKG. To that end, we applied a uniformly labeled [U-<sup>13</sup>C]glutamine tracer and determined MIDs of TCA cycle metabolites (Fig. 4A for atom transitions).

As expected, under hypoxic conditions we observed a drop in oxidative TCA cycle activity and a strong induction of reductive carboxylation, inferred from decreased citrate M4 and increased citrate M5 isotopologues (Fig. 4, *B–D*). This pattern was also reflected by decreasing malate M4 (oxidative route) and increasing malate M3 (reductive route) isotopologues (Fig. 4E). However, when cells were stimulated with LPS at normoxic conditions, reductive carboxylation of αKG was not increased (Fig. 4D).

Using the glutamine tracer, we observed that the major carbon source of αKG was glutamine and that upon LPS stimulation and under hypoxia the abundance of M5 isotopologues increased, suggesting an increase in glutamine influx and a decreasing glucose contribution (Fig. 4F). Although hypoxia results in increased usage of αKG for reductive carboxylation and decreased αKG oxidation (14, 15), we did not find evidence that LPS stimulation under normoxia compromises the relative glutamine carbon flux through αKG dehydrogenase, indicated by a similar enrichment pattern of αKG and malate.

To analyze glutamine metabolism in more detail, we quantified glutamine uptake from the medium and glutamate release from the cells. Although hypoxia did not result in increased glutamine uptake, we observed a strong increase of glutamine uptake upon LPS stimulation under both oxygen levels (Fig. 4G). Because glutamate is produced from glutamine and can be

## PDH Flux Is Important for Activation of M(LPS) Macrophages

released from the cell, we quantified glutamate release to infer glutamine anaplerosis to the TCA cycle. Although we observed increased glutamate release upon LPS stimulation, the net uptake of glutamine in LPS-stimulated cells was still higher compared with untreated controls (control 12.84 versus LPS 20.5 fmol/cell/h) (Fig. 4, *G* and *H*). As indicated by the intracellular metabolite levels (Fig. 1*K*), we also observed a trend of increased consumption of branched chain amino acids from the medium upon LPS stimulation (Fig. 4*I*). However, these differences were only significant in the case of leucine. Nevertheless, we believe that the influence of branched chain amino acids on central metabolism is higher upon LPS activation.

To better understand the impact of the different carbon sources to the TCA cycle metabolites, we calculated the carbon contributions of glucose and glutamine to citrate,  $\alpha$ KG, malate, and itaconate (Fig. 4*J*). We observed a small decrease in glucose contribution to citrate upon LPS activation. However, based on the [ $U$ - $^{13}$ C]glucose-derived MIDs, this decrease mostly originated from decreased citrate cycling through the oxidative TCA cycle (compare M3, M4, and M5 isotopologues in Fig. 3*B*) or increased glutamine influx, rather than decreased pyruvate flux through PDH (M2 isotopologue). Hypoxia resulted in a stronger reduction of glucose contribution to citrate, which was a result of PDH inhibition. Along with the decrease in glucose contribution, the glutamine contribution to citrate was increased upon LPS, especially under hypoxia, where glutamine is the major carbon source of citrate. For  $\alpha$ KG and malate, the glucose contribution was significantly lower compared with citrate, indicating that major parts of the citrate pool are not used for further oxidation through the oxidative TCA cycle, but for anabolic processes such as lipid synthesis or itaconate synthesis. In line with this observation, we observed higher glucose contribution to itaconate, compared with  $\alpha$ KG and malate. Moreover, upon LPS stimulation, and especially with hypoxia, we observed an increase of other carbon sources than glucose or glutamine, which is in line with potentially increased uptake of branched chain amino acids (Figs. 1*K* and 4*I*).

In summary, we observed that glutamine is the major carbon source of the TCA cycle in M(LPS) macrophages and is the main substrate for TCA oxidation. Glucose carbon still enters the cycle at citrate; however, significant amounts of the citrate pool are not further oxidized through IDH but are distributed to other metabolic pathways. Glutamine serves to replenish this lack of carbon by increased uptake upon LPS stimulation.

**LPS Causes an Increase in Lipogenesis in RAW 264 Cells**—Besides transcriptional and metabolic adaptations to inflammation, it has been described that pro-inflammatory macrophages also undergo morphological changes from small and spherical to a larger and more attached form (Fig. 5*A*). To demonstrate the surface enlargement during LPS activation, we monitored cell size by using two orthogonal microscopy approaches (Fig. 5*B*), demonstrating an increase in cell surface and thus pointing to an increased demand on lipids needed for membrane formation. Furthermore, M(LPS) macrophages increase intracellular and extracellular vesicle formation during pathogen defense (36). Therefore, M(LPS) macrophages have an increased demand for lipids, needed for morphological changes and vesicle formation. To meet this demand, LPS-

activated macrophages need to prioritize their metabolism toward lipogenesis and to repress lipid oxidation. In line with this necessary metabolic shift, we observed decreased expression of carnitine palmitoyltransferase 1 (*Cpt1*), the gene of the protein that imports palmitate into the mitochondrion for lipid oxidation and subsequent energy production (Fig. 5*C*). A reduction of  $\beta$ -oxidation is in line with reports of decreased oxidative metabolism in M(LPS) macrophages (37) and supports the observed increased demand for lipids. High activity of lipid degradation, simultaneously to their synthesis, would be a waste of energy.

To generate lipids from central metabolism, cells export mitochondrial citrate into the cytoplasm where it is hydrolyzed via ATP-dependent citrate lyase to provide acetyl-coA for lipogenesis. In this preferred case, citrate utilization is for anabolic processes rather than the TCA cycle. To analyze the contribution of glucose and glutamine to palmitate, an end point of fatty acid synthesis, we determined the MIDs of and the carbon contributions to palmitate after both the application of [ $U$ - $^{13}$ C]glucose and [ $U$ - $^{13}$ C]glutamine as tracers in independent experiments (Fig. 5, *D* and *E*). We observed that under normoxia, nearly 50% of the carbon in palmitate originated from glucose. Under hypoxic conditions, a shift in isotopologues indicated that the glucose contribution was reduced while glutamine contribution was increased, suggesting increased reductive carboxylation under hypoxia, but not as a result of LPS stimulation. Although dependent on the pool sizes of the metabolites, increased production of itaconate and palmitate from glucose-derived citrate in M(LPS) macrophages indicates reduced citrate oxidation through the TCA cycle in M(LPS) macrophages.

**Pyruvate Flux to Citrate Is Important for LPS Activation in RAW 264 Cells**—To investigate the importance of the PDH flux in M(LPS) macrophages, we used a pharmacological approach to impair pyruvate oxidation through PDH by inhibiting the pyruvate transporter with the specific inhibitor UK5099 (38). Using this inhibitor together with the [ $U$ - $^{13}$ C]glucose tracer, we observed a significant decrease of citrate M2 isotopologues, indicating reduced relative pyruvate oxidation through PDH (Fig. 6*A*). Addition of LPS to UK509-treated cells could not restore the abundance of M2 citrate, because pyruvate supply is impaired by the inhibition of the transporter. Analysis of intracellular metabolite levels revealed that inhibition of pyruvate transport into the mitochondrion resulted in decreased amounts of citrate, originating from reduced substrate levels for citrate synthase (Fig. 6*B*). Intriguingly, we also observed decreased amounts of the inflammatory marker metabolites itaconate and succinate under pro-inflammatory conditions (Fig. 6, *C* and *D*). Decreased amounts of itaconate and succinate could either result from decreased glucose flux into the TCA cycle, similar to hypoxia, or from a metabolic alteration in M(LPS) macrophages. To analyze these hypotheses, we investigated the gene expression profiles of pro-inflammatory marker genes (Fig. 6, *E*–*H*). Although *Il1b* gene expression was not significantly decreased (Fig. 6*E*), we observed that UK5099 treatment of LPS-stimulated macrophages resulted in decreased expression levels of *iNos*, *Irg1*, and *Tnf $\alpha$*  (Fig. 6, *F*–*H*), indicating that in this case and in contrast to hypoxia, the observed decreased itaconate level roots back to decreased *Irg1*



## PDH Flux Is Important for Activation of M(LPS) Macrophages

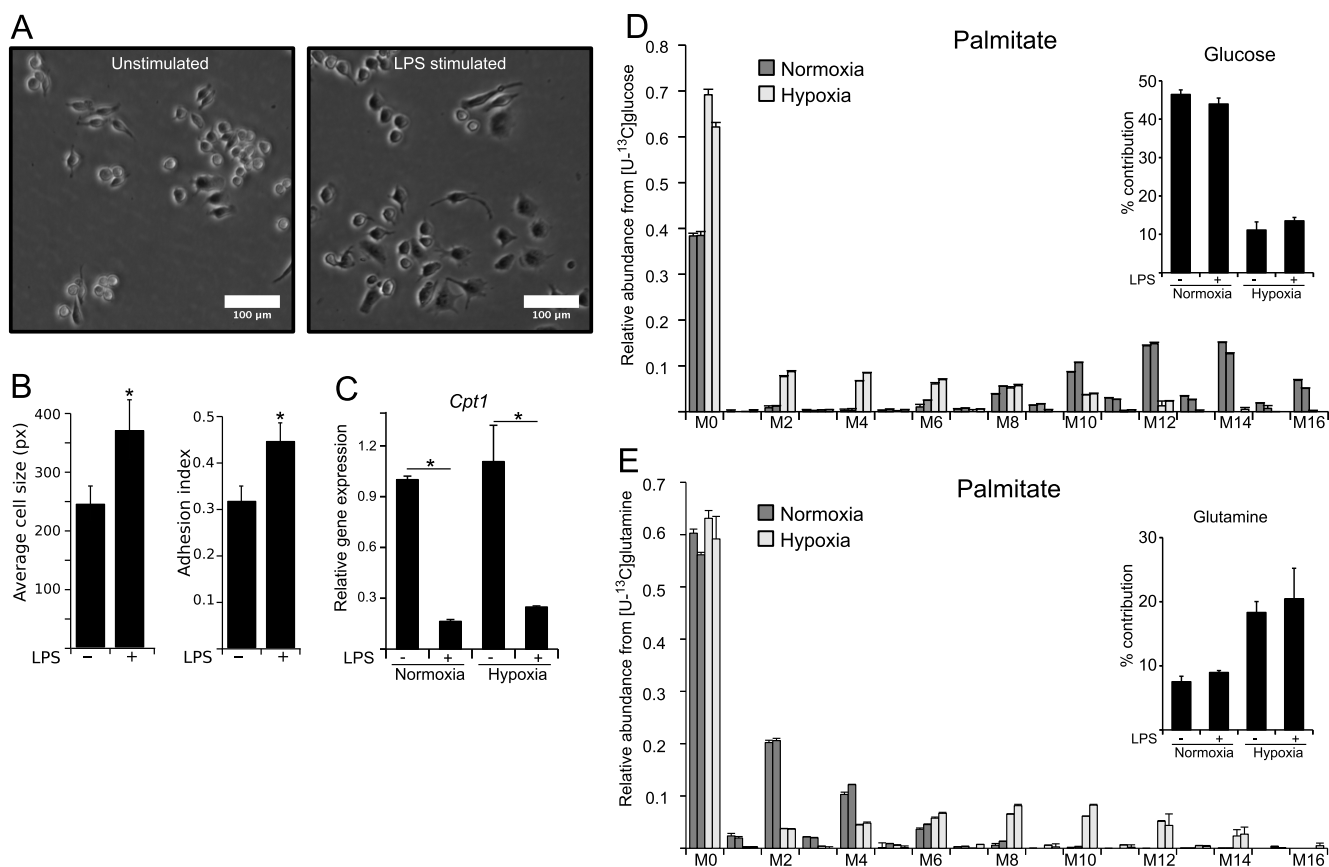


**FIGURE 5. Morphological changes upon LPS activation require sustained lipogenesis in macrophages.** *A*, microscopy (bright field image) of RAW macrophages unstimulated or stimulated with 10 ng/ml LPS for 6 h. *White bar* indicates 100  $\mu$ m. *B*, mean average of cell size (pixels) (*left*) and analysis of adhesion index (*right*) of LPS-stimulated and -non-stimulated cells obtained from bright field microscopy. Analysis demonstrates morphological adaptation of macrophages during LPS activation. For further details regarding the analysis approach, see under "Experimental Procedures." *C*, relative gene expression of carnitine palmitoyl transferase1 (*Cpt1*) normalized to normoxia control (*Ctrl*) (-LPS), indicating inhibition of  $\beta$ -oxidation upon LPS stimulation. *D* and *E*, MID of palmitate using [U-<sup>13</sup>C]glucose (*D*) and [U-<sup>13</sup>C]glutamine (*E*) as a tracer. Contribution of each carbon source is depicted in the *top right corner* of each panel. *Error bars* indicate S.E. (Welsh's *t* test, \*,  $p < 0.01$ ,  $n \geq 3$ ). One representative experiment with three individual wells per condition is presented. Each experiment was performed at least three times, except for *C*. Presented is the mean  $\pm$  S.E. over three independent experiments. (Welsh's *t* test, \*,  $p < 0.01$ ,  $n = 3$ ).

levels. Moreover, application of UK5099 to LPS-stimulated cells resulted in increased *Cpt1* expression levels, similar to untreated controls, although *Pdk1* expression was still reduced, due to the fact that pyruvate import into the mitochondrion was inhibited and thus regulation of PDH not necessary (Fig. 6, *I* and *J*). To exclude a potential toxic effect of UK5099 on RAW 264 cells, we performed a viability assay and did not observe significant changes in viability (Fig. 6*K*). To further exclude the possibility of timing effects due to simultaneous addition of LPS and UK5099, we repeated the experiments with a modified experimental setup, where we first activated the cells with LPS for 3 h and then added UK5099 for an additional 6 h to investigate whether this intervention can repress the pro-inflammatory profile of M(LPS) macrophages (Fig. 6*L*). Following this approach, we also observed significantly decreased citrate, itaconate, and succinate levels (Fig. 6, *M–O*) and significantly decreased expression of *Tnfa*, *iNos*, *Irg1*, and *Il1b* (Fig. 6, *P–S*). These results indicate that inhibition of pyruvate import into the mitochondrion can indeed suppress pro-inflammatory responses in M(LPS) macrophages. Finally, we investigated the effect of carbon contribution to palmitate for these conditions, using [U-<sup>13</sup>C]glucose as a tracer, in combination with UK5099. In line with decreased citrate, itaconate, and

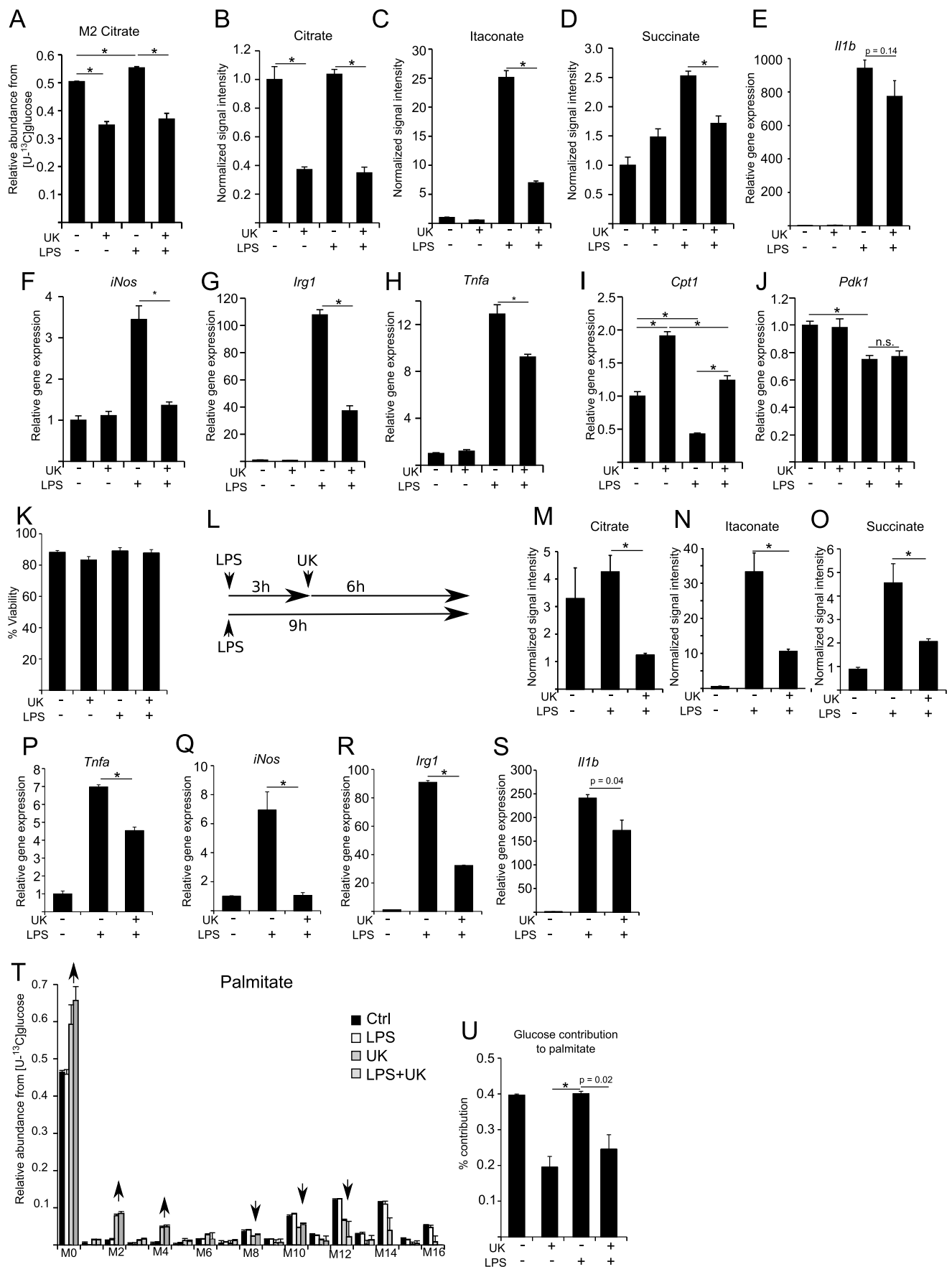
succinate levels upon UK5099 treatment, we also observed lower carbon contribution from glucose to palmitate (Fig. 6, *T* and *U*).

In summary, these data demonstrate that the pyruvate flux through PDH is important for LPS activation in macrophages. Apparently, altered metabolic fluxes or changes in metabolite concentrations enable a feedback mechanism to regulate cellular gene expression profiles. Hence, metabolic intervention can be used to attenuate activation of M(LPS) macrophages.

### Discussion

M(LPS) macrophages require extensive reprogramming to enable host defense mechanisms. Although M(IL4) macrophages increase oxidative metabolism optimized for tissue repair (39), M(LPS) macrophages develop a Warburg-like phenotype by increasing glycolysis and lactate release (3). It has been demonstrated that pro-inflammatory activation results in the stabilization of HIF1 $\alpha$ , HIF1 complex formation with monomeric or dimeric PKM2, along with an increased expression of M(LPS)-associated cytokines and bacterial defense mechanisms (29). While under hypoxia HIF1 not only increases the glycolytic activity but also represses PDH activity through PDK1, it was speculated that glucose flux

## PDH Flux Is Important for Activation of M(LPS) Macrophages



through PDH is also repressed in M(LPS) macrophages (3, 40). However, this would diminish the carbon supply necessary for lipogenesis and synthesis of the antimicrobial metabolite itaconate.

In this work, we demonstrate that the PDH flux plays an important role in maintaining full LPS-specific activation and that pharmacological intervention to prevent pyruvate oxidation represses pro-inflammatory activation. Although an active PDH flux has been speculated for early macrophage differentiation and for dendritic cells before (3, 41), our results demonstrate that pyruvate oxidation through PDH is fully active in mature M(LPS) macrophages and that this is even essential to sustain LPS activation. Moreover, we discovered that this process is facilitated by repressed *Pdk1* expression and no increase in PDK1 protein abundance, as well as significantly lower phosphorylation of PDH compared with hypoxic conditions, illustrating that M(LPS) macrophages sustain an active pyruvate flux through PDH.

Under hypoxia, HIF1 decreases pyruvate oxidation through PDH by inducing *Pdk1* (32). In contrast to hypoxia, we demonstrated that although glycolysis is increased and oxygen consumption is decreased (29) in M(LPS) macrophages, pyruvate oxidation through PDH is not inhibited, because PDK1 abundance is not increased. Active PDH facilitates a stable citrate pool, which in turn prevents increased reductive carboxylation of  $\alpha$ KG by thermodynamic means (16). M(LPS) macrophages have been shown to increase their expression of the mitochondrial citrate carrier to transport citrate from the mitochondrion into the cytosol (42), and we have shown that M(LPS) macrophages have an increased lipid demand. Because we demonstrated that reductive carboxylation of  $\alpha$ KG is not increased, the high demand of citrate has to be mostly supplied by glucose through PDH.

When PDH flux is repressed, citrate is increasingly generated by reductive carboxylation of  $\alpha$ KG, which is mostly derived from glutamine (43). An increased demand on glutamine in M(LPS) macrophages has been reported before (44). Here, we describe in detail how this glutamine is utilized. In M(LPS) macrophages most glutamine is preferentially used for glutaminolysis rather than for reductive carboxylation of  $\alpha$ KG. Besides ATP-dependent citrate lyase-derived oxaloacetate, increased glutaminolysis additionally provides oxaloacetate, which is needed as an acceptor for pyruvate-derived acetyl-CoA and the synthesis of citrate. It also replenishes the TCA cycle to compensate for increased lipogenesis and the loss of carbon that is used for the synthesis of itaconate.

It is known that LPS activation results in decreased oxygen consumption, which suggests that TCA cycle activity is decreased and would provide less NADH to be oxidized via the ETC (29, 45, 46). However, we found evidence that the oxidative TCA cycle is still running and is fueled by increased amounts of glutamine. TCA cycle-derived NADH can be used for alternative routes and would consequently not be oxidized via the ETC and thus would also result in reduced oxygen consumption rates. Mitochondrially derived NADH can alternatively be converted to NADPH by nicotinamide nucleotide transhydrogenase (17, 47), which is utilized by M(LPS) macrophages for ROS production via NADPH oxidase, needed for antibacterial activity (48), or transferred to the cytoplasm (49) where it is needed for lipogenesis. Therefore, it is possible that M(LPS) macrophages use increased amounts of TCA cycle-derived NADH for the generation of NADPH rather than oxidizing it via the ETC, which fits to the reported decreased oxygen consumption rates (6, 45, 46). Additionally, the ETC can be directly inhibited by nitrosylation (50, 51) promoted by increased expression of *iNos*, which we have shown to be increased upon LPS stimulation. Therefore, decreased oxygen consumption in M(LPS) macrophages due to decreased ETC activity is reasonable, but a decreased ETC activity does not necessarily have to result in decreased oxidative TCA cycle activity.

Although we could demonstrate that PDH activity is important in M(LPS) macrophages, the mechanism of how *Pdk1* repression is facilitated despite the presence of HIF1 needs additional research. One possibility would be a weaker stabilization because HIF1 $\alpha$  is not as abundant as in hypoxic cells. However, in this case, we would still expect a similar mode of action and therefore a moderate induction of *Pdk1*. LPS activation exhibits distinct regulatory modules (2), and we conclude that these specific networks overlap with the classical HIF1 signature to mediate LPS-specific activation. Because we demonstrated that M(LPS) macrophages depend on the PDH flux to induce cytokine expression and synthesis of itaconate, it appears that a specific HIF1-induced upstream regulator exists which specifically prevents *Pdk1* expression. In this way, increased glucose uptake and lactate release can still be facilitated by HIF1, whereas PDK1 activity is prevented by an additional regulator. Overall, this points toward a context-dependent HIF1 response.

With the hypoxia model, we demonstrated that the decreased pyruvate flux through PDH results in decreased levels of the antimicrobial metabolite itaconate as well as decreased levels of succinate. However, gene expression of *Irg1* was unchanged. We conclude that, under hypoxia, decreased metabolite levels are a

**FIGURE 6. Inhibition of pyruvate transport into mitochondria suppresses pro-inflammatory responses in M(LPS) macrophages.** A, application of the specific pyruvate transport inhibitor UK5099 to inhibit flux through PDH. Cells were treated with 100  $\mu$ M UK5099 for 6 h with or without 10 ng/ml LPS at normoxia. Prior to treatment start, cells were cultivated for 24 h in [U-<sup>13</sup>C]glucose. Presented are citrate M2 isotopologues as a readout for relative glucose flux through PDH. B–D, intracellular metabolite levels of citrate, itaconate, and succinate upon LPS stimulation and after application of 100  $\mu$ M UK5099. Metabolite levels were determined using GC/MS and normalized to cell number. E–J, relative gene expression of *Il1 $\beta$* , *iNos*, *Irg1*, *Tnf $\alpha$* , *Cpt1*, and *Pdk1* normalized to normoxia control (*Ctrl*) (–LPS), upon LPS stimulation and after application of 100  $\mu$ M UK5099 for 6 h. K, viability assay to test a potential effect of UK5099 on cell viability. Assay was performed using trypan blue, dead and live cells were counted. L, to validate the effect of UK5099 a modified experimental setup has additionally been performed. Cells were first activated with 10 ng/ml LPS for 3 h and then UK5099 was added to the cells for additional 6 h. In total, LPS activation was 9 h in this case. Non-UK5099 treated and non-activated cells served as control. M–O, intracellular metabolite levels for citrate, itaconate, and succinate (analysis as in B–D). P–S, relative gene expression analysis of *Tnf $\alpha$* , *iNos*, *Irg1*, and *Il1 $\beta$* . T and U, MID of palmitate using [U-<sup>13</sup>C]glucose as a tracer. Experimental setup as in A. U, glucose contribution to palmitate, determined from T. Error bars indicate S.E. (Welsh's *t* test, \*, *p* < 0.01, *n* = 3). One representative experiment with three individual wells per condition is presented. Each experiment was performed at least three times.



10. Tannahill, G. M., Curtis, A. M., Adamik, J., Palsson-McDermott, E. M., McGettrick, A. F., Goel, G., Frezza, C., Bernard, N. J., Kelly, B., Foley, N. H., Zheng, L., Gardet, A., Tong, Z., Jany, S. S., Corr, S. C., *et al.* (2013) Succinate is an inflammatory signal that induces IL-1 $\beta$  through HIF-1 $\alpha$ . *Nature* **496**, 238–242
11. Denko, N. C. (2008) Hypoxia, HIF1 and glucose metabolism in the solid tumour. *Nat. Rev. Cancer* **8**, 705–713
12. Filipp, F. V., Scott, D. A., Ronai, Z. A., Osterman, A. L., and Smith, J. W. (2012) Reverse TCA cycle flux through isocitrate dehydrogenases 1 and 2 is required for lipogenesis in hypoxic melanoma cells. *Pigment Cell Melanoma Res.* **25**, 375–383
13. Mullen, A. R., Wheaton, W. W., Jin, E. S., Chen, P.-H., Sullivan, L. B., Cheng, T., Yang, Y., Linehan, W. M., Chandel, N. S., and DeBerardinis, R. J. (2012) Reductive carboxylation supports growth in tumour cells with defective mitochondria. *Nature* **481**, 385–388
14. Wise, D. R., Ward, P. S., Shay, J. E., Cross, J. R., Gruber, J. J., Sachdeva, U. M., Platt, J. M., DeMatteo, R. G., Simon, M. C., and Thompson, C. B. (2011) Hypoxia promotes isocitrate dehydrogenase-dependent carboxylation of -ketoglutarate to citrate to support cell growth and viability. *Proc. Natl. Acad. Sci. U.S.A.* **108**, 19611–19616
15. Metallo, C. M., Gameiro, P. A., Bell, E. L., Mattaini, K. R., Yang, J., Hiller, K., Jewell, C. M., Johnson, Z. R., Irvine, D. J., Guarente, L., Kelleher, J. K., Vander Heiden, M. G., Iliopoulos, O., and Stephanopoulos, G. (2012) Reductive glutamine metabolism by IDH1 mediates lipogenesis under hypoxia. *Nature* **481**, 380–384
16. Fendt, S.-M., Bell, E. L., Keibler, M. A., Olenchock, B. A., Mayers, J. R., Wasylenko, T. M., Vokes, N. I., Guarente, L., Vander Heiden, M. G., and Stephanopoulos, G. (2013) Reductive glutamine metabolism is a function of the  $\alpha$ -ketoglutarate to citrate ratio in cells. *Nat. Commun.* **4**, 2236
17. Mullen, A. R., Hu, Z., Shi, X., Jiang, L., Boroughs, L. K., Kovacs, Z., Boriack, R., Rakheja, D., Sullivan, L. B., Linehan, W. M., Chandel, N. S., and DeBerardinis, R. J. (2014) Oxidation of  $\alpha$ -ketoglutarate is required for reductive carboxylation in cancer cells with mitochondrial defects. *Cell Rep.* **7**, 1679–1690
18. Hellwig-Bürgel, T., Rutkowski, K., Metzen, E., Fandrey, J., and Jelkmann, W. (1999) Interleukin-1 $\beta$  and tumor necrosis factor- $\alpha$  stimulate DNA binding of hypoxia-inducible factor-1. *Blood* **94**, 1561–1567
19. Jung, Y., Isaacs, J. S., Lee, S., Trepel, J., Liu, Z. G., and Neckers, L. (2003) Hypoxia-inducible factor induction by tumour necrosis factor in normoxic cells requires receptor-interacting protein-dependent nuclear factor  $\kappa$ B activation. *Biochem. J.* **370**, 1011–1017
20. Simon, M. C. (2010) *Diverse Effects of Hypoxia on Tumor Progression*. Springer, Berlin
21. Nishi, K., Oda, T., Takabuchi, S., Oda, S., Fukuda, K., Adachi, T., Semenza, G. L., Shingu, K., and Hirota, K. (2008) LPS induces hypoxia-inducible factor 1 activation in macrophage-differentiated cells in a reactive oxygen species-dependent manner. *Antioxid. Redox Signal.* **10**, 983–995
22. Walther, J. L., Metallo, C. M., Zhang, J., and Stephanopoulos, G. (2012) Optimization of 13C isotopic tracers for metabolic flux analysis in mammalian cells. *Metab. Eng.* **14**, 162–171
23. Metallo, C. M., Walther, J. L., Stephanopoulos, G. (2009) Evaluation of 13C isotopic tracers for metabolic flux analysis in mammalian cells. *J. Biotechnol.* **144**, 167–174
24. Sapcariu, S. C., Kanashova, T., Weindl, D., Ghelfi, J., Dittmar, G., and Hiller, K. (2014) Simultaneous extraction of proteins and metabolites from cells in culture. *MethodsX* **1**, 74–80
25. Hiller, K., Hangebrauk, J., Jäger, C., Spura, J., Schreiber, K., and Schomburg, D. (2009) Metabolite Detector: comprehensive analysis tool for targeted and nontargeted GC/MS based metabolome analysis. *Anal. Chem.* **81**, 3429–3439
26. Leek, R. D., and Harris, A. L. (2002) Tumor-associated macrophages in breast cancer. *J. Mammary Gland Biol. Neoplasia* **7**, 177–189
27. Lewis, J. S., Lee, J. A., Underwood, J. C., Harris, A. L., and Lewis, C. E. (1999) Macrophage responses to hypoxia: relevance to disease mechanisms. *J. Leukocyte Biol.* **66**, 889–900
28. Murdoch, C. (2004) Mechanisms regulating the recruitment of macrophages into hypoxic areas of tumors and other ischemic tissues. *Blood* **104**, 2224–2234
29. Palsson-McDermott, E. M., Curtis, A. M., Goel, G., Lauterbach, M. A., Sheedy, F. J., Gleeson, L. E., van den Bosch, M. W., Quinn, S. R., Domingo-Fernandez, R., Johnston, D. G., Jiang, J. K., Jiang, J. K., Israelsen, W. J., Keane, J., Thomas, C., *et al.* (2015) Pyruvate kinase M2 regulates Hif-1 $\alpha$  activity and IL-1 $\beta$  induction and is a critical determinant of the Warburg effect in LPS-activated macrophages. *Cell Metab.* **21**, 65–80
30. Strelko, C. L., Lu, W., Dufort, F. J., Seyfried, T. N., Chiles, T. C., Rabinowitz, J. D., and Roberts, M. F. (2011) Itaconic acid is a mammalian metabolite induced during macrophage activation. *J. Am. Chem. Soc.* **133**, 16386–16389
31. Blouin, C. C., Pagé, E. L., Soucy, G. M., and Richard, D. E. (2004) Hypoxic gene activation by lipopolysaccharide in macrophages: implication of hypoxia-inducible factor 1. *Blood* **103**, 1124–1130
32. Kim, J. W., Tchernyshyov, I., Semenza, G. L., Dang, C. V. (2006) HIF-1-mediated expression of pyruvate dehydrogenase kinase: a metabolic switch required for cellular adaptation to hypoxia. *Cell Metab.* **3**, 177–185
33. Patel, M. S., and Korotchkina, L. G. (2006) Regulation of the pyruvate dehydrogenase complex. *Biochem. Soc. Trans.* **34**, 217–222
34. King, A., Selak, M. A., and Gottlieb, E. (2006) Succinate dehydrogenase and fumarate hydratase: linking mitochondrial dysfunction and cancer. *Oncogene* **25**, 4675–4682
35. Demaria, M., Giorgi, C., Lebedzinska, M., Esposito, G., D'Angeli, L., Bartoli, A., Gough, D. J., Turkson, J., Levy, D. E., Watson, C. J., Wiecekowski, M. R., Provero, P., Pinton, P., and Poli, V. (2010) A STAT3-mediated metabolic switch is involved in tumour transformation and STAT3 addiction. *Ageing* **2**, 823–842
36. Garzetti, L., Menon, R., Finardi, A., Bergami, A., Sica, A., Martino, G., *et al.* (2014) Activated macrophages release microvesicles containing polarized M1 or M2 mRNAs. *J. Leukocyte Biol.* **95**, 817–825
37. O'Neill, L. A., and Hardie, D. G. (2013) Metabolism of inflammation limited by AMPK and pseudo-starvation. *Nature* **493**, 346–355
38. Yang, C., Ko, B., Hensley, C. T., Jiang, L., Wasti, A. T., Kim, J., Sudderth, J., Calvaruso, M. A., Lumata, L., Mitsche, M., Rutter, J., Merritt, M. E., and DeBerardinis, R. J. (2014) Glutamine oxidation maintains the TCA cycle and cell survival during impaired mitochondrial pyruvate transport. *Mol. Cell* **56**, 414–424
39. Vats, D., Mukundan, L., Odegaard, J. I., Zhang, L., Smith, K. L., Morel, C. R., Wagner, R. A., Greaves, D. R., Murray, P. J., and Chawla, A. (2006) Oxidative metabolism and PGC-1 $\beta$  attenuate macrophage-mediated inflammation. *Cell Metab.* **4**, 13–24
40. Tan, Z., Xie, N., Cui, H., Moellering, D. R., Abraham, E., Thannickal, V. J., and Liu, G. (2015) Pyruvate dehydrogenase kinase 1 participates in macrophage polarization via regulating glucose metabolism. *J. Immunol.* **194**, 6082–6089
41. Everts, B., Amiel, E., Huang, S. C., Smith, A. M., Chang, C.-H., Lam, W. Y., Redmann, V., Freitas, T. C., Blagih, J., van der Windt, G. J., Artyomov, M. N., Jones, R. G., Pearce, E. L., and Pearce, E. J. (2014) TLR-driven early glycolytic reprogramming via the kinases TBK1-IKK $\epsilon$  supports the anabolic demands of dendritic cell activation. *Nat. Immunol.* **15**, 323–332
42. Infantino, V., Convertini, P., Cucci, L., Panaro, M. A., Di Noia, M. A., Calvello, R., Palmieri, F., and Iacobazzi, V. (2011) The mitochondrial citrate carrier: a new player in inflammation. *Biochem. J.* **438**, 433–436
43. Wise, D. R., and Thompson, C. B. (2010) Glutamine addiction: a new therapeutic target in cancer. *Trends Biochem. Sci.* **35**, 427–433
44. Newsholme, P., Curi, R., Pithon Curi, T.C., Murphy, C. J., Garcia, C., and Pires de Melo, M. (1999) Glutamine metabolism by lymphocytes, macrophages, and neutrophils: its importance in health and disease. *J. Nutr. Biochem.* **10**, 316–324
45. Jha, A. K., Huang, S. C., Sergushichev, A., Lampropoulou, V., Ivanova, Y., Loginicheva, E., Chmielewski, K., Stewart, K. M., Ashall, J., Everts, B., Pearce, E. J., Driggers, E. M., and Artyomov, M. N. (2015) Network integration of parallel metabolic and transcriptional data reveals metabolic modules that regulate macrophage polarization. *Immunity* **42**, 419–430
46. Krawczyk, C. M., Holowka, T., Sun, J., Blagih, J., Amiel, E., DeBerardinis, R. J., Cross, J. R., Jung, E., Thompson, C. B., Jones, R. G., and Pearce, E. J. (2010) Toll-like receptor-induced changes in glycolytic metabolism regulate dendritic cell activation. *Blood* **115**, 4742–4749

## PDH Flux Is Important for Activation of M(LPS) Macrophages

47. Gameiro, P. A., Laviolette, L. A., Kelleher, J. K., Iliopoulos, O., and Stephanopoulos, G. (2013) Cofactor balance by nicotinamide nucleotide transhydrogenase (NNT) coordinates reductive carboxylation and glucose catabolism in the tricarboxylic acid (TCA) cycle. *J. Biol. Chem.* **288**, 12967–12977
48. West, A. P., Brodsky, I. E., Rahner, C., Woo, D. K., Erdjument-Bromage, H., Tempst, P., Walsh, M. C., Choi, Y., Shadel, G. S., and Ghosh, S. (2011) TLR signalling augments macrophage bactericidal activity through mitochondrial ROS. *Nature* **472**, 476–480
49. Houtkooper, R. H., Cantó, C., Wanders, R. J., and Auwerx, J. (2010) The secret life of  $\text{NAD}^+$ : an old metabolite controlling new metabolic signaling pathways. *Endocr. Rev.* **31**, 194–223
50. Clementi, E., Brown, G. C., Feelisch, M., and Moncada, S. (1998) Persistent inhibition of cell respiration by nitric oxide: crucial role of S-nitrosylation of mitochondrial complex I and protective action of glutathione. *Proc. Natl. Acad. Sci. U.S.A.* **95**, 7631–7636
51. Drapier, J. C., and Hibbs, J. B. (1988) Differentiation of murine macrophages to express nonspecific cytotoxicity for tumor cells results in L-arginine-dependent inhibition of mitochondrial iron-sulfur enzymes in the macrophage effector cells. *J. Immunol.* **140**, 2829–2838

**Pro-inflammatory Macrophages Sustain Pyruvate Oxidation through Pyruvate Dehydrogenase for the Synthesis of Itaconate and to Enable Cytokine Expression**

Johannes Meiser, Lisa Krämer, Sean C. Sapcariu, Nadia Battello, Jenny Ghelfi, Aymeric Fouquier D'Herouel, Alexander Skupin and Karsten Hiller

*J. Biol. Chem.* 2016, 291:3932-3946.

doi: 10.1074/jbc.M115.676817 originally published online December 17, 2015

---

Access the most updated version of this article at doi: [10.1074/jbc.M115.676817](https://doi.org/10.1074/jbc.M115.676817)

Alerts:

- [When this article is cited](#)
- [When a correction for this article is posted](#)

[Click here](#) to choose from all of JBC's e-mail alerts

This article cites 49 references, 16 of which can be accessed free at <http://www.jbc.org/content/291/8/3932.full.html#ref-list-1>

---

# Bridging the gap between non-targeted stable isotope labeling and metabolic flux analysis

---

Daniel Weindl, Thekla Cordes, Nadia Battello, Sean C Sapcariu, Xiangyi Dong, Andre Wegner, and Karsten Hiller

*Cancer & Metabolism*, accepted for publication

## Contributions

- Conduction of experimental work and analysis of the data underlying figure 5E



## METHODOLOGY

# Bridging the gap between non-targeted stable isotope labeling and metabolic flux analysis

Daniel Weindl<sup>1</sup>, Thekla Cordes<sup>1,2</sup>, Nadia Battello<sup>1</sup>, Sean C Sapcariu<sup>1</sup>, Xiangyi Dong<sup>1</sup>, Andre Wegner<sup>1</sup> and Karsten Hiller<sup>1\*</sup>

\*Correspondence:

[karsten.hiller@uni.lu](mailto:karsten.hiller@uni.lu)

<sup>1</sup>Luxembourg Centre for Systems Biomedicine, University of Luxembourg, 6, avenue du Swing, 4367, Belvaux, Luxembourg  
Full list of author information is available at the end of the article

### Abstract

**Background:** Metabolism gained increasing interest for the understanding of diseases and to pinpoint therapeutic intervention points. However, classical metabolomics techniques only provide a very static view on metabolism. Metabolic flux analysis methods, on the other hand, are highly targeted, requiring detailed knowledge on metabolism beforehand and cannot account for unanticipated reactions.

**Results:** We present a novel workflow to analyze non-targeted metabolome-wide stable isotope labeling data to detect metabolic flux changes in a non-targeted manner. Furthermore, we show how similarity-analysis of isotopic enrichment patterns can be used for pathway contextualization of unidentified compounds. We illustrate our approach with the analysis of changes in cellular metabolism of human adenocarcinoma cells in response to decreased oxygen availability. Starting without *a priori* knowledge, we detect metabolic flux changes, leading to an increased glutamine contribution to acetyl-CoA production, reveal biosynthesis of *N*-acetylaspartate by *N*-acetyltransferase 8-like (NAT8L) in lung cancer cells and show that *NAT8L* silencing inhibits proliferation of A549, JHH-4, PH5CH8 and BEAS-2B cells.

**Conclusion:** Differential stable isotope labeling analysis provides qualitative metabolic flux information in a non-targeted manner. Furthermore, similarity analysis of enrichment patterns provides information on metabolically closely related compounds. *N*-acetylaspartate and NAT8L are important players in cancer cell metabolism, a context in which they have not received much attention yet.

**Keywords:** stable isotope labeling; metabolomics; non-targeted; flux analysis; mass isotopomer distribution analysis; NTFD; cancer; NAT8L; *N*-acetylaspartate

### Background

Over the last decades, cellular metabolism gained increasing interest to pinpoint potential therapeutic intervention points to treat complex diseases. Metabolomics research, analyzing changes in metabolite levels, deepened our understanding of cellular metabolism, which led to the discovery of unanticipated metabolites [1] and disease biomarkers [2, 3]. However, metabolite levels alone provide only a very static view on metabolism. For a systems understanding of metabolism, the underlying metabolic fluxes are much more important and informative because they provide a much closer functional link to an observed phenotype [4]. Metabolic fluxes through these pathways do not only depend on metabolite concentrations, but are modulated by intricate regulatory mechanisms [5]. For that reason, they cannot be deduced from metabolite levels alone.

To that end metabolic flux analysis techniques such as flux balance analysis (FBA) and  $^{13}\text{C}$  metabolic flux analysis ( $^{13}\text{C}$ -MFA) have been developed. FBA employs genome-scale metabolic networks [6] and aims to balance cellular influxes and effluxes with an optimal set of intracellular fluxes [7, 8]. On the other hand,  $^{13}\text{C}$ -MFA uses much smaller metabolic networks, but combines cellular influxes and effluxes with experimental data obtained from stable isotope labeling experiments [9, 10]. Isotopic labeling patterns are usually analyzed by mass spectrometry (MS) in the form of mass isotopomer distributions (MIDs), which are the mass-aggregated relative isotopologue abundances. Since MIDs of metabolites from a given tracer within a given metabolic network are solely a function of the metabolic fluxes, they can be used to estimate these underlying fluxes [11, 12]. Using mathematical optimization techniques, a set of fluxes is determined which can explain the experimentally observed MIDs for a defined metabolic network model [9, 10].

A drawback, that all current metabolic flux analysis techniques have in common, is that they rely on the exact topological knowledge of the metabolic network of interest. However, knowledge of metabolic networks of most organisms is still not comprehensive, as for example recently shown for mammalian macrophages which were found to produce an unanticipated antimicrobial compound [1].

As stated above, MIDs from stable isotope labeling experiments hold metabolic flux information. This is exploited in  $^{13}\text{C}$ -MFA, but only in a highly targeted manner. However, there are methods available for the non-targeted MID determination of compounds in complex mixtures after either gas chromatography MS (GC-MS) [13, 14] or liquid chromatography MS (LC-MS) analysis [15–17]. These methods do not rely on any biological knowledge, and thus, are able to account for any unanticipated metabolite. To date, only very few studies performed non-targeted MID analyses and obtained novel biological insights [15, 18]. Mostly, non-targeted detection of stable isotope labeling has been applied in a qualitative manner to separate metabolites produced by the cell from analytical background [19–21]. One major problem is still the lack of appropriate tools to extract biological information out of the mass spectrometric data [22]. In particular, studies covering multiple experimental conditions or time-points generate complex data and require proper tools for efficient analysis and visualization of isotope labeling data.

In this article, we present a novel workflow for stable isotope labeling analysis that allows for the non-targeted detection of 1) pathway activity, highlighting unexpected parts of metabolism; 2) relative flux changes or differential pathway activity between conditions; and 3) the pathway contextualization of unidentified compounds and their vicinity to other metabolites. This workflow can be used for data-driven analyses and hypothesis generation which can be tested in subsequent targeted approaches. We illustrate our workflow by analyzing changes in cellular metabolism of human lung cancer cells in response to varying oxygen availability ranging from atmospheric 21%  $\text{O}_2$  down to 1%  $\text{O}_2$ . Starting without *a priori* knowledge, we detected metabolic flux changes, which led to an increased glutamine contribution to acetyl-CoA, show that A549 lung cancer cells produce *N*-acetylaspartate, a compound which is well known to have an important function in neuronal tissue, but was until very recently [23] not known to be produced in other tissues, and show that silencing its biosynthetic enzyme NAT8L exerts a negative growth effect.

## Methods

### Chemicals

Stable isotope labeled tracers were bought from Cambridge Isotope Laboratories, all other chemicals were bought from Sigma-Aldrich. All solvents were of grade *Chromasolv* or higher.

### Cell culture & stable isotope labeling

Human lung adenocarcinoma A549 cells (ATCC CCL-185, [24]) were cultivated in D5030 medium (Dulbecco's modified Eagle's medium without glucose, glutamine, phenol red, sodium pyruvate and sodium bicarbonate), supplemented with 10% dialyzed fetal bovine serum and either 12.5 mM glucose, 12.5 mM [1,2-<sup>13</sup>C<sub>2</sub>]-D-glucose and 4 mM glutamine, or with 25 mM glucose, 2 mM glutamine and 2 mM [U-<sup>13</sup>C]-L-glutamine. Cells were seeded into 12-well multi-well plates at a density of  $3 \times 10^5$  cells in 0.75 ml growth medium and cultivated at 37 °C, in an atmosphere with 5% CO<sub>2</sub> and 95% air with oxygen levels of 1%, 5%, 10%, 15%, and 21%. Before applying the tracer-containing medium for 24 h, cells and media were equilibrated to the respective oxygen levels for 24 h. Under each condition, 3–4 wells were used for metabolite extraction.

### Metabolite extraction and GC-MS analysis

Intracellular metabolites were extracted and polar metabolites were analyzed by GC-MS as described in [25]. In short, a liquid-liquid extraction was performed using chloroform:methanol:water. The quenching step using ice cold methanol was performed at the respective oxygen levels. An aliquot of the polar phase was dried, dissolved in pyridine containing methoxyamine hydrochloride and trimethylsilylated using *N*-methyl-*N*-(trimethylsilyl) trifluoroacetamide (MSTFA).

### GC-MS data processing and determination of isotopic enrichment

Deconvolution of mass spectra and targeted MID analysis were performed using MetaboliteDetector version 2.820150209R [26]. The following MetaboliteDetector peak picking and deconvolution settings were used: Minimum number of peaks: 25; Peak threshold: 5; Minimum peak height: 5; Bins/scan: 10; Required base peak intensity: 0; Deconvolution width: 3 scans. An even-numbered *n*-alkane mixture (C<sub>10</sub>–C<sub>40</sub>) was measured for retention index calibration.

Non-targeted detection of stable isotope labeling and mass isotopologue analysis were performed using an in-house software based on the NTFD algorithm [13, 14, 27]. For data analysis we considered all compounds which the NTFD algorithm detected at least under one experimental condition two mass spectrometric fragments with a coefficient of MID determination of  $R^2 > 0.98$ ,  $\sum |M_i| < 1.05$ ,  $M_0$  abundance of  $0.45 < M_0 < 1$  and minimal enrichment  $1 - M_0 \geq 0.05$ . These parameters are described in more detail in [27]. Because in non-targeted analysis the maximal length of the MID vector is unknown, trailing mass isotopomer abundances of below 0.01 have been considered as noise and been removed. Compounds were identified based on RI and mass spectrum matching against an in-house reference library. Known contaminants like siloxanes were excluded from further analysis. Analytes were identified based on RI and mass spectrum matching against an in-house reference library.

### Mass isotopomer abundance variation

To detect compounds with most varying labeling patterns across different experimental conditions, we analyzed the maximal standard deviation in relative mass isotopomer abundance for every compound that was detected in at least three out of five conditions:

$$\text{variation score} = \max \sigma_j \quad | \quad \sigma_j = \sqrt{\frac{1}{n} \cdot \sum_{i=0}^n (\bar{p}_j - p_{j,i})^2}$$

where  $p_{i,j}$  is the relative abundance of the  $M_j$  isotopologue of the given compound in the  $i$ -th dataset and  $\bar{p}_j$  the average  $M_j$  abundance across all  $n$  datasets. The MIDs of the heaviest common fragments across all conditions were used and the MIDs of unlabeled compounds were not considered. Compounds with the top five MID variation scores after [1,2-<sup>13</sup>C<sub>2</sub>]glucose and [U-<sup>13</sup>C]glutamine labeling are shown in [Figure 3A](#) (only one of two glutamate TMS derivatives is shown).

### MID distance calculation

For calculation of MID distances, MIDs of the largest fragment with  $R^2 > 0.95$  of each compound was used. Correction for natural isotope abundance was performed using the NTFD algorithm [27]. A Needleman-Wunsch alignment was performed on the MID vectors minimizing the absolute differences in relative mass isotopomer abundances using a gap penalty of 0.4 ([Figure 1B](#)). Subsequently, the pairwise distances of all aligned MID vectors were determined ([Figure 1A](#)). Therefore, the Canberra distance of two MID vectors  $A$  and  $B$  was calculated as  $d_{A,B} = \sum_{i=1}^n \frac{|A_i - B_i|}{|A_i| + |B_i|}$  and normalized by the sum of the dimensions of the MID vectors ( $d_{A,B}^{norm} = \frac{d_{A,B}}{\dim A + \dim B}$ ). The most similar compounds are shown in [Figure 4](#); edge color represents the experimental condition at which the high similarity was observed. In case of multiple TMS derivatives of the same metabolite only one is shown.

### MID deconvolution of aspartyl and acetyl moiety of *N*-acetylaspartate

The mass spectrometric fragment ions  $m/z$  304 and  $m/z$  245 of NAA 2TMS represent the  $[M-CH_3]^+$  and  $[M-CH_3-CH_3CONH_2]^+$  fragments, respectively (Supplemental Figure S5). The two fragments differ by the acetamido-group ( $CH_3CONH_2$ ). The MID of NAA (given by  $[M-CH_3]^+$ ) is the convolution or Cauchy product [12] of the MIDs of the aspartyl moiety ( $M_{Asp}$ , given by  $[M-CH_3-CH_3CONH_2]^+$ ) and the acetamido moiety ( $M_{Ac}$ ) of the molecule:

$$\begin{pmatrix} M_{0,NAA} \\ M_{1,NAA} \\ M_{2,NAA} \\ M_{3,NAA} \\ M_{4,NAA} \\ M_{5,NAA} \\ M_{6,NAA} \end{pmatrix} = \begin{pmatrix} M_{0,Asp} & 0 & 0 \\ M_{1,Asp} & M_{0,Asp} & 0 \\ M_{2,Asp} & M_{1,Asp} & M_{0,Asp} \\ M_{3,Asp} & M_{2,Asp} & M_{1,Asp} \\ M_{4,Asp} & M_{3,Asp} & M_{2,Asp} \\ 0 & M_{4,Asp} & M_{3,Asp} \\ 0 & 0 & M_{4,Asp} \end{pmatrix} \cdot \begin{pmatrix} M_{0,Ac} \\ M_{1,Ac} \\ M_{2,Ac} \end{pmatrix}$$

This equation system was populated with the raw mass spectral intensities and solved for  $M_{Ac}$  using a weighted least squares approach using the `nlsLM` routine of the `minpack.lm` package (version 1.1-8) for the R statistics environment (version 3.1.2). The determined acetyl MIDs were corrected for natural isotope abundance.

#### siRNA transfection

For knockdown experiments, siRNA were reverse transfected into A549 cells using Lipofectamine RNAiMAX (Invitrogen/Life Technologies). For each well (12-well plate), 20 pmol siRNA were diluted in 200  $\mu$ l Opti-MEM I reduced-serum medium (Invitrogen/Life Technologies), supplemented with 2.5  $\mu$ l Lipofectamine RNAiMAX, gently mixed, and incubated for 20 min at room temperature. The prepared solution was spread in a well 5 min before 100,000 cells in 800  $\mu$ l of DMEM 5796 growth medium containing 10% FBS were added. The plate was gently mixed and incubated (37 °C, 5% CO<sub>2</sub>) for up to 72 h. ON-TARGETplus non-targeting and NAT8L-targeting siRNA were obtained from Dharmacon/GEHealthcare (see Supplemental Table S6 for target sequences).

#### Growth assay

For growth assays with A549 cells, cells were transfected and cultivated at 2% oxygen as described above. After 72 h, cells were detached using trypsin, and cell numbers and viability were determined using a Vi-CELL XR Cell Viability Analyzer (Beckman Coulter). Cell viability was above 95% in all samples. Cell numbers are presented as mean of three independent experiments, each consisting of 3-wells per condition (Figure 5).

Human bronchial epithelial BEAS-2B cells (ATCC CRL-9609), human hepatocellular carcinoma JHH-4 cells (JCRB Cell Bank) and non-neoplastic hepatocyte PH5CH8 cells [28] were transfected with non-targeting or NAT8L-targeting siRNA as described above and cultivated at normoxia. Cells were seeded in 12-well plates at densities of 95,000 cell/well for PH5CH8, 57,000 cells/well for JHH-4 and 100,000 cells/well for BEAS-2B. After 24 h, transfection medium was replaced by DMEM 5796 growth medium containing 10% FBS (JHH-4 and PH5CH8) or LHC-9 medium (BEAS-2B). LHC-9 medium was prepared from LHC-8 media (Gibco) by adding 33 nM retinoic acid (Lonza) and 2.75  $\mu$ M epinephrine (Lonza). After 72 h, cell numbers were determined as described above. Cell numbers are presented as mean of three independent experiments, each consisting of three wells per condition.

#### Metabolome analysis

For semi-quantification of metabolite levels after NAT8L silencing (Figure 5), cells were incubated at 21% O<sub>2</sub> for two days after transfection. Metabolites were extracted and analyzed by GC-MS as described above. Data was analyzed using MetaboliteDetector with settings as described above, but a deconvolution width of 5 scans. Non-targeted batch quantification was performed over all data files and mass spectrometric intensities were normalized to summed analyte signal of each sample after exclusion of known contaminants. Replicates represent metabolite extracts from different cell populations ( $n = 3$ ).

## Results

### Mass isotopologue analysis

The starting point of our workflow is a stable isotope labeling experiment. After mass spectrometric measurements of labeled and unlabeled metabolite extracts, MIDs, corrected for natural isotope abundance, can be obtained in a non-targeted manner [15, 16, 27]. We analyze these metabolome-wide MIDs, the mass isotopologue, to detect changes in metabolic fluxes and exploit MID similarity between compounds for their pathway contextualization.

#### *Locating flux changes by non-targeted mass isotopomer abundance variation analysis*

Since changes in MIDs can only be a consequence of altered metabolic fluxes, we can reveal metabolic flux changes by detecting changes in the mass isotopologue [29]. Therefore, MIDs of identical compounds are matched across different experimental conditions to detect differences in relative mass isotopomer abundances. As a measure of variation, for each isotopically enriched compound we calculate the maximal standard deviation of relative mass isotopomer abundance across the different experimental conditions (see Experimental Procedures). We assume that large flux changes will lead to large changes in mass isotopomer abundances, although this might neglect flux changes that make a small relative contribution to a given metabolite pool. Thus, to find the most significant flux changes, we rank metabolites by their aforementioned variation score. Like any MID analysis, this approach is limited by the facts that 1) MIDs alone can only provide relative flux information (flux ratios), and therefore, 2) not all changes in metabolic fluxes manifest in MID changes. Furthermore, as in conventional metabolomics approaches, metabolite pools of subcellular compartments are usually mixed during metabolite extraction which might reduce their informative value. Apart from that, this systematic analysis of relative mass isotopomer abundance variation detects flux changes without the requirement of any biochemical *a priori* knowledge on the system of interest or the identification of the respective compounds. It is only biased by analytical restrictions and the choice of the isotopic tracer and will consider any unanticipated reaction or metabolite which cannot be accounted for by current flux analysis techniques.

#### *MID-similarity assisted compound identification*

For subsequent interpretation of the detected changes in mass isotopomer abundances, the respective compounds need to be identified. This is usually achieved by matching their mass spectra against reference libraries [30], but the available libraries are far from comprehensive. Although thousands of chromatographic / mass spectrometric features, and among them at least several hundreds of metabolites can be analytically detected [20, 31, 32], only a fraction thereof can be identified, rendering compound identification a major bottleneck in current metabolomics research [33]. When the detected features or at least their pathways or compound classes are identified, they can provide more biological insights in addition to their function as biomarkers. Hence, compound identification is, however cumbersome, still highly important.

For compounds that are not present in reference libraries, other means for identification are required. Here, we present an approach based on MID-similarity. As described above, the MID of any metabolite is determined by those of its precursors and the flux ratio of the producing reactions. Within linear pathways, the MIDs of all compounds are identical, except if there are gains or losses of isotopically enriched fragments of the molecules. Here we exploit the reverse conclusion, assuming that compounds with identical or highly similar MIDs are more likely to be intermediates of the same pathway or lie in the same area of the metabolic network. Therefore, by analyzing the MID similarity of different compounds, they can be grouped to metabolic pathways. Strictly speaking, this high MID similarity is only granted in linear pathways. However, in converging pathways, if one flux is much larger than the other, or there is only a dilution with the unlabeled isotopologue, then the labeling pattern of the dominating precursor is mostly conserved in the product MID and the reaction sequence can be seen as pseudo-linear. In this case, the MID similarity is still significant. Empirically, this is the case for many metabolic reactions.

To analyze MID similarity for pathway contextualization of unidentified compounds, we pairwise compare MIDs of all isotopically enriched compounds (Figure 1A). To account for potential losses or additions of isotopically enriched fragments to the molecules which would shift the MIDs, we perform a Needleman-Wunsch alignment [34] on the MID vectors prior to the similarity calculation (Figure 1B). As a similarity measure, we compare the Canberra distances of all pairwise aligned MIDs. This pairwise comparison results in a distance or similarity matrix. After applying an empirically determined distance cutoff, we create a network of compounds with higher MID similarity. The resulting graph is likely to show metabolically connected compounds. However, the MID similarity can — dependent on tracer and pathways — be ambiguous. The specificity can be increased by using distinct tracers and multiple experimental conditions (Figure 1A). Edges in the graph occurring in multiple conditions are more likely to be biologically meaningful.

In summary, MID similarity between compounds can indicate proximity within the metabolic network. This can be used to associate unidentified compounds with identified ones, and to map them to specific pathways. This itself is valuable information and can furthermore be a strong hint for subsequent compound identification. For both identified and unidentified compounds such an MID similarity analysis can reveal new biosynthetic pathways or help to distinguish between different known ones.

#### *Method summary*

The proposed workflow starts with stable isotope labeling experiments, mass spectrometric analysis, and the non-targeted detection of isotopically enriched compounds (Figure 2B). In addition to MIDs, such an analysis yields, for each compound, the labeled and unlabeled mass spectra, as well as the chromatographic retention time, often normalized as retention index (RI). Qualitative analysis of isotopic enrichment provides information on active fluxes and the general fate of the metabolic tracer. MIDs from different experimental conditions are systematically analyzed to detect changes in metabolic fluxes. MID similarity may indicate

metabolic proximity, hence, MIDs of compounds of interest are compared to all other MIDs for pathway contextualization, discovery of potential precursors, or to facilitate identification of unidentified compounds.

Overall, this non-targeted approach provides information on: 1) active pathways, 2) changed fluxes, and 3) compound identities. This information holds biological insights itself and will furthermore generate hypotheses for subsequent analyses (Figure 2A).

An additional advantage of non-targeted isotope labeling analysis is that, depending on the proper tracer choice, it clearly shows whether a given compound is formed by the organism or was externally introduced as ingredient of an undefined growth medium or as contamination and thus provides an additional quality control. Furthermore, an advantage of the analysis of MIDs over metabolite levels is that they are more robust to technical variation than metabolite levels.

#### Mass isotopome analysis in hypoxic cancer cells

We illustrate the developed approach by analyzing human lung cancer cell metabolism under different oxygen levels. We have chosen this condition, because hypoxia induces strong changes in cellular metabolism which have been studied intensively in cancer cells [35–39]. The large number of previous studies would allow us to readily confirm our findings and to validate our approach. Furthermore, it was interesting to see if our approach was able to identify novel features. To this end, we performed stable isotope labeling experiments with [1,2-<sup>13</sup>C<sub>2</sub>]glucose and [U-<sup>13</sup>C]glutamine under oxygen levels ranging from 1% O<sub>2</sub> to atmospheric 21% O<sub>2</sub>. We chose glucose and glutamine as isotopic tracers because they are the major carbon sources of most mammalian cells, and therefore, lead to a good metabolome coverage of isotopic enrichment. After GC-MS analysis of the metabolite extracts, we determined all isotopically enriched compounds along with their MIDs in an automated and non-targeted manner. We detected 24 compounds which were labeled from [U-<sup>13</sup>C]glutamine and 60 labeled from [1,2-<sup>13</sup>C<sub>2</sub>]glucose (Supplemental Tables S1–S2).

#### *Non-targeted flux profiling reveals changes in intermediary metabolism*

To detect hypoxia-induced metabolic flux changes in a non-targeted manner, we applied the aforementioned mass isotopomer abundance variation analysis and focused on the 5 compounds with the highest variation resulting from [U-<sup>13</sup>C]glutamine and [1,2-<sup>13</sup>C<sub>2</sub>]glucose labeling. Three compounds were common to both datasets, two were unique to one set (Figure 3A, only one out of two glutamate TMS derivatives is shown).

With decreasing O<sub>2</sub> levels, the compounds with high MID variation after glucose labeling showed an increase in the unlabeled (M<sub>0</sub>) fraction and a concomitant decrease in the abundances of heavier mass isotopomers, indicating decreased glucose contribution to their biosynthesis (Figure 3A). The compounds with changed MIDs after glutamine labeling had an either relatively constant or slightly increasing enrichment. Additionally, three of these compounds showed a switch of the most abundant mass isotopomer indicating a change of their biosynthesis route (Figure 3A).



While the detection of these changes in labeling patterns was fully non-targeted and did not require the compounds to be identified, the further interpretation requires their identification, as well as detailed knowledge on the metabolic network, including carbon atom transitions. Hence, to interpret the observed changes in isotopic labeling, we tried to identify the corresponding compounds by matching their mass spectra against an in-house reference library. We identified the highest-ranking metabolites from glutamine labeling as the trimethylsilyl (TMS) derivatives of malate, glutamate, citrate and *N*-acetylaspartate (NAA) (Figure 3A). From glucose labeling we identified citrate and malate, NAA and adenosine monophosphate (AMP). One compound remained unidentified; its mass spectrum could not be found in any of the common mass spectrum reference libraries such as the Golm Metabolome Database (GMD) or the NIST mass spectral library.

Citrate, malate, and glutamate and NAA are all associated with the citric acid cycle. With decreasing O<sub>2</sub> levels, their isotopic enrichment from [U-<sup>13</sup>C]glutamine changes significantly due to increasing reductive carboxylation of 2-oxoglutarate by isocitrate dehydrogenase (IDH) [36, 37] (Figure 3B). This reductive IDH flux increased severalfold with decreasing O<sub>2</sub>. At the same time, isotopic enrichment from [1,2-<sup>13</sup>C<sub>2</sub>]glucose was significantly reduced, indicating a relative decrease in glucose-carbon entering the citric acid cycle as a result of pyruvate dehydrogenase (PDH) inhibition [40].

For this mass isotopomer abundance variation analysis we used the heaviest mass spectrometric fragment that was detected as isotopically enriched. For malate, citrate and glutamate, the selected fragment all contained the full carbon backbone of the native metabolites. However, for NAA and AMP the MIDs represent only a substructure of the analytes, so that interpretation is only possible if the fragmentation is known. The MIDs shown for fragment *m/z* 169 of AMP 5TMS (Figure 3A) most likely represent the ribose moiety of AMP [41]. These labeling changes might hint towards changed fluxes through the pentose phosphate pathway, but require further validation. The MIDs of fragment *m/z* 245 of NAA exhibited very high similarity to malate, suggesting that this fragment contains only the aspartate moiety, but not the acetyl moiety of NAA (Figure 3A). Combinatorial analysis of possible fragment formulas using FFC [42] indicated that this fragment most likely arises from loss of the acetamido-moiety of NAA which was confirmed by stable isotope labeling (Supplemental Figure S5). This turned out to be of interest because it allows for the deconvolution of the MIDs of the aspartyl- and acetyl-moiety of NAA and hence can be used as a proxy to assess acetyl-CoA labeling under isotopic steady state conditions (Figure 3C). The determined isotopic enrichment of the NAA acetyl-moiety provides additional evidence for progressive increase of carboxylation of 2-oxoglutarate to provide acetyl-CoA for fatty acid biosynthesis under hypoxia [36].

#### *MID-similarity assisted compound identification*

Among the compounds with highly varying MIDs, as well as among the isotopically enriched compounds in general, there were several compounds which we were not able to identify using our in-house or any other commonly available reference library. However, to be able to interpret the observed MID changes, knowledge on their metabolic origin is imperative.

To show that the aforementioned MID similarity analysis can be a valuable tool to aid compound identification, we first performed MID similarity analysis on the already identified NAA. The compounds with the most similar labeling patterns after [U-<sup>13</sup>C]glutamine labeling were aspartate, malate and pyroglutamate (Figure 4A), and alanine and citrate after [1,2-<sup>13</sup>C<sub>2</sub>]glucose (Figure 4B). Aspartate is the direct precursor of NAA and the other compounds are only a few reactions away, demonstrating that MID similarity analysis can indeed provide valuable hints on metabolically closely related compounds (Figure 4C).

Next, we performed the same analysis to aid identification of the yet unidentified compound RI 2578 which popped up in the MID variation analysis (Figure 3A). The heaviest fragment that was detected as isotopically enriched showed very high MID similarity to citrate after [U-<sup>13</sup>C]glutamine labeling, suggesting that the unidentified compounds must be closely related to citrate (Figure 4D). The compounds with high MID similarity after [1,2-<sup>13</sup>C<sub>2</sub>]glucose labeling, glycerol 3-phosphate and pyroglutamate, are very distantly related, and therefore, are less informative (Figure 4E). The analyzed fragment *m/z* 363 has only about half the mass of the heaviest fragment *m/z* 666 of the spectrum (Supplemental Figure S7). For the heaviest fragment, no enrichment patterns could be determined due to its low abundance and low enrichment. We assumed the heaviest fragment *m/z* 666 was the [M-CH<sub>3</sub>]<sup>+</sup> ion, a fragment ion that is commonly observed after electron ionization of TMS derivatives in place of the molecular ion [M]<sup>+</sup>. In order to identify compound RI 2578, we searched the HMDB database [43] for the mass of the native metabolite, assuming due to its retention index 5 or 6 TMS groups in the molecule. Of the 38 database hits, β-citrylglutamate (β-CG) was the candidate that could account for the observed high MID similarity to citrate (Figure 4D,F). Unfortunately, there was neither an authentic standard of β-CG commercially available to confirm this tentative identification, nor was there an electron ionization mass spectrum published. However, as discussed below, there is biological evidence supporting this identification.

#### NAT8L-mediated NAA biosynthesis in lung cancer cells

We were intrigued by finding NAA in lung cancer cells, with its isotopic enrichment clearly indicating its *de novo* biosynthesis there, although so far biosynthesis was assumed to be restricted to neuronal tissue. Therefore, we followed up on this finding to investigate whether NAA plays a significant role in cancer cells. The recent study by Lou *et al.* [23], reporting some of the results presented below, was only published during the preparation of this manuscript.

In neurons, NAA is known to be produced by NAT8L [44]. To confirm NAT8L as the producing enzyme in A549 cells, we transfected them with *NAT8L* targeting siRNA and analyzed polar metabolite extracts by GC-MS. Upon *NAT8L* silencing, NAA levels were drastically reduced (Figure 5A), confirming NAT8L-mediated biosynthesis of NAA. Besides, NAA, we also observed production of another neuropeptide, *N*-acetylaspartylglutamate (NAAG), by A549 cells. NAAG is synthesized from NAA by RIMKLA and RIMKLB, the latter of which also catalyzes the formation of β-CG as alternative product [45]. Both *RIMKLA* and *RIMKLB* were found to be expressed in A549 as determined by qPCR analysis (data not shown). Upon transfection with *NAT8L* targeting siRNA, NAAG levels dropped below the detection limit (Figure 5B), whereas the levels of putative β-CG increased (Figure 5C).

As mentioned above, there was unfortunately no authentic standard available to confirm the identity of RI 2578 as  $\beta$ -CG. Yet, its identification is corroborated by mass spectrometric fragmentation (Supplemental Figure S7), stable isotope labeling data as well as the correlation of NAT8L silencing with an increase in levels of RI 2578.

#### *Loss of NAT8L function impairs cell proliferation*

Others have observed a positive correlation between NAA levels and malignancy of prostate tumors [46] and identified NAA as a potential diagnostic blood biomarker for cancer [23]. To determine whether NAA or NAT8L have an effect on cell proliferation, we performed growth assays after siRNA-mediated *NAT8L* silencing. After 72h, the number of cells transfected with NAT8L-targeting siRNA was 28% lower than the ones transfected with a non-targeting siRNA, suggesting a substantial role of NAA or NAT8L in A549 cells (Figure 5D). To confirm this finding, we repeated the experiments using bronchial epithelial BEAS-2B cells, hepatocellular carcinoma JHH-4 cells and non-neoplastic hepatocyte PH5CH8 cells. All three cell lines showed a similar reduction in cell numbers of about 20–30% after transfection with *NAT8L* targeting siRNA (Figure 5E).

## Discussion

Non-targeted data acquisition and analysis approaches are valuable tools to generate initial hypotheses, especially when little *a priori* information is available on the organism or subject of interest. We showed how stable isotope labeling experiments and subsequent non-targeted mass isotopologue analysis can be used for metabolic flux profiling and hypothesis generation (Figure 2A).

To demonstrate our novel non-targeted stable isotope labeling analysis workflow, we performed stable isotope labeling experiments with human adenocarcinoma cells incubated in the presence of  $^{13}\text{C}$ -labeled glucose and glutamine at various oxygen levels and analyzed the resulting mass isotopologue. We illustrated that our approach can be used to extract biologically meaningful information instead of mere statistical differences. Although we applied our workflow on GC-MS data, it can also directly be used in LC-MS experiments which may provide higher metabolome coverage.

We globally analyzed mass isotopomer abundance variation across different experimental conditions to detect metabolic flux changes in a non-targeted manner. MIDs after stable isotope labeling are determined by metabolic fluxes. This relationship is already exploited in  $^{13}\text{C}$ -MFA, but only in a highly targeted manner. Here, we applied a global differential MID analysis to detect metabolic flux changes without considering the identity of the respective compounds. Therefore, even if such flux changes occurred in yet unknown reactions, they would pop up in this analysis, rendering compound identification dispensable at this stage of the analysis. Since for many organisms or cell types the metabolic network is not fully known, such a non-targeted and data-driven approach is highly desirable. It will not replace subsequent targeted experiments, but it can be a valuable scouting strategy to not miss unanticipated reactions or metabolites and to validate the assumptions required for example for  $^{13}\text{C}$ -MFA.

To demonstrate and validate our approach we analyzed cellular metabolism of lung cancer cells at different oxygen levels. The data-driven analysis of isotopic

enrichment correctly identified enhanced reductive carboxylation of 2-oxoglutarate to isocitrate by IDH and subsequent cleavage of citrate by ACLY to produce cytosolic acetyl-CoA which flows into increased fatty acid biosynthesis [36–38] (Figure 3). This inversion of IDH flux directionality is an important feature of cancer cells since it allows for the generation of acetyl-CoA from glutamine under hypoxia when acetyl-CoA production from glucose is strongly inhibited. The non-targeted detection of these previously reported findings validate our approach.

We argued that, because MID similarity often correlates with metabolic proximity, comparison of MIDs of different compounds can reveal metabolic similarity. Addressing a current bottleneck in non-targeted metabolomics studies, we demonstrated how the similarity in MIDs after stable isotope labeling can facilitate compound identification. Knowledge of biochemically related compounds helps to constrain database searches and it can help to elucidate unknown biosynthetic pathways by revealing potential precursors. Although MID similarity analysis will not always allow for compound identification, it can still be used to put unknown compounds into the context of certain biochemical pathways or to provide hypotheses on chemical substructures. MID similarity can, dependent on tracer and pathways, sometimes be ambiguous. However, this ambiguity can be reduced by the use of distinct tracers and multiple experimental conditions as done in this study. Analysis of MID similarity can additionally provide valuable hints on the composition of a given mass spectrometric fragment, as shown above for NAA.

A related approach to our MID similarity analysis is the recently described “metabolic turnover analysis” [47] which analyzes correlations in mass isotopomer abundances to determine metabolic distances. Whereas Nakayama *et al.* [47] analyzed time-series data from a transient labeling experiment, we compare MIDs from only one single time-point. The dynamic nature of metabolic turnover analysis has the advantage, that it can reveal the sequence of intermediates of linear pathways, an information that is lost in isotopic steady state. However, this extra information comes at the cost of a more complex experimental setup.

We demonstrated the value of our MID similarity analysis in the case of the already identified NAA and an unidentified compound, the spectrum of which was not present in any of the common reference libraries (Figure 4). This MID similarity analysis constrained the database search for the given nominal mass to only one candidate structure. This putative identification is corroborated by mass spectrometric fragmentation, isotope labeling and a gene silencing experiment.

Using stable isotope labeling and siRNA-mediated gene silencing we showed that A549 lung cancer cells produce NAA and its downstream metabolite and neuropeptide NAAG (Figure 5). NAA is highly abundant in the brain and was long thought to only be produced in neuronal tissues. Its functions are still not fully understood, but several potential roles are discussed [48, 49]. In the context of cancer, NAA has not received much attention, except for tumors of the brain where NAA concentrations are high *per se*. Increased levels of NAA were detected in ovarian tumors [50–54] and a positive correlation between urinary NAA levels and malignancy of prostate cancer cells has been observed [46]. Only during the preparation of this manuscript, two independent studies focusing on NAA and NAT8L were published [23, 55]. At the time of our study, it was not yet clear whether increased NAA levels

in cancer cells are due to endogenous biosynthesis or accumulation of exogenous NAA. Here, using  $^{13}\text{C}$ -labeling, we showed that lung adenocarcinoma cells are able to produce this metabolite via the NAT8L enzyme. Production of NAA is not limited to A549 cells; we also detected NAA in prostate (RWPE-2) and liver (HepG2) cancer cell lines and in bronchial epithelial cells (BEAS-2B) non-neoplastic hepatocytes (PH5CH8) (unpublished observations). Lou *et al.* investigated NAA levels and *NAT8L* expression levels in lung cancer in parallel and independently of our studies and their findings were published during the preparation of our manuscript [23]. Here we confirm their report on NAA production in A549 cells and show furthermore that the NAA downstream metabolite NAAG is produced and that *NAT8L* silencing inhibits cell proliferation (Figure 5). Production of NAA and a negative effect of NAT8L silencing on proliferation has also been reported by Zand *et al.* in ovarian cancer cells [55]. Furthermore, they showed a lower survival rate of cancer patients with higher NAT8L and NAA levels. These data hint towards a more integral role of NAA in cancer cells, more than a mere biomarker or byproduct, which needs to be investigated further.

Nothing is known about the mechanistic role of either NAA, NAAG or NAT8L in cancer yet. Exogenous NAA was found to increase proliferation of glioma stem-like cells [56]. Pessentheiner *et al.* reported that NAT8L plays an important role in lipid metabolism in brown adipocytes [57]. Its functional role there is yet unclear, but the authors hypothesized an *N*-acetylaspartate-based acetyl-CoA shuttle across the mitochondrial membrane, as suggested for neurons [58, 59] and similar to the intercellular acetyl-transport observed in the brain [48]. In this model, NAA is exported from the mitochondria, deacetylated by cytosolic aspartoacylase (ASPA) and the resulting acetate is activated by cytosolic acetyl-CoA synthase (ACSS2). Such a shuttling mechanism to provide cytosolic acetyl-CoA would also be advantageous for cancer cells which are known to have increased fatty acid biosynthesis. NAA-based acetyl-CoA shuttling would decouple acetyl-transport from citrate synthesis for oxidation in the citric acid cycle. Furthermore, it would explain recent findings on the importance of ACSS2 in cancer cells [60–62]. The inhibition of cell proliferation we observed here upon *NAT8L* silencing would be in line with NAA-mediated acetyl transport. Lack of NAT8L could induce a shortage of cytosolic acetyl-CoA for fatty acid biosynthesis and other metabolic processes which would eventually reduce cell proliferation. More data are required to unravel the exact mechanism by which NAT8L confers a growth advantage to these cells. This acetyl-shuttling relies on mitochondrial NAA biosynthesis. However, there is no consent about subcellular localization of NAT8L [63–68].

If NAT8L was only localized in the cytosol, NAA could still play an important role as precursor of NAAG, which we also detected in A549 cells. NAAG was reported as an agonist at type II metabotropic glutamate receptors [69, 70] which are also expressed by cancer cells [71] and have been shown to promote cell proliferation [72]. The observed reduction in cell proliferation after *NAT8L* silencing could therefore be due to reduced levels of NAAG.

An alternative product of RIMKLB, one of the NAAG-producing enzymes, is  $\beta$ -CG [45] which we putatively identified in A549 cells. Very little is known about the function of this metabolite. It was suggested to act as an iron carrier, able to

reactivate aconitase activity and increasing cell viability [73]. It is unclear whether  $\beta$ -CG plays a specific role in A549 cells, or whether it only forms as a side product of RIMKLB.

Besides any biological role, NAA is of analytical interest because of its mass spectrometric fragmentation. Under isotopic steady state conditions, it can be used to deduce labeling of the acetyl-CoA pool from which it is synthesized (Figure 3). Acetyl-CoA is a hub of many anabolic and catabolic reactions, linking fatty acid, carbohydrate and amino acids metabolism, and is a substrate for protein acetylation. Acetyl-CoA is not directly accessible via GC-MS measurements, but its isotopic enrichment can alternatively be deduced from labeling patterns of fatty acids by isotopomer spectral analysis (ISA) [74]. However, this requires additional sample processing and measurements and is further complicated by the fact that cellular fatty acids can be derived from medium components directly or by elongation or be synthesized *de novo*. When the localization of NAT8L is resolved, NAA may furthermore provide a means to analyze isotopic enrichment of a compartment-specific acetyl-CoA pool.

Analyzing isotopic enrichment of the acetyl-moiety of NAA at different oxygen levels revealed that with decreasing oxygen availability, acetyl-CoA was progressively increasingly derived from glutamine instead of glucose, whereas their combined contribution was relatively stable.

## Conclusions

We applied stable isotope labeling and illustrated a novel non-targeted mass isotopologue analysis approach to systematically analyze the metabolic hypoxia response of human lung cancer cells. We employed non-targeted mass isotopomer abundance variation analysis for non-targeted metabolic flux change profiling and showed how MID similarity can assist compound identification, addressing a major bottleneck of current metabolomics research. This approach can also account for unknown or unanticipated reactions, thus bridging the gap between non-targeted metabolomics and  $^{13}\text{C}$ -MFA. With this data-driven analysis we detected known hypoxia-induced metabolic effects, validating our approach. Furthermore, this analysis led to the discovery of a potentially important role of NAA in cancer cell metabolism, which needs to be investigated further. In summary, this non-targeted approach provided biological insights and proved to be a fruitful methodology for hypothesis generation for subsequent more targeted analyses.

### Competing interests

The authors declare that they have no competing interests.

### Author's contributions

TC performed experiments underlying figures 3 & 4, DW and XD performed experiments underlying figures 5A–D, NB and SCS performed experiments underlying figure 5E; DW and KH developed the data analysis workflow; DW implemented the data analysis workflow and performed data analysis; AW and DW designed the manuscript; DW drafted the manuscript; AW and KH critically revised the manuscript. All authors read and approved the final manuscript.

### Acknowledgements

This project was supported by the Fonds National de la Recherche (FNR) Luxembourg (ATTRACT A10/03). SCS acknowledges funding from the HICE virtual institute. We thank our collaborator Prof. Nobuyuki Kato (Okayama University) for providing the PH5CH8 cells.

### Author details

<sup>1</sup>Luxembourg Centre for Systems Biomedicine, University of Luxembourg, 6, avenue du Swing, 4367, Belvaux, Luxembourg. <sup>2</sup>Department of Bioengineering, University of California, Gilman Drive, 92037, San Diego, La Jolla, USA.

### References

1. Michelucci, A., Cordes, T., Ghelfi, J., Pailot, A., Reiling, N., Goldmann, O., Binz, T., Wegner, A., Tallam, A., Rausell, A., Buttini, M., Linster, C.L., Medina, E., Balling, R., Hiller, K.: Immune-responsive gene 1 protein links metabolism to immunity by catalyzing itaconic acid production. *Proc Natl Acad Sci U S A* **110**(19), 7820–7825 (2013). doi:[10.1073/pnas.1218599110](https://doi.org/10.1073/pnas.1218599110)
2. Mayers, J.R., Wu, C., Clish, C.B., Kraft, P., Torrence, M.E., Fiske, B.P., Yuan, C., Bao, Y., Townsend, M.K., Tworoger, S.S., Davidson, S.M., Papagiannakopoulos, T., Yang, A., Dayton, T.L., Ogino, S., Stampfer, M.J., Giovannucci, E.L., Qian, Z.R., Rubinson, D.A., Ma, J., Sesso, H.D., Gaziano, J.M., Cochrane, B.B., Liu, S., Wactawski-Wende, J., Manson, J.E., Pollak, M.N., Kimmelman, A.C., Souza, A., Pierce, K., Wang, T.J., Gerszten, R.E., Fuchs, C.S., Vander Heiden, M.G., Wolpin, B.M.: Elevation of circulating branched-chain amino acids is an early event in human pancreatic adenocarcinoma development. *Nat Med* **20**(10), 1193–1198 (2014). doi:[10.1038/nm.3686](https://doi.org/10.1038/nm.3686)
3. Wei, R.: Metabolomics and its practical value in pharmaceutical industry. *Curr Drug Metab* **12**(4), 345–358 (2011). doi:[10.2174/138920011795202947](https://doi.org/10.2174/138920011795202947)
4. Sauer, U.: Metabolic networks in motion: <sup>13</sup>C-based flux analysis. *Mol Syst Biol* **2**, 62 (2006). doi:[10.1038/msb4100109](https://doi.org/10.1038/msb4100109)
5. Wegner, A., Meiser, J., Weindl, D., Hiller, K.: How metabolites modulate metabolic flux. *Current Opinion in Biotechnology* **34**(0), 16–22 (2015). doi:[10.1016/j.copbio.2014.11.008](https://doi.org/10.1016/j.copbio.2014.11.008)
6. Thiele, I., Swainston, N., Fleming, R.M.T., Hoppe, A., Sahoo, S., Aurich, M.K., Haraldsdottir, H., Mo, M.L., Rolfsson, O., Stobbe, M.D., Thorleifsson, S.G., Agren, R., Bölling, C., Bordel, S., Chavali, A.K., Dobson, P., Dunn, W.B., Endler, L., Hala, D., Hucka, M., Hull, D., Jameson, D., Jamshidi, N., Jonsson, J.J., Juty, N., Keating, S., Nookaew, I., Le Novère, N., Malys, N., Mazein, A., Papin, J.A., Price, N.D., Selkov, E. Sr, Sigurdsson, M.I., Simeonidis, E., Sonnenschein, N., Smallbone, K., Sorokin, A., van Beek, J.H.G.M., Weichart, D., Goryanin, I., Nielsen, J., Westerhoff, H.V., Kell, D.B., Mendes, P., Palsson, B.O.: A community-driven global reconstruction of human metabolism. *Nat Biotechnol* **31**(5), 419–425 (2013). doi:[10.1038/nbt.2488](https://doi.org/10.1038/nbt.2488)
7. Orth, J.D., Thiele, I., Palsson, B.O.: What is flux balance analysis? *Nat Biotechnol* **28**(3), 245–248 (2010). doi:[10.1038/nbt.1614](https://doi.org/10.1038/nbt.1614)
8. Lewis, N.E., Nagarajan, H., Palsson, B.O.: Constraining the metabolic genotype-phenotype relationship using a phylogeny of in silico methods. *Nat Rev Microbiol* **10**(4), 291–305 (2012). doi:[10.1038/nrmicro2737](https://doi.org/10.1038/nrmicro2737)
9. Wiechert, W.: <sup>13</sup>C metabolic flux analysis. *Metab Eng* **3**(3), 195–206 (2001). doi:[10.1006/mben.2001.0187](https://doi.org/10.1006/mben.2001.0187)
10. Antoniewicz, M.R., Kelleher, J.K., Stephanopoulos, G.: Determination of confidence intervals of metabolic fluxes estimated from stable isotope measurements. *Metab Eng* **8**(4), 324–337 (2006). doi:[10.1016/j.ymben.2006.01.004](https://doi.org/10.1016/j.ymben.2006.01.004)
11. Wiechert, W., de Graaf, A.A.: Bidirectional reaction steps in metabolic networks: I. modeling and simulation of carbon isotope labeling experiments. *Biotechnol Bioeng* **55**(1), 101–117 (1997). doi:[10.1002/\(SICI\)1097-0290\(19970705\)55:1<101::AID-BIT12>3.0.CO;2-P](https://doi.org/10.1002/(SICI)1097-0290(19970705)55:1<101::AID-BIT12>3.0.CO;2-P)
12. Antoniewicz, M.R., Kelleher, J.K., Stephanopoulos, G.: Elementary metabolite units (emu): a novel framework for modeling isotopic distributions. *Metab Eng* **9**(1), 68–86 (2007). doi:[10.1016/j.ymben.2006.09.001](https://doi.org/10.1016/j.ymben.2006.09.001)
13. Hiller, K., Wegner, A., Weindl, D., Cordes, T., Metallo, C.M., Kelleher, J.K., Stephanopoulos, G.: NTFD—a stand-alone application for the non-targeted detection of stable isotope-labeled compounds in GC/MS data. *Bioinformatics* **29**(9), 1226–1228 (2013). doi:[10.1093/bioinformatics/btt119](https://doi.org/10.1093/bioinformatics/btt119)
14. Hiller, K., Metallo, C.M., Kelleher, J.K., Stephanopoulos, G.: Nontargeted elucidation of metabolic pathways using stable-isotope tracers and mass spectrometry. *Anal Chem* **82**(15), 6621–6628 (2010). doi:[10.1021/ac1011574](https://doi.org/10.1021/ac1011574)
15. Creek, D.J., Chokkathukalam, A., Jankevics, A., Burgess, K.E.V., Breitling, R., Barrett, M.P.: Stable isotope-assisted metabolomics for network-wide metabolic pathway elucidation. *Anal Chem* **84**(20), 8442–8447 (2012). doi:[10.1021/ac3018795](https://doi.org/10.1021/ac3018795)
16. Huang, X., Chen, Y.-J., Cho, K., Nikolskiy, I., Crawford, P.A., Patti, G.J.: X13CMS: global tracking of isotopic labels in untargeted metabolomics. *Anal Chem* **86**(3), 1632–1639 (2014). doi:[10.1021/ac403384n](https://doi.org/10.1021/ac403384n)
17. Chokkathukalam, A., Jankevics, A., Creek, D.J., Achcar, F., Barrett, M.P., Breitling, R.: mzMatch-ISO: an R tool for the annotation and relative quantification of isotope-labelled mass spectrometry data. *Bioinformatics* **29**(2), 281–283 (2013). doi:[10.1093/bioinformatics/bts674](https://doi.org/10.1093/bioinformatics/bts674)
18. Gaglio, D., Metallo, C.M., Gameiro, P.A., Hiller, K., Danna, L.S., Balestrieri, C., Alberghina, L., Stephanopoulos, G., Chiaradonna, F.: Oncogenic k-ras decouples glucose and glutamine metabolism to support cancer cell growth. *Mol Syst Biol* **7**, 523 (2011). doi:[10.1038/msb.2011.56](https://doi.org/10.1038/msb.2011.56)
19. Yang, S., Hoggard, J.C., Lidstrom, M.E., Synovec, R.E.: Comprehensive discovery of <sup>13</sup>C labeled metabolites in the bacterium *Methylobacterium extorquens* AM1 using gas chromatography-mass spectrometry. *J Chromatogr A* **1317**, 175–185 (2013). doi:[10.1016/j.chroma.2013.08.059](https://doi.org/10.1016/j.chroma.2013.08.059)
20. Bueschl, C., Kluger, B., Lemmens, M., Adam, G., Wiesenberger, G., Maschietto, V., Marocco, A., Strauss, J., Bödi, S., Thallinger, G., Krska, R., Schuhmacher, R.: A novel stable isotope labelling assisted workflow for improved untargeted LC–HRMS based metabolomics research. *Metabolomics*, 1–16 (2013). doi:[10.1007/s11306-013-0611-0](https://doi.org/10.1007/s11306-013-0611-0)
21. Weindl, D., Wegner, A., Jäger, C., Hiller, K.: Isotopologue ratio normalization for non-targeted metabolomics. *J Chromatogr A* **1389**, 112–119 (2015). doi:[10.1016/j.chroma.2015.02.025](https://doi.org/10.1016/j.chroma.2015.02.025)
22. Chokkathukalam, A., Kim, D.-H., Barrett, M.P., Breitling, R., Creek, D.J.: Stable isotope-labeling studies in metabolomics: new insights into structure and dynamics of metabolic networks. *Bioanalysis* **6**(4), 511–524 (2014). doi:[10.4155/bio.13.348](https://doi.org/10.4155/bio.13.348)

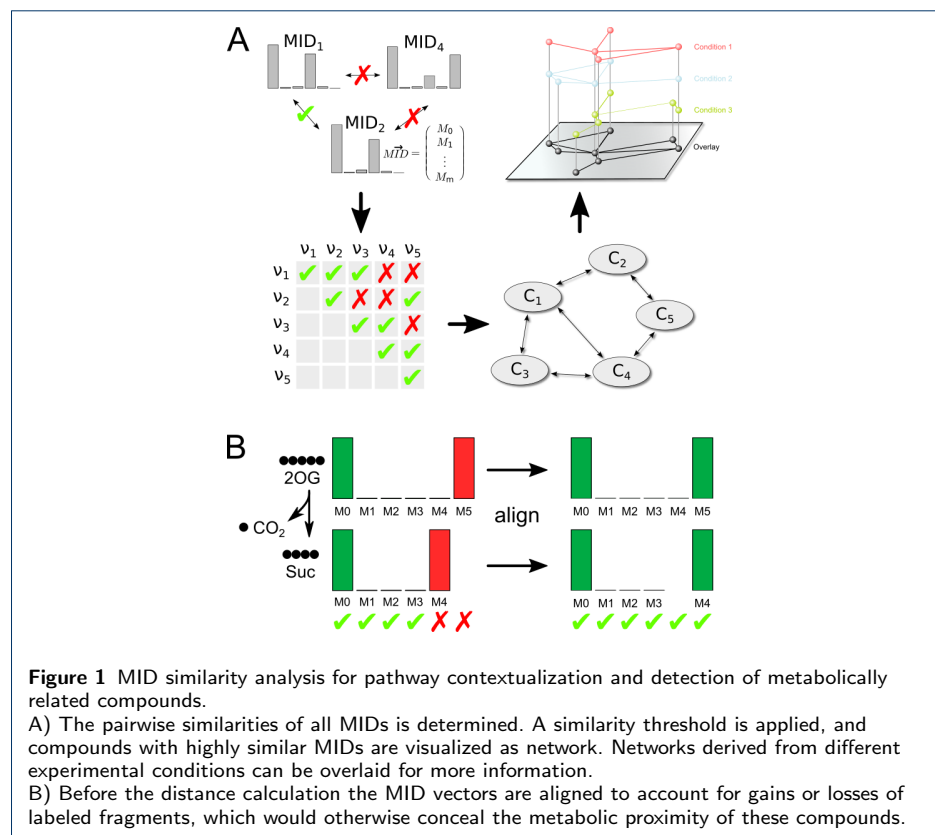
23. Lou, T.-F., Sethuraman, D., Dospoy, P., Srivastva, P., Kim, H.S., Kim, J., Ma, X., Chen, P.-H., Huffman, K.E., Frink, R.E., Larsen, J.E., Lewis, C.M., Um, S.-W., Kim, D.-H., Ahn, J.-M., DeBerardinis, R.J., White, M., Minna, J.D., Yoo, H.: Cancer-specific production of *N*-acetylaspartate via NAT8L overexpression in non-small cell lung cancer and its potential as a circulating biomarker. *Cancer Prevention Research* (2015). doi:[10.1158/1940-6207.CAPR-14-0287](https://doi.org/10.1158/1940-6207.CAPR-14-0287)
24. Giard, D.J., Aaronson, S.A., Todaro, G.J., Arnstein, P., Kersey, J.H., Dosik, H., Parks, W.P.: In vitro cultivation of human tumors: establishment of cell lines derived from a series of solid tumors. *J Natl Cancer Inst* **51**(5), 1417–1423 (1973). doi:[10.1093/jnci/51.5.1417](https://doi.org/10.1093/jnci/51.5.1417)
25. Sapcariu, S.C., Kanashova, T., Weindl, D., Ghelfi, J., Dittmar, G., Hiller, K.: Simultaneous extraction of proteins and metabolites from cells in culture. *MethodsX* **1**(0), 74–80 (2014). doi:[10.1016/j.mex.2014.07.002](https://doi.org/10.1016/j.mex.2014.07.002)
26. Hiller, K., Hangebrauk, J., Jäger, C., Spura, J., Schreiber, K., Schomburg, D.: MetaboliteDetector: comprehensive analysis tool for targeted and nontargeted GC/MS based metabolome analysis. *Anal Chem* **81**(9), 3429–3439 (2009). doi:[10.1021/ac802689c](https://doi.org/10.1021/ac802689c)
27. Weindl, D., Wegner, A., Hiller, K.: Non-targeted tracer fate detection. In: Metallo, C.M. (ed.) *Metabolic Analysis Using Stable Isotopes. Methods in Enzymology*, vol. 561, pp. 277–302. Academic Press, Waltham, MA (2015). doi:[10.1016/bs.mie.2015.04.003](https://doi.org/10.1016/bs.mie.2015.04.003)
28. Ikeda, M., Sugiyama, K., Mizutani, T., Tanaka, T., Tanaka, K., Sekihara, H., Shimotohno, K., Kato, N.: Human hepatocyte clonal cell lines that support persistent replication of hepatitis c virus. *Virus Res* **56**(2), 157–167 (1998)
29. Weindl, D., Wegner, A., Hiller, K.: Metabolome-wide analysis of stable isotope labeling - is it worth the effort? *Frontiers in Physiology* **6**(344) (2015). doi:[10.3389/fphys.2015.00344](https://doi.org/10.3389/fphys.2015.00344)
30. Wegner, A., Sapcariu, S.C., Weindl, D., Hiller, K.: Isotope cluster based compound matching in gas chromatography/mass spectrometry for non-targeted metabolomics. *Anal Chem* (2013). doi:[10.1021/ac303774z](https://doi.org/10.1021/ac303774z)
31. Zhou, R., Tseng, C.-L., Huan, T., Li, L.: IsoMS: automated processing of LC-MS data generated by a chemical isotope labeling metabolomics platform. *Anal Chem* **86**(10), 4675–4679 (2014). doi:[10.1021/ac5009089](https://doi.org/10.1021/ac5009089)
32. Bouatra, S., Aziat, F., Mandal, R., Guo, A.C., Wilson, M.R., Knox, C., Bjorn Dahl, T.C., Krishnamurthy, R., Saleem, F., Liu, P., Dame, Z.T., Poelzer, J., Huynh, J., Yallou, F.S., Psychogios, N., Dong, E., Bogumil, R., Roehring, C., Wishart, D.S.: The human urine metabolome. *PLoS One* **8**(9), 73076 (2013). doi:[10.1371/journal.pone.0073076](https://doi.org/10.1371/journal.pone.0073076)
33. Sévin, D.C., Kuehne, A., Zamboni, N., Sauer, U.: Biological insights through nontargeted metabolomics. *Current Opinion in Biotechnology* **34**(0), 1–8 (2015). doi:[10.1016/j.copbio.2014.10.001](https://doi.org/10.1016/j.copbio.2014.10.001). *Systems Biology • Nanobiotechnology*
34. Needleman, S.B., Wunsch, C.D.: A general method applicable to the search for similarities in the amino acid sequence of two proteins. *J Mol Biol* **48**(3), 443–453 (1970). doi:[10.1016/0022-2836\(70\)90057-4](https://doi.org/10.1016/0022-2836(70)90057-4)
35. Masson, N., Ratcliffe, P.J.: Hypoxia signaling pathways in cancer metabolism: the importance of co-selecting interconnected physiological pathways. *Cancer Metab* **2**(1), 3 (2014). doi:[10.1186/2049-3002-2-3](https://doi.org/10.1186/2049-3002-2-3)
36. Metallo, C.M., Gameiro, P.A., Bell, E.L., Mattaini, K.R., Yang, J., Hiller, K., Jewell, C.M., Johnson, Z.R., Irvine, D.J., Guarente, L., Kelleher, J.K., Heiden, M.G.V., Iliopoulos, O., Stephanopoulos, G.: Reductive glutamine metabolism by IDH1 mediates lipogenesis under hypoxia. *Nature* **481**(7381), 380–384 (2012). doi:[10.1038/nature10602](https://doi.org/10.1038/nature10602)
37. Wise, D.R., Ward, P.S., Shay, J.E.S., Cross, J.R., Gruber, J.J., Sachdeva, U.M., Platt, J.M., DeMatteo, R.G., Simon, M.C., Thompson, C.B.: Hypoxia promotes isocitrate dehydrogenase-dependent carboxylation of  $\alpha$ -ketoglutarate to citrate to support cell growth and viability. *Proc Natl Acad Sci U S A* **108**(49), 19611–19616 (2011). doi:[10.1073/pnas.111773108](https://doi.org/10.1073/pnas.111773108)
38. Zaidi, N., Lupien, L., Kuemmerle, N.B., Kinlaw, W.B., Swinnen, J.V., Smans, K.: Lipogenesis and lipolysis: the pathways exploited by the cancer cells to acquire fatty acids. *Prog Lipid Res* **52**(4), 585–589 (2013). doi:[10.1016/j.plipres.2013.08.005](https://doi.org/10.1016/j.plipres.2013.08.005)
39. Fendt, S.-M., Bell, E.L., Keibler, M.A., Olenchock, B.A., Mayers, J.R., Wasylenko, T.M., Vokes, N.I., Guarente, L., Vander Heiden, M.G., Stephanopoulos, G.: Reductive glutamine metabolism is a function of the  $\alpha$ -ketoglutarate to citrate ratio in cells. *Nat Commun* **4**, 2236 (2013). doi:[10.1038/ncomms3236](https://doi.org/10.1038/ncomms3236)
40. Kim, J.-w., Tchernyshyov, I., Semenza, G.L., Dang, C.V.: Hif-1-mediated expression of pyruvate dehydrogenase kinase: a metabolic switch required for cellular adaptation to hypoxia. *Cell Metab* **3**(3), 177–185 (2006). doi:[10.1016/j.cmet.2006.02.002](https://doi.org/10.1016/j.cmet.2006.02.002)
41. Gehrke, C.W., Desgres, J.A., Keith, G., Gerhardt, K.O., Agris, P.F., Sierzputowska-Gracz, H., Tempesta, M.S., Kuo, K.C.: Chapter 5 structural elucidation of nucleosides in nucleic acids. In: Gehrke, C.W., Kuo, K.C.T. (eds.) *Chromatography and Modification of Nucleosides — Analytical Methods for Major and Modified Nucleosides: HPLC, GC, MS, NMR, UV and FT-IR. Journal of Chromatography Library*, vol. 45, Part A, pp. 159–223. Elsevier, Amsterdam, NL (1990). doi:[10.1016/S0301-4770\(08\)61471-2](https://doi.org/10.1016/S0301-4770(08)61471-2). <http://www.sciencedirect.com/science/article/pii/S0301477008614712>
42. Wegner, A., Weindl, D., Jäger, C., Sapcariu, S.C., Dong, X., Stephanopoulos, G., Hiller, K.: Fragment formula calculator (FFC): Determination of chemical formulas for fragment ions in mass spectrometric data. *Anal Chem* **86**(4), 2221–2228 (2014). doi:[10.1021/ac403879d](https://doi.org/10.1021/ac403879d)
43. Wishart, D.S., Jewison, T., Guo, A.C., Wilson, M., Knox, C., Liu, Y., Djoumbou, Y., Mandal, R., Aziat, F., Dong, E., Bouatra, S., Sinelnikov, I., Arndt, D., Xia, J., Liu, P., Yallou, F., Bjorn Dahl, T., Perez-Pineiro, R., Eisner, R., Allen, F., Neveu, V., Greiner, R., Scalbert, A.: Hmdb 3.0—the human metabolome database in 2013. *Nucleic Acids Res* **41**(Database issue), 801–807 (2013). doi:[10.1093/nar/gks1065](https://doi.org/10.1093/nar/gks1065)
44. Wiame, E., Tyteca, D., Pierrrot, N., Collard, F., Amyere, M., Noel, G., Desmedt, J., Nassogne, M.-C., Vikkula, M., Octave, J.-N., Vincent, M.-F., Courtoy, P.J., Boltshauser, E., van Schaftingen, E.: Molecular identification of aspartate *n*-acetyltransferase and its mutation in hypoacetylaspartia. *Biochem J* **425**(1), 127–136 (2010). doi:[10.1042/BJ20091024](https://doi.org/10.1042/BJ20091024)
45. Collard, F., Stroobant, V., Lamosa, P., Kapanda, C.N., Lambert, D.M., Muccioli, G.G., Poupaert, J.H.,



- Oppendoes, F., Van Schaftingen, E.: Molecular identification of *N*-acetylasparylglutamate synthase and beta-citrylglutamate synthase. *J Biol Chem* **285**(39), 29826–29833 (2010). doi:[10.1074/jbc.M110.152629](https://doi.org/10.1074/jbc.M110.152629)
46. Sreekumar, A., Poisson, L.M., Rajendiran, T.M., Khan, A.P., Cao, Q., Yu, J., Laxman, B., Mehra, R., Lonigro, R.J., Li, Y., Nyati, M.K., Ahsan, A., Kalyana-Sundaram, S., Han, B., Cao, X., Byun, J., Omenn, G.S., Ghosh, D., Pennathur, S., Alexander, D.C., Berger, A., Shuster, J.R., Wei, J.T., Varambally, S., Beecher, C., Chinnaiyan, A.M.: Metabolomic profiles delineate potential role for sarcosine in prostate cancer progression. *Nature* **457**(7231), 910–914 (2009). doi:[10.1038/nature07762](https://doi.org/10.1038/nature07762)
  47. Nakayama, Y., Putri, S.P., Bamba, T., Fukusaki, E.: Metabolic distance estimation based on principle component analysis of metabolic turnover. *J Biosci Bioeng* (2014). doi:[10.1016/j.jbiosc.2014.02.014](https://doi.org/10.1016/j.jbiosc.2014.02.014)
  48. Moffett, J.R., Ross, B., Arun, P., Madhavarao, C.N., Namboodiri, A.M.A.: *N*-acetylasparylglutamate in the CNS: from neurodiagnostics to neurobiology. *Prog Neurobiol* **81**(2), 89–131 (2007). doi:[10.1016/j.pneurobio.2006.12.003](https://doi.org/10.1016/j.pneurobio.2006.12.003)
  49. Moffett, J.R., Arun, P., Ariyannur, P.S., Namboodiri, A.M.: *N*-acetylasparylglutamate reductions in brain injury: impact on post-injury neuroenergetics, lipid synthesis and protein acetylation. *Frontiers in Neuroenergetics* **5**(11) (2013). doi:[10.3389/fnene.2013.00011](https://doi.org/10.3389/fnene.2013.00011)
  50. Kolwijck, E., Wevers, R.A., Engelke, U.F., Woudenberg, J., Bulten, J., Blom, H.J., Massuger, L.F.A.G.: Ovarian cyst fluid of serous ovarian tumors contains large quantities of the brain amino acid *N*-acetylasparylglutamate. *PLoS One* **5**(4), 10293 (2010). doi:[10.1371/journal.pone.0010293](https://doi.org/10.1371/journal.pone.0010293)
  51. Hascalik, S., Celik, O., Sarac, K., Alkan, A., Mizrak, B.: Clinical significance of *N*-acetyl-L-aspartate resonance in ovarian mucinous cystadenoma. *Int J Gynecol Cancer* **16**(1), 423–426 (2006). doi:[10.1111/j.1525-1438.2006.00200.x](https://doi.org/10.1111/j.1525-1438.2006.00200.x)
  52. Boss, E.A., Moolenaar, S.H., Massuger, L.F., Boonstra, H., Engelke, U.F., de Jong, J.G., Wevers, R.A.: High-resolution proton nuclear magnetic resonance spectroscopy of ovarian cyst fluid. *NMR Biomed* **13**(5), 297–305 (2000)
  53. Fong, M.Y., McDunn, J., Kakar, S.S.: Identification of metabolites in the normal ovary and their transformation in primary and metastatic ovarian cancer. *PLoS One* **6**(5), 19963 (2011). doi:[10.1371/journal.pone.0019963](https://doi.org/10.1371/journal.pone.0019963)
  54. Ben Sellem, D., Elbayed, K., Neuville, A., Moussallieh, F.-M., Lang-Averous, G., Piotto, M., Bellocq, J.-P., Namer, I.J.: Metabolomic characterization of ovarian epithelial carcinomas by hrmas-nmr spectroscopy. *J Oncol* **2011**, 174019 (2011). doi:[10.1155/2011/174019](https://doi.org/10.1155/2011/174019)
  55. Zand, B., Previs, R.A., Zacharias, N.M., Rupaimoole, R., Mitamura, T., Nagaraja, A.S., Guindani, M., Dalton, H.J., Yang, L., Baddour, J., Achreja, A., Hu, W., Pecot, C.V., Ivan, C., Wu, S.Y., McCullough, C.R., Gharpure, K.M., Shoshan, E., Pradeep, S., Mangala, L.S., Rodriguez-Aguayo, C., Wang, Y., Nick, A.M., Davies, M.A., Armaiz-Pena, G., Liu, J., Lutgendorf, S.K., Baggerly, K.A., Eli, M.B., Lopez-Berestein, G., Nagrath, D., Bhattacharya, P.K., Sood, A.K.: Role of increased *n*-acetylasparylglutamate levels in cancer. *J Natl Cancer Inst* **108**(6) (2016). doi:[10.1093/jnci/djv426](https://doi.org/10.1093/jnci/djv426)
  56. Long, P.M., Moffett, J.R., Namboodiri, A.M.A., Viapiano, M.S., Lawler, S.E., Jaworski, D.M.: *N*-acetylasparylglutamate (NAA) and *N*-acetylasparylglutamate (NAAG) promote growth and inhibit differentiation of glioma stem-like cells. *J Biol Chem* **288**(36), 26188–26200 (2013). doi:[10.1074/jbc.M113.487553](https://doi.org/10.1074/jbc.M113.487553)
  57. Pessentheiner, A.R., Pelzmann, H.J., Walenta, E., Schweiger, M., Groschner, L.N., Graier, W.F., Kolb, D., Uno, K., Miyazaki, T., Nitta, A., Rieder, D., Prokesch, A., Bogner-Strauss, J.G.: NAT8L (*N*-acetyltransferase 8-like) accelerates lipid turnover and increases energy expenditure in brown adipocytes. *J Biol Chem* **288**(50), 36040–36051 (2013). doi:[10.1074/jbc.M113.491324](https://doi.org/10.1074/jbc.M113.491324)
  58. D'Adamo, J. A.F., Gidez, L.I., Yatsu, F.M.: Acetyl transport mechanisms. involvement of *N*-acetyl aspartic acid in de novo fatty acid biosynthesis in the developing rat brain. *Experimental Brain Research* **5**(4), 267–273 (1968). doi:[10.1007/BF00235902](https://doi.org/10.1007/BF00235902)
  59. Patel, T.B., Clark, J.B.: Lipogenesis in the brain of suckling rats. studies on the mechanism of mitochondrial-cytosolic carbon transfer. *Biochem J* **188**(1), 163–168 (1980)
  60. Mashimo, T., Pichumani, K., Vemireddy, V., Hatanpaa, K.J., Singh, D.K., Sirasanagandla, S., Nannepaga, S., Piccirillo, S.G., Kovacs, Z., Foong, C., Huang, Z., Barnett, S., Mickey, B.E., DeBerardinis, R.J., Tu, B.P., Maher, E.A., Bachoo, R.M.: Acetate is a bioenergetic substrate for human glioblastoma and brain metastases. *Cell* **159**(7), 1603–1614 (2014). doi:[10.1016/j.cell.2014.11.025](https://doi.org/10.1016/j.cell.2014.11.025)
  61. Kamphorst, J., Chung, M., Fan, J., Rabinowitz, J.: Quantitative analysis of acetyl-CoA production in hypoxic cancer cells reveals substantial contribution from acetate. *Cancer & Metabolism* **2**(1), 23 (2014). doi:[10.1186/2049-3002-2-23](https://doi.org/10.1186/2049-3002-2-23)
  62. Schug, Z.T., Peck, B., Jones, D.T., Zhang, Q., Grosskurth, S., Alam, I.S., Goodwin, L.M., Smethurst, E., Mason, S., Blyth, K., McGarry, L., James, D., Shanks, E., Kalna, G., Saunders, R.E., Jiang, M., Howell, M., Lassailly, F., Thin, M.Z., Spencer-Dene, B., Stamp, G., van den Broek, N.J.F., Mackay, G., Bulusu, V., Kamphorst, J.J., Tardito, S., Strachan, D., Harris, A.L., Aboagye, E.O., Critchlow, S.E., Wakelam, M.J.O., Schulze, A., Gottlieb, E.: Acetyl-coa synthetase 2 promotes acetate utilization and maintains cancer cell growth under metabolic stress. *Cancer Cell* **27**(1), 57–71 (2015). doi:[10.1016/j.ccell.2014.12.002](https://doi.org/10.1016/j.ccell.2014.12.002)
  63. Arun, P., Moffett, J.R., Namboodiri, A.M.A.: Evidence for mitochondrial and cytoplasmic *N*-acetylasparylglutamate synthesis in SH-SY5Y neuroblastoma cells. *Neurochem Int* **55**(4), 219–225 (2009). doi:[10.1016/j.neuint.2009.03.003](https://doi.org/10.1016/j.neuint.2009.03.003)
  64. Ariyannur, P.S., Madhavarao, C.N., Namboodiri, A.M.A.: *N*-acetylasparylglutamate synthesis in the brain: mitochondria vs. microsomes. *Brain Res* **1227**, 34–41 (2008). doi:[10.1016/j.brainres.2008.06.040](https://doi.org/10.1016/j.brainres.2008.06.040)
  65. Ariyannur, P.S., Moffett, J.R., Manickam, P., Pattabiraman, N., Arun, P., Nitta, A., Nabeshima, T., Madhavarao, C.N., Namboodiri, A.M.A.: Methamphetamine-induced neuronal protein NAT8L is the NAA biosynthetic enzyme: implications for specialized acetyl coenzyme A metabolism in the CNS. *Brain Res* **1335**, 1–13 (2010). doi:[10.1016/j.brainres.2010.04.008](https://doi.org/10.1016/j.brainres.2010.04.008)
  66. Tahay, G., Wiame, E., Tyteca, D., Courtoy, P.J., Van Schaftingen, E.: Determinants of the enzymatic activity and the subcellular localization of aspartate *N*-acetyltransferase. *Biochem J* **441**(1), 105–112 (2012). doi:[10.1042/BJ20111179](https://doi.org/10.1042/BJ20111179)
  67. Toriumi, K., Ikami, M., Kondo, M., Mouri, A., Koseki, T., Ibi, D., Furukawa-Hibi, Y., Nagai, T., Mamiya, T.,

- Nitta, A., Yamada, K., Nabeshima, T.: SHAT1/NAT8L regulates neurite outgrowth via microtubule stabilization. *J Neurosci Res* **91**(12), 1525–1532 (2013). doi:10.1002/jnr.23273
68. Madhavarao, C.N., Chinopoulos, C., Chandrasekaran, K., Namboodiri, M.A.A.: Characterization of the *N*-acetylaspartate biosynthetic enzyme from rat brain. *J Neurochem* **86**(4), 824–835 (2003)
69. Wroblewska, B., Wroblewski, J.T., Pshenichkin, S., Surin, A., Sullivan, S.E., Neale, J.H.: *N*-acetylaspartylglutamate selectively activates mglur3 receptors in transfected cells. *J Neurochem* **69**(1), 174–181 (1997)
70. Neale, J.H.: *N*-acetylaspartylglutamate is an agonist at mglur<sub>3</sub> in vivo and in vitro. *J Neurochem* **119**(5), 891–895 (2011). doi:10.1111/j.1471-4159.2011.07380.x
71. Stepulak, A., Luksch, H., Gebhardt, C., Uckermann, O., Marzahn, J., Siffringer, M., Rzeski, W., Staufner, C., Brocke, K.S., Turski, L., Ikonomidou, C.: Expression of glutamate receptor subunits in human cancers. *Histochem Cell Biol* **132**(4), 435–445 (2009). doi:10.1007/s00418-009-0613-1
72. Guo, J., Zhou, X., Chen, Y., Bai, M., Yang, X., Zhao, K., Hao, W., Wei, W., Zhang, Y.: mglur3 promotes proliferation of human embryonic cortical neural progenitor cells by activating erk1/2 and jnk2 signaling pathway in vitro. *Cell Mol Biol (Noisy-le-grand)* **60**(2), 42–49 (2014)
73. Hamada-Kanazawa, M., Narahara, M., Takano, M., Min, K.S., Tanaka, K., Miyake, M.:  $\beta$ -citryl-l-glutamate acts as an iron carrier to activate aconitase activity. *Biol Pharm Bull* **34**(9), 1455–1464 (2011)
74. Kharroubi, A.T., Masterson, T.M., Aldaghas, T.A., Kennedy, K.A., Kelleher, J.K.: Isotopomer spectral analysis of triglyceride fatty acid synthesis in 3T3-L1 cells. *Am J Physiol* **263**(4 Pt 1), 667–675 (1992)

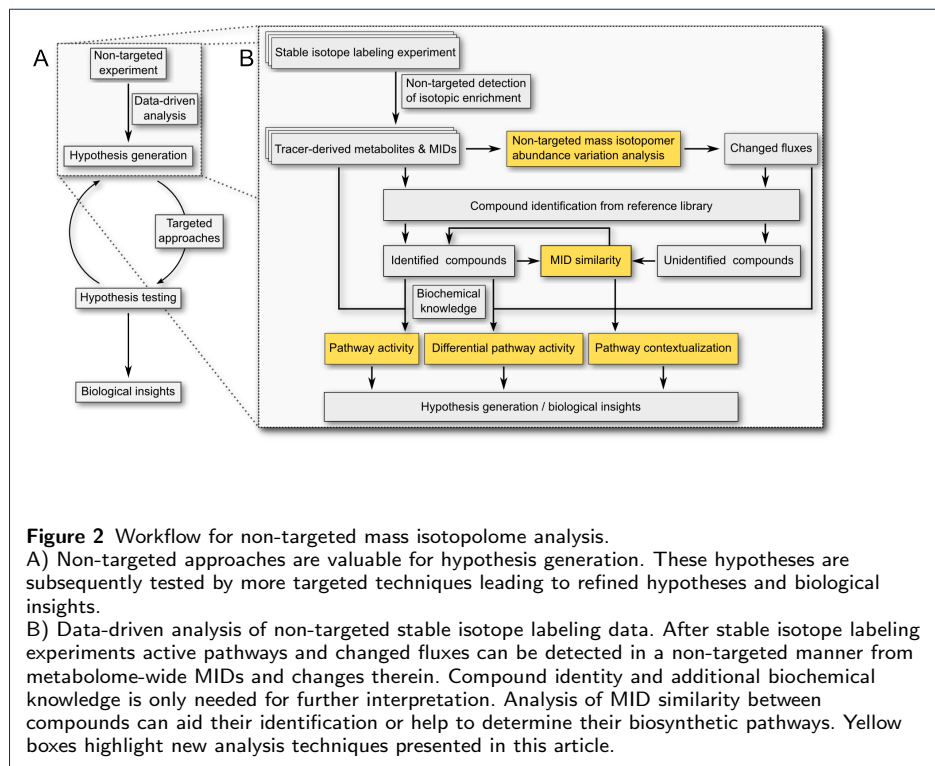
## Figures



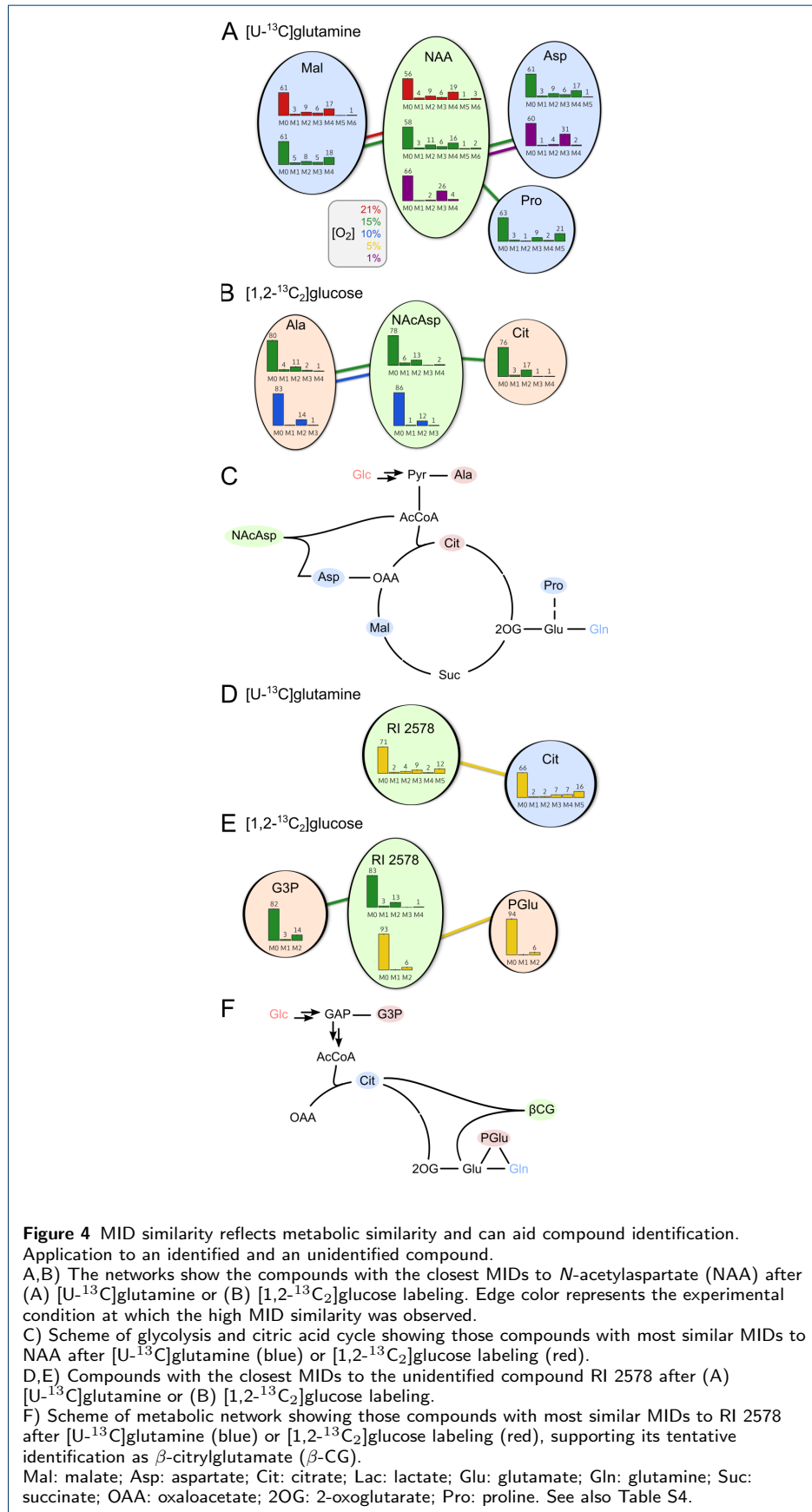
## Additional Files

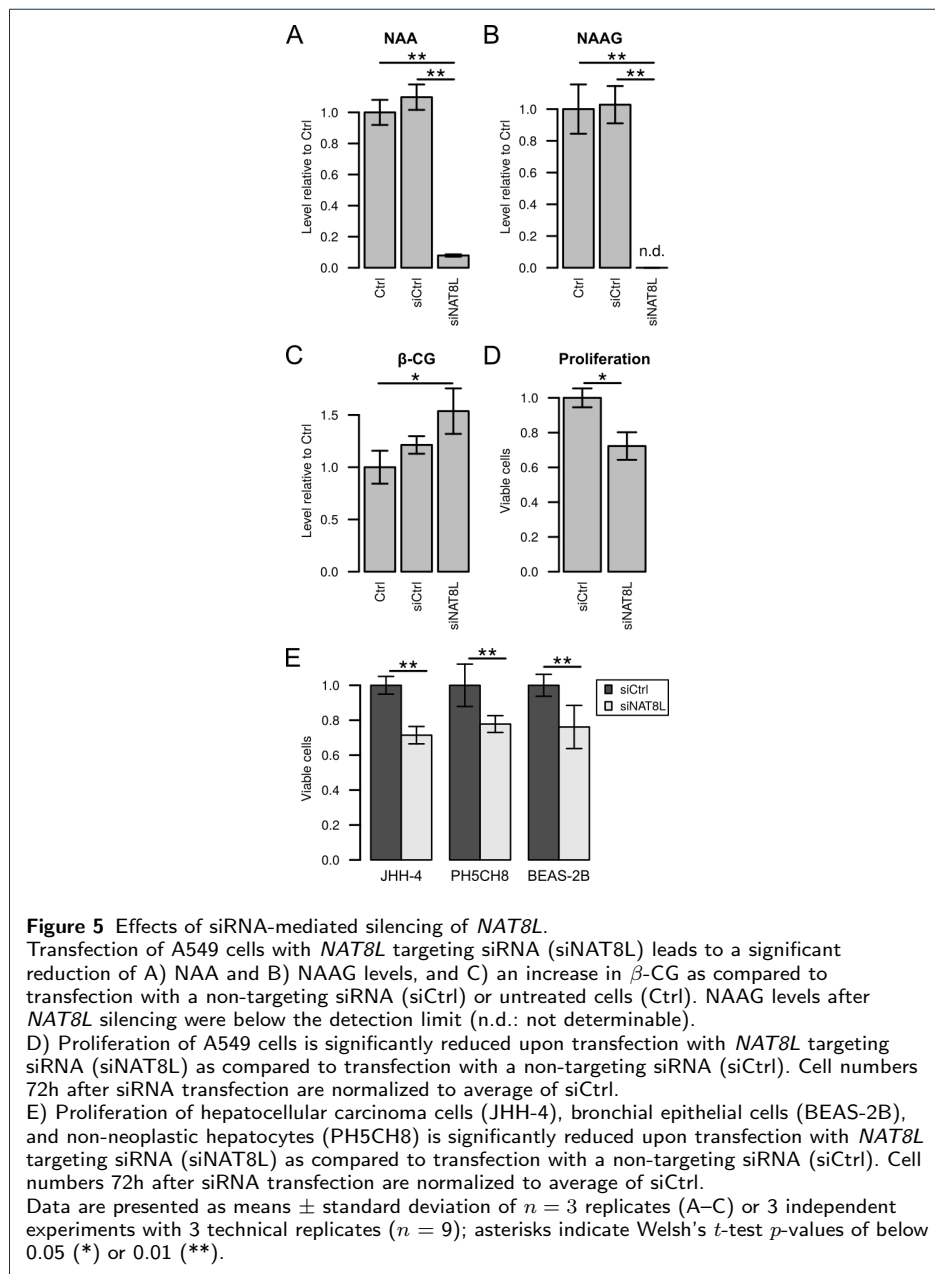
Additional file 1 — Supplemental information

List of isotopically enriched compounds and their mass isotopomer distributions; selected mass spectra.









# Bibliography

- Aggarwal, B. B., A. B. Kunnumakkara, K. B. Harikumar, S. R. Gupta, S. T. Tharakan, C. Koca, S. Dey, and B. Sung (2009). Signal transducer and activator of transcription-3, inflammation, and cancer: How intimate is the relationship? *Annals of the New York Academy of Sciences* 1171, 59–76.
- Aguilar, E., I. Marin de Mas, E. Zodda, S. Marin, F. Morrish, V. Selivanov, Ó. Meca-Cortés, H. Delowar, M. Pons, I. Izquierdo, T. Celià-Terrassa, P. de Atauri, J. J. Centelles, D. Hockenbery, T. M. Thomson, and M. Cascante (2016). Metabolic Reprogramming and Dependencies Associated with Epithelial Cancer Stem Cells Independent of the Epithelial-Mesenchymal Transition Program. *Stem cells (Dayton, Ohio)* 34(5), 1163–76.
- Allen, J. W., S. R. Khetani, R. S. Johnson, and S. N. Bhatia (2006). In vitro liver tissue model established from transgenic mice: role of HIF-1alpha on hypoxic gene expression. *Tissue engineering* 12(11), 3135–3147.
- Altenberg, B. and K. O. Greulich (2004). Genes of glycolysis are ubiquitously overexpressed in 24 cancer classes. *Genomics* 84(6), 1014–1020.
- Anastasiou, D., G. Poulogiannis, J. M. Asara, M. B. Boxer, J.-k. Jiang, M. Shen, G. Bellinger, A. T. Sasaki, J. W. Locasale, D. S. Auld, C. J. Thomas, M. G. Vander Heiden, and L. C. Cantley (2011). Inhibition of pyruvate kinase M2 by reactive oxygen species contributes to cellular antioxidant responses. *Science (New York, N.Y.)* 334(6060), 1278–83.
- Ando, M., I. Uehara, K. Kogure, Y. Asano, W. Nakajima, Y. Abe, K. Kawauchi, and N. Tanaka (2010). Interleukin 6 enhances glycolysis through expression of the glycolytic enzymes hexokinase 2 and 6-phosphofructo-2-kinase/fructose-2,6-bisphosphatase-3. *Journal of Nihon Medical School* 77(2), 97–105.
- Appelhoff, R. J., Y.-M. Tian, R. R. Raval, H. Turley, A. L. Harris, C. W. Pugh, P. J. Ratcliffe, and J. M. Gleadle (2004). Differential function of the prolyl hydroxylases PHD1, PHD2, and PHD3 in the regulation of hypoxia-inducible factor. *The Journal of biological chemistry* 279(37), 38458–65.

- Aravalli, R. N., C. J. Steer, and E. N. K. Cressman (2008). Molecular mechanisms of hepatocellular carcinoma. *Hepatology* 48(6), 2047–2063.
- Arita, K., A. P. South, G. Hans-Filho, T. H. Sakuma, J. Lai-Cheong, S. Clements, M. Odashiro, D. N. Odashiro, G. Hans-Neto, N. R. Hans, M. V. Holder, B. S. Bhogal, S. T. Hartshorne, M. Akiyama, H. Shimizu, and J. A. McGrath (2008). Oncostatin M Receptor- $\beta$  mutations underlie familial primary localized cutaneous amyloidosis. *American Journal of Human Genetics* 82(1), 73–80.
- Arredondo, J., A. I. Chernyavsky, D. L. Jolkovsky, K. E. Pinkerton, and S. a. Grando (2006). Receptor-mediated tobacco toxicity: cooperation of the Ras/Raf-1/MEK1/ERK and JAK-2/STAT-3 pathways downstream of alpha7 nicotinic receptor in oral keratinocytes. *The FASEB journal : official publication of the Federation of American Societies for Experimental Biology* 20(12), 2093–2101.
- Astuti, D., F. Latif, A. Dallol, P. L. Dahia, F. Douglas, E. George, F. Sköldbberg, E. S. Husebye, C. Eng, and E. R. Maher (2001). Gene mutations in the succinate dehydrogenase subunit SDHB cause susceptibility to familial pheochromocytoma and to familial paraganglioma. *American journal of human genetics* 69(1), 49–54.
- Atkin, B. M., M. F. Utter, and M. B. Weinberg (1979). Pyruvate carboxylase and phosphoenolpyruvate carboxykinase activity in leukocytes and fibroblasts from a patient with pyruvate carboxylase deficiency. *Pediatric research* 13(1), 38–43.
- Balkwill, F. and A. Mantovani (2001). Inflammation and cancer: Back to Virchow? *Lancet* 357(9255), 539–545.
- Battello, N., A. D. Zimmer, C. Goebel, X. Dong, I. Behrmann, C. Haan, K. Hiller, and A. Wegner (2016). The role of HIF-1 in oncostatin M-dependent metabolic reprogramming of hepatic cells. *Cancer & Metabolism* 4(1), 3.
- Bauer, D. E., G. Hatzivassiliou, F. Zhao, C. Andreadis, and C. B. Thompson (2005). ATP citrate lyase is an important component of cell growth and transformation. *Oncogene* 24(41), 6314–6322.
- Baysal, B. E. (2000). Mutations in SDHD, a Mitochondrial Complex II Gene, in Hereditary Paraganglioma. *Science* 287(5454), 848–851.
- Bo Wang, Shuhao Hsu, Wendy Frankel, K. G. and S. T. Jacob (2013). Stat3-mediated activation of miR-23a suppresses gluconeogenesis in hepatocellular carcinoma by downregulating G6PC and PGC-1 $\alpha$ . *Hepatology* 56(1), 186–197.
- Bollrath, J., T. J. Phesse, V. A. von Burstin, T. Putoczki, M. Bennecke, T. Bateman, T. Nebelsiek, T. Lundgren-May, Ö. Canli, S. Schwitalla, V. Matthews, R. M. Schmid,



- T. Kirchner, M. C. Arkan, M. Ernst, and F. R. Greten (2009). gp130-Mediated Stat3 Activation in Enterocytes Regulates Cell Survival and Cell-Cycle Progression during Colitis-Associated Tumorigenesis. *Cancer Cell* 15(2), 91–102.
- Bowker-Kinley, M. M., W. I. Davis, P. Wu, R. A. Harris, and K. M. Popov (1998). Evidence for existence of tissue-specific regulation of the mammalian pyruvate dehydrogenase complex. *The Biochemical journal* 329(1), 191–6.
- Brahimi-Horn, M. C. and J. Pouyssegur (2004). The hypoxia-inducible factor and tumor progression along the angiogenic pathway. *International Review of Cytology* 242, 157–213.
- Brand, A., J. Engelmann, and D. Leibfritz (1992). A <sup>13</sup>C NMR study on fluxes into the TCA cycle of neuronal and glial tumor cell lines and primary cells. *Biochimie* 74(9-10), 941–948.
- Bronte-Tinkew, D. M., M. Terebiznik, A. Franco, M. Ang, D. Ahn, H. Mimuro, C. Sasakawa, M. J. Ropeleski, R. M. Peek, and N. L. Jones (2009). Helicobacter pylori cytotoxin-associated gene a activates the signal transducer and activator of transcription 3 pathway in vitro and in vivo. *Cancer Research* 69(2), 632–639.
- Bruick, R. K. and S. L. Mcknight (2001). R EPORTS A Conserved Family of Prolyl-4-Hydroxylases That Modify HIF. *Science (New York, N.Y.)* 294(November), 1337–1340.
- Brunelle, J. K., E. L. Bell, N. M. Quesada, K. Vercauteren, V. Tiranti, M. Zeviani, R. C. Scarpulla, and N. S. Chandel (2005). Oxygen sensing requires mitochondrial ROS but not oxidative phosphorylation. *Cell Metabolism* 1(6), 409–414.
- Buescher, J. M., M. R. Antoniewicz, L. G. Boros, S. C. Burgess, H. Brunengraber, C. B. Clish, R. J. DeBerardinis, O. Feron, C. Frezza, B. Ghesquiere, E. Gottlieb, K. Hiller, R. G. Jones, J. J. Kamphorst, R. G. Kibbey, A. C. Kimmelman, J. W. Locasale, S. Y. Lunt, O. D. K. Maddocks, C. Malloy, C. M. Metallo, E. J. Meuillet, J. Munger, K. Nöh, J. D. Rabinowitz, M. Ralser, U. Sauer, G. Stephanopoulos, J. St-Pierre, D. A. Tennant, C. Wittmann, M. G. Vander Heiden, A. Vazquez, K. Vousden, J. D. Young, N. Zamboni, and S.-M. Fendt (2015). A roadmap for interpreting (<sup>13</sup>C) metabolite labeling patterns from cells. *Current opinion in biotechnology* 34(34), 189–201.
- Calvisi, D. F., S. Ladu, A. Gorden, M. Farina, E. A. Conner, J. S. Lee, V. M. Factor, and S. S. Thorgeirsson (2006). Ubiquitous Activation of Ras and Jak/Stat Pathways in Human HCC. *Gastroenterology* 130(4), 1117–1128.
- Carow, B. and M. E. Rottenberg (2014). SOCS3, a major regulator of infection and inflammation. *Frontiers in Immunology* 5(FEB), 1–13.

- Catlett-Falcone, R., T. H. Landowski, M. M. Oshiro, J. Turkson, A. Levitzki, R. Savino, G. Ciliberto, L. Moscinski, J. L. Fernández-Luna, G. Nuñez, W. S. Dalton, and R. Jove (1999). Constitutive activation of Stat3 signaling confers resistance to apoptosis in human U266 myeloma cells. *Immunity* 10(1), 105–115.
- Chan, K. S., S. Sano, K. Kiguchi, J. Anders, N. Komazawa, J. Takeda, and J. DiGiovanni (2004). Disruption of Stat3 reveals a critical role in both the initiation and the promotion stages of epithelial carcinogenesis. *Journal of Clinical Investigation* 114(5), 720–728.
- Cheng, T., J. Sudderth, C. Yang, A. R. Mullen, E. S. Jin, J. M. Matés, and R. J. DeBerardinis (2011). Pyruvate carboxylase is required for glutamine-independent growth of tumor cells. *Proceedings of the National Academy of Sciences of the United States of America* 108(21), 8674–9.
- Chi, J.-T., Z. Wang, D. S. A. Nuyten, E. H. Rodriguez, M. E. Schaner, A. Salim, Y. Wang, G. B. Kristensen, A. Helland, A.-L. Børresen-Dale, A. Giaccia, M. T. Longaker, T. Hastie, G. P. Yang, M. J. van de Vijver, and P. O. Brown (2006). Gene expression programs in response to hypoxia: cell type specificity and prognostic significance in human cancers. *PLoS medicine* 3(3), e47.
- Christofk, H. R., M. G. Vander Heiden, M. H. Harris, A. Ramanathan, R. E. Gerszten, R. Wei, M. D. Fleming, S. L. Schreiber, and L. C. Cantley (2008). The M2 splice isoform of pyruvate kinase is important for cancer metabolism and tumour growth. *Nature* 452(7184), 230–233.
- Christofk, H. R., M. G. Vander Heiden, N. Wu, J. M. Asara, and L. C. Cantley (2008). Pyruvate kinase M2 is a phosphotyrosine-binding protein. *Nature* 452(7184), 181–186.
- Clifford, S. C., M. E. Cockman, a. C. Smallwood, D. R. Mole, E. R. Woodward, P. H. Maxwell, P. J. Ratcliffe, and E. R. Maher (2001). Contrasting effects on HIF-1 $\alpha$  regulation by disease-causing pVHL mutations correlate with patterns of tumourigenesis in von Hippel-Lindau disease. *Human molecular genetics* 10(10), 1029–1038.
- Cockman, M. E., N. Masson, D. R. Mole, P. Jaakkola, G. W. Chang, S. C. Clifford, E. R. Maher, C. W. Pugh, P. J. Ratcliffe, and P. H. Maxwell (2000). Hypoxia inducible factor- $\alpha$  binding and ubiquitylation by the von Hippel-Lindau tumor suppressor protein. *Journal of Biological Chemistry* 275(33), 25733–25741.
- Crosby, M. E., C. M. Devlin, P. M. Glazer, G. a. Calin, and M. Ivan (2009). Emerging roles of microRNAs in the molecular responses to hypoxia. *Current pharmaceutical design* 15(33), 3861–6.
- Curi, R., P. Newsholme, and E. A. Newsholme (1988). Metabolism of pyruvate by isolated rat mesenteric lymphocytes, lymphocyte mitochondria and isolated mouse macrophages. *Biochemical Journal* 250(2), 383–388.

- Dauer, D. J., B. Ferraro, L. Song, B. Yu, L. Mora, R. Buettner, S. Enkemann, R. Jove, and E. B. Haura (2005). Stat3 regulates genes common to both wound healing and cancer. *Oncogene* 24(21), 3397–408.
- Davis, S., T. H. Aldrich, N. Stahl, L. Pan, T. Taga, T. Kishimoto, N. Y. Ip, and G. D. Yancopoulos (1993). LIFR beta and gp130 as heterodimerizing signal transducers of the tripartite CNTF receptor. *Science (New York, N.Y.)* 260(June), 1805–1808.
- DeBerardinis, R. J., J. J. Lum, G. Hatzivassiliou, and C. B. Thompson (2008). The Biology of Cancer: Metabolic Reprogramming Fuels Cell Growth and Proliferation. *Cell Metabolism* 7(1), 11–20.
- DeBerardinis, R. J., A. Mancuso, E. Daikhin, I. Nissim, M. Yudkoff, S. Wehrli, and C. B. Thompson (2007). Beyond aerobic glycolysis: transformed cells can engage in glutamine metabolism that exceeds the requirement for protein and nucleotide synthesis. *Proceedings of the National Academy of Sciences of the United States of America* 104(49), 19345–50.
- Demaria, M., C. Giorgi, M. Lebedzinska, G. Esposito, L. D’angeli, A. Bartoli, D. J. Gough, J. Turkson, D. E. Levy, C. J. Watson, M. R. Wieckowski, P. Provero, P. Pinton, and V. Poli (2010). A STAT3-mediated metabolic switch is involved in tumour transformation and STAT3 addiction. *Aging* 2(11), 823–842.
- Demaria, M., S. Misale, C. Giorgi, V. Miano, A. Camporeale, J. Campisi, P. Pinton, and V. Poli (2012). STAT3 can serve as a hit in the process of malignant transformation of primary cells. *Cell death and differentiation* 19(8), 1390–7.
- Des Rosiers, C., L. Di Donato, B. Comte, A. Laplante, C. Marcoux, F. David, C. A. Fernandez, and H. Brunengraber (1995). Isotopomer analysis of citric acid cycle and gluconeogenesis in rat liver: Reversibility of isocitrate dehydrogenase and involvement of ATP-citrate lyase in gluconeogenesis. *Journal of Biological Chemistry* 270(17), 10027–10036.
- Dey, G., A. Radhakrishnan, N. Syed, J. K. Thomas, A. Nadig, K. Srikumar, P. P. Mathur, A. Pandey, S. K. Lin, R. Raju, and T. S. K. Prasad (2013). Signaling network of Oncostatin M pathway. *Journal of Cell Communication and Signaling* 7(2), 103–108.
- Dimova, E. Y. and T. Kietzmann (2010). Hypoxia-Inducible Factors: Post-translational Crosstalk of Signaling Pathways. *Transcription Factors: Methods and Protocols* 647(2), 215–236.
- Dombrackas, J. D., B. D. Santarsiero, and A. D. Mesecar (2005). Structural basis for tumor pyruvate kinase M2 allosteric regulation and catalysis. *Biochemistry* 44(27), 9417–29.
- Edinger, A. L. and C. B. Thompson (2002). Akt maintains cell size and survival by increasing mTOR-dependent nutrient uptake. *Molecular biology of the cell* 13(7), 2276–88.

- El-Serag, H. B. and K. L. Rudolph (2007). Hepatocellular Carcinoma: Epidemiology and Molecular Carcinogenesis. *Gastroenterology* 132(7), 2557–2576.
- Elks, C. M. and J. M. Stephens (2015). Oncostatin M modulation of lipid storage. *Biology* 4(1), 151–60.
- Ema, M., S. Taya, N. Yokotani, K. Sogawa, Y. Matsuda, and Y. Fujii-Kuriyama (1997). A novel bHLH-PAS factor with close sequence similarity to hypoxia-inducible factor 1alpha regulates the VEGF expression and is potentially involved in lung and vascular development. *Proceedings of the National Academy of Sciences of the United States of America* 94(9), 4273–8.
- Epstein, A. C. R., J. M. Gleadle, L. A. McNeill, K. S. Hewitson, J. O'Rourke, D. R. Mole, M. Mukherji, E. Metzen, M. I. Wilson, A. Dhanda, Y. M. Tian, N. Masson, D. L. Hamilton, P. Jaakkola, R. Barstead, J. Hodgkin, P. H. Maxwell, C. W. Pugh, C. J. Schofield, and P. J. Ratcliffe (2001). C. elegans EGL-9 and mammalian homologs define a family of dioxygenases that regulate HIF by prolyl hydroxylation. *Cell* 107(1), 43–54.
- Ernst, M., M. Najdovska, D. Grail, T. Lundgren-May, M. Buchert, H. Tye, V. B. Matthews, J. Armes, P. S. Bhathal, N. R. Hughes, E. G. Marcusson, J. G. Karras, S. Na, J. D. Sedgwick, P. J. Hertzog, and B. J. Jenkins (2008). STAT3 and STAT1 mediate IL-11-dependent and inflammation-associated gastric tumorigenesis in gp130 receptor mutant mice. *Journal of Clinical Investigation* 118(5), 1727–1738.
- Fabiano, A. J. and J. Qiu (2015). Post-stereotactic radiosurgery brain metastases: A review. *Journal of Neurosurgical Sciences* 59(2), 157–167.
- Faris, M., B. Ensoli, N. Stahl, G. Yancopoulos, A. Nguyen, S. Wang, and A. E. Nel (1996). Differential activation of the extracellular signal-regulated kinase, Jun kinase and Janus kinase-Stat pathways by oncostatin M and basic fibroblast growth factor in AIDS-derived Kaposi's sarcoma cells. *AIDS (London, England)* 10(4), 369–78.
- Fausto, N. (1999). Mouse liver tumorigenesis: models, mechanisms, and relevance to human disease. *Seminars in liver disease* 19(3), 243–252.
- Fendt, S.-M., E. L. Bell, M. A. Keibler, B. A. Olenchock, J. R. Mayers, T. M. Wasylenko, N. I. Vokes, L. Guarente, M. G. Vander Heiden, and G. Stephanopoulos (2013). Reductive glutamine metabolism is a function of the  $\alpha$ -ketoglutarate to citrate ratio in cells. *Nature communications* 4, 2236.
- Filipp, F. V., D. A. Scott, Z. A. Ronai, A. L. Osterman, and J. W. Smith (2012). Reverse TCA cycle flux through isocitrate dehydrogenases 1 and 2 is required for lipogenesis in hypoxic melanoma cells. *Pigment Cell & Melanoma Research* 25(3), 375–383.

- Firth, J. D., B. L. Ebert, and P. J. Ratcliffe (1995). Hypoxic regulation of lactate dehydrogenase A: Interaction between hypoxia-inducible factor 1 and cAMP response elements. *Journal of Biological Chemistry* 270(36), 21021–21027.
- Fong, G.-H. and K. Takeda (2008). Role and regulation of prolyl hydroxylase domain proteins. *Cell death and differentiation* 15(4), 635–641.
- Frank, D. A. (2007). STAT3 as a central mediator of neoplastic cellular transformation. *Cancer Letters* 251(2), 199–210.
- Frezza, C., L. Zheng, D. A. Tennant, D. B. Papkovsky, B. A. Hedley, G. Kalna, D. G. Watson, and E. Gottlieb (2011). Metabolic profiling of hypoxic cells revealed a catabolic signature required for cell survival. *PLoS ONE* 6(9).
- Fukuda, R., K. Hirota, F. Fan, Y. D. Jung, L. M. Ellis, and G. L. Semenza (2002). Insulin-like growth factor 1 induces hypoxia-inducible factor 1-mediated vascular endothelial growth factor expression, which is dependent on MAP kinase and phosphatidylinositol 3-kinase signaling in colon cancer cells. *Journal of Biological Chemistry* 277(41), 38205–38211.
- Fukuda, R., H. Zhang, J. whan Kim, L. Shimoda, C. V. Dang, and G. L. Semenza (2007). HIF-1 Regulates Cytochrome Oxidase Subunits to Optimize Efficiency of Respiration in Hypoxic Cells. *Cell* 129(1), 111–122.
- Galluzzi, L., O. Kepp, M. G. Vander Heiden, and G. Kroemer (2013). Metabolic targets for cancer therapy. *Nat. Rev. Drug Discov.* 12(11), 829–46.
- Gameiro, P. A., J. Yang, A. M. Metelo, R. Prez-Carro, R. Baker, Z. Wang, A. Arreola, W. K. Rathmell, A. Olumi, P. Lpez-Larrubia, G. Stephanopoulos, and O. Iliopoulos (2013). In vivo HIF-mediated reductive carboxylation is regulated by citrate levels and sensitizes VHL-deficient cells to glutamine deprivation. *Cell Metabolism* 17(3), 372–385.
- Ganesh, K., A. Das, R. Dickerson, S. Khanna, N. L. Parinandi, G. M. Gordillo, C. K. Sen, and S. Roy (2012). Prostaglandin E induces oncostatin M expression in human chronic wound macrophages through Axl receptor tyrosine kinase pathway. *Journal of immunology (Baltimore, Md. : 1950)* 189(5), 2563–73.
- Gao, S. P., K. G. Mark, K. Leslie, W. Pao, N. Motoi, W. L. Gerald, W. D. Travis, W. Bornmann, D. Veach, B. Clarkson, and J. F. Bromberg (2007). Mutations in the EGFR kinase domain mediate STAT3 activation via IL-6 production in human lung adenocarcinomas. *Journal of Clinical Investigation* 117(12), 3846–3856.
- Gao, X., H. Wang, J. J. Yang, X. Liu, and Z. R. Liu (2012). Pyruvate kinase M2 regulates gene transcription by acting as a protein kinase. *Molecular Cell* 45(5), 598–609.

- Garcia, R., T. L. Bowman, G. Niu, H. Yu, S. Minton, C. a. Muro-Cacho, C. E. Cox, R. Falcone, R. Fairclough, S. Parsons, A. Laudano, A. Gazit, A. Levitzki, A. Kraker, and R. Jove (2001). Constitutive activation of Stat3 by the Src and JAK tyrosine kinases participates in growth regulation of human breast carcinoma cells. *Oncogene* 20(20), 2499–2513.
- Gearing, D. P., M. R. Comeau, D. J. Friend, S. D. Gimpel, C. J. Thut, J. McGourty, K. K. Brasher, J. a. King, S. Gillis, and B. Mosley (1992). The IL-6 signal transducer, gp130: an oncostatin M receptor and affinity converter for the LIF receptor. *Science (New York, N.Y.)* 255(5050), 1434–1437.
- Giannitrapani, L., M. Cervello, M. Soresi, M. Notarbartolo, M. Rosa, L. Virruso, N. D'Alessandro, and G. Montalto (2006). Circulating IL-6 and sIL-6R in Patients with Hepatocellular Carcinoma. *Annals of the New York Academy of Sciences* 963(1), 46–52.
- Gough, D. J., A. Corlett, K. Schlessinger, J. Wegrzyn, A. C. Larner, and D. E. Levy (2009). Mitochondrial STAT3 supports Ras-dependent oncogenic transformation. *Science (New York, N.Y.)* 324(5935), 1713–6.
- Grassian, A. R., C. M. Metallo, J. L. Coloff, G. Stephanopoulos, and J. S. Brugge (2011). Erk regulation of pyruvate dehydrogenase flux through PDK4 modulates cell proliferation. *Genes & development* 25(16), 1716–33.
- Grivennikov, S., E. Karin, J. Terzic, D. Mucida, G. Y. Yu, S. Vallabhapurapu, J. Scheller, S. Rose-John, H. Cheroutre, L. Eckmann, and M. Karin (2009). IL-6 and Stat3 Are Required for Survival of Intestinal Epithelial Cells and Development of Colitis-Associated Cancer. *Cancer Cell* 15(2), 103–113.
- Grove, R. I., C. E. Mazzucco, S. F. Radka, M. Shoyab, and P. A. Kiener (1991). Oncostatin M up-regulates low density lipoprotein receptors in HepG2 cells by a novel mechanism. *J Biol Chem* 266(27), 18194–18199.
- Gu, M., R. P. Singh, S. Dhanalakshmi, C. Agarwal, and R. Agarwal (2007). Silibinin inhibits inflammatory and angiogenic attributes in photocarcinogenesis in SKH-1 hairless mice. *Cancer Research* 67(7), 3483–3491.
- Gu, Y., S. Moran, J. Hogenesch, L. Wartman, and C. Bradfield (1998). Molecular characterization and chromosomal localization of a third alpha-class hypoxia inducible factor subunit, HIF3alpha. *Gene Expression* 7(3), 205–213.
- Guzy, R. D., B. Hoyos, E. Robin, H. Chen, L. Liu, K. D. Mansfield, M. C. Simon, U. Hammerling, and P. T. Schumacker (2005). Mitochondrial complex III is required for hypoxia-induced ROS production and cellular oxygen sensing. *Cell Metabolism* 1(6), 401–408.

- Gygi, S. P., Y. Rochon, B. R. Franza, and R. Aebersold (1999). Correlation between protein and mRNA abundance in yeast. *Molecular and cellular biology* 19(3), 1720–1730.
- Haan, C. and I. Behrmann (2007). A cost effective non-commercial ECL-solution for Western blot detections yielding strong signals and low background. *Journal of Immunological Methods* 318(1-2), 11–19.
- Halama, A., B. S. Guerrouahen, J. Pasquier, I. Diboun, E. D. Karoly, K. Suhre, and A. Raffi (2015). Metabolic signatures differentiate ovarian from colon cancer cell lines. *Journal of translational medicine* 13, 223.
- Halfter, H., R. Lotfi, R. Westermann, P. Young, E. B. Ringelstein, and F. T. Stogbauer (1998). Inhibition of growth and induction of differentiation of glioma cell lines by oncostatin M (OSM). *Growth Factors* 15(2), 135–147.
- Hamada, T., A. Sato, T. Hirano, T. Yamamoto, G. Son, M. Onodera, I. Torii, T. Nishigami, M. Tanaka, A. Miyajima, S. Nishiguchi, J. Fujimoto, and T. Tsujimura (2007). Oncostatin M gene therapy attenuates liver damage induced by dimethylnitrosamine in rats. *Am J Pathol* 171(3), 872–881.
- Hanahan, D. and R. A. Weinberg (2000). The hallmarks of cancer. *Cell* 100(1), 57–70.
- Hanahan, D. and R. A. Weinberg (2011). Hallmarks of cancer: The next generation. *Cell* 144(5), 646–674.
- Hatzivassiliou, G., F. Zhao, D. E. Bauer, C. Andreadis, A. N. Shaw, D. Dhanak, S. R. Hingorani, D. A. Tuveson, and C. B. Thompson (2005). ATP citrate lyase inhibition can suppress tumor cell growth. *Cancer Cell* 8(4), 311–321.
- Haverkorn van Rijsewijk, B. R. B., A. Nanchen, S. Nallet, R. J. Kleijn, and U. Sauer (2011). Large-scale <sup>13</sup>C-flux analysis reveals distinct transcriptional control of respiratory and fermentative metabolism in *Escherichia coli*. *Molecular systems biology* 7, 477.
- He, G. and M. Karin (2011). NF- $\kappa$ B and STAT3 - key players in liver inflammation and cancer. *Cell research* 21(1), 159–68.
- He, G., G. Y. Yu, V. Temkin, H. Ogata, C. Kuntzen, T. Sakurai, W. Sieghart, M. Peck-Radosavljevic, H. L. Leffert, and M. Karin (2010). Hepatocyte IKK $\beta$ /NF- $\kappa$ B Inhibits Tumor Promotion and Progression by Preventing Oxidative Stress-Driven STAT3 Activation. *Cancer Cell* 17(3), 286–297.
- Hedekov, C. J. (1968). Early Effects of Phytohaemagglutinin on Glucose Metabolism of Normal Human Lymphocytes. *The Biochemical journal* 110(2), 373–80.

- Heinrich, P. C., I. Behrmann, G. Müller-Newen, F. Schaper, and L. Graeve (1998). Interleukin-6-type cytokine signalling through the gp130/Jak/STAT pathway. *The Biochemical Journal* 334, 297–314.
- Hemann, U., C. Gerhartz, B. Heesel, J. Sasse, G. Kurapkat, J. Grötzingerl, A. Wollmert, Z. Zhong, J. E. Darnell, L. Graeve, P. C. Heinrich, and F. Horn (1996). Differential activation of acute phase response factor/Stat3 and Stat1 via the cytoplasmic domain of the interleukin 6 signal transducer gp130: II. Src homology SH2 domains define the specificity of stat factor activation. *Journal of Biological Chemistry* 271(22), 12999–13007.
- Henkel, J., D. Gärtner, C. Dorn, C. Hellerbrand, N. Schanze, S. R. Elz, and G. P. Püschel (2011). Oncostatin M produced in Kupffer cells in response to PGE2: possible contributor to hepatic insulin resistance and steatosis. *Laboratory investigation; a journal of technical methods and pathology* 91(7), 1107–17.
- Hermanns, H. M. (2015). Oncostatin M and interleukin-31: Cytokines, receptors, signal transduction and physiology. *Cytokine and Growth Factor Reviews* 26(5), 545–558.
- Hewitson, K. S., B. M. R. Liénard, M. A. McDonough, I. J. Clifton, D. Butler, A. S. Soares, N. J. Oldham, L. A. McNeill, and C. J. Schofield (2007). Structural and mechanistic studies on the inhibition of the hypoxia-inducible transcription factor hydroxylases by tricarboxylic acid cycle intermediates. *Journal of Biological Chemistry* 282(5), 3293–3301.
- Hiller, K., J. Hangebrauk, C. Jäger, J. Spura, K. Schreiber, and D. Schomburg (2009). Metabolite detector: Comprehensive analysis tool for targeted and nontargeted GC/MS based metabolome analysis. *Analytical Chemistry* 81(9), 3429–3439.
- Hiller, K., C. Metallo, and G. Stephanopoulos (2011). Elucidation of cellular metabolism via metabolomics and stable-isotope assisted metabolomics. *Current pharmaceutical biotechnology* 12(7), 1075–1086.
- Hiller, K., C. M. Metallo, J. K. Kelleher, and G. Stephanopoulos (2010). Nontargeted elucidation of metabolic pathways using stable-isotope tracers and mass spectrometry. *Analytical Chemistry* 82(15), 6621–6628.
- Hitosugi, T., S. Kang, M. G. Vander Heiden, T.-W. Chung, S. Elf, K. Lythgoe, S. Dong, S. Lonial, X. Wang, G. Z. Chen, J. Xie, T.-L. Gu, R. D. Polakiewicz, J. L. Roesel, T. J. Boggon, F. R. Khuri, D. G. Gilliland, L. C. Cantley, J. Kaufman, and J. Chen (2009). Tyrosine phosphorylation inhibits PKM2 to promote the Warburg effect and tumor growth. *Science signaling* 2(97), ra73.
- Hodge, D. R., E. M. Hurt, and W. L. Farrar (2005). The role of IL-6 and STAT3 in inflammation and cancer. *European journal of cancer (Oxford, England : 1990)* 41(16), 2502–12.



- Holleran, A. L., D. A. Briscoe, G. Fiskum, and J. K. Kelleher (1995). Glutamine metabolism in AS-30D hepatoma cells. Evidence for its conversion into lipids via reductive carboxylation. *Molecular and Cellular Biochemistry* 152(2), 95–101.
- Holmes, E., A. W. Nicholls, J. C. Lindon, S. Ramos, M. Spraul, P. Neidig, S. C. Connor, J. Connelly, S. J. P. Damment, J. Haselden, and J. K. Nicholson (1998). Development of a model for classification of toxin-induced lesions using <sup>1</sup>H NMR spectroscopy of urine combined with pattern recognition. *NMR in Biomedicine* 11(4-5), 235–244.
- Horn, D., W. C. Fitzpatrick, P. T. Gompper, V. Ochs, M. Bolton-Hansen, J. Zarling, N. Malik, G. J. Todaro, and P. S. Linsley (1990). Regulation of cell growth by recombinant oncostatin M. *Growth factors (Chur, Switzerland)* 2(2-3), 157–65.
- Hsu, P. P. and D. M. Sabatini (2008). Cancer cell metabolism: Warburg and beyond. *Cell* 134(5), 703–707.
- Hu, C.-j., L.-y. Wang, L. a. Chodosh, B. Keith, and M. C. Simon (2003). Differential Roles of hypoxia-inducible factor 1 alpha (HIF-1 alpha) and HIF-2 alpha in hypoxic gene regulation. *Molecular and Cellular Biology* 23(24), 9361–9374.
- Huang, L. E., J. Gu, M. Schau, and H. F. Bunn (1998). Regulation of hypoxia-inducible factor 1-alpha is mediated by an O<sub>2</sub>-dependent degradation domain via the ubiquitin-proteasome pathway. *Proceedings of the National Academy of Sciences of the United States of America* 95(14), 7987–92.
- Ichihara, M., T. Hara, H. Kim, T. Murate, and a. Miyajima (1997). Oncostatin M and leukemia inhibitory factor do not use the same functional receptor in mice. *Blood* 90(1), 165–173.
- Ikeda, M., K. Sugiyama, T. Tanaka, K. Tanaka, H. Sekihara, K. Shimotohno, and N. Kato (1998). Lactoferrin markedly inhibits hepatitis C virus infection in cultured human hepatocytes. *Biochemical and biophysical research communications* 245(2), 549–53.
- Inoue, H., W. Ogawa, M. Ozaki, S. Haga, M. Matsumoto, K. Furukawa, N. Hashimoto, Y. Kido, T. Mori, H. Sakaue, K. Teshigawara, S. Jin, H. Iguchi, R. Hiramatsu, D. LeRoith, K. Takeda, S. Akira, and M. Kasuga (2004). Role of STAT-3 in regulation of hepatic gluconeogenic genes and carbohydrate metabolism in vivo. *Nat Med* 10(2), 168–174.
- Isaacs, J. S., J. J. Yun, D. R. Mole, S. Lee, C. Torres-Cabala, Y. L. Chung, M. Merino, J. Trepel, B. Zbar, J. Toro, P. J. Ratcliffe, W. M. Linehan, and L. Neckers (2005). HIF overexpression correlates with biallelic loss of fumarate hydratase in renal cancer: Novel role of fumarate in regulation of HIF stability. *Cancer Cell* 8(2), 143–153.

- Ivan, M., K. Kondo, H. Yang, W. Kim, J. Valiando, M. Ohh, A. Salic, J. M. Asara, W. S. Lane, and W. G. Kaelin (2001). HIF- $\alpha$  targeted for VHL-mediated destruction by proline hydroxylation: implications for O<sub>2</sub> sensing. *Science (New York, N.Y.)* 292(5516), 464–468.
- Iyer, N. V., L. E. Kotch, F. Agani, S. W. Leung, E. Laughner, R. H. Wenger, M. Gassmann, J. D. Gearhart, A. M. Lawler, A. Y. Yu, and G. L. Semenza (1998). Cellular and developmental control of O<sub>2</sub> homeostasis by hypoxia-inducible factor 1 $\alpha$ . *Genes and Development* 12(2), 149–162.
- Jaakkola, P., D. R. Mole, Y. M. Tian, M. I. Wilson, J. Gielbert, S. J. Gaskell, A. von Kriegsheim, H. F. Hebestreit, M. Mukherji, C. J. Schofield, P. H. Maxwell, C. W. Pugh, and P. J. Ratcliffe (2001). Targeting of HIF- $\alpha$  to the von Hippel-Lindau ubiquitylation complex by O<sub>2</sub>-regulated prolyl hydroxylation. *Science* 292(5516), 468–72.
- Jeong, J. W., M. K. Bae, M. Y. Ahn, S. H. Kim, T. K. Sohn, M. H. Bae, M. A. Yoo, E. J. Song, K. J. Lee, and K. W. Kim (2002). Regulation and destabilization of HIF-1 $\alpha$  by ARD1-mediated acetylation. *Cell* 111(5), 709–20.
- Jiang, B. H., G. L. Semenza, C. Bauer, and H. H. Marti (1996). Hypoxia-inducible factor 1 levels vary exponentially over a physiologically relevant range of O<sub>2</sub> tension. *The American journal of physiology* 271(45), C1172–C1180.
- Jitrapakdee, S., M. St Maurice, I. Rayment, W. W. Cleland, J. C. Wallace, and P. V. Attwood (2008). Structure, mechanism and regulation of pyruvate carboxylase. *The Biochemical journal* 413(3), 369–87.
- Jung, J. E., H. S. Kim, C. S. Lee, Y. J. Shin, Y. N. Kim, G. H. Kang, T. Y. Kim, Y. S. Juhn, S. J. Kim, J. W. Park, S. K. Ye, and M. H. Chung (2008). STAT3 inhibits the degradation of HIF-1 $\alpha$  by pVHL-mediated ubiquitination. *Experimental & molecular medicine* 40(5), 479–85.
- Jung, J. E., H. G. Lee, I. H. Cho, D. H. Chung, S.-H. Yoon, Y. M. Yang, J. W. Lee, S. Choi, J.-W. Park, S.-K. Ye, and M.-H. Chung (2005). STAT3 is a potential modulator of HIF-1-mediated VEGF expression in human renal carcinoma cells. *The FASEB journal : official publication of the Federation of American Societies for Experimental Biology* 19(10), 1296–1298.
- Jurica, M. S., A. Mesecar, P. J. Heath, W. Shi, T. Nowak, and B. L. Stoddard (1998). The allosteric regulation of pyruvate kinase by fructose-1,6-bisphosphate. *Structure (London, England : 1993)* 6(2), 195–210.
- Kamiya, a., T. Kinoshita, Y. Ito, T. Matsui, Y. Morikawa, E. Senba, K. Nakashima, T. Taga, K. Yoshida, T. Kishimoto, and a. Miyajima (1999). Fetal liver development requires a

- paracrine action of oncostatin M through the gp130 signal transducer. *The EMBO journal* 18(8), 2127–2136.
- Kanani, H., P. K. Chrysanthopoulos, and M. I. Klapa (2008). Standardizing GC-MS metabolomics. *Journal of Chromatography B: Analytical Technologies in the Biomedical and Life Sciences* 871(2), 191–201.
- Kerbey, A. L., P. J. Randle, R. H. Cooper, S. Whitehouse, H. T. Pask, and R. M. Denton (1976). Regulation of pyruvate dehydrogenase in rat heart. Mechanism of regulation of proportions of dephosphorylated and phosphorylated enzyme by oxidation of fatty acids and ketone bodies and of effects of diabetes: role of coenzyme A, acetyl-coenzyme A and red. *The Biochemical journal* 154(2), 327–48.
- Kerr, D., G. Grahame, and G. Nakouzi (2012). Assays of pyruvate dehydrogenase complex and pyruvate carboxylase activity. *Methods in molecular biology (Clifton, N.J.)* 837, 93–119.
- Kerr, D. S., L. Ho, C. M. Berlin, K. F. Lanoue, J. Towfighi, C. L. Hoppel, M. M. Lusk, C. M. Gondek, and M. S. Patel (1987). Systemic deficiency of the first component of the pyruvate dehydrogenase complex. *Pediatric research* 22(3), 312–8.
- Kim, J. W., I. Tchernyshyov, G. L. Semenza, and C. V. Dang (2006). HIF-1-mediated expression of pyruvate dehydrogenase kinase: A metabolic switch required for cellular adaptation to hypoxia. *Cell Metabolism* 3(3), 177–185.
- Klausen, P., L. Pedersen, J. Jurlander, and H. Baumann (2000). Oncostatin M and interleukin 6 inhibit cell cycle progression by prevention of p27kip1 degradation in HepG2 cells. *Oncogene* 19(32), 3675–83.
- Koek, M. M., B. Muilwijk, M. J. Van Der Werf, and T. Hankemeier (2006). Microbial metabolomics with gas chromatography/mass spectrometry. *Analytical Chemistry* 78(4), 1272–1281.
- Kortylewski, M., H. Xin, M. Kujawski, H. Lee, Y. Liu, T. Harris, C. Drake, D. Pardoll, and H. Yu (2009). Regulation of the IL-23 and IL-12 Balance by Stat3 Signaling in the Tumor Microenvironment. *Cancer Cell* 15(2), 114–123.
- Krieg, M., R. Haas, H. Brauch, T. Acker, I. Flamme, and K. H. Plate (2000). Up-regulation of hypoxia-inducible factors HIF-1alpha and HIF-2alpha under normoxic conditions in renal carcinoma cells by von Hippel-Lindau tumor suppressor gene loss of function. *Oncogene* 19(48), 5435–5443.

- Kuhajda, F. P., K. Jenner, F. D. Wood, R. a. Hennigar, L. B. Jacobs, J. D. Dick, and G. R. Pasternack (1994). Fatty acid synthesis: a potential selective target for antineoplastic therapy. *Proceedings of the National Academy of Sciences of the United States of America* 91(14), 6379–6383.
- Kujawski, M., M. Kortylewski, H. Lee, A. Herrmann, H. Kay, and H. Yu (2008). Stat3 mediates myeloid cell-dependent tumor angiogenesis in mice. *Journal of Clinical Investigation* 118(10), 3367–3377.
- Kuper, H., H. O. Adami, and D. Trichopoulos (2000). Infections as a major preventable cause of human cancer. *Journal of Internal Medicine* 248(3), 171–183.
- Laughner, E., P. Taghavi, K. Chiles, C. Patrick, G. L. Semenza, and P. C. Mahon (2001). HER2 ( neu ) signaling increases the rate of synthesis of hypoxia-inducible factor 1 $\alpha$  (HIF-1 $\alpha$ ) synthesis: novel mechanism for HIF-1-mediated vascular endothelial growth factor expression. *American Society for Microbiology* 21(12), 3995–4004.
- Lei, Z., D. V. Huhman, and L. W. Sumner (2011). Mass spectrometry strategies in metabolomics. *Journal of Biological Chemistry* 286(29), 25435–25442.
- Liang, H., T. M. Block, M. Wang, B. Nefsky, R. Long, J. Hafner, A. S. Mehta, J. Marrero, R. Gish, and P. A. Norton (2012). Interleukin-6 and oncostatin M are elevated in liver disease in conjunction with candidate hepatocellular carcinoma biomarker GP73. *Cancer Biomarkers* 11(4), 161–171.
- Liou, J. C., M. Matney, P. Anz-Meador, D. J. Kessler, M. Jansen, and J. R. Theall (2001). The new NASA orbital debris engineering model ORDEM2000. *European Space Agency, (Special Publication) ESA SP 1(473)*, 309–313.
- Liu, X., Z. Ser, and J. W. Locasale (2014). Development and quantitative evaluation of a high-resolution metabolomics technology. *Analytical chemistry* 86(4), 2175–84.
- Lunt, S. Y., V. Muralidhar, A. M. Hosios, W. J. Israelsen, D. Y. Gui, L. Newhouse, M. Ogrodzinski, V. Hecht, K. Xu, P. N. M. Acevedo, D. P. Hollern, G. Bellinger, T. L. Dayton, S. Christen, I. Elia, A. T. Dinh, G. Stephanopoulos, S. R. Manalis, M. B. Yaffe, E. R. Andrechek, S. M. Fendt, and M. G. Vander Heiden (2015). Pyruvate kinase isoform expression alters nucleotide synthesis to impact cell proliferation. *Molecular Cell* 57(1), 95–107.
- Lussey-Lepoutre, C., K. E. R. Hollinshead, C. Ludwig, M. Menara, A. Morin, L.-J. Castro-Vega, S. J. Parker, M. Janin, C. Martinelli, C. Ottolenghi, C. Metallo, A.-P. Gimenez-Roqueplo, J. Favier, and D. A. Tennant (2015). Loss of succinate dehydrogenase activity results in dependency on pyruvate carboxylation for cellular anabolism. *Nature Communications* 6, 8784.

- Ma, X.-T., S. Wang, Y.-J. Ye, R.-Y. Du, Z.-R. Cui, and M. Somsouk (2004). Constitutive activation of Stat3 signaling pathway in human colorectal carcinoma. *World journal of gastroenterology : WJG* 10(11), 1569–73.
- Mansfield, K. D., R. D. Guzy, Y. Pan, R. M. Young, T. P. Cash, P. T. Schumacker, and M. C. Simon (2005). Mitochondrial dysfunction resulting from loss of cytochrome c impairs cellular oxygen sensing and hypoxic HIF- $\alpha$  activation. *Cell Metabolism* 1(6), 393–399.
- Mantovani, A., P. Allavena, A. Sica, and F. Balkwill (2008). Cancer-related inflammation. *Nature* 454(7203), 444.
- Masson, N., R. S. Singleton, R. Sekirnik, D. C. Trudgian, L. J. Ambrose, M. X. Miranda, Y.-M. Tian, B. M. Kessler, C. J. Schofield, and P. J. Ratcliffe (2012). The FIH hydroxylase is a cellular peroxide sensor that modulates HIF transcriptional activity.
- Maxwell, P. H., G. U. Dachs, J. M. Gleadle, L. G. Nicholls, A. L. Harris, I. J. Stratford, O. Hankinson, C. W. Pugh, and P. J. Ratcliffe (1997). Hypoxia-inducible factor-1 modulates gene expression in solid tumors and influences both angiogenesis and tumor growth. *Proceedings of the National Academy of Sciences of the United States of America* 94(15), 8104–9.
- Maxwell, P. H., M. S. Wiesener, G. W. Chang, S. C. Clifford, E. C. Vaux, M. E. Cockman, C. C. Wykoff, C. W. Pugh, E. R. Maher, and P. J. Ratcliffe (1999). The tumour suppressor protein VHL targets hypoxia-inducible factors for oxygen-dependent proteolysis. *Nature* 399(6733), 271–275.
- Mazurek, S. (2011). Pyruvate kinase type M2: a key regulator of the metabolic budget system in tumor cells. *The international journal of biochemistry & cell biology* 43(7), 969–80.
- Mazurek, S., C. B. Boschek, F. Hugo, and E. Eigenbrodt (2005). Pyruvate kinase type M2 and its role in tumor growth and spreading. *Seminars in cancer biology* 15(4), 300–8.
- Meiser, J., L. Krämer, S. C. Saccariu, N. Battello, J. Ghelfi, A. F. D’Herouel, A. Skupin, and K. Hiller (2016). Pro-inflammatory Macrophages Sustain Pyruvate Oxidation through Pyruvate Dehydrogenase for the Synthesis of Itaconate and to Enable Cytokine Expression. *The Journal of biological chemistry* 291(8), 3932–46.
- Metallo, C. M., P. A. Gameiro, E. L. Bell, K. R. Mattaini, J. Yang, K. Hiller, C. M. Jewell, Z. R. Johnson, D. J. Irvine, L. Guarente, J. K. Kelleher, M. G. V. Heiden, O. Iliopoulos, and G. Stephanopoulos (2011). Reductive glutamine metabolism by IDH1 mediates lipogenesis under hypoxia. *Nature* 481(VN-(7381)), 380–384.
- Metallo, C. M., J. L. Walther, G. Stephanopoulos, P. S. Ward, J. Patel, D. R. Wise, O. Abdelwahab, B. D. Bennett, H. A. Collier, J. R. Cross, V. R. Fantin, C. V. Hedvat, E. Alexander,

- J. D. Rabinowitz, M. Carroll, S. M. Su, K. A. Sharp, L. Ross, and C. B. Thompson (2009). Evaluation of  $^{13}\text{C}$  isotopic tracers for metabolic flux analysis in mammalian cells. *BioTechniques* 144(3), 167–174.
- Minton, D. R., L. Fu, Q. Chen, B. D. Robinson, S. S. Gross, D. M. Nanus, and L. J. Gudas (2015). Analyses of the transcriptome and metabolome demonstrate that HIF-1 $\alpha$  mediates altered tumor metabolism in clear cell renal cell carcinoma. *PLoS ONE* 10(4), 167–174.
- Mishra, P. and S. Ambs (2015). Metabolic Signatures of Human Breast Cancer. *Molecular & cellular oncology* 2(3), 1367–671.
- Miyajima, A., T. Kinoshita, M. Tanaka, A. Kamiya, Y. Mukoyama, and T. Hara (2000). Role of oncostatin M in hematopoiesis and liver development. *Cytokine and Growth Factor Reviews* 11(3), 177–183.
- Mole, D. R., C. Blancher, R. R. Copley, P. J. Pollard, J. M. Gleadle, J. Ragousis, and P. J. Ratcliffe (2009). Genome-wide association of hypoxia-inducible factor (HIF)-1 $\alpha$  and HIF-2 $\alpha$  DNA binding with expression profiling of hypoxia-inducible transcripts. *Journal of Biological Chemistry* 284(25), 16767–16775.
- Mora Linda, B., R. Buettner, J. Seigne, J. Diaz, N. Ahmad, R. Garcia, T. Bowman, R. Falcone, R. Fairclough, A. Cantor, C. Muro-Cacho, S. Livingston, J. Karras, J. Pow-Sang, and R. Jove (2002). Constitutive activation of Stat3 in human prostate tumors and cell lines: direct inhibition of Stat3 signaling induces apoptosis of prostate cancer cells. *Cancer Res* 62(22), 6659–6666.
- Moreno-Sánchez, R., S. Rodríguez-Enríquez, A. Marín-Hernández, and E. Saavedra (2007). Energy metabolism in tumor cells. *FEBS Journal* 274(6), 1393–1418.
- Moroz, E., S. Carlin, K. Dyomina, S. Burke, H. T. Thaler, R. Blasberg, and I. Serganova (2009). Real-time imaging of HIF-1 $\alpha$  stabilization and degradation. *PLoS ONE* 4(4), e5077.
- Mullen, A. R., W. W. Wheaton, E. S. Jin, P.-H. Chen, L. B. Sullivan, T. Cheng, Y. Yang, W. M. Linehan, N. S. Chandel, and R. J. DeBerardinis (2011). Reductive carboxylation supports growth in tumour cells with defective mitochondria. TL - 481. *Nature* 481 VN-(7381), 385–388.
- Murakami, M., M. Hibi, N. Nakagawa, T. Nakagawa, K. Yasukawa, K. Yamanishi, T. Taga, and T. Kishimoto (1993). IL-6-induced homodimerization of gp130 and associated activation of a tyrosine kinase. *Science (New York, N.Y.)* 260(5115), 1808–10.
- Nair, B. C., A. L. DeVico, S. Nakamura, T. D. Copeland, Y. Chen, A. Patel, T. O’Neil, S. Oroszlan, R. C. Gallo, and M. G. Sarngadharan (1992). Identification of a major growth factor for AIDS-Kaposi’s sarcoma cells as oncostatin M. *Science* 255(5050), 1430–1432.

- Nakamura, K., H. Nonaka, H. Saito, M. Tanaka, and A. Miyajima (2004). Hepatocyte proliferation and tissue remodeling is impaired after liver injury in oncostatin M receptor knockout mice. *Hepatology* 39(3), 635–644.
- Naugler, W. E., T. Sakurai, S. Kim, S. Maeda, K. Kim, A. M. Elsharkawy, and M. Karin (2007). Gender disparity in liver cancer due to sex differences in MyD88-dependent IL-6 production. *Science (New York, N.Y.)* 317(5834), 121–4.
- Newsholme, E. a., B. Crabtree, and M. S. Ardawi (1985). The role of high rates of glycolysis and glutamine utilization in rapidly dividing cells. *Bioscience reports* 5(5), 393–400.
- Niemann, S. and U. Müller (2000). Mutations in SDHC cause autosomal dominant paraganglioma, type 3. *Nature genetics* 26(3), 268–270.
- Niklas, J., V. Sandig, and E. Heinzle (2011). Metabolite channeling and compartmentation in the human cell line AGE1.HN determined by <sup>13</sup>C labeling experiments and <sup>13</sup>C metabolic flux analysis. *Journal of bioscience and bioengineering* 112(6), 616–23.
- Niu, G., J. Briggs, J. Deng, Y. Ma, H. Lee, M. Kortylewski, M. Kujawski, H. Kay, W. D. Cress, R. Jove, and H. Yu (2008). Signal transducer and activator of transcription 3 is required for hypoxia-inducible factor-1 $\alpha$  RNA expression in both tumor cells and tumor-associated myeloid cells. *Molecular cancer research : MCR* 6(7), 1099–1105.
- Niu, G., K. L. Wright, M. Huang, L. Song, E. Haura, J. Turkson, S. Zhang, T. Wang, D. Sinibaldi, D. Coppola, R. Heller, L. M. Ellis, J. Karras, J. Bromberg, D. Pardoll, R. Jove, and H. Yu (2002). Constitutive Stat3 activity up-regulates VEGF expression and tumor angiogenesis. *Oncogene* 21(October), 2000–2008.
- Noguchi, Y., J. D. Young, J. O. Aleman, M. E. Hansen, J. K. Kelleher, and G. Stephanopoulos (2009). Effect of anaplerotic fluxes and amino acid availability on hepatic lipoapoptosis. *The Journal of biological chemistry* 284(48), 33425–36.
- Olcaydu, D., A. Harutyunyan, R. Jäger, T. Berg, B. Gisslinger, I. Pabinger, H. Gisslinger, and R. Kralovics (2009). A common JAK2 haplotype confers susceptibility to myeloproliferative neoplasms. *Nature genetics* 41(4), 450–4.
- Ortiz-Barahona, A., D. Villar, N. Pescador, J. Amigo, and L. del Peso (2010). Genome-wide identification of hypoxia-inducible factor binding sites and target genes by a probabilistic model integrating transcription-profiling data and in silico binding site prediction. *Nucleic Acids Research* 38(7), 2332–2345.
- Papandreou, I., R. A. Cairns, L. Fontana, A. L. Lim, and N. C. Denko (2006). HIF-1 mediates adaptation to hypoxia by actively downregulating mitochondrial oxygen consumption. *Cell Metabolism* 3(3), 187–197.

- Parkin, D. M. (2001). Global cancer statistics in the year 2000. *Lancet Oncology* 2(9), 533–543.
- Parlo, R. A. and P. S. Coleman (1984a). Enhanced rate of citrate export from cholesterol-rich hepatoma mitochondria. The truncated Krebs cycle and other metabolic ramifications of mitochondrial membrane cholesterol. *Journal of Biological Chemistry* 259(16), 9997–10003.
- Parlo, R. A. and P. S. Coleman (1984b). Enhanced rate of citrate export from cholesterol-rich hepatoma mitochondria. The truncated Krebs cycle and other metabolic ramifications of mitochondrial membrane cholesterol. *Journal of Biological Chemistry* 259(16), 9997–10003.
- Parlo, R. A. and P. S. Coleman (1986). Continuous pyruvate carbon flux to newly synthesized cholesterol and the suppressed evolution of pyruvate-generated CO<sub>2</sub> in tumors: Further evidence for a persistent truncated Krebs cycle in hepatomas. *BBA - Molecular Cell Research* 886(2), 169–176.
- Pawlus, M. R., L. Wang, and C.-J. Hu (2014a). STAT3 and HIF1 $\alpha$  cooperatively activate HIF1 target genes in MDA-MB-231 and RCC4 cells. *Oncogene* 33(13), 1670–9.
- Pawlus, M. R., L. Wang, and C.-J. Hu (2014b). STAT3 and HIF1 $\alpha$  cooperatively activate HIF1 target genes in MDA-MB-231 and RCC4 cells. *Oncogene* 33(13), 1670–9.
- Pennica, D., K. L. King, K. J. Shaw, E. Luis, J. Rullamas, S. M. Luoh, W. C. Darbonne, D. S. Knutzon, R. Yen, and K. R. Chien (1995). Expression cloning of cardiotrophin 1, a cytokine that induces cardiac myocyte hypertrophy. *Proceedings of the National Academy of Sciences of the United States of America* 92(4), 1142–1146.
- Pfeiffer, T., S. Schuster, and S. Bonhoeffer (2001). Cooperation and competition in the evolution of ATP-producing pathways. *Science (New York, N.Y.)* 292(5516), 504–507.
- Pizer, E. S., F. D. Wood, H. S. Heine, F. E. Romantsev, G. R. Pasternack, and F. P. Kuhajda (1996). Inhibition of fatty acid synthesis delays disease progression in a xenograft model of ovarian cancer. *Cancer Research* 56(6), 1189–1193.
- Pollard, P. J., B. Spencer-Dene, D. Shukla, K. Howarth, E. Nye, M. El-Bahrawy, M. Deheragoda, M. Joannou, S. McDonald, A. Martin, P. Igarashi, S. Varsani-Brown, I. Rosewell, R. Poulson, P. Maxwell, G. W. Stamp, and I. P. M. Tomlinson (2007). Targeted inactivation of Fh1 causes proliferative renal cyst development and activation of the hypoxia pathway. *Cancer Cell* 11(4), 311–319.
- Quintero, M., N. Mackenzie, and P. A. Brennan (2004). Hypoxia-inducible factor 1 (HIF-1) in cancer. *European Journal of Surgical Oncology* 30(5), 465–468.



- Ramadoss, P., N. E. Unger-Smith, F. S. Lam, and A. N. Hollenberg (2009). STAT3 targets the regulatory regions of gluconeogenic genes in vivo. *Molecular endocrinology (Baltimore, Md.)* 23(6), 827–837.
- Richards, C. D. (2013). The enigmatic cytokine oncostatin M and roles in disease. *ISRN inflammation 2013*, 512103.
- Richards, C. D., T. J. Brown, M. Shoyab, H. Baumann, and J. Gauldie (1992). Recombinant oncostatin M stimulates the production of acute phase proteins in HepG2 cells and rat primary hepatocytes in vitro. *J Immunol* 148(6), 1731–1736.
- Robb, L., D. J. Hilton, T. A. Willson, and C. G. Begley (1996). Structural analysis of the gene encoding the murine interleukin-11 receptor alpha-chain and a related locus. *The Journal of biological chemistry* 271(23), 13754–61.
- Roberts, L. D., A. L. Souza, R. E. Gerszten, and C. B. Clish (2012). Targeted metabolomics. *Current protocols in molecular biology / edited by Frederick M. Ausubel ... [et al.] Chapter 30*, Unit 30.2.1–24.
- Roche, T. E., J. C. Baker, X. Yan, Y. Hiromasa, X. Gong, T. Peng, J. Dong, a. Turkan, and S. a. Kasten (2001). Distinct regulatory properties of pyruvate dehydrogenase kinase and phosphatase isoforms. *Progress in nucleic acid research and molecular biology* 70, 33–75.
- Sakurai, T., G. He, A. Matsuzawa, G. Y. Yu, S. Maeda, G. Hardiman, and M. Karin (2008). Hepatocyte Necrosis Induced by Oxidative Stress and IL-1 $\alpha$  Release Mediate Carcinogen-Induced Compensatory Proliferation and Liver Tumorigenesis. *Cancer Cell* 14(2), 156–165.
- Samavati, L., R. Rastogi, W. Du, M. Hüttemann, A. Fite, and L. Franchi (2009). STAT3 tyrosine phosphorylation is critical for interleukin 1 beta and interleukin-6 production in response to lipopolysaccharide and live bacteria. *Molecular Immunology* 46(8-9), 1867–1877.
- Sano, S., K. S. Chan, M. Kira, K. Kataoka, S. Takagi, M. Tarutani, S. Itami, K. Kiguchi, M. Yokoi, K. Sugasawa, T. Mori, F. Hanaoka, J. Takeda, and J. DiGiovanni (2005). Signal transducer and activator of transcription 3 is a key regulator of keratinocyte survival and proliferation following UV irradiation. *Cancer Research* 65(13), 5720–5729.
- Sapcariu, S. C., T. Kanashova, D. Weindl, J. Ghelfi, G. Dittmar, and K. Hiller (2014). Simultaneous extraction of proteins and metabolites from cells in culture. *MethodsX* 1(1), 74–80.
- Schoedel, J., S. Oikonomopoulos, J. Ragoussis, C. W. Pugh, P. J. Ratcliffe, and D. R. Mole (2011). High-resolution genome-wide mapping of HIF-binding sites by ChIP-seq. *Blood* 117(23), e207–17.

- Schofield, C. J. and Z. Zhang (1999). Structural and mechanistic studies on 2-oxoglutarate-dependent oxygenases and related enzymes. *Current Opinion in Structural Biology* 9(6), 722–731.
- Schwab, W. (2003). Metabolome diversity: Too few genes, too many metabolites? *Phytochemistry* 62(6), 837–849.
- Scott, D. A., A. D. Richardson, F. V. Filipp, C. A. Knutzen, G. G. Chiang, Z. A. Ronai, A. L. Osterman, and J. W. Smith (2011). Comparative metabolic flux profiling of melanoma cell lines: Beyond the Warburg effect. *Journal of Biological Chemistry* 286(49), 42626–42634.
- Scrutton, M. C. and M. D. White (1974). Purification and properties of human liver pyruvate carboxylase. *Biochemical medicine* 9(3), 217–92.
- Seagroves, T. N., H. E. Ryan, H. Lu, B. G. Wouters, M. Knapp, P. Thibault, K. Laderoute, and R. S. Johnson (2001). Transcription factor HIF-1 is a necessary mediator of the pasteur effect in mammalian cells. *Molecular and cellular biology* 21(10), 3436–44.
- Selak, M. A., S. M. Armour, E. D. MacKenzie, H. Boulahbel, D. G. Watson, K. D. Mansfield, Y. Pan, M. C. Simon, C. B. Thompson, and E. Gottlieb (2005). Succinate links TCA cycle dysfunction to oncogenesis by inhibiting HIF- $\alpha$  prolyl hydroxylase. *Cancer Cell* 7(1), 77–85.
- Semenza, G. L. (2003). Targeting HIF-1 for cancer therapy. *Nature Reviews Cancer* 3(10), 721–732.
- Semenza, G. L. (2011). HIF-1 : upstream and downstream of cancer metabolism. *Current opinion in genetics & development* 20(1), 1–10.
- Semenza, G. L. (2012). Hypoxia-inducible factors in physiology and medicine. *Cell* 148(3), 399–408.
- Semenza, G. L., P. H. Roth, H. M. Fang, and G. L. Wang (1994). Transcriptional regulation of genes encoding glycolytic enzymes by hypoxia-inducible factor 1. *Journal of Biological Chemistry* 269(38), 23757–23763.
- Semenza, G. L. and G. L. Wang (1992). A nuclear factor induced by hypoxia via de novo protein synthesis binds to the human erythropoietin gene enhancer at a site required for transcriptional activation. *Molecular and cellular biology* 12(12), 5447–5454.
- Sheu, K. F., C. W. Hu, and M. F. Utter (1981). Pyruvate dehydrogenase complex activity in normal and deficient fibroblasts. *The Journal of clinical investigation* 67(5), 1463–71.
- Shuai, K. and B. Liu (2003). Regulation of JAK-STAT signalling in the immune system. *Nature reviews. Immunology* 3(11), 900–911.

- Shuai, K. and B. Liu (2005). Regulation of gene-activation pathways by PIAS proteins in the immune system. *Nature reviews. Immunology* 5(8), 593–605.
- Spannbauer, M. M. and C. Trautwein (2009). Frequent in-frame somatic deletions activate gp130 in inflammatory hepatocellular tumors. *Hepatology* 49(4), 1387–1389.
- Spura, J., L. Christian Reimer, P. Wieloch, K. Schreiber, S. Buchinger, and D. Schomburg (2009). A method for enzyme quenching in microbial metabolome analysis successfully applied to gram-positive and gram-negative bacteria and yeast. *Analytical Biochemistry* 394(2), 192–201.
- Stahl, N., T. J. Farruggella, T. G. Boulton, Z. Zhong, J. E. Darnell, and G. D. Yancopoulos (1995). Choice of STATs and other substrates specified by modular tyrosine-based motifs in cytokine receptors. *Science* 267(5202), 1349–1353.
- Stickle, N., J. Chung, J. Klco, R. Hill, W. Kaelin, and M. Ohh (2004). pVHL modification by NEDD8 is required for fibronectin matrix assembly and suppression of tumor development. *Mol Cell Biol* 24(8), 3251–3261.
- Stolze, I. P., Y. M. Tian, R. J. Appelhoff, H. Turley, C. C. Wykoff, J. M. Gleadle, and P. J. Ratcliffe (2004). Genetic analysis of the role of the asparaginyl hydroxylase factor inhibiting hypoxia-inducible factor (HIF) in regulating HIF transcriptional target genes. *Journal of Biological Chemistry* 279(41), 42719–42725.
- Sturek, M. (2011). Ca<sup>2+</sup> regulatory mechanisms of exercise protection against coronary artery disease in metabolic syndrome and diabetes. *Journal of applied physiology (Bethesda, Md. : 1985)* 111(2), 573–86.
- Sun, R. C. and N. C. Denko (2014). Hypoxic regulation of glutamine metabolism through HIF1 and SIAH2 supports lipid synthesis that is necessary for tumor growth. *Cell Metabolism* 19(2), 285–292.
- Sun, X., J. Zhang, L. Wang, and Z. Tian (2008). Growth inhibition of human hepatocellular carcinoma cells by blocking STAT3 activation with decoy-ODN. *Cancer Letters* 262(2), 201–213.
- Tomlinson, I. P. M., N. A. Alam, A. J. Rowan, E. Barclay, E. E. M. Jaeger, D. Kelsell, I. Leigh, P. Gorman, H. Lamlum, S. Rahman, R. R. Roylance, S. Olpin, S. Bevan, K. Barker, N. Hearle, R. S. Houlston, M. Kiuru, R. Lehtonen, A. Karhu, S. Vilkki, P. Laiho, C. Eklund, O. Vierimaa, K. Aittomäki, M. Hietala, P. Sistonen, A. Paetau, R. Salovaara, R. Herva, V. Launonen, and L. a. Aaltonen (2002). Germline mutations in FH predispose to dominantly inherited uterine fibroids, skin leiomyomata and papillary renal cell cancer. *Nature genetics* 30(april), 406–410.

- Treins, C., S. Giorgetti-Peraldi, J. Murdaca, G. L. Semenza, and E. Van Obberghen (2002). Insulin stimulates hypoxia-inducible factor 1 through a phosphatidylinositol 3-kinase/target of rapamycin-dependent signaling pathway. *Journal of Biological Chemistry* 277(31), 27975–27981.
- Uhlén, M., L. Fagerberg, B. M. Hallström, C. Lindskog, P. Oksvold, A. Mardinoglu, Å. Sivertsson, C. Kampf, E. Sjöstedt, A. Asplund, I. Olsson, K. Edlund, E. Lundberg, S. Navani, C. A.-K. Szigartyo, J. Odeberg, D. Djureinovic, J. O. Takanen, S. Hober, T. Alm, P.-H. Edqvist, H. Berling, H. Tegel, J. Mulder, J. Rockberg, P. Nilsson, J. M. Schwenk, M. Hamsten, K. von Feilitzen, M. Forsberg, L. Persson, F. Johansson, M. Zwahlen, G. von Heijne, J. Nielsen, and F. Pontén (2015). Proteomics. Tissue-based map of the human proteome. *Science (New York, N.Y.)* 347(6220), 1260419.
- Van Wagoner, N. J., C. Choi, P. Repovic, and E. N. Benveniste (2000). Oncostatin M regulation of interleukin-6 expression in astrocytes: Biphasic regulation involving the mitogen-activated protein kinases ERK1/2 and p38. *Journal of Neurochemistry* 75(2), 563–575.
- Vander Heiden, M. G., L. C. Cantley, and C. B. Thompson (2009). Understanding the Warburg effect: the metabolic requirements of cell proliferation. *Science (New York, N.Y.)* 324(5930), 1029–33.
- Vengellur, A., B. G. Woods, H. E. Ryan, R. S. Johnson, and J. J. LaPres (2003). Gene expression profiling of the hypoxia signaling pathway in hypoxia-inducible factor 1alpha null mouse embryonic fibroblasts. *Gene Expr.* 11(3-4), 181–197.
- Villas-Bôas, S. G., J. Højer-Pedersen, M. Åkesson, J. Smedsgaard, and J. Nielsen (2005). Global metabolite analysis of yeast: Evaluation of sample preparation methods. *Yeast* 22(14), 1155–1169.
- Vollmer, S., V. Kappler, J. Kaczor, D. Flügel, C. Rolvering, N. Kato, T. Kietzmann, I. Behrmann, and C. Haan (2009). Hypoxia-inducible factor 1 $\alpha$  is up-regulated by oncostatin M and participates in oncostatin M signaling. *Hepatology* 50(1), 253–260.
- Wang, G. L., B. H. Jiang, E. A. Rue, and G. L. Semenza (1995). Hypoxia-inducible factor 1 is a basic-helix-loop-helix-PAS heterodimer regulated by cellular O<sub>2</sub> tension. *Proceedings of the National Academy of Sciences of the United States of America* 92(12), 5510–5514.
- Wang, G. L. and G. L. Semenza (1995). Purification and characterization of Hypoxia-inducible Factor 1. *The Journal of biological chemistry* 270(Issue of January 20), 1230–1237.
- Wang, T., C. Marquardt, and J. Foker (1976). Aerobic glycolysis during lymphocyte proliferation. *Nature* 261(5562), 702–705.

- Wang, X., S. Chen, and Z. Zhang (2001). Expression of surviving gene and its relationship with expression of P53, c-myc, k-ras proteins in non-small-cell lung cancer. *Zhonghua Jie He He Hu Xi Za Zhi* 24(6), 371–374.
- Wang, Y. and G. M. Fuller (1994). Phosphorylation and internalization of gp130 occur after {IL-6} activation of Jak2 kinase in hepatocytes. *Molecular biology of the cell* 5(7), 819–828.
- Want, E. J., B. F. Cravatt, and G. Siuzdak (2005). The expanding role of mass spectrometry in metabolite profiling and characterization. *ChemBioChem* 6(11), 1941–1951.
- Warburg, O. (1928). Stoffwechsel der Karzinomzelle. In *Verhandlungen der Deutschen Gesellschaft für Innere Medizin SE - 2*, pp. 11–18.
- Warburg, O. (1956). On respiratory impairment in cancer cells. *Science (New York, N.Y.)* 124(3215), 269–70.
- Warren, G. B. and K. F. Tipton (1974). Pig liver pyruvate carboxylase. Purification, properties and cation specificity. *The Biochemical journal* 139(2), 297–310.
- Wegner, A., S. C. Sapcariu, D. Weindl, and K. Hiller (2013). Isotope cluster-based compound matching in gas chromatography/mass spectrometry for non-targeted metabolomics. *Analytical Chemistry* 85(8), 4030–4037.
- Wegner, A., D. Weindl, C. Jäger, S. C. Sapcariu, X. Dong, G. Stephanopoulos, and K. Hiller (2014). Fragment formula calculator (FFC): Determination of chemical formulas for fragment ions in mass spectrometric data. *Analytical Chemistry* 86(4), 2221–2228.
- Wegrzyn, J., R. Potla, Y.-J. Chwae, N. B. V. Sepuri, Q. Zhang, T. Koeck, M. Derecka, K. Szczepanek, M. Szelag, A. Gornicka, A. Moh, S. Moghaddas, Q. Chen, S. Bobbili, J. Cichy, J. Dulak, D. P. Baker, A. Wolfman, D. Stuehr, M. O. Hassan, X.-Y. Fu, N. Avadhani, J. I. Drake, P. Fawcett, E. J. Lesnefsky, and A. C. Larner (2009). Function of mitochondrial Stat3 in cellular respiration. *Science (New York, N.Y.)* 323(5915), 793–7.
- Wei, L.-H., M.-L. Kuo, C.-A. Chen, C.-H. Chou, K.-B. Lai, C.-N. Lee, and C.-Y. Hsieh (2003). Interleukin-6 promotes cervical tumor growth by VEGF-dependent angiogenesis via a STAT3 pathway. *Oncogene* 22(10), 1517–27.
- Wenger, R. H., D. P. Stiehl, and G. Camenisch (2005). Integration of oxygen signaling at the consensus HRE. *Science's STKE : signal transduction knowledge environment* 2005(306), re12.
- Wise, D. R., P. S. Ward, J. E. S. Shay, J. R. Cross, J. J. Gruber, U. M. Sachdeva, J. M. Platt, R. G. DeMatteo, M. C. Simon, and C. B. Thompson (2011). Hypoxia promotes isocitrate dehydrogenase-dependent carboxylation of  $\alpha$ -ketoglutarate to citrate to support

- cell growth and viability. *Proceedings of the National Academy of Sciences of the United States of America* 108(49), 19611–6.
- Wong, V. W.-S., J. Yu, A. S.-L. Cheng, G. L.-H. Wong, H.-Y. Chan, E. S.-H. Chu, E. K.-O. Ng, F. K.-L. Chan, J. J.-Y. Sung, and H. L.-Y. Chan (2009). High serum interleukin-6 level predicts future hepatocellular carcinoma development in patients with chronic hepatitis B. *International journal of cancer. Journal international du cancer* 124(12), 2766–70.
- Wu, M. Z., Y. P. Tsai, M. H. Yang, C. H. Huang, S. Y. Chang, C. C. Chang, S. C. Teng, and K. J. Wu (2011). Interplay between HDAC3 and WDR5 is essential for hypoxia-induced epithelial-mesenchymal transition. *Molecular Cell* 43(5), 811–822.
- Xia, X., M. E. Lemieux, W. Li, J. S. Carroll, M. Brown, X. S. Liu, and A. L. Kung (2009). Integrative analysis of HIF binding and transactivation reveals its role in maintaining histone methylation homeostasis. *Proceedings of the National Academy of Sciences of the United States of America* 106(11), 4260–5.
- Xu, Q., J. Briggs, S. Park, G. Niu, M. Kortylewski, S. Zhang, T. Gritsko, J. Turkson, H. Kay, G. L. Semenza, J. Q. Cheng, R. Jove, and H. Yu (2005). Targeting Stat3 blocks both HIF-1 and VEGF expression induced by multiple oncogenic growth signaling pathways. *Oncogene* 24(36), 5552–5560.
- Yang, M., A. E. Donaldson, C. E. Marshall, J. Shen, and L. Iacovitti (2004). Studies on the differentiation of dopaminergic traits in human neural progenitor cells in vitro and in vivo. *Cell Transplantation* 13(5), 535–547.
- Yoo, H., M. R. Antoniewicz, G. Stephanopoulos, and J. K. Kelleher (2008). Quantifying reductive carboxylation flux of glutamine to lipid in a brown adipocyte cell line. *Journal of Biological Chemistry* 283(30), 20621–20627.
- Yu, H., D. Pardoll, and R. Jove (2009). STATs in cancer inflammation and immunity: a leading role for STAT3. *Nature reviews. Cancer* 9(11), 798–809.
- Zamboni, N. and U. Sauer (2009). Novel biological insights through metabolomics and 13C-flux analysis. *Current opinion in microbiology* 12(5), 553–8.
- Zarling, J. M., M. Shoyab, H. Marquardt, M. B. Hanson, M. N. Lioubin, and G. J. Todaro (1986). Oncostatin M: a growth regulator produced by differentiated histiocytic lymphoma cells. *Proceedings of the National Academy of Sciences of the United States of America* 83(24), 9739–43.
- Zhang, Q., V. Raje, V. A. Yakovlev, A. Yacoub, K. Szczepanek, J. Meier, M. Derecka, Q. Chen, Y. Hu, J. Sisler, H. Hamed, E. J. Lesnfsky, K. Valerie, P. Dent, and A. C. Larner

- (2013). Mitochondrial localized Stat3 promotes breast cancer growth via phosphorylation of serine 727. *Journal of Biological Chemistry* 288(43), 31280–31288.
- Zhou, Y., P. Abidi, A. Kim, W. Chen, T. T. Huang, F. B. Kraemer, and J. Liu (2007). Transcriptional activation of hepatic ACSL3 and ACSL5 by oncostatin M reduces hypertriglyceridemia through enhanced  $\beta$ -oxidation. *Arteriosclerosis, Thrombosis, and Vascular Biology* 27(10), 2198–2205.
- Zimmer, A. D. (2015). *Differential effects of IL-6 type cytokines, their interplay with hypoxia and resulting effects on the metabolism*. Ph. D. thesis, University of Luxembourg; Faculty of Science, Technology and Communication.
- Zimmermann, M., U. Sauer, and N. Zamboni (2014). Quantification and mass isotopomer profiling of  $\alpha$ -keto acids in central carbon metabolism. *Analytical chemistry* 86(6), 3232–7.
- Znoyko, I., N. Sohara, S. S. Spicer, M. Trojanowska, and A. Reuben (2005). Expression of oncostatin M and its receptors in normal and cirrhotic human liver. *Journal of Hepatology* 43(5), 893–900.